BioMed Research International

Toxicology of Metals and Metalloids

Guest Editors: Fernando Barbosa Júnior, Marcelo Farina, Susana Viegas, and Wilma De Grava Kempinas

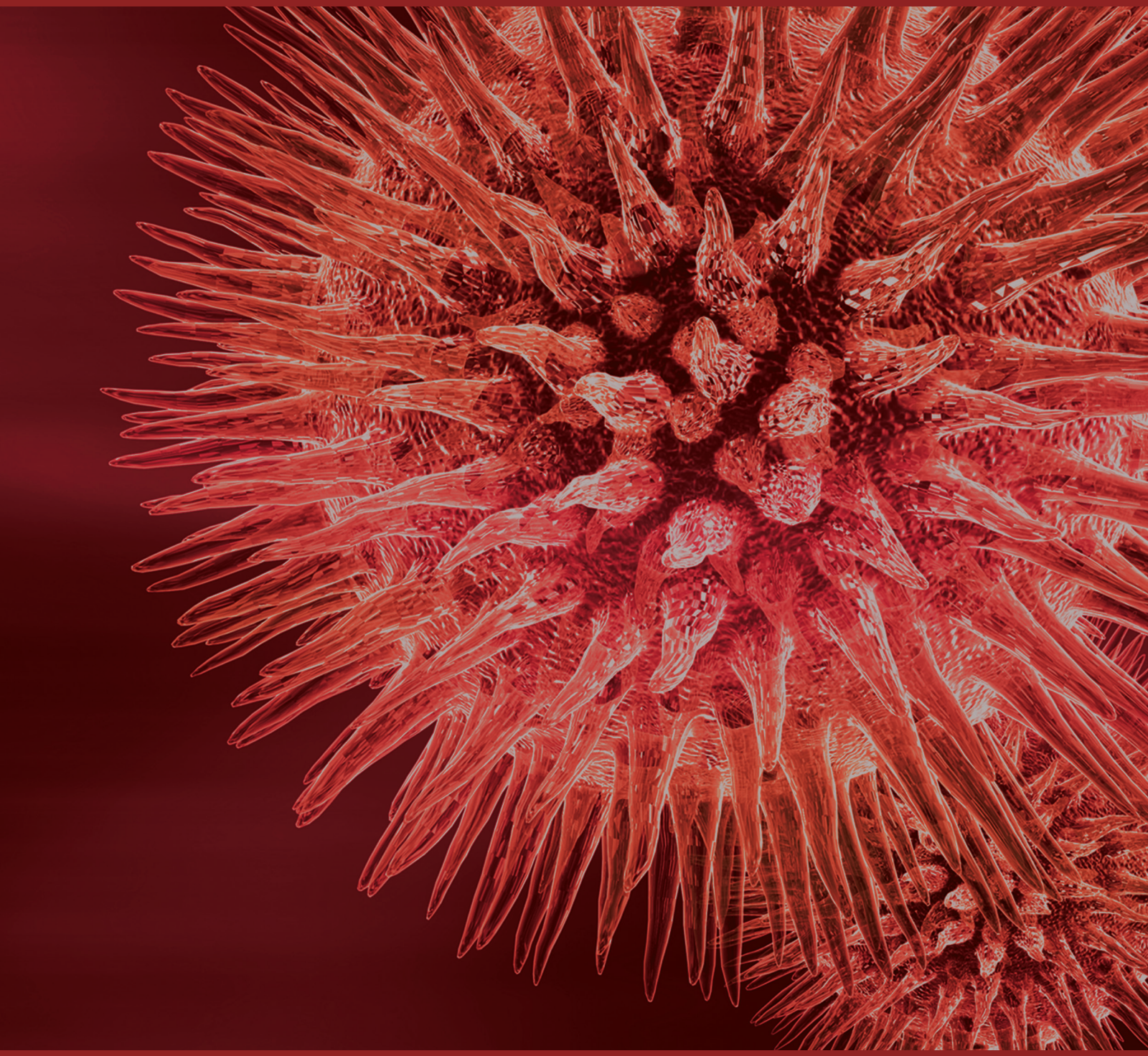

Toxicology of Metals and Metalloids

BioMed Research International

Toxicology of Metals and Metalloids

Guest Editors: Fernando Barbosa Júnior, Marcelo Farina, Susana Viegas, and Wilma De Grava Kempinas

Contents

Hindawi Publishing Corporation
BioMed Research International
Volume 2014, Article ID 253738, 2 pages
http://dx.doi.org/10.1155/2014/253738

Editorial
Toxicology of Metals and Metalloids

Fernando Barbosa Júnior,[1] Marcelo Farina,[2] Susana Viegas,[3] and Wilma De Grava Kempinas[4]

[1] *Departamento de Análises Clínicas, Toxicológicas e Bromatológicas, Faculdade de Ciências Farmacêuticas de Ribeirão Preto, Universidade de São Paulo, 14040903 Ribeirão Preto, SP, Brazil*
[2] *Departamento de Bioquímica, Centro de Ciências Biológicas, Universidade Federal de Santa Catarina, 88040900 Florianópolis, SC, Brazil*
[3] *Grupo de Investigação Ambiente e Saúde, Escola Superior de Tecnologia da Saúde de Lisboa and Instituto Politécnico de Lisboa, 1990-096 Lisboa, Portugal*
[4] *Departamento de Morfologia, Instituto de Biociências de Botucatu, Universidade Estadual Paulista, 18618970 Botucatu, SP, Brazil*

Correspondence should be addressed to Fernando Barbosa Júnior; fbarbosa@fcfrp.usp.br

Received 29 April 2014; Accepted 29 April 2014; Published 22 May 2014

Metal toxicology is one of the oldest areas of study of toxicology and one of the oldest environmental problems. Metals and metalloids are toxic elements at the top of the priority list of hazardous substances of the Agency for Toxic Substances and Disease Registry (ATSDR). However, several gaps of knowledge still exist that are related to their toxicity, mainly concerning the mechanisms of action. This special issue affords the opportunity to bring together the results of nine papers covering several aspects of the toxicology of metals and metalloids in *in vitro* and *in vivo* experimental models, as well as in exposed populations.

The molecular mechanisms mediating manganese- (Mn-) induced neurotoxicity, particularly in the immature central nervous system, are not completely understood. Based on that, T. V. Peres et al. suggested that altered intracellular MAPKs signaling pathways may represent an early event concerning the effects of Mn exposure in the immature brain.

In vitro cytotoxicity of β-SiC nanowires (ceramic material with a potential use as hard tissue replacement) was investigated by W. Xie et al. The authors have found that 100 nm long SiC nanowires increased oxidative stress in MC3T3-E1 cells, as determined by the concentrations of MDA (as a marker of lipid peroxidation) and 8-OHdG (indicator of oxidative DNA damage). Moreover, after treatment with 100 nm long SiC nanowires, the mitochondria were swelled and disintegrated, and the production of ATP and the total oxygen uptake were also decreased significantly.

G. Espinosa-Reyes et al. assessed the impact of mining activities on biotic communities within the District of Villa de la Paz in Mexico. Authors have observed that the concentrations of As and Pb in soil were higher than the Mexican's regulations for urban or agricultural areas.

Many phytoremediation technologies have been used for the remediation of metal polluted areas. This is a low cost process with several distinct advantages including improvement of the soil quality, cost-effective and technically feasible process, plants which serve as sufficient biomass for rapid remediation, promoting high rhizosphere activity, and finally restoration in a reasonable time frame. Based on that, M. Sabeen et al. showed the potential of *Arundo donax* L. for phytoextraction of cadmium (Cd) from contaminated soil and water.

T. S. Gonçalves et al. evaluated the cytotoxicity induced by orthodontic bands through survival tests on *Saccharomyces cerevisiae*, a microorganism that presents several genetic and biochemical characteristics similar to human cells. Three groups of bands were evaluated: silver soldered (SSB), laser soldered (LSB), and bands without any solder

(WSB). Authors found SSBs to be cytotoxic, whilst LSBs were not, confirming that laser soldering may be a more biocompatible alternative for use in connecting wires to orthodontic appliances.

The chemical effects of uranium in rats following a chronic ingestion were investigated by I. Dublineau and coworkers. Biochemical and hematological indicators were measured and several different types of investigations (molecular, functional, and structural) were conducted in different organs. The specific sensitivity of the organs to uranium was deduced from nondeleterious biological effects, with the following thresholds (in mg/L): 0.2 for brain, >2 for liver, >10 for kidneys, and >20 for intestine, indicating a no-observed-adverse-effect level (NOAEL) threshold for uranium superior to 120 mg/L. Based on the chemical uranium toxicity, the tolerable daily intake calculation yields a guideline value for humans of 1350 g/L. This value was higher than the WHO value of 30 g/L, indicating that this WHO guideline for uranium content in drinking water is very protective and might be reconsidered.

Methylmercury (MeHg) is one of the most poisonous environmental contaminants, causing toxic effects in humans and experimental animals. Then, potential protective effects of several nutrients against MeHg-induced toxicity have been evaluated. C. L. Dalla Corte et al. investigate the efficacy of diphenyl diselenide [(PhSe)2] in attenuating methylmercury-(MeHg-) induced toxicity in rats. Cotreatment with (PhSe)2 protected hepatic and cerebral mitochondrial thiols from depletion by MeHg but failed to completely reverse MeHg's effect on hepatic and cerebral mitochondrial dysfunction or hepatic, cerebral, and renal inhibition of TrxR activity. Additionally, the cotreatment with (PhSe)2 increased Hg accumulation in the liver (50.5%) and brain (49.4%) and increased the MeHg-induced motor deficits and body-weight loss. Their results indicate that (PhSe)2 can increase Hg body burden as well as the neurotoxic effects induced by MeHg exposure in rats. On the other hand, R. Frenedoso da Silva et al. observed that Maná-cubiu (*Solanum sessiliflorum* Dunal), a native fruit from the Amazon rich in iron, zinc, niacin, pectin, and citric acid, when coadministered with MeHg minimizes the damages caused by the exposure to MeHg on sperm quantity and quality and the histological aspect of the testis and epididymis of rats.

A. Á. Soares de Oliveira et al. evaluated the effects of polymorphisms in glutathione- (GSH-) related genes (GSTM1, GSTT1, GSTP1, GCLM, and GCLC) in the distribution of Hg in the blood compartments in humans exposed to methylmercury (MeHg). They observed that GSH-related polymorphisms might change the metabolism of MeHg by modifying the distribution of mercury species (inorganic mercury and methylmercury) in the plasma compartment and the partitioning between Hg in plasma and in blood.

We hope that the new findings on the toxic effects of metals and metalloids presented here can contribute to environmental and health policies, leading to a safer planet.

Acknowledgment

We would like to thank all the reviewers that have contributed their time and insight to this special issue.

Fernando Barbosa Júnior
Marcelo Farina
Susana Viegas
Wilma De Grava Kempinas

Hindawi Publishing Corporation
BioMed Research International
Volume 2014, Article ID 312901, 9 pages
http://dx.doi.org/10.1155/2014/312901

Research Article

The β-SiC Nanowires (~100 nm) Induce Apoptosis via Oxidative Stress in Mouse Osteoblastic Cell Line MC3T3-E1

Weili Xie,[1,2] Qi Xie,[2] Meishan Jin,[2] Xiaoxiao Huang,[1] Xiaodong Zhang,[1] Zhengkai Shao,[3] and Guangwu Wen[1,4]

[1] *School of Materials Science and Engineering, Harbin Institute of Technology, Harbin 150001, China*
[2] *Department of Prosthodontics, School of Stomatology, Harbin Medical University, Harbin 150001, China*
[3] *Department of Neurosurgery, The First Affiliated Hospital of Harbin Medical University, Harbin 150001, China*
[4] *School of Materials Science and Engineering, Harbin Institute of Technology at Weihai, Weihai 264209, China*

Correspondence should be addressed to Guangwu Wen; guangwuwen@yeah.net

Received 23 July 2013; Revised 26 November 2013; Accepted 28 November 2013; Published 21 May 2014

Academic Editor: Marcelo Farina

Silicon carbide (SiC), a compound of silicon and carbon, with chemical formula SiC, the beta modification (β-SiC), with a zinc blende crystal structure (similar to diamond), is formed at temperature below 1700°C. β-SiC will be the most suitable ceramic material for the future hard tissue replacement, such as bone and tooth. The *in vitro* cytotoxicity of β-SiC nanowires was investigated for the first time. Our results indicated that 100 nm long SiC nanowires could significantly induce the apoptosis in MC3T3-E1 cells, compared with 100 μm long SiC nanowires. And 100 nm long SiC nanowires increased oxidative stress in MC3T3-E1 cells, as determined by the concentrations of MDA (as a marker of lipid peroxidation) and 8-OHdG (indicator of oxidative DNA damage). Moreover, transmission electron microscopy (TEM) was performed to evaluate the morphological changes of MC3T3-E1 cells. After treatment with 100 nm long SiC nanowires, the mitochondria were swelled and disintegrated, and the production of ATP and the total oxygen uptake were also decreased significantly. Therefore, β-SiC nanowires may have limitations as medical material.

1. Introduction

SiC nanowires are considered to have extensive potential applications due to the excellent mechanical, electrical, and optical properties [1, 2]. During the past decades, efforts have been focused on the synthesis of SiC nanowires. Recently, we fabricated ultra-large-scale SiC nanowires by directly annealing SiOC nanocomposites. Owing to the outstanding physical and chemical stability, SiC nanowires might show good performances in biotechnology and life sciences.

Recent studies have disclosed that nanomaterials are excellent vectors for targeting and delivery of medicines [3, 4]. Nevertheless, the *in vitro* toxicity of SiC nanomaterials has not been investigated. The suitability of nanomaterials must be supported by rigorous studies of their potential toxicity [5, 6]. Thus, in the development of nanomaterials the potential nanomaterial induction of adverse cellular reactions must be considered. Silica nanoparticles, for example, have been demonstrated to have low toxicity if administered in moderate concentration [7]. But, the nanoparticles tend to agglomerate and to lead to protein aggregation at a concentration of 25 μg/mL [8]. Further studies showed that toxic effects of nanowires in HepG2 cells and human epithelial cells only occur at higher concentrations (more than 100 μg/mL) [9]. On the other hand, studies have shown that nanowires readily bind the large protein fibronectin and are readily internalized when incubated with mammalian cells [10].

Osteoblasts synthesize and regulate the deposition and mineralization of the extracellular matrix. Most transformed osteoblast cell lines, although of uniform phenotype, do not exhibit the normal linkage of differentiation and growth arrest [11]. Recent studies have shown that H_2O_2, as active oxygen species, had both stimulatory and inhibitory effects on MC3T3-E1 cell viability depending on the concentration and treatment duration [12, 13]. Oxidative stress, resulting from excessive levels of reactive oxygen species, represents a major cause of cellular damage and death in a plethora of pathological conditions including osteoporosis,

in which there are markedly increased blood levels of oxidative stress markers [14, 15]. And oxidative stress induced caspase-independent apoptosis of MC3T3-E1 cell *in vitro* [16]. The present study was designed to investigate the SiC nanowires induced apoptosis through ROS generation and oxidative stress via Bax/Bal-2 and caspase pathways in mouse osteoblastic cell line MC3T3-E1. Based on the results described above, we employed TEM to characterize the SiC nanowires before exposure and to investigate the effect of SiC with different lengths on cytotoxicity of MC3T3-E1 cell.

2. Materials and Methods

2.1. Chemicals. In the present study, β-SiC nanowires were synthesized by directly annealing the amorphous SiOC nanocomposites in Ar atmosphere [17]. High-sugar Dulbecco's modified Eagle's medium (DMEM) and fetal bovine serum (FBS) were purchased from Gibco (USA). Penicillin-streptomycin was purchased from Sangon (Shanghai, China). WST-8 was purchased from Dojindo Laboratories (Japan). 3-(4,5-Dimethylthiazol-2-yl)-2,5-diphenyltetrazolium bromide (MTT), 2,7-dichlorodihydro-fluorescein diacetate (DCF-DA), propidium iodide (PI), and Hoechst 33342 were purchased from Sigma-Aldrich Chemical Company. Annexin V-FITC Apoptosis Detection Kit I was purchased from BD Biosciences (USA). The primary anti-Bax, anti-Bcl-2, anti-caspase-3, and anti-actin were purchased from Santa Cruz Biotechnology (Santa Cruz, CA, USA).

2.2. Preparation and Characterization of SiC Nanowires. The β-SiC nanowires were dispersed in deionized (DI) water, phosphate-buffered saline (PBS), or a culture medium and characterized by X-ray diffraction (XRD, Shimadzu XRD-6000) and transmission electron microscopy (TEM, Philips CM12), respectively.

2.3. Cell Culture. Preosteoblast subclones (MC3T3-E1) cells were obtained from the Cell Bank of Shanghai Institutes for Biological Sciences, Chinese Academy of Science, China. The cells were cultured in DMEM with 10% FBS, 100 U/mL penicillin, and 100 μg/mL streptomycin at 37°C in humidified environment with 5% of CO_2.

2.4. Cell Morphology Observation. After the incubation, control cells as well as MC3T3-E1 cells treated by different types and concentrations of β-SiC nanowires were harvested, gently washed with 0.01 M PBS (pH 7.4), and fixed by 2.5% glutaraldehyde for two hours. Then, the cells were incubated at 37°C for 5 min and embedded into 0.1% agar. The agar was subsequently fixed by 2.5% glutaraldehyde in PBS at 4°C for at least 2 h. The cell samples were washed with PBS and refixed by 1% osmium tetroxide at 4°C for 2 h, dehydrated in epoxy resin [18]. Ultrathin cross sections (~60 nm) of the cells were observed under TEM microscope (Hitachi-7650, Japan).

2.5. MTT Assay. Cell viability was determined using a 3-(4,5-dimethylthiazol-2-yl)-2,5-diphenyltetrazolium bromide (MTT) assay. Briefly, the cells were seeded in 96-well dishes at 1×10^4 to 2×10^4 cells per well and pretreated with or without β-SiC nanowires for 24 h. Each well was then supplemented with 10 μL of MTT (Sigma) and incubated for 4 h at 37°C. The medium was then removed, and 150 μL of dimethyl sulfoxide (Sigma) was added to solubilize the MTT formazan. The optical density was read at 490 nm.

2.6. Apoptosis Assay by Flow Cytometry. Double staining for annexin V-fluorescein isothiocyanate (FITC) and propidium iodide (PI) was carried out with annexin V-FITC apoptosis detection kit. After the treatment, cells were washed twice in cold PBS/sodium azide and centrifuged at 80 ×g for 5 min. The pellets were resuspended in binding buffer at density of 1×10^6 cells/mL. A sample (100 μL) of the solution was transferred to a culture tube and double-stained with 5 μL of annexin V-FITC and 5 μL of PI. After incubation in the dark for 15 min at room temperature, 400 μL of binding buffer was added to the mixture. The intensity of annexin V-FITC and PI was recorded by FACScan flow cytometry (BD Biosciences, USA) and analyzed with Cell Quest software. A total of 10,000 cells in each sample was analyzed and the percentage of positive cells was determined for each histogram.

2.7. Nuclear Staining with Hoechst 33342/PI. Hoechst 33342/PI were added to each well and incubated for 10 min at 37°C. The stained cells were visualized under a fluorescent microscope, equipped with a CoolSNAP-Pro color digital camera to examine the degree of nuclear condensation.

2.8. Western Blot. Cells were cultured and treated as described above and then lysed with ice-cold lysis buffer containing 50 mmol/L Tris-HCl, pH 7.4; 1% NP-40; 150 mmol/L NaCl; 1 mmol/L EDTA; 1 mmol/L phenylmethylsulphonyl fluoride; and complete proteinase inhibitor mixture (one tablet per 10 mL; Roche Molecular Biochemicals, Indianapolis, IN, USA). After protein content determination using a DC Protein Assay kit (Bio-Rad Laboratories, Hercules, CA, USA) and subsequently incubation with dilute solution (1 : 1000) of primary antibodies including anti-Bax, anti-Bcl-2, anti-caspase3, and anti-actin (Santa Cruz Biotechnology Inc, Santa Cruz, CA). The membranes were then exposed to the secondary antibodies, that is, alkaline phosphatase-labeled goat anti-rabbit immunoglobulin (Santa Cruz), at a dilution of 1 : 1000, followed by exposure to X-ray film [19]. The protein bands were detected using an enhanced chemiluminescence western blotting detection kit (Amersham, Little Chalfont, Buckinghamshire, UK).

2.9. Detection of the Level of Superoxide Anion ($O_2^{\bullet-}$), MDA, 8-OHdG, and MnSOD. We used the probe dihydroethidium (DHE; Molecular Probes, Eugene, OR, USA) to detect intracellular $O_2^{\bullet-}$. $O_2^{\bullet-}$ oxidizing DHE to ethidium, which generates a red fluorescent signal. Fluorescence spectrometry of cell $O_2^{\bullet-}$ production was performed according to previous methods [20].

Cell samples were prepared as a 10% homogenate in 0.9% saline using a homogenizer on ice according to their respective weight. Then the homogenate was centrifuged, and

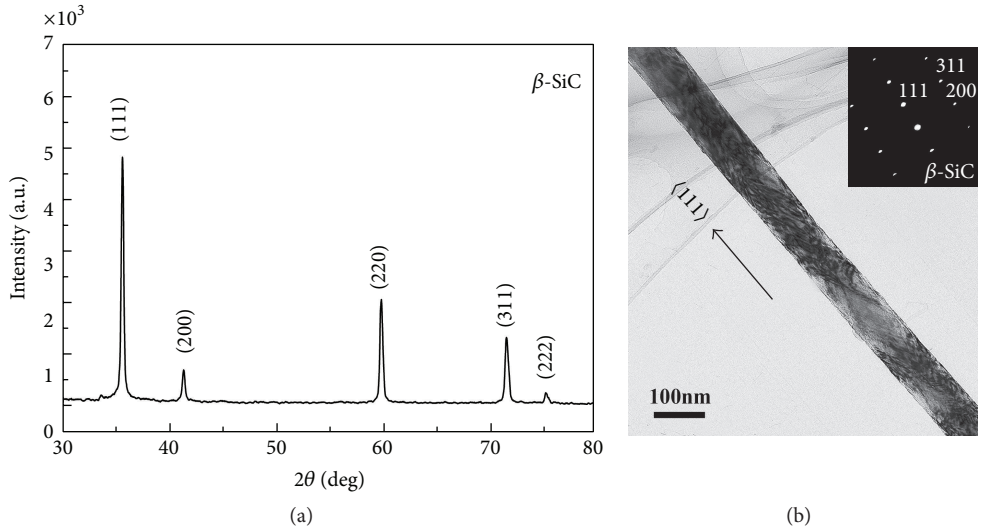

Figure 1: Characterization of nanowires, XRD, and TEM patterns of SiC nanowires. (a) XRD pattern of the SiC nanowires; (b) TEM image of single SiC nanowires and the corresponding SAED pattern.

the supernatant was collected and diluted. The assay of the MDA levels was performed according to the manufacturer's instructions for the MDA detection kit. Competitive ELISA for 8-OHdG was performed according to the manufacturer's protocol. Sample DNA assays were performed in triplicate. Standard 8-OHdG was assayed over a concentration range of 0.125–20 ng/mL in duplicate for each experiment. The average concentration of 8-OHdG per microgram of DNA for each group was calculated for each sample. Controls without added DNA and appropriate blanks were also incorporated into experiments.

The enzyme activity of MnSOD was measured in 5–10 μg of cell protein using a kit. The method utilized tetrazolium salt to quantify $O_2^{\bullet-}$ generated by xanthine oxidase and hypoxanthine. The standard curve was generated by using a quality-controlled SOD standard. MnSOD activity was determined by performing the assay in the presence of potassium cyanide to inhibit Cu-ZnSOD, thus measuring the residual MnSOD activity.

2.10. ATP Assay. The level of intracellular ATP was determined using the ATP Bioluminescence Assay Kit. Cultured cells were lysed with a lysis buffer, followed by centrifugation at 12,000 ×g for 1 min at 4°C. Finally, the level of ATP was determined by mixing 50 μL of the supernatant with 50 μL of luciferase reagent, which catalyzed the light production from ATP and substrate. The emitted light was linearly related to the ATP concentration and measured by using a microplate luminometer.

2.11. Oxygen Consumption. To evaluate the ability of cellular oxygen consumption (VO_2) during nanowires treatment, the Micro Respirometry System (Strathkelvin, Mitocell S200) was employed to measure oxygen content of culture media. Before the assay, MC3T3-E1 cells were pretreated in low oxygen conditions for 2 h in suspension culture with nanowires.

2.12. Statistics. All data was expressed as Mean ± S.D. of three independent experiments. The significance of the variability among the trials was analysed using GraphPad Prism (version 5.0) software.

3. Results

3.1. Characterization of Nanowires. The size and crystalline structure of nanowires were determined using TEM microscopy and X-ray diffraction (XRD). The average radius of 100 nm long and 100 μm long β-SiC nanowires was ~47 nm. The mean length of the two types of nanowires was 100 nm ± 42 nm and 100 μm ± 23 μm, respectively. Figure 1(a) shows the typical XRD pattern of the SiC nanowires used in our experiments. All the sharp diffraction peaks can be well indexed as β-SiC (JCPDS 29-1129). As shown in Figure 1(b), the SiC nanowire was straight and uniform with diameter of 100 nm and the corresponding SAED pattern analysis revealed that the nanowire was β-SiC single crystal and the growth direction was along.

3.2. 100 nm Long β-SiC Nanowires Induced Apoptosis in MC3T3-E1 Cells. Dysfunction induced by the decreased population of cells was regarded as an important factor in the pathogenesis of various metabolic diseases. To investigate the effect of β-SiC nanowires on MC3T3-E1 cells, cell viability was determined by using MTT assays. After MC3T3-E1 cells were exposed to β-SiC nanowires (100 nm or 100 μm) at 6.25, 12.5, 25, 50, and 100 μg/mL for 24 h, cell viability was only decreased in a concentration-dependent manner of 100 nm long β-SiC nanowires (Figure 2(a)). To further examine the effects of 100 nm long β-SiC nanowires on cell apoptosis, two different methods were used. Quantitative evaluation of apoptosis through annexin V-FITC/PI staining was analyzed by flow cytometry. As shown in Figure 2(c), the rate of apoptotic cells was raised to 28.5% with

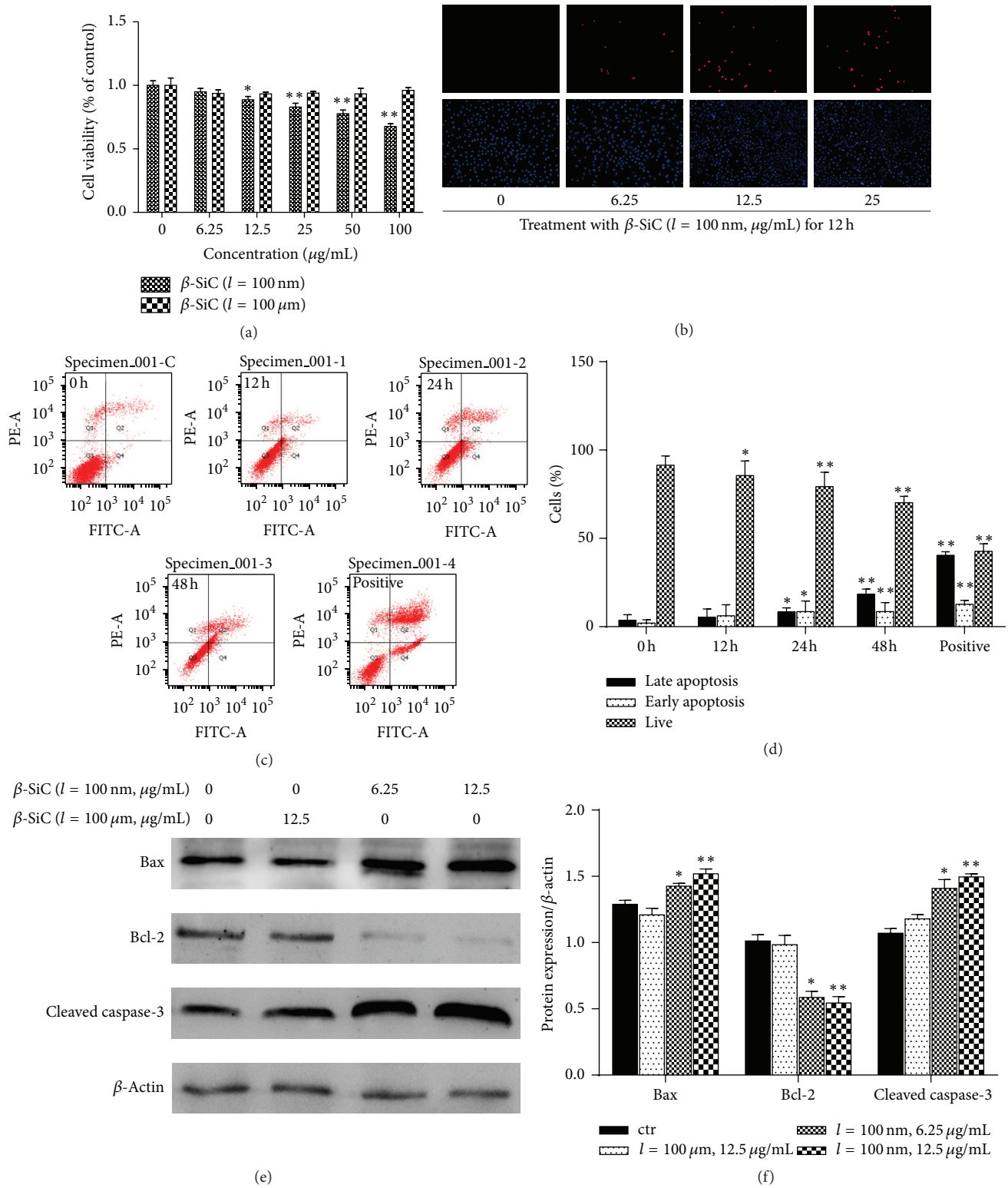

FIGURE 2: The effect of β-SiC nanowires on the cytotoxicity of MC3T3-E1 cells. (a) After 24 h exposure to 6.25, 12.5, 25, 50, and 100 μg/mL of β-SiC nanowires (100 nm, 100 μm), MTT assay was used to evaluate the viability of MC3T3-E1 cells. (b) Representative photographs of double staining of PI and Hoechst 33342. The apoptotic cells were observed as PI intense signal after double staining. (c) Cells were stained with annexin V-FITC and PI, analyzed by flow cytometry. H_2O_2 treated cells were used as positive control. (d) Cells were treated with 12.5 μg/mL of 100 nm long β-SiC nanowires (100 nm) for 12 h, 24 h, and 48 h. The distribution of viable, early apoptotic, later apoptotic, and necrotic cells was analyzed. The data are expressed as percentage of total cells. (e) The expression of apoptotic genes was analyzed by western blot in MC3T3-E1 cells. Values are the means ± SD ($n = 3$) of three individual experiments. (f) Gray value percentage of target protein and β-actin. $^{*}P < 0.05$, $^{**}P < 0.01$ versus ctr (0 μg/mL).

the treatment of 100 nm long β-SiC nanowires (12.5 μg/mL) for 48 h. Determination of DNA content by Hoechst/PI staining indicated that 100 nm long β-SiC nanowires increased the amount of dead cells in MC3T3-E1 cells (Figure 2(b)). And treatment with 100 nm long β-SiC for 24 h caused a change of the expression level of Bcl-2, Bax, and caspase-3 proteins as markers of cytokine-induced apoptosis (Figure 2(e)). Thus, β-SiC nanowires (length = nm) showed significant cytotoxicity in MC3T3-E1 cells, compared with β-SiC nanowires (length = μm).

3.3. 100 nm Long β-SiC Nanowires Increase Oxidative Stress in MC3T3-E1 Cells. Oxidative stress had been implicated in the pathogenesis of osteocytes apoptosis [21]. To estimate the oxidative effect of different β-SiC nanowires, superoxide anion (DHE), MDA, and 8-OHdG levels and MnSOD activity in MC3T3-E1 cells were measured. As an initial indicator of ROS, DHE staining was used, which was a probe for $O_2^{\bullet-}$ and produced red fluorescence as a result of the complex between ethidium and DNA as described by previous study [22]. To quantitate changes in $O_2^{\bullet-}$ levels, we measured total DHE fluorescence in MC3T3-E1 cell. $O_2^{\bullet-}$ levels were induced in the group treated with 100 nm long β-SiC nanowires, and 100 μm long β-SiC nanowires had no such effects (Figure 3(a)). MnSOD is a pivotal enzyme scavenging ROS *in vivo*. MnSOD activity in MC3T3-E1 cells was significantly increased after treatment with 100 nm long β-SiC nanowires (Figure 3(b)). Oxidative stress, as determined by the concentrations of MDA (as a marker of lipid peroxidation) and 8-OHdG (indicator of oxidative DNA damage), remained elevated in the 100 nm long β-SiC group. Administration of 100 μm long β-SiC could not increase MDA and 8-OHdG levels (Figures 3(c) and 3(d)) in MC3T3-E1 cell. Therefore, 100 nm long β-SiC induced oxidative stress in MC3T3-E1 cells.

3.4. 100 nm Long β-SiC Nanowires Impair Energy Metabolism in MC3T3-E1 Cells. Cell apoptosis resulted in decreased energy metabolism and increased production of ROS, especially those linked to mitochondrial signaling events. The TEM images of MC3T3-E1 cells cultured in medium containing β-SiC nanowires were shown in Figure 4. All types of cytoplasmic organelles were observed in normal cell (Figure 4(a)) and the cells treated by 100 μm long β-SiC nanowires. β-SiC nanowires were internalized into plasma, even into the nucleus (Figure 4(b)). The chromatin agglomerated with the microvillus disappeared (Figure 4(c)). Dissolved cytoplasm and swelled endoplasmic reticulum were observed after the cells were treated with β-SiC nanowires. The mitochondria were swelled and disintegrated (Figure 4(d)). As 100 nm long β-SiC nanowires accelerated the amount of MC3T3-E1 cells, the production of the total oxygen uptake (Figure 4(e)) and ATP (Figure 4(f)) was also reduced significantly, compared with the group treated with 100 μm long β-SiC nanowires or the control group. Taken together, it suggested that the mitochondrial signal transduction pathway might be involved in 100 nm long β-SiC nanowires induced apoptosis in MC3T3-E1 cells.

4. Discussion

Nanoparticles are the particles less than 100 nm in size, which may possess significant health impairments to human bodies [23]. Earlier studies have shown that nanoparticles can penetrate the stratum corneum of epidermis of skin and reach the dermal layer [24]. Nevertheless, the corresponding toxicity of nanoparticles was not tested. The present study was, therefore, designed to measure the cytotoxicity of β-SiC nanowires of different sizes *in vitro*.

Compared with *in vivo* studies, *in vitro* assays are less ethically ambiguous and easier to control and reproduce. In the case of *in vitro* assay, it is important to recognize that cell cultures are sensitive to changes in their environment such as fluctuations in pH, temperature, and nutrient and waste concentrations, in addition to the concentration of the potentially toxic agent being tested. As several nanoparticles can adsorb dyes and be redox active, it is also important that the cytotoxicity assay is appropriately selected [25, 26]. Hence, control of the experimental conditions is crucial to ensure that the measured cell changes correspond to the toxicity of the added nanoparticles versus the unstable culture conditions. In our studies, all experiments were performed under controlled conditions. The preliminary MTT assay revealed that β-SiC nanowires did not adsorb dyes (data not shown). Apoptosis is a form of programmed cell death which enabled a cell to direct its own destruction. Apoptosis had been evidenced indirectly by three independent methods in our studies (Figure 2). And the expression of related proteins of apoptotic pathway was induced by 100 nm long β-SiC nanowires (Figure 2). Oxidative stress was one of the key mechanisms in cellular defense after the uptake of nanoparticles [27–29]. Nanoparticles could induce intracellular oxidative stress by disturbing the balance between the oxidant and antioxidant processes [30, 31]. In the present study, generation and scavenging of free radicals in cells are performed by an oxidation-reduction system containing a plurality of enzymes. Normally, cell mitochondria generate a small quantity of ROS, which is easily removed by antioxidase. However, when free radicals are generated in a large quantity and accumulated through chain reactions, whose situation exceeds the scavenging activity of the antioxidant defense system, the cells are in the state of oxidative stress, thereby causing cytotoxicity damage [32]. MnSOD is a critical link in the free radical scavenging toxification process for cells. We found that, with the increase of concentration of 100 nm long β-SiC nanowires, there was a significant decrease in the levels of MnSOD activity, which indicates that the ability to scavenge free radicals of the cells reduces substantially and the cells are in the state of oxidative stress. This study employs MDA as the index for reflecting peroxidation level of lipids in cells. Experimental results show that MDA content of the cells increases substantially with the increase of concentration of 100 nm long β-SiC nanowires, which indicates nanowires can induce the cells to generate lipid peroxidation, thereby leading cell function damage and breaking dynamic equilibrium of reactive oxygen and antioxidant substances in the cells. The level of oxidative stress in cells shows substantial correlation with proliferation

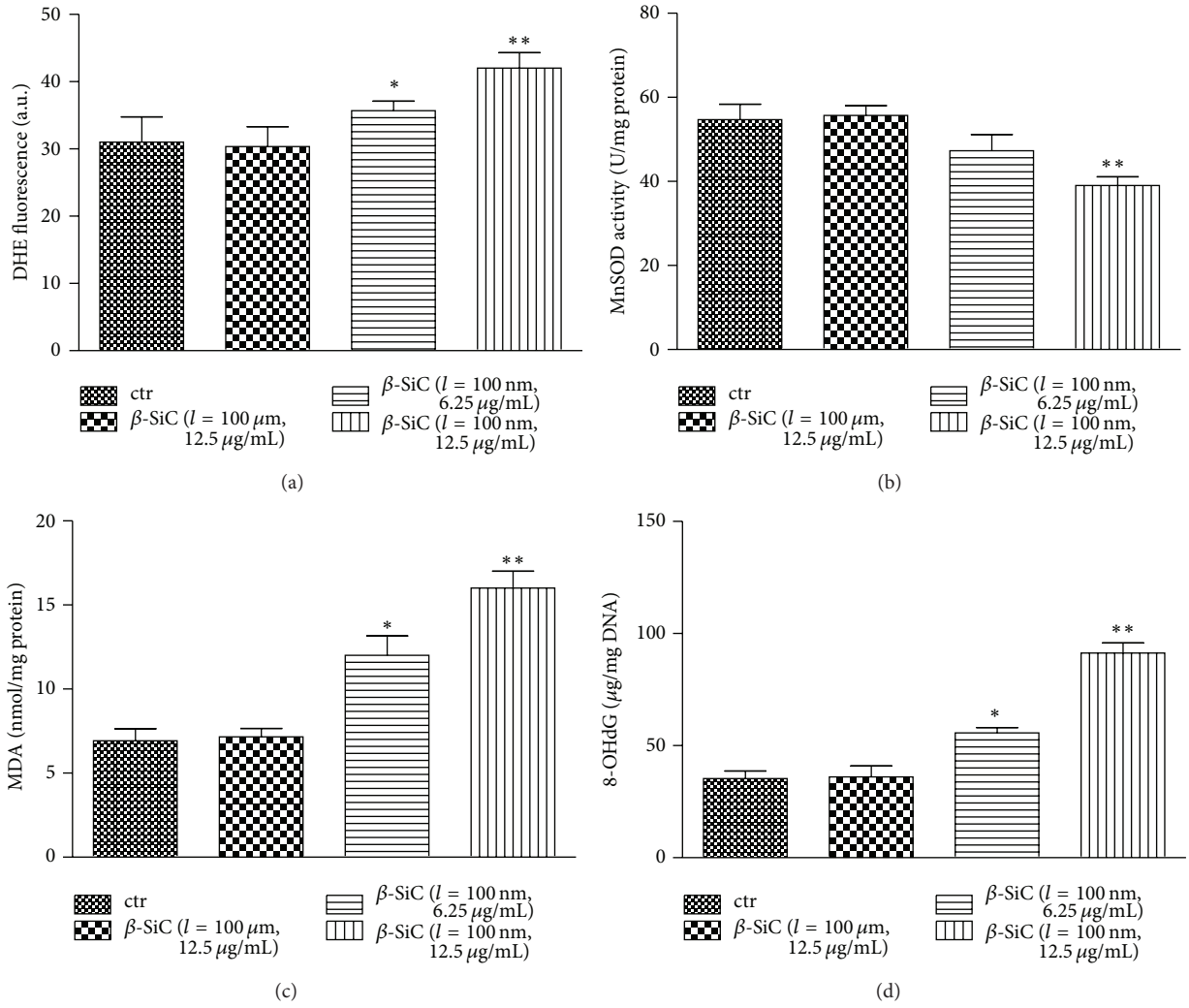

Figure 3: Effects of different β-SiC nanowires on oxidative stress in MC3T3-E1 cells. (a) Superoxide level (DHE), (b) MnSOD activity, (c) MDA production, and (d) 8-OHdG level were measured according to the manufacturer's instructions for each assay. Values are the means ± SD ($n = 3$) of three independent experiments. $^{*}P < 0.05$, $^{**}P < 0.01$ versus control.

rate of cells, thus indicating that generation of free radicals and oxidative stress are the main ways for the nanometer materials to cause cytotoxicity damage. As previous study had reported [31], oxidative stress induced transcriptional activation of nuclear respiratory factor 2 (Nrf-2), mitogen activated protein kinase (MAPK), and nuclear factor-κB (NF-κB). Our results indicated oxidative damage to the inner membrane and organelles (Figure 4). We investigated the characterization of β-SiC nanowires through TEM and XRD observation. The results of TEM and XRD confirmed the suitability for investigation of actual cytotoxicity of these nanowires. The TEM images also revealed internalization of 100 nm long β-SiC nanowires into MC3T3-E1 cells. The β-SiC nanowires were enclosed in cellular nucleus and lysosomal, while other nanowires were engulfed. This result is in line with the report that β-SiC nanowires could be incorporated into cellular membranes [33]. However, details of the intrusion process and its potential effect on organelles need to be further elucidated. When MC3T3-E1 cells are exposed to β-SiC nanowires, we believe, the nanowires are endocytosed from the extracellular fluid: one portion of the plasma membrane is then invaginated and pinched off to form a membrane-bound vesicle.

Increment of permeability in lysosomal membrane is the early event in apoptosis that initiates changes in the mitochondria and activates downstream signal pathway, indicating the active role of lysosomes in apoptosis [34–36]. In present study, however, the increased oxidative stress in cells treated by β-SiC nanowires predicted similar apoptotic event that compared with the control group there was a time-dependent increase of necrotic and late apoptotic cells, as reflected by flow cytometry. The similar phenomenon was also revealed by TEM scanning. The damage caused by 100 nm long nanowires was principally mediated through the injury of nucleus and cellular homeostasis, as well as the enhancement of lysosome proliferation via

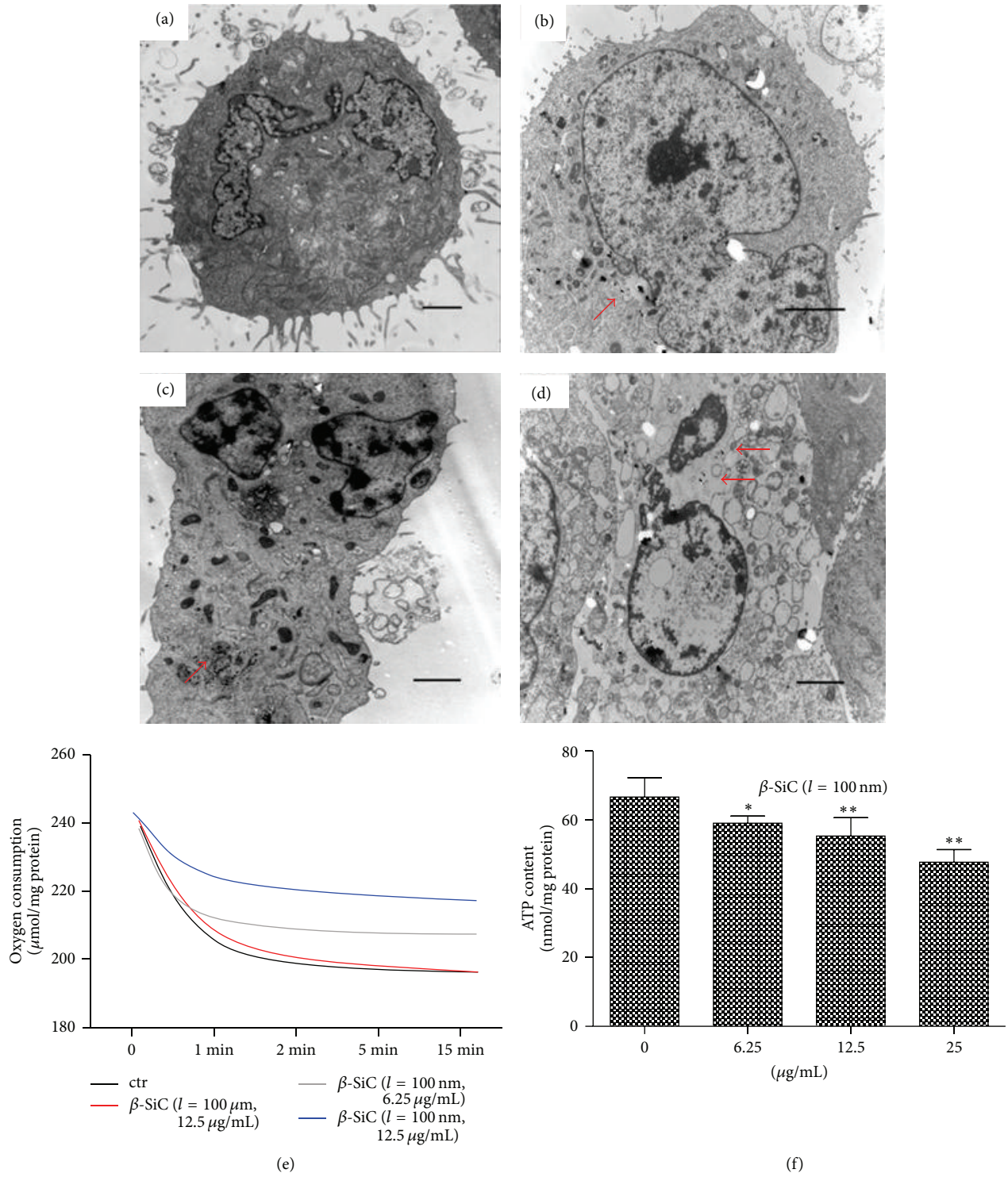

FIGURE 4: Effects of different β-SiC nanowires on energy metabolism in MC3T3-E1 cells. TEM image of β-SiC nanowires internalization in MC3T3-E1 cells treated with 12.5 μg/mL of 100 nm long β-SiC nanowires ((a)–(d)). Scale bar = 2 μm; red arrows indicate nanowires internalization. Before the oxygen consumption test (e), MC3T3-E1 cells were pretreated in low oxygen conditions for 2 h in suspension culture with different β-SiC nanowires. (f) The intracellular ATP concentrations were evaluated after exposure to different β-SiC nanowires for 24 h. Values are the means ± SD ($n = 3$) of three independent experiments. $^{*}P < 0.05$, $^{**}P < 0.01$ versus control.

concentration-dependent manner, while the 100 μm long β-SiC nanowires induced less cytotoxicity than that of 100 nm long β-SiC nanowires. It thus indicates that 100 μm long β-SiC nanowires possess favourable biocompatibility and may possess prospect in the biomedical field. Nevertheless, further investigations are required to elucidate the potential cytotoxicity of different cell lines to β-SiC nanowires and to assess the biocompatibility and biological safety of such nanowires both *in vitro* and *in vivo*.

5. Conclusion

Our results demonstrate that the β-SiC nanowires with different lengths result in different cytotoxic effects on MC3T3-E1 cells. As compared with 100 μm long β-SiC nanowires, 100 nm long nanowires induced significant increase in the levels of superoxide anion, malondialdehyde, 8-hydroxy-2-deoxyguanosine, and MnSOD (manganese superoxide dismutase) activity. Additionally, 100 nm long nanowires led to apoptosis by oxidative stress in MC3T3-E1 cells.

Conflict of Interests

All authors declare that there is no conflict of interests and agree with the contents of the paper for publication and support open access publishing to allow unlimited access and high publicity of their published paper.

Authors' Contribution

Weili Xie, Qi Xie, and Meishan Jin contributed equally to the work.

Acknowledgments

This research was financially supported by National High Technology Research and Development Program 863 (no. 2007AA03Z340), Natural Science Foundation of China (NSFC, Grant nos. 51202045, 51021002, 51172050, 51102063, 51372052, and 50672018), the Fundamental Research Funds for the Central Universities (Grant no. HIT. NSRIF. 2013004), and Key Technology Research and Development Program of Hei Longjiang Province (GC12C305-3).

References

[1] T. Zimmermann, S. Albrecht, and G. Von Gagern, "Molecular-biological investigations of the multicenter stage-III study (SIC-study)," *Medizinische Klinik*, vol. 94, no. 3, pp. 58–61, 1999.

[2] A. M. Morales and C. M. Lieber, "A laser ablation method for the synthesis of crystalline semiconductor nanowires," *Science*, vol. 279, no. 5348, pp. 208–211, 1998.

[3] J.-H. Kim, Y.-S. Kim, K. Park et al., "Antitumor efficacy of cisplatin-loaded glycol chitosan nanoparticles in tumor-bearing mice," *Journal of Controlled Release*, vol. 127, no. 1, pp. 41–49, 2008.

[4] M. Goldberg, R. Langer, and X. Jia, "Nanostructured materials for applications in drug delivery and tissue engineering," *Journal of Biomaterials Science, Polymer Edition*, vol. 18, no. 3, pp. 241–268, 2007.

[5] Z. Li, S. Zhu, K. Gan et al., "Poly-L-lysine-modified silica nanoparticles: a potential oral gene delivery system," *Journal of Nanoscience and Nanotechnology*, vol. 5, no. 8, pp. 1199–1203, 2005.

[6] Z. Ye and R. I. Mahato, "Role of nanomedicines in cell-based therapeutics," *Nanomedicine*, vol. 3, no. 1, pp. 5–8, 2008.

[7] H. Yang, C. Liu, D. Yang, H. Zhang, and Z. Xi, "Comparative study of cytotoxicity, oxidative stress and genotoxicity induced by four typical nanomaterials: the role of particle size, shape and composition," *Journal of Applied Toxicology*, vol. 29, no. 1, pp. 69–78, 2009.

[8] M. Chen and A. Von Mikecz, "Formation of nucleoplasmic protein aggregates impairs nuclear function in response to SiO_2 nanoparticles," *Experimental Cell Research*, vol. 305, no. 1, pp. 51–62, 2005.

[9] S. Qi, C. Yi, W. Chen, C.-C. Fong, S.-T. Lee, and M. Yang, "Effects of silicon nanowires on HepG2 cell adhesion and spreading," *ChemBioChem*, vol. 8, no. 10, pp. 1115–1118, 2007.

[10] T. Nishibe, S. O'Donnel, E. Pikoulis et al., "Effects of fibronectin bonding on healing of high porosity expanded polytetrafluoroethylene grafts in pigs," *Journal of Cardiovascular Surgery*, vol. 42, no. 5, pp. 667–673, 2001.

[11] A. A. Fatokun, T. W. Stone, and R. A. Smith, "Hydrogen peroxide-induced oxidative stress in MC3T3-E1 cells: the effects of glutamate and protection by purines," *Bone*, vol. 39, no. 3, pp. 542–551, 2006.

[12] J. K. Zhang, L. Yang, G. L. Meng et al., "Protective effect of tetrahydroxystilbene glucoside against hydrogen peroxide-induced dysfunction and oxidative stress in osteoblastic MC3T3-E1 cells," *European Journal of Pharmacology*, vol. 689, no. 1–3, pp. 31–37, 2012.

[13] E. M. Choi, G.-H. Kim, and Y. S. Lee, "Protective effects of dehydrocostus lactone against hydrogen peroxide-induced dysfunction and oxidative stress in osteoblastic MC3T3-E1 cells," *Toxicology in Vitro*, vol. 23, no. 5, pp. 862–867, 2009.

[14] F. Grassi, G. Tell, M. Robbie-Ryan et al., "Oxidative stress causes bone loss in estrogen-deficient mice through enhanced bone marrow dendritic cell activation," *Proceedings of the National Academy of Sciences of the United States of America*, vol. 104, no. 38, pp. 15087–15092, 2007.

[15] T. S. Blackwell, J. W. Christman, T. Hagan et al., "Oxidative stress and NF-κB activation: correlation in patients following allogeneic bone marrow transplantation," *Antioxidants and Redox Signaling*, vol. 2, no. 1, pp. 93–102, 2000.

[16] D. Liang, L. Xiang, M. Yang et al., "ZnT7 can protect MC3T3-E1 cells from oxidative stress-induced apoptos is via PI3K/Akt and MAPK/ERK signaling pathways," *Cell Signal*, vol. 25, no. 5, pp. 1126–1135, 2013.

[17] X. Zhang, X. Huang, G. Wen et al., "Novel SiOC nanocomposites for high-yield preparation of ultra-large-scale SiC nanowires," *Nanotechnology*, vol. 21, no. 38, Article ID 385601, 2010.

[18] P. Pozarowski and A. Górski, "Immunology of ulcerative colitis—interactions of T lymphocytes with extracellular matrix proteins," *Polskie Archiwum Medycyny Wewntrznej*, vol. 97, no. 5, pp. 486–491, 1997.

[19] Y. Wang, L. Gao, Y. Li, H. Chen, and Z. Sun, "Nifedipine protects INS-1 β-cell from high glucose-induced ER stress and apoptosis," *International Journal of Molecular Sciences*, vol. 12, no. 11, pp. 7569–7580, 2011.

[20] S.-Q. He, Y.-H. Zhang, S. K. Venugopal et al., "Delivery of antioxidative enzyme genes protects against ischemia/

reperfusion-induced liver injury in mice," *Liver Transplantation*, vol. 12, no. 12, pp. 1869–1879, 2006.

[21] A. Kikuyama, K. Fukuda, S. Mori, M. Okada, H. Yamaguchi, and C. Hamanishi, "Hydrogen peroxide induces apoptosis of osteocytes: involvement of calcium ion and caspase activity," *Calcified Tissue International*, vol. 71, no. 3, pp. 243–248, 2002.

[22] K. Sabeur and B. A. Ball, "Detection of superoxide anion generation by equine spermatozoa," *American Journal of Veterinary Research*, vol. 67, no. 4, pp. 701–706, 2006.

[23] K. Pulskamp, S. Diabaté, and H. F. Krug, "Carbon nanotubes show no sign of acute toxicity but induce intracellular reactive oxygen species in dependence on contaminants," *Toxicology Letters*, vol. 168, no. 1, pp. 58–74, 2007.

[24] C. Bennat and C. C. Müller-Goymann, "Skin penetration and stabilization of formulations containing microfine titanium dioxide as physical UV filter," *International Journal of Cosmetic Science*, vol. 22, no. 4, pp. 271–283, 2000.

[25] N. Lewinski, V. Colvin, and R. Drezek, "Cytotoxicity of nanopartides," *Small*, vol. 4, no. 1, pp. 26–49, 2008.

[26] E. Jan, S. J. Byrne, M. Cuddihy et al., "High-content screening as a universal tool for fingerprinting of cytotoxicity of nanoparticles," *ACS Nano*, vol. 2, no. 5, pp. 928–938, 2008.

[27] E. Kefaloyianni, C. Gaitanaki, and I. Beis, "ERK1/2 and p38-MAPK signalling pathways, through MSK1, are involved in NF-κB transactivation during oxidative stress in skeletal myoblasts," *Cellular Signalling*, vol. 18, no. 12, pp. 2238–2251, 2006.

[28] M. Mohammadzadeh, R. Halabian, A. Gharehbaghian et al., "Nrf-2 overexpression in mesenchymal stem cells reduces oxidative stress-induced apoptosis and cytotoxicity," *Cell Stress and Chaperones*, vol. 17, no. 5, pp. 553–565, 2012.

[29] S. K. Katiyar and S. M. Meeran, "Obesity increases the risk of UV radiation-induced oxidative stress and activation of MAPK and NF-κB signaling," *Free Radical Biology and Medicine*, vol. 42, no. 2, pp. 299–310, 2007.

[30] J.-R. Gurr, A. S. S. Wang, C.-H. Chen, and K.-Y. Jan, "Ultrafine titanium dioxide particles in the absence of photoactivation can induce oxidative damage to human bronchial epithelial cells," *Toxicology*, vol. 213, no. 1-2, pp. 66–73, 2005.

[31] A. Nel, T. Xia, L. Mädler, and N. Li, "Toxic potential of materials at the nanolevel," *Science*, vol. 311, no. 5761, pp. 622–627, 2006.

[32] A. A. Shvedova, V. Castranova, E. R. Kisin et al., "Exposure to carbon nanotube material: assessment of nanotube cytotoxicity using human keratinocyte cells," *Journal of Toxicology and Environmental Health Part A*, vol. 66, no. 20, pp. 1909–1926, 2003.

[33] W. G. Wamer, J.-J. Yin, and R. R. Wei, "Oxidative damage to nucleic acids photosensitized by titanium dioxide," *Free Radical Biology and Medicine*, vol. 23, no. 6, pp. 851–858, 1997.

[34] X. Bi, A. P. Yong, J. Zhou, C. M. Gall, and G. Lynch, "Regionally selective changes in brain lysosomes occur in the transition from young adulthood to middle age in rats," *Neuroscience*, vol. 97, no. 2, pp. 395–404, 2000.

[35] M. E. Guicciardi, J. Deussing, H. Miyoshi et al., "Cathepsin B contributes to TNF-α-mediated hepatocyte apoptosis by promoting mitochondrial release of cytochrome c," *Journal of Clinical Investigation*, vol. 106, no. 9, pp. 1127–1137, 2000.

[36] L. Foghsgaard, D. Wissing, D. Mauch et al., "Cathepsin B acts as a dominant execution protease in tumor cell apoptosis induced by tumor necrosis factor," *Journal of Cell Biology*, vol. 153, no. 5, pp. 999–1009, 2001.

Hindawi Publishing Corporation
BioMed Research International
Volume 2014, Article ID 309631, 9 pages
http://dx.doi.org/10.1155/2014/309631

Research Article

Phytoremediation Potential of Maná-Cubiu (*Solanum sessiliflorum* Dunal) for the Deleterious Effects of Methylmercury on the Reproductive System of Rats

Raquel Frenedoso da Silva,[1] Gabriela Missassi,[1] Cibele dos Santos Borges,[1] Eloísa Silva de Paula,[2] Maria Fernanda Hornos Carneiro,[2] Denise Grotto,[2] Fernando Barbosa Junior,[2] and Wilma De Grava Kempinas[1]

[1] *Department of Morphology, Institute of Biosciences, Univ Estadual Paulista-UNESP, Distrito de Rubião Junior s/nº, 18618-970 Botucatu, SP, Brazil*
[2] *Department of Clinical Analyses, Toxicology and Food Sciences, School of Pharmaceutical Sciences of Ribeirão Preto, University of São Paulo, Avenida do Café s/nº, 14040-903 Ribeirão Preto, SP, Brazil*

Correspondence should be addressed to Wilma De Grava Kempinas; kempinas@ibb.unesp.br

Received 18 November 2013; Revised 11 February 2014; Accepted 11 February 2014; Published 19 March 2014

Academic Editor: Susana Viegas

Methylmercury, organic form of mercury, can increase the number of abnormal sperm and decrease sperm concentration and testosterone levels possibly due to the damage caused by reactive species to germ and Leydig cells. Maná-cubiu (*Solanum sessiliflorum* Dunal) is a native fruit from Amazon rich in iron, zinc, niacin, pectin, and citric acid, used in foods, beverages, and medicinal purposes, since it has been useful for treatment of various diseases caused by oxidative stress or nutritional deficiency. Therefore, this study evaluated the phytoremediation potential of this fruit on damages caused by exposure to MeHg on sperm quantity and quality and the histological aspect of the testis and epididymis. Wistar male rats ($n = 20$) were randomly allocated into four groups: Control group (received distilled water), MeHg group (140 μg/Kg), *Solanum* group (1% of fruit Maná-cubiu on chow), and *Solanum* plus MeHg group (same treatment as MeHg and Solanum group). The organs were weighted, histopathology; sperm morphology and counts were obtained. The results showed reduction in body weight gain, testis weights, reduced sperm production, and increased histopathological abnormalities in the MeHg-treated group. However, treatment with *Solanum* plus MeHg revealed a protective effect of this fruit on damages caused by MeHg.

1. Introduction

Mercury (Hg) is a trace metal widely used and marketed for centuries and may be found in air, water, foods of plant and animal origin, and even in pharmaceuticals such as vaccines [1, 2]. Sulfate-reducing bacteria present in rivers, lakes, and oceans methylate inorganic Hg, transforming it into its organic form methylmercury (MeHg) [3], which can be transferred to humans through the food chain, mainly by eating fish predators.

Cellular damage caused by MeHg is mainly due to increased production of reactive oxygen species (ROS) that causes oxidative stress [4]. In addition, interactions occur between Hg and thiol groups of proteins, forming complexes that bind to important proteins as glutathione, cysteine, and superoxide dismutase, inactivating them, reducing the antioxidant defenses of cells [5, 6]. Glutathione is a major suppressor of ROS, being the result of a complex mechanism that defends the cell from oxidative damage. Its reduced form, the reduced gluthatione (GSH), is able to eliminate the reactive species molecules and plays central role in maintenance of redox state of the cell [7, 8].

Hg has proven deleterious effects on male reproductive system that have been extensively investigated over the past years [9, 10]. The oral exposure of rats to mercury derivatives reduces the serum testosterone levels [2], testicular weight,

and sperm production, besides causing DNA fragmentation [9]. A study of our research group showed that changes caused by exposure to MeHg, such as decreased sperm concentration and increase of sperm with abnormal head, can be attributed to low levels of testosterone [11]. The reduction in the levels of this hormone may be due to damage caused by reactive species to Leydig cells, impairing its synthesis in the testis of exposed animals [12].

It has been demonstrated that consumption of antioxidants present in certain foods can prevent toxic effects caused by exposure to trace metals, once it protects the cell from DNA damage and changes its redox state induced by MeHg [5]. In this sense, the maná-cubiu (*Solanum sessiliflorum* Dunal), a native fruit from the Amazon, is often used in foods and beverages as well as in the production of cosmetics and plant-derived medicines due to the antioxidant properties of its bioactive compounds—iron (Fe), selenium (Se), manganese (Mn), zinc (Zn), citric acid, carotenoids, and phenolic compounds [13, 14]. Marx et al. [15] present a detailed analysis of the main components of the maná-cibiu fruit.

Despite the antioxidant health effects attributed to its consumption, there are no studies regarding the effects of the maná-cubiu on the MeHg toxicity in male reproductive system. Therefore, the objective of this work was to evaluate the phytoremediation potential of maná-cubiu on the damages caused by chronic exposure to MeHg in the rat sperm parameters and the histological aspect of the testis and epididymis.

2. Material and Methods

2.1. Animals. Wistar male rats weighting 100 g were supplied by the Central Laboratory Animal Breeding Center (University of São Paulo, Ribeirão Preto, Brazil) and allocated individually in polypropylene cages, with laboratory grade pine shavings as bedding. Rats were maintained under controlled temperature (22–25°C) and lighting conditions (12 L/12 D photoperiod). Rat chow and filtered tap water were provided *ad libitum*. Experimental procedures were in accordance with the guidelines of the Committee on Care and Use of Experimental Animal Resources, University of São Paulo, Brazil (Approved protocol number: 12.1.1599.53.8).

2.2. Experimental Design. The animals were randomly allocated into four groups ($n = 5$ per group): Control group, MeHg group, *Solanum* group, and *Solanum* plus MeHg group. The MeHg group rats received daily oral gavage doses of 140 μg/Kg of CH_3HgCl; the *Solanum* group rats received chow containing 1% of fruit pulp maná-cubiu lyophilized; the MeHg + *Solanum* group rats received the same treatment than group MeHg and *Solanum*; and the Control group rats received distilled water. The animals were treated for 100 days, weighted each 14 days, and, at the end of treatment, were euthanized with super doses of ketamine and xilasine. The following parameters were GSH level in total blood, body and reproductive organ weights, sperm morphology, sperm counts in the testis, and epididymis and testicular and epididymal histopathology.

2.3. Minerals Determination in Solanum sessiliflorum by ICP-MS. Before digestion of the fruit, 15 g was separated by quartering as described by [16] and divided into two plastic tubes. The contents of each tube were ground for 3 minutes in a ball mill (TECNAL TE 350, Brazil) and sifted in a 106 μm sieve (BERTEL, Brazil). Then, samples were digested in closed vessels using a microwave oven decomposition system (MILESTONE ETHOS D, Italy) according to the method proposed by [17]. Briefly, fruit samples (250 mg) were accurately weighed in a PFA digestion vessel and then 5 mL of nitric acid 20% v/v + 2 mL of 30% (v/v) H_2O_2 were added. The vessel was placed inside the microwave oven and decomposition was carried out according to the following program: (a) 160°C (power of 1000 W) for 4.5 minutes; (b) 160°C (power of 0 W) for 0.5 minutes; (c) 230°C (power of 1000 W) for 20 minutes; and (d) 0°C (power of 0 W) for 20 minutes. After that, the solutions were left to cool and the volume was made up to 50 mL with Milli-Q water. Rhodium was then added as an internal standard to a final concentration of 10 $\mu g \cdot L^{-1}$.

All measurements were conducted using an ICP-MS (Elan DRC II PerkinElmer, Norwalk, CT) with high-purity argon (99.999%, White Martins, Brazil), which used a Meinhard concentric nebulizer (Spectron/Glass Expansion, Ventura, CA) connected to a cyclonic spray chamber. A radiofrequency (rf) of 1200 W power was selected in pulse mode with autolens one. Sample data were acquired by using 20 sweeps/reading, 1 reading/replicate, and a dwell time of 50 ms. Argon nebulizer gas flow rate was optimized daily from 0.5 to 0.9 L/min. Data were acquired in counts per second (cps). The following isotopes were selected: Mn, Se, Fe, Zn, Co, and Mg.

2.4. Reduced Glutathione (GSH) Assay. Reduced thiols in total blood, represented by GSH quantification, were determined by the method of Ellman [18]. Blood (0.15 mL) was hemolyzed by 10% TritonX-100 (0.1 mL) and precipitated with 0.1 mL of TCA. After centrifugation at 3000 g and 4°C for 10 min, the supernatant aliquots were reacted to 50 mL of DTNB. The final reaction product was read at 412 nm in a spectrophotometer. GSH levels were expressed as millimoles per milliliter of blood.

2.5. Reproductive Organ Weights. Immediately after the euthanasia, testis, epididymis, ventral prostate, and seminal vesicle (without the coagulating gland) were removed and their wet weights (absolute and relative to body weight) were measured.

2.6. Sperm Morphology. Sperm were removed from the left vas deferens by internal rising with 1 mL formol-saline solution with the aid of a syringe and needle. To analyze sperm morphology, smears were prepared on histological slides that were left to dry for 90 minutes and observed in a phase-contrast microscope (400x magnification) [19]. Two

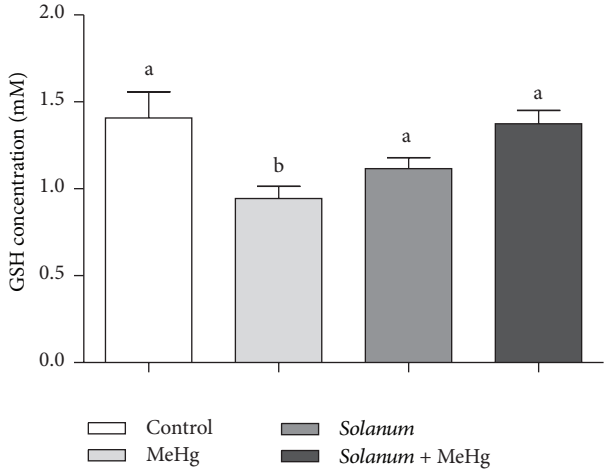

Figure 1: GSH quantification of control and treated animals. One-way analysis of variance (ANOVA) test followed by Tukey test was performed. [a, b]Mean values with the same letter do not differ statistically; P values < 0.05 were considered significant.

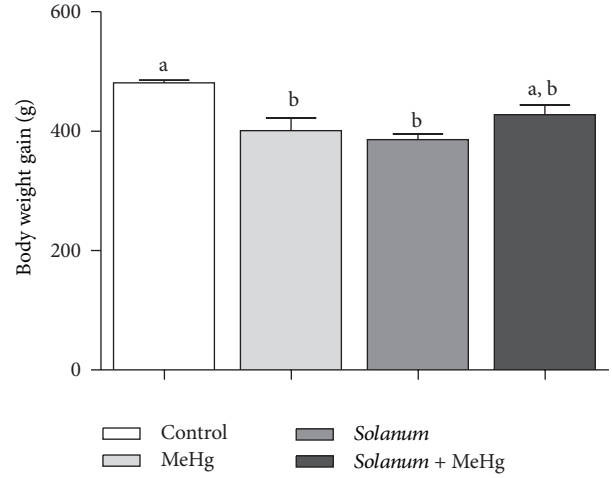

Figure 2: Weight gain of control and treated animals. Values expressed as mean ± SEM. One-way analysis of variance (ANOVA) test followed by Tukey test was performed. [a, b]Mean values with the same letter do not differ statistically; P values < 0.05 were considered significant.

hundred spermatozoa were analyzed per animal. Morphological abnormalities were classified into two general categories: head morphology and tail morphology [20]. Sperm were also classified as to the presence or absence of the cytoplasmic droplet.

2.7. Daily Sperm Production per Testis, Sperm Number, and Transit Time in the Epididymis. The right testis and epididymis were used for sperm counts. Homogenization-resistant testicular spermatids (stage 19 of spermiogenesis) in the testis were counted as described previously [21]. Briefly, the testis was decapsulated, weighed soon after collection, and homogenized in 5 mL NaCl 0.9% containing Triton X100 at 0.5%, followed by sonication for 30 s. After a 10-fold dilution, one sample was transferred to Neubauer chambers (four fields per animal), and late spermatids were counted. To calculate the daily sperm production (DSP), the number of homogenization resistant spermatids was divided by 6.1, the number of days these spermatids are present in the seminiferous epithelium. In the same manner, caput/corpus and cauda epididymidis portions were cut into small fragments with scissors and homogenized, and sperm were counted as described for the testis. The sperm transit time through the epididymis was determined by dividing the number of sperm in each portion by the DSP.

2.8. Histological Analysis of Testis and Epididymis. The left testis and epididymis were fixed in Bouin solution for 24 h. The pieces were dehydrated in a graded ethanol series and routinely processed for embedding in paraffin, sectioned at 5 μm, and subsequently stained with hematoxylin and eosin (H&E). Testis and epididymis sections were examined by light microscopy following specific guidelines for toxicological studies [22].

2.9. Statistical Analysis. Data are presented as mean ± standard error of mean (SEM) for parametric variables (ANOVA test followed by Dunnett was used). For comparison of nonparametric variables Mann-Whitney test or Kruskal-Wallis followed by Dunn test was used and expressed as median and interquartile range. Differences were considered significant when $P < 0.05$. The statistical analyses were performed by GraphPadInStat (version 5).

3. Results

3.1. Minerals Determination in Solanum sessiliflorum by ICP-MS. The analysis performed showed that maná-cubiu fruit has the following chemical composition: Mn: 9.189 μg/g; Se: 0.162 μg/g; Fe: 36.952 μg/g; Zn: 17.358 μg/g. Also, the fruit presents cobalt (Co—0.054 μg/g) and magnesium (Mg—2.815.518 μg/g).

3.2. Reduced Glutathione (GSH) Assay. GSH quantification showed that MeHg reduced levels of this enzyme in blood.

On the other hand, *Solanum* + MeHg group showed GSH levels similar to Control group (Figure 1).

3.3. Body Weight Gain and Reproductive Organ Weights. Significant reductions in the body weight gain (Figure 2) and final body weight (Table 1) were reported in both MeHg and *Solanum*-treated groups. Also, the animals treated with MeHg showed a reduction in the testis weight. However, animals that received both treatments, that is, *Solanum* plus MeHg, showed comparable final body weight and testicular weight compared to the control group (Table 1).

3.4. Sperm Morphology. Analysis of sperm morphology revealed that MeHg group had lower percentage of morphologically normal spermatozoa, whereas the predominant abnormality was in the sperm head. Interestingly the group treated with MeHg plus *Solanum* showed no change in sperm morphology. A large amount of spermatozoa presented

Table 1: Body weight and reproductive organ weights of male rats.

Parameters	Control ($n = 5$)	MeHg ($n = 5$)	*Solanum* ($n = 6$)	*Solanum* + MeHg ($n = 6$)
Absolute weights				
Final body weight (g)	597.0 ± 5.7[a]	533.5 ± 13.9[b]	508.3 ± 10.0[b]	550.3 ± 18.3[a,b]
Testis (mg)	2,613 ± 87.02[a]	1,955 ± 15.23[b]	2,358 ± 86.92[a,b]	2,224 ± 33.83[a,b]
Epididymis (mg)	885.9 ± 30.2	755.5 ± 65.0	795.1 ± 35.8	779.3 ± 35.9
Ventral prostate (mg)	453.2 ± 35.4	434.7 ± 41.5	429.1 ± 55.0	542.3 ± 63.9
Full seminal vesicle (mg)	1,619 ± 182.3	1,592 ± 150.9	1,440 ± 66.7	1,500 ± 90.9
Empty seminal vesicle (mg)	630.9 ± 41.1	628.7 ± 71.7	586.5 ± 27.2	574.6 ± 32.8
Relative weights				
Testis (mg/100 g)	4.36 ± 0.14[a,b]	3.63 ± 0.20[a]	4.64 ± 1.74[b]	4.05 ± 2.42[a,b]
Epididymis (mg/100 g)	1.48 ± 0.04	1.40 ± 0.08	1.57 ± 0.09	1.42 ± 0.05
Ventral prostate (mg/100 g)	0.75 ± 0.05	0.80 ± 0.05	0.84 ± 0.10	0.98 ± 0.05
Full seminal vesicle (mg/100 g)	2.69 ± 0.28	2.94 ± 0.20	2.85 ± 0.18	2.72 ± 0.14
Empty seminal vesicle (mg/100 g)	1.05 ± 0.06	1.16 ± 0.10	1.16 ± 0.07	1.04 ± 0.05

Values expressed as mean ± SEM. One-way analysis of variance (ANOVA) test followed by Tukey test was performed. [a,b]Mean values with the same letter do not differ statistically; P values < 0.05 were considered significant.

Table 2: Sperm morphology of control and treated animals.

Parameters	Control	MeHg	*Solanum*	*Solanum* + MeHg
Normal sperm	92.00 (91.50–93.38)[a]	75.00 (66.38–82.13)[b]	92.50 (86.63–94.38)[a]	89.75 (84.50–95.00)[a,b]
Abnormalities of the sperm head	6.00 (5.00–7.25)[a]	19.75 (12.75–31.13)[b]	6.50 (5.12–11.13)[a,b]	9.25 (2.37–13.00)[a,b]
Abnormalities of the flagellum	1.75 (0.37–2.12)[a,b]	4.00 (2.37–6.50)[a]	1.00 (0.50–1.75)[b]	2.00 (0.37–6.50)[a,b]
Presence of cytoplasmic droplet	15.00 (9.87–15.75)	19.00 (14.38–24.13)	23.00 (21.75–28.63)	34.00 (23.38–37.00)

N = 6/group. Values expressed as median and interquartile range (first and third). Kruskal-Wallis analysis of variance test followed by Dunn's test was performed. [a,b]Medians with the same letter do not differ statistically; P values < 0.05 were considered significant.

cytoplasmic droplet in all experimental groups, especially on *Solanum* + MeHg. *Solanum* group showed an improvement on flagellum morphology compared to other groups (Table 2).

3.5. Daily Sperm Production per Testis, Sperm Number, and Transit Time in the Epididymis. The treatment with MeHg decreased the DSP and epididymal sperm number compared to Control group. This harmful effect was prevented by the use of *Solanum*, as shown by the results of the group MeHg plus *Solanum* (Table 3).

3.6. Histological Analysis of Testis and Epididymis. Histopathological evaluation showed a significant increase in the percentage of abnormal seminiferous tubules in the MeHg treated group relative to the Control and *Solanum* group. The abnormalities found were predominantly seminiferous tubules with vacuolization and degeneration (Figures 3 and 4). Epididymal evaluation showed an increased incidence of cell bodies in the lumen of the caput and cauda epididymis in the MeHg treated group (Figure 4).

4. Discussion

Methylmercury is the most toxic form of mercury due to its lipophilic properties, which enable it to overcome some cellular barriers [1]. Several studies have described its neurotoxic [23, 24], hepatotoxic [25, 26], and cardiotoxic action [27]. Also, this substance has deleterious effects on the male and female reproductive systems [9, 28].

Maná-cubiu presents several compounds in its composition that have relevant antioxidant properties as phenolic compounds, hydrophilic extracts, and carotenoids, which are capable of scavenging reactive species of oxygen and nitrogen [13], as well as chemical elements essential to assist in the proper diet as zinc and selenium [5, 14, 29]. Considering the constituents of maná-cubiu and their beneficial effects, the present study evaluated the phytoremediation potential of this fruit on the deleterious effects on rat sperm quantity and quality promoted by MeHg.

Changes in body weight are indicative signs of systemic toxicity [30] and its reduction may be related to the effects of exposure to toxic substances. There was a reduction in body weight gain of animals treated with MeHg, as shown previously by Fossato da Silva et al. [11]. Moreover, animals exposed to MeHg had decreased testis weights, possibly due to the toxic effects of MeHg on this organ. The determination of organ weights is an important parameter for assessing the risk of toxicity on the male reproductive system [30]. Although there was a reduction in the weight gain in the *Solanum*-treated group, the reproductive organ weights were comparable among groups.

The toxicity caused by MeHg is closely related to oxidative stress that develops as a consequence of an imbalance

Table 3: Sperm counts and transit time of male rats from control and treated groups.

Parameters	Control	MeHg	*Solanum*	*Solanum* + MeHg
Sperm head count ($\times 10^6$/testis)	288.40 ± 8.72[a]	208.00 ± 24.11[b]	289.20 ± 12.08[a]	267.90 ± 18.83[a,b]
Sperm head count ($\times 10^6$/g testis)	117.50 ± 4.59	112.00 ± 9.55	124.20 ± 9.22	121.4 ± 7.13
Daily sperm production ($\times 10^6$/testis)	47.27 ± 1.43[a]	34.09 ± 3.95[b]	47.40 ± 1.98[a]	43.92 ± 3.09[a,b]
Daily sperm production ($\times 10^6$/g testis)	19.26 ± 0.75	18.35 ± 1.56	20.35 ± 1.51	19.90 ± 1.17
Caput/corpus epididymis sperm count ($\times 10^6$/organ)	236.70 ± 19.36[a]	155.30 ± 22.05[b]	195.80 ± 21.76[a,b]	175.90 ± 7.83[a,b]
Caput/corpus epididymis sperm count ($\times 10^6$/g organ)	521.40 ± 26.61[a]	397.00 ± 34.22[b]	510.80 ± 26.78[a]	475.10 ± 12.61[a,b]
Transit time in the caput/corpus epididymis (days)	4.98 ± 0.29	4.49 ± 0.48	4.15 ± 0.43	4.12 ± 0.40
Cauda epididymis sperm count (10^6/organ)	415.10 ± 25.26	285.50 ± 44.96	351.00 ± 36.33	339.80 ± 29.96
Cauda epididymis sperm count (10^6/g organ)	1295.00 ± 50.68[a]	961.50 ± 59.96[a]	1116.00 ± 49.41[a,b]	1105.00 ± 20.14[a,b]
Transit time in the cauda epididymis (days)	8.77 ± 0.43	8.11 ± 0.41	7.34 ± 0.37	8.02 ± 1.12

$N = 6$/group. Values expressed as mean ± SEM. One-way analysis of variance (ANOVA) test followed by Tukey test was performed. [a,b]Mean values with the same letter do not differ statistically; P values < 0.05 were considered significant.

between excessive production of reactive species of oxygen (ROS) and impaired antioxidant defense system after exposure [31, 32]. These reactive species are bioproducts of oxygen metabolism, constantly produced in normal cells by mitochondria, especially by sperm during capacitation process, but its action is neutralized by cell antioxidant system [33]. However, when testicular and epididymal cells are exposed to harmful factors such as excessive heat, radiation, chemicals, or trace metals, there is an overproduction of these molecules potentially causing male infertility [34, 35], since ROS can cause damages to sperm function and DNA integrity [36], especially if the defense system is lagged. In this work, we showed that MeHg is capable of decreasing the GSH concentration present in blood of treated animals, as also observed by Barcelos et al. [5] and Grotto et al. [6], indicating that the toxicity is related to oxidative stress and to the imbalance of cellular antioxidant system. The protective antioxidant effect of *Solanum* is proved since GSH levels are restored in group *Solanum* + MeHg.

Histological evaluation of the male reproductive tract requires a good understanding of the form and function of the organs in order to distinguish changes in the normal morphology correlating with the animal reproductive status [22]. McNeil and Bhatnagar [37] showed that injury to seminiferous tubules and increased vacuolization were related to the dietary amount of MeHg. In accordance, our study showed that treated animals had degeneration of seminiferous tubules, absence of germ cells, and increased vacuolization in the seminiferous epithelium, possibly caused by a higher apoptotic index of germ cells caused by MeHg chronic exposure. At least part of these dead germ cells was seen in a higher incidence in the lumen of the epididymis of the MeHg-treated rats.

The possible increase in ROS production in the testis can cause significant damage to mitochondrial and nuclear DNA due to the alteration on the expression of genes such as Bcl-2 and Bax involved in molecular mechanisms promoters of germ cells apoptosis in response to oxidative stress [38]. Since MeHg increases the expression of these genes which promotes apoptosis, we observed a reduction in daily sperm production and this can be correlated with decreased testicular weight and histopathological changes observed. The reduced sperm number found in the epididymis reflected the lower DSP. On the other hand, sperm parameters in the *Solanum* plus MeHg group were comparable with the control group, indicating a possible protective effect of maná-cubiu. Facing the constant risk of oxidative stress which germ cells are subject to, which may impair reproductive physiology, the gonads need antioxidant protection during gamete production. Substances with antioxidant properties have achieved success in the treatment of infertility, such as maná-cubiu fruit, which exhibits antioxidant activity being able to decrease the production of reactive oxygen species.

This protective effect may be associated with possible antioxidant activity of niacin, a compound present in large quantities in fruit, which protects cell from DNA damage and can change the redox state induced by MeHg [5] or by the action of some chemical elements in the fruit, such as Zn, Fe, and Se. It is known that Zn and Fe participate of oxidation and reduction processes, and Zn as cofactors of Cu-Zn superoxide dismutase prevents deleterious effects of ROS on spermatozoa [39]. Thus, the improvements in histopathology, sperm production, and testicular weight may be related to coadministration of *Solanum* and MeHg.

The cytodifferentiation of the spermatozoa during spermiogenesis is responsible for morphological changes

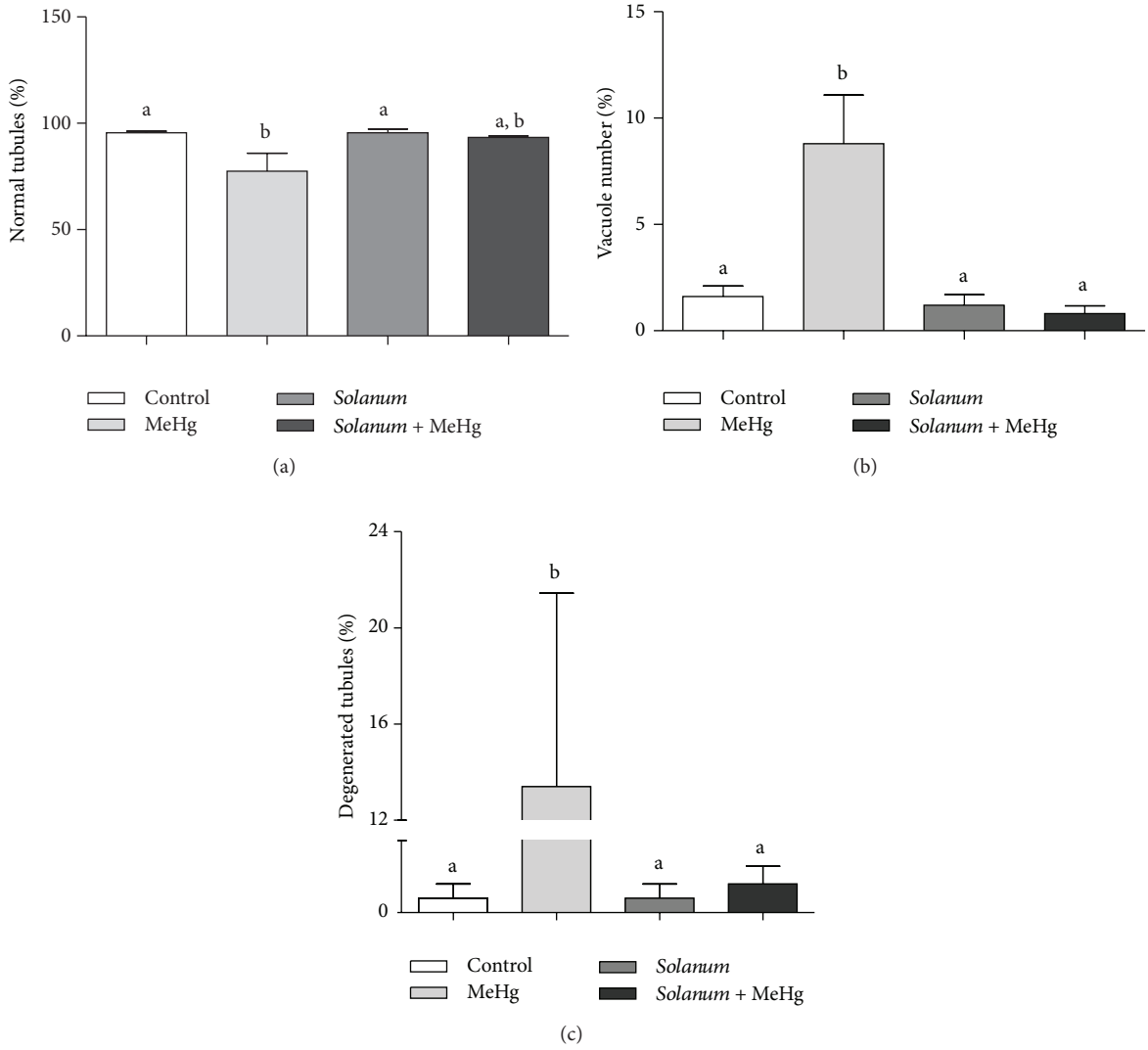

Figure 3: Histopathological evaluation of the testis. Values expressed as mean ± SEM. Kruskal-Wallis analysis of variance test followed by Dunn's test was performed. [a,b]Mean values with the same letter do not differ statistically; P-values < 0.05 were considered significant.

that define this specialized cell, and Zn deficiency may lead to degeneration of cells involved in spermatozoa processing after meiotic division [40]. Besides, at this stage, the germ cell loses large amount of their cytoplasm, and along with it, some of the enzymes of the antioxidant system, making these cells unable to regenerate from damage caused by ROS [41]. Therefore, abnormal sperm morphology has been associated with oxidative stress [42]. Fossato da Silva et al. [11] found a higher number of abnormal sperm in animals treated with MeHg, and this abnormality was mainly in the sperm head. Our results also showed a higher number of abnormalities in the sperm head caused by exposure to MeHg proving the deleterious action of reactive species in the normal development of spermatozoa. Once normal sperm morphology is better criterion for predicting fertility than sperm counts [43]; animals exposed to MeHg can present fertility problems.

The *Solanum* plus MeHg group showed an improvement in sperm morphology possibly due to maná-cubiu antioxidant activity. Once Zn directly influenced sperm morphology [44], it was demonstrated that low levels of Zn can increase percentages of broken flagellum [45]. In this study, we observed an improvement of flagellum morphology in *Solanum* group, showing that maná-cubiu utilization, rich in Zn, has a positive effect on sperm.

5. Conclusion

In conclusion, the present work confirmed previous results showing that chronic exposure to MeHg compromises GSH levels, sperm count, and quality, as well as the germinative epithelium of adult rats. Moreover, we also show the phytoremediation potential of maná-cubiu fruit, preventing deleterious effects caused by MeHg on the male reproductive system.

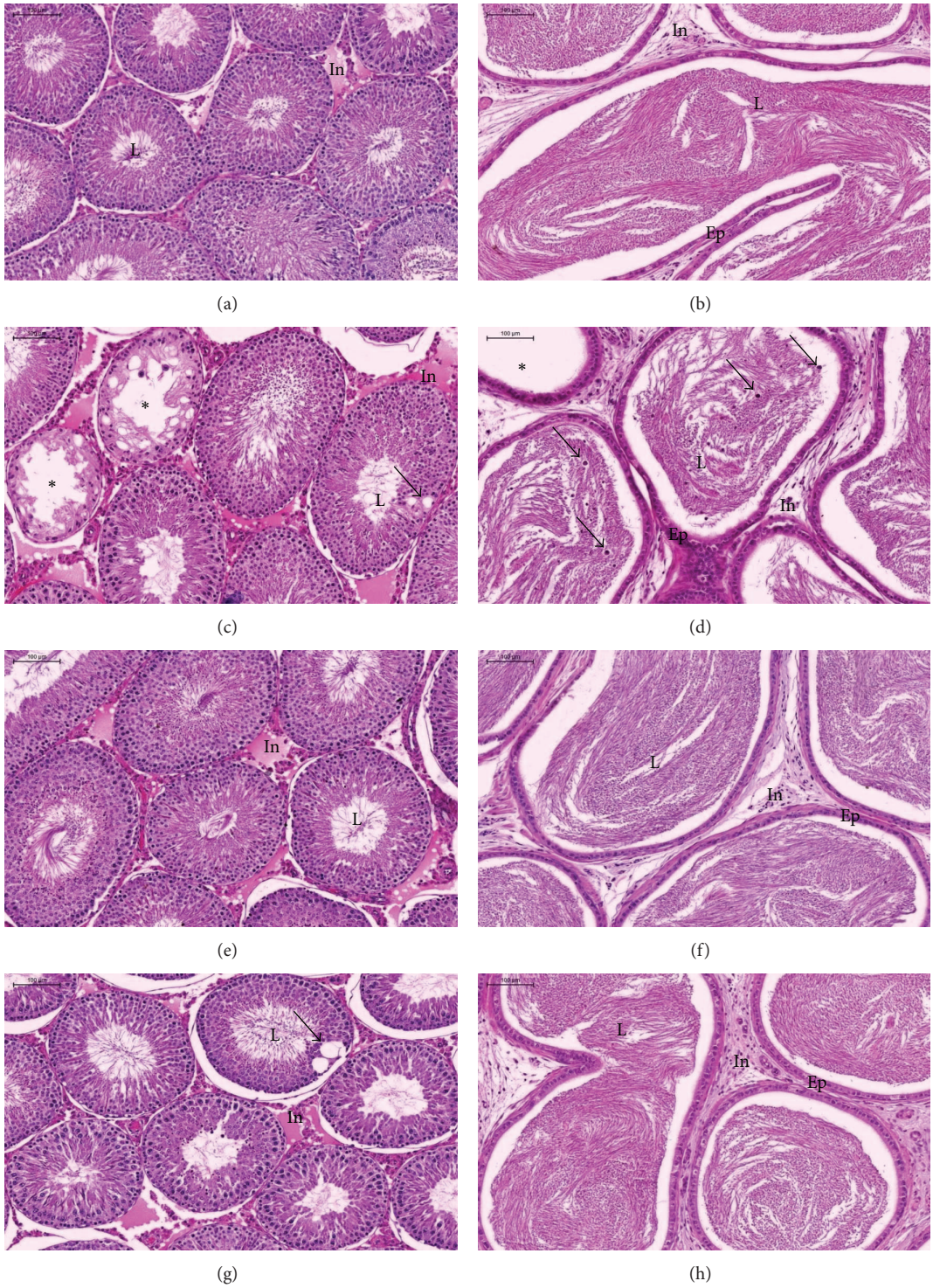

FIGURE 4: Histological aspect of the testis and cauda epididymis (n = 5/group): (a, b) control group, (c, d) MeHg group, (e, f) *Solanum* group, and (g, h) MeHg + *Solanum* group. GC: germ cells; L: lumen; In: interstitial tissue; Ep: epithelium. Observe the presence of vacuoles (arrow) and degenerated seminiferous epithelium (asterisk) in the testis and empty segments (asterisk) and cell bodies in the lumen (arrow) in the epididymis. Final magnification: 200x.

Conflict of Interests

The authors declare that there is no conflict of interests regarding the publication of this paper.

Acknowledgments

The authors would like to acknowledge José Eduardo Bozano from Department of Morphology, Institute of Biosciences, and Carlos César Ramos from Department of Pathology, Medicine School, UNESP—Univ Estadual Paulista for the technical support. This work was supported by Fundação de Amparo à Pesquisa do Estado de São Paulo (FAPESP), Grant no. 13/05560-4.

References

[1] F. Zahir, S. J. Rizwi, S. K. Haq, and R. H. Khan, "Low dose mercury toxicity and human health," *Environmental Toxicology and Pharmacology*, vol. 20, no. 2, pp. 351–360, 2005.

[2] M. A. Boujbiha, K. Hamden, F. Guermazi et al., "Testicular toxicity in mercuric chloride treated rats: association with oxidative stress," *Reproductive Toxicology*, vol. 28, no. 1, pp. 81–89, 2009.

[3] F. M. M. Morel, A. M. L. Kraepiel, and M. Amyot, "The chemical cycle and bioaccumulation of mercury," *Annual Review of Ecology and Systematics*, vol. 29, pp. 543–566, 1998.

[4] S. Ceccatelli, E. Daré, and M. Moors, "Methylmercury-induced neurotoxicity and apoptosis," *Chemico-Biological Interactions*, vol. 188, no. 2, pp. 301–308, 2010.

[5] G. R. M. Barcelos, D. Grotto, J. M. Serpeloni et al., "Protective properties of quercetin against DNA damage and oxidative stress induced by methylmercury in rats," *Archives of Toxicology*, vol. 85, no. 9, pp. 1151–1157, 2011.

[6] D. Grotto, J. Vicentini, J. P. Friedmann Angeli et al., "Evaluation of protective effects of fish oil against oxidative damage in rats exposed to methylmercury," *Ecotoxicology and Environmental Safety*, vol. 74, no. 3, pp. 487–493, 2011.

[7] H. C. Chou and H. L. Chan, "Effect of glutathione reductase knockdown in response to UVB-induced oxidative stress in human lung adenocarcinoma," *Proteome Science*, vol. 12, article 2, 2014.

[8] W. J. Carr, R. E. Oberley-Deegan, Y. Zhang, C. C. Oberley, L. W. Oberley, and M. Dunnwald, "Antioxidant proteins and reactive oxygen species are decreased in a murine epidermal side population with stem cell-like characteristics," *Histochemistry and Cell Biology*, vol. 135, no. 3, pp. 293–304, 2011.

[9] S. Homma-Takeda, Y. Kugenuma, T. Iwamuro, Y. Kumagai, and N. Shimojo, "Impairment of spermatogenesis in rats by methylmercury: involvement of stage- and cell-specific germ cell apoptosis," *Toxicology*, vol. 169, no. 1, pp. 25–35, 2001.

[10] J. Dufresne and D. G. Cyr, "Effects of short-term methylmercury exposure on metallothionein mRNA levels in the testis and epididymis of the rat," *Journal of Andrology*, vol. 20, no. 6, pp. 769–778, 1999.

[11] D. A. Fossato da Silva, C. T. Teixeira, W. R. Scarano et al., "Effects of methylmercury on male reproductive functions in Wistar rats," *Reproductive Toxicology*, vol. 31, no. 4, pp. 431–439, 2011.

[12] M. D. Maines and R. D. Mayer, "Inhibition of testicular cytochrome P-450-dependent steroid biosynthesis by cis-platinum. Reversal by human chorionic gonadotropin," *Journal of Biological Chemistry*, vol. 260, no. 10, pp. 6063–6068, 1985.

[13] E. Rodrigues, L. R. Mariutti, and A. Z. Mercadante, "Carotenoids and phenolic compounds from *Solanum sessiliflorum*, an unexploited Amazonian fruit, and their scavenging capacities against reactive oxygen and nitrogen species," *Journal of Agricultural and Food Chemistry*, vol. 61, pp. 3022–3029, 2013.

[14] L. K. O. Yuyama, S. H. M. Macedo, J. P. L. Aguiar et al., "Macro and micro nutrients quantification of some cubiu ethnovarieties (*Solanum sessiliflorum* Dunal)," *Acta Amazonica*, vol. 37, no. 3, pp. 425–429, 2007.

[15] F. Marx, E. H. A. Andrade, and J. G. Maia, "Chemical composition of the fruit of *Solanum sessiliflorum*," *Food Research and Technology*, vol. 206, no. 5, pp. 364–366, 1998.

[16] CAC, "General Guide-lines on Sampling CAC-GL-50," Codex Alimentarius Commission, 2004.

[17] E. P. Nardi, F. S. Evangelista, L. Tormen et al., "The use of inductively coupled plasma mass spectrometry (ICP-MS) for the determination of toxic and essential elements in different types of food samples," *Food Chemistry*, vol. 112, no. 3, pp. 727–732, 2009.

[18] G. L. Ellman, "Tissue sulfhydryl groups," *Archives of Biochemistry and Biophysics*, vol. 82, no. 1, pp. 70–77, 1959.

[19] J. Seed, R. E. Chapin, E. D. Clegg et al., "Methods for assessing sperm motility, morphology, and counts in the rat, rabbit, and dog: a consensus report," *Reproductive Toxicology*, vol. 10, no. 3, pp. 237–244, 1996.

[20] R. Filler, "Methods for evaluation of rats epididymal sperm morphology," in *Male Reproductive Toxicology*, R. E. Chapin and J. H. Heindel, Eds., pp. 334–343, Academic Pres, San Diego, Calif, USA, 1993.

[21] G. W. Robb, R. P. Amann, and G. J. Killian, "Daily sperm production and epididymal sperm reserves of pubertal and adult rats," *Journal of Reproduction and Fertility*, vol. 54, no. 1, pp. 103–107, 1978.

[22] G. L. Foley, "Overview of male reproductive pathology," *Toxicologic Pathology*, vol. 29, no. 1, pp. 49–63, 2001.

[23] M. Farina, M. Aschner, and J. B. T. Rocha, "Oxidative stress in MeHg-induced neurotoxicity," *Toxicology and Applied Pharmacology*, vol. 256, no. 3, pp. 405–417, 2011.

[24] B. Xu, Z. F. Xu, Y. Deng, W. Liu, and H. B. Yang, "Protective effects of MK-801 on methylmercury-induced neuronal injury in rat cerebral cortex: involvement of oxidative stress and glutamate metabolism dysfunction," *Toxicology*, vol. 300, pp. 112–120, 2012.

[25] F. J. Dieguez-Acuña, W. W. Polk, M. E. Ellis, P. L. Simmonds, J. V. Kushleika, and J. S. Woods, "Nuclear factor κB activity determines the sensitivity of kidney epithelial cells to apoptosis: implications for mercury-induced renal failure," *Toxicological Sciences*, vol. 82, no. 1, pp. 114–123, 2004.

[26] A. Yasutake, A. Nakano, K.-I. Miyamoto, and K. Eto, "Chronic effects of methylmercury in rats—I. Biochemical aspects," *Tohoku Journal of Experimental Medicine*, vol. 182, no. 3, pp. 185–196, 1997.

[27] N. Sørensen, K. Murata, E. Budtz-Jørgensen, P. Weihe, and P. Grandjean, "Prenatal methylmercury exposure as a cardiovascular risk factor at seven years of age," *Epidemiology*, vol. 10, no. 4, pp. 370–375, 1999.

[28] F. de Rosis, S. P. Anastasio, and L. Selvaggi, "Female reproductive health in two lamp factories: effects of exposure to inorganic mercury vapour and stress factors," *British Journal of Industrial Medicine*, vol. 42, no. 7, pp. 488–494, 1985.

[29] D. F. da Silva Filho, L. K. O. Yuyama, J. Paiva Lopes Aguiar, M. C. Oliveira, and L. H. P. Martins, "Caracterização e avaliação do potencial agronômico e nutricional de etnovariedades de cubiu (*Solanum sessiliflorum* Dunal) da Amazônia," *Acta Amazonica*, vol. 35, no. 4, pp. 399–406, 2005.

[30] E. D. Clegg, D. Perreault, and G. R. Klinefelter, "Assessment of male reproductive toxicity," in *Principles and Methods of Toxicology*, A. W. Hayes, Ed., pp. 1263–1300, Taylor & Francis, Philadelphia, Pa, USA, 2001.

[31] M. Polunas, A. Halladay, R. B. Tjalkens, M. A. Philbert, H. Lowndes, and K. Reuhl, "Role of oxidative stress and the mitochondrial permeability transition in methylmercury cytotoxicity," *NeuroToxicology*, vol. 32, no. 5, pp. 526–534, 2011.

[32] A. Agarwal and R. A. Saleh, "Utility of oxidative stress test in the male infertility clinic," *National Journal of Andrology*, vol. 8, no. 1, pp. 1–9, 2002.

[33] G. Lavranos, M. Balla, A. Tzortzopoulou, V. Syriou, and R. Angelopoulou, "Investigating ROS sources in male infertility: a common end for numerous pathways," *Reproductive Toxicology*, vol. 34, pp. 298–307, 2012.

[34] K. Makker, A. Agarwal, and R. Sharma, "Oxidative stress & male infertility," *Indian Journal of Medical Research*, vol. 129, no. 4, pp. 357–367, 2009.

[35] M. Cocuzza, S. C. Sikka, K. S. Athayde, and A. Agarwal, "Clinical relevance of oxidative stress and sperm chromation damage in male infertility: an evidence based analysis," *International Brazilian Journal of Urology*, vol. 33, no. 5, pp. 603–621, 2007.

[36] F. Lanzafame, S. la Vignera, E. Vicari, and A. E. Calogero, "Oxidative stress and medical antioxidant treatment in male infertility," *Reproductive BioMedicine Online*, vol. 19, no. 5, pp. 638–659, 2009.

[37] S. I. McNeil and M. K. Bhatnagar, "Ultrastructure of the testis of Pekin ducks fed methyl mercury chloride: seminiferous epithelium," *American Journal of Veterinary Research*, vol. 46, no. 9, pp. 2019–2025, 1985.

[38] N. Kaushal and M. P. Bansal, "Dietary selenium variation-induced oxidative stress modulates CDC2/cyclin B1 expression and apoptosis of germ cells in mice testis," *Journal of Nutritional Biochemistry*, vol. 18, no. 8, pp. 553–564, 2007.

[39] U. Marzec-Wroblewska, P. Kaminski, and P. Lakota, "Influence of chemical elements on mammalian spermatozoa," *Folia Biologica*, vol. 58, pp. 7–15, 2012.

[40] M. P. Cigánková Viera, A. Viera, and J. Bíreš, "Morphological changes of testes in zinc deficient boars," *Acta Veterinaria*, vol. 58, pp. 89–97, 2008.

[41] R. K. Sharma and A. Agarwal, "Role of reactive oxygen species in male infertility," *Urology*, vol. 48, no. 6, pp. 835–850, 1996.

[42] F. Mazzilli, T. Rossi, M. Marchesini, C. Ronconi, and F. Dondero, "Superoxide anion in human semen related to seminal parameters and clinical aspects," *Fertility and Sterility*, vol. 62, no. 4, pp. 862–868, 1994.

[43] D. S. Guzick, J. W. Overstreet, P. Factor-Litvak et al., "Sperm morphology, motility, and concentration in fertile and infertile men," *New England Journal of Medicine*, vol. 345, no. 19, pp. 1388–1393, 2001.

[44] P. Massányi, J. Trandzik, P. Nad et al., "Concentration of copper, iron, zinc, cadmium, lead, and nickel in bull and ram semen and relation to the occurrence of pathological spermatozoa," *Journal of Environmental Science and Health A*, vol. 39, no. 11-12, pp. 3005–3014, 2004.

[45] P. Massányi, J. Trandzik, P. Nad et al., "Seminal concentration of trace elements in fox and relationships to spermatozoa quality," *Journal of Environmental Science and Health A*, vol. 40, no. 5, pp. 1097–1105, 2005.

Hindawi Publishing Corporation
BioMed Research International
Volume 2014, Article ID 940952, 8 pages
http://dx.doi.org/10.1155/2014/940952

Research Article

Genetic Polymorphisms in Glutathione (GSH-) Related Genes Affect the Plasmatic Hg/Whole Blood Hg Partitioning and the Distribution between Inorganic and Methylmercury Levels in Plasma Collected from a Fish-Eating Population

Andréia Ávila Soares de Oliveira,[1] Marilesia Ferreira de Souza,[2] André van Helvoort Lengert,[2] Marcelo Tempesta de Oliveira,[2] Rossana Batista de Oliveira Godoy Camargo,[2] Gilberto Úbida Leite Braga,[1] Ilce Mara de Syllos Cólus,[2] Fernando Barbosa Jr.,[1] and Gustavo Rafael Mazzaron Barcelos[1]

[1] *Department of Clinical Analyses, Toxicology and Food Sciences, School of Pharmaceutical Sciences of Ribeirão Preto, University of São Paulo, Avenida do Café s/nº, 14040-903 Ribeirão Preto, SP, Brazil*
[2] *Department of General Biology, Center for Biological Sciences, State University of Londrina, Rodovia Celso Garcia Cid km 380, 86051-990 Londrina, PR, Brazil*

Correspondence should be addressed to Gustavo Rafael Mazzaron Barcelos; barcelos@fcfrp.usp.br

Received 18 October 2013; Accepted 8 January 2014; Published 18 February 2014

Academic Editor: Wilma De Grava Kempinas

This study aims to evaluate the effects of polymorphisms in glutathione (GSH-) related genes (*GSTM1*, *GSTT1*, *GSTP1*, *GCLM*, and *GCLC*) in the distribution of Hg in the blood compartments in humans exposed to methylmercury (MeHg). Subjects ($n = 88$), exposed to MeHg from fish consumption, were enrolled in the study. Hg species in the plasma compartment were determined by LC-ICP-MS, whereas genotyping was performed by PCR assays. Mean total Hg levels in plasma (THgP) and whole blood (THgB) were 10 ± 4.2 and 37 ± 21, whereas mean evels of plasmatic MeHg (MeHgP), inorganic Hg (IHgP), and HgP/HgB were 4.3 ± 2.9, 5.8 ± 2.3 μg/L, and 0.33 ± 0.15, respectively. *GSTM1* and *GCLC* polymorphisms influence THgP and MeHgP (multivariate analyses, $P < 0.050$). Null homozygotes for *GSTM1* showed higher THgP and MeHgP levels compared to subjects with *GSTM1* (THgP $\beta = 0.22$, $P = 0.035$; MeHgP $\beta = 0.30$, $P = 0.050$) and persons carrying at least one T allele for *GCLC* had significant higher MeHgP ($\beta = 0.59$, $P = 0.046$). Also, polymorphic *GCLM* subjects had lower THgP/THgB than those with the nonvariant genotype. Taken together, data of this study suggest that GSH-related polymorphisms may change the metabolism of MeHg by modifying the distribution of mercury species iin plasma compartment and the HgP/HgB partitioning.

1. Introduction

Mercury (Hg) exposure during early life is associated with impaired neurodevelopment [1–4] and later in life, with adverse effects on the cardiovascular system [5, 6]. Fish is the major source of Hg exposure in fish-eating communities, where the methylmercury (MeHg) is the main species and presents the highest toxicity [7]. In the Amazonian region, several riverside populations, who have fish as the main source of proteins, are chronically exposed to high levels of MeHg [8].

For biomonitoring Hg exposure, several biomarkers have been proposed [9–12]. For instance, urinary levels of Hg frequently estimate the level of exposure to Hg vapors or inorganic Hg (IHg) whereas blood Hg and/or hair Hg predicts MeHg exposure [13].

According to Lorscheider et al. [14], most of the MeHg in our body is attached to hemoglobin (Hb) in red blood cells, with a small fraction coupled to GSH that contributes approximately to 1% of all circulating blood MeHg. Therefore, the use of whole blood as a biomarker of Hg exposure barely

reflects available Hg, since only 1% or less of the metal is in the mobile form (Hg-cysteine) that effectively reaches the target organs [15]. Due to a higher portion of unbound Hg in comparison to blood, plasmatic Hg may be considered a fraction more freely available for exchange with target tissues than Hg levels in whole blood [16]. In this context, some recent publications demonstrate interesting and relevant associations between plasmatic Hg and outcomes in MeHg exposed subjects [17, 18].

On the other hand, it is generally accepted that Hg predominates in plasma in its inorganic form [19, 20]. However, data supporting this judgment are very limited and based on populations exposed to very low levels of Hg and only exposed to IHg. Moreover, data on the total plasmatic Hg/whole blood Hg (THgP/THgB) partitioning are totally inexistent for MeHg exposed populations.

Hg elimination in humans is linked to the glutathione (GSH) detoxification system in bile and several enzymes of this pathway may be involved in its elimination, such as the glutamyl-cysteine-ligases (GCLs) and the glutathione-S-transferases (GSTs) [21]. Many GSH-related enzymes are highly polymorphic and epidemiological studies have found that some polymorphisms in GSH-related genes are associated with the metabolism of Hg [22–28] and result in differences of Hg retention. Moreover, since the polymorphisms of GSH-related genes are associated to differences in Hg retention in the body, these genetic variations may also modify the partitioning of Hg between red cells and plasma for a given Hg whole blood which can be also associated with different toxicologically labile fraction of circulatory Hg.

Then, the aim of the present study was to evaluate the effects of polymorphisms in (*GSTM1*, *GSTT1*, *GSTP1*, *GCLM,* and *GCLC*) on the distribution of mercury species (MeHg and IHg) in the plasma compartment, as well as on the differences in the THgP/THgB partitioning in a group of persons exposed to the metal via consumption of contaminated fish in the Amazonian region of Brazil.

2. Materials and Methods

2.1. Study Design and Population. We carried out a cross-sectional study with participants from several riverside communities situated on the banks of the Tapajós River, one of the major tributaries of the Amazon River. Recruitment was conducted in 12 villages through a door-to-door invitation followed by community meetings. 88 subjects agreed to participate in the study.

The riverside communities of Brazilian Amazon are different from other populations of Brazil. The persons have a very specific diet; around 80% of the protein intake comes from fish and the consumption of vegetables and fruits is basically restricted to the region's typical ones [29]. In most of the villages of the study, there are no industrial activities or roads or vehicles, although a few motorized boats are used for fishing and transportation. Moreover, there is no gold-mining close to these communities and no participants reported to have amalgam fillings. Therefore, the only source of Hg exposure is through the intake of contaminated fish, where Hg is predominantly found in MeHg form [8].

Villagers' data were collected using two interviewer-administered questionnaires. One questionnaire covered sociodemographic, life-style, and health information (gender, age, village of residence, place of birth, length of time in the region, educational level, subsistence activities, exposure to other contaminants, frequency and quantity of smoking, drinking and drug habits, medical history and medication). The second was a 7-day recall food consumption frequency questionnaire. For fish consumption, a list was prepared which included most of the fish species present in the region. For each day, participants indicated the number of meals containing fish as well as the fish species that were consumed. Anthropometric measurements (weight, height, and waist circumference) were also taken by a trained technician.

Written consent was provided by all study participants. This study was approved by Ethics Committee of the University of São Paulo at Ribeirão Preto (Brazil), protocol number CEP/FCFRP-71.

2.2. Samples Collection and Hg Analyses. Blood samples were collected in trace metal-free vacuum tubes (BD Vacutainer, Franklin Lakes, NJ, USA) containing heparin. Plasma Hg species were determined using HPLC-ICP-MS (ELAN DRCII, SCIEX, Norwalk, CT, USA), according the method proposed by Souza et al. [30]. Samples (250 μL; in triplicate) were placed in 15 mL polypropylene test tubes with 2.75 mL of a solution containing 0.10% v/v HCl + 0.050% m/v L-cysteine + 0.10% v/v 2-mercaptoethanol and then sonicated for 15 min in ultrasonic bath (UNIQUE, Brazil). The resulting solution was centrifuged and filtered through 0.20 μm Nylon filters (Millipore, USA) and 100 μL were injected in HPLC-ICP-MS. All separations were performed at room temperature under isocratic conditions. The isocratic mobile phase was 3% v/v methanol + 97% v/v (0.5% v/v 2-mercaptoethanol + 0.05% v/v formic acid). The flow rate was 1.2 mL/min. Data evaluation was performed using Chromera software (version 2.1.0.1631) supplied with the instrument, and quantifications were based on peak areas by external calibration. This method determines three species of Hg, but only MeHg and IHg were detected in the plasma samples that we analyzed.

Hg determination of quality control was guaranteed by analyzing standard reference materials from the U.S. National Institute of Standards and Technologies (NIST 966-Toxic Metals in Bovine Blood, certified value 31 ± 1.7 μg/L and mean found value 31 ± 0.30 μg/L). Moreover, various secondary reference materials, provided by the National Institute of Public Health of Quebec, Canada (INSP External Quality Assessment Scheme (EQAS) for Trace Elements in Blood, Plasma and Hair), were also analyzed. For these reference materials recoveries of Hg were between 93 and 105% (based on target values).

2.3. DNA Isolation and Genotyping. Genomic DNA was extracted from peripheral blood using the Easy-DNA kit (Invitrogen, Carlsbad, CA, USA) according to the manufacturer's instructions and stored at −20°C until analyses. *GSTM1* and *GSTT1* deletions were genotyped using multiplex-PCR as described by Abdel-Rahman et al. [31], with *CYP1A1*

(exon 7) as an internal control to ensure good quality of the DNA. The primers, dNTPs, *Taq* polymerase, and magnesium chloride, were obtained from Invitrogen (Carlsbad, CA, USA). After amplification, PCR products were subjected to electrophoresis on a 2.0% agarose gel (Invitrogen, Carlsbad, CA, USA) and visualized using ethidium bromide (Sigma-Aldrich, St. Louis, MO, USA). DNA from samples positive for the *GSTM1* and *GSTT1* genes yielded bands of 215 and 480 bp, respectively, while the internal positive control (*CYP1A1*) PCR product yielded a 312 bp fragment. *GSTP1* $Ile^{105}Val$ (rs1695), *GCLM*-588 (rs41303970), and *GCLC*-129 (rs17883901) were genotyped by real-time PCR using TaqMan assays (Applied Biosystems, Carlsbad, CA, USA) as described by Custodio et al. [24] on a Quantica Real Time PCR System (TECHNE; Staffordshire, UK).

2.4. Statistical Analysis. Hardy-Weinberg equilibrium was analyzed with the conventional Chi-square test. Age, fish intake, and biomarkers of Hg were analyzed as continuous variables; gender, genotypes, alcohol consumption, and smoking as categorical variables. We considered participants that consumed at least five drinks per week as alcohol users and smokers those who smoke at least five cigarettes per day for the last five years.

Correlations (Spearman's; rho) were performed in order to examine the associations between age, gender, fish intake, alcohol consumption, smoking, and Hg biomarkers. After that, Student's t-tests were performed to assess the variations between the Hg biomarkers among the different genotypes.

Finally, multivariate general linear models were employed to evaluate the influence of genetic effects on Hg biomarkers. In order to adjust for other variables influencing Hg concentrations, the impacts of age, gender, body mass index, fish intake, alcohol consumption, and smoking on Hg levels were analyzed in a univariate model and variables were included in the multivariate model if they had a P value <0.20, that is, in the present study, age, gender, and fish intake. All Hg biomarkers were ln-transformed through the analyses, because the nontransformed values were not normally distributed.

Results were defined as statistically significant for a value of $P \leq 0.050$. Analyses were performed using SPSS 20 Statistics software (IBM; Armonk, NY, USA).

3. Results

3.1. General Characteristics. Sociodemographic characteristics and Hg concentrations for all participants enrolled are described in Table 1. The age ranged between 15 and 80 years; the distribution between the sexes was homogenous and fish consumption (portion of fish per day; 150–200 g per meal) varied from one to four portions per day (2.5 ± 1.5). Alcohol was consumed by 34% and 23% of the study participants were smokers. No participants reported to have amalgam fillings. THgB, THgP, MeHgP, and IHgP were 37 ± 21, 10 ± 4.3, 4.3 ± 2.9, and 5.8 ± 2.3 μg/L, respectively; THgP/THgB ranged from 0.13 to 0.91.

Table 1: General characteristics of riverside persons living in Amazonian region, Brazil.

	N	Mean ± SD	Median	Range
Participants	88	—	—	—
Age (years)	88	41 ± 16	41	15–80
Female/male	37/51	—	—	—
Body mass index	88	25 ± 4.6	24	17–42
Portion fish/day[a]	86	2.5 ± 1.5	3.0	1.0–4.0
1	15	—	—	—
2	26	—	—	—
3	13	—	—	—
4	32	—	—	—
Smoking (yes)	88 (20)	—	—	—
Alcohol (yes)	88 (30)	—	—	—
THgB[b] (μg/L)	88	37 ± 21	29	8.4–83
THgP[c] (μg/L)	88	10 ± 4.3	9.6	2.4–27
THgP/THgB[f]	88	0.33 ± 0.15	0.29	0.13–0.91
MeHgP[d] (μg/L)	88	4.3 ± 2.9	3.6	0.67–18
IHgP[e] (μg/L)	88	5.8 ± 2.3	5.7	1.1–13

[a]One portion of fish: 150–200 g; two participants did not answer the questionnaire concerning fish intake.
[b]Total Hg in blood.
[c]Total Hg in plasma.
[d]Methylmercury in plasma.
[e]Inorganic Hg in plasma.
[f]Ratio between total Hg in plasma and total Hg in blood.

Table 2 presents genetic background data and comparative allele frequencies of Caucasians and Africans found in earlier studies (http://www.hapmap.org/, populations CEU; CEPH (Utah residents with ancestry from northern and Western Europe; and YRI; Yoruba in Ibadan, Nigeria)), because the study population has a genetic background from European colonizers and African slaves. All allelic frequencies were in Hardy-Weinberg equilibrium; in general, for the five polymorphisms analyzed, the genetic/allelic frequencies were more similar to those found in the reference African population than the European ones.

3.2. Correlations between Fish Intake, Lifestyle, and Hg Biomarkers. Correlations between the variables enrolled in the present work are present in Table 3. Interestingly, here, fish consumption was only positively correlated to MeHgP ($r_S = 0.32$, $P < 0.0010$). Moreover, THgB, THgP, MeHgP, and IHgP were highly correlated and the highest correlation was found between THgP and MeHgP ($r_S = 0.81$, $P < 0.0010$). Age was positively correlated to THgB, THgP and IHgP, while no correlations were found between Hg biomarkers and gender. Also, a negative correlation was found between THgB and THgP/THgB ($r_S = 0.71$, $P < 0.0010$) (Figure 1). No correlations were found between smoking and alcohol consumption and Hg biomarkers.

3.3. Genetic Effects and Hg Partitioning between Plasma and Whole Blood. Table 4 shows the concentrations of Hg biomarkers among the different genotypes. It can be seen

Table 2: Genotype, allele frequencies of *GSTM1*, *GSTT1*, *GSTP1*, *GCLM*, and *GCLC* polymorphisms of riverside persons living in the Amazonian region of the Tapajós River, Brazil.

Genotypes	Genotype frequencies		MAF[a]		Reference MAF	
					European	African
GSTM1	Present	Null	—	—	Null[c]	Null[c]
Deletion	0.66	0.34	—	—	0.13–0.54	0.47
GSTT1	Present	Null	—	—	Null[c]	Null[c]
Deletion	0.60	0.40	—	—	0.11–0.28	0.37
GSTP1 (Ile[105]Val)	Ile/Ile	Ile/Val + Val/Val	Val (G)	HWE[b]	Val (G)[d]	Val (G)[g]
rs1695	0.37	0.63	0.40	Yes	0.42	0.39
GCLM-588 (C/T)	CC	CT + TT	T	HWE	T[e]	T[h]
rs41303970	0.48	0.52	0.33	Yes	0.10	0.25
GCLC-128 (C/T)	CC	CT + TT	T	HWE	T[f]	T[f]
rs17883901	0.95	0.050	0.030	Yes	0.060	0.010

[a]Minor allele frequency.
[b]HWE: Hardy-Weinberg equilibrium. For the *GSTM1* and *GSTT1* deletions it was not possible to calculate HWE, because the methodology used does not distinguish between hetero- and homozygous genotypes.
[c]Reference values from Mo et al. [32].
[d]Reference values for ss1390210 from HapMap-CEU.
[e]Reference values for ss230641266 from pilot_1_CEU_low_coverage_panel.
[f]Reference values for ss66860389 from CEU_GENO_PANEL; YRI_GENO_PANEL.
[g]Reference values for ss1390210 from HapMap-YRI.
[h]Reference values for ss218528824 from pilot_1_YRI_low_coverage_panel.

Table 3: Correlations (Spearman's; r_s) between age, gender, body mass index (BMI), alcohol consumption, smoking, total Hg in blood (THgB) and total Hg, methylmercury, and inorganic Hg in plasma (THgP, MeHgP, and IHgP, resp.).

	Age	Gender	BMI	Fish intake	Alcohol	Smoking	THgB	THgP	THgP/THgB	MeHgP	IHgP
Age	—	−0.13	0.18	−0.17	−0.20	−0.16	0.27*	0.21*	−0.16	0.059	0.27*
Gender[a]	−0.13	—	0.051	−0.32**	−0.030	0.19	−0.11	−0.036	0.13	0.057	−0.12
BMI	0.18	0.051	—	−0.15	0.12	0.022	−0.072	0.0090	0.071	−0.075	0.12
Fish intake[b]	−0.17	−0.32	−0.15	—	0.12	−0.030	0.20	0.21	−0.075	0.32**	−0.0090
Alcohol	−0.20	−0.030	0.12	0.12	—	0.16	−0.077	0.086	0.17	0.096	0.041
Smoking	−0.16	0.19	0.022	−0.030	0.16	—	−0.043	−0.12	−0.032	−0.098	−0.060
THgB	0.27*	−0.11	−0.072	0.20	−0.077	−0.043	—	0.66**	0.71**	0.61**	0.48**
THgP	0.21*	−0.036	0.0090	0.21	0.086	−0.12	0.66**	—	0.040	0.81**	0.77**
THgP/THgB	−0.16	0.13	0.071	−0.075	0.17	−0.032	0.71**	0.040	—	−0.11	0.11
MeHgP	0.059	0.057	−0.075	0.32**	0.096	−0.098	0.61**	0.81**	−0.11	—	0.32**
IHgP	0.27*	−0.12	0.12	−0.0090	0.041	−0.060	0.48**	0.77**	0.11	0.32**	—

[a]Female was considered as reference. [b]Fisk intake ranged from one to four portions per day.
*Statistically significant $P < 0.050$; **statistically significant $P < 0.010$.

that participants with the *GSTM1* null genotype had higher levels of THgB and IHgP than subjects that expressed the enzyme. Also, persons carrying at least one allele T for *GCLC* had higher levels of THgP, MeHgP and IHgP compared to those with the nonvariant genotype, while polymorphic *GLCM* individuals had lower percentage of THgP in the blood stream.

Table 5 summarizes the genetic effects obtained from multivariate regressions for concentrations of Hg biomarkers, adjusted for fish intake, gender, and age. *GSTM1* and *GCLC* polymorphisms modified THgP and MeHgP (multivariate analyses, $P < 0.050$). Null homozygotes for *GSTM1* accumulated more THgP and MeHgP compared to subjects with *GSTM1* ($\beta = 0.22$, $P = 0.035$ and $\beta = 0.30$, $P = 0.050$, resp.).

Genetic effects were also seen concerning *GCLs* polymorphisms. Persons who are carrying at least one T allele for *GCLC* had higher THgP as well as MeHgP concentration ($\beta = 0.45$, $P = 0.046$; $\beta = 0.69$, $P = 0.038$, resp.). Interestingly, *GCLM* polymorphism altered the relation between the levels of THgP and THgB; that is, participants who carried the polymorphic allele tended to have lower levels of THgP than those with the nonvariant genotype ($\beta = -0.21$, $P = 0.050$) (Figure 2).

4. Discussion

The present work shows that polymorphisms in glutathione-related genes modify the relationship between exposure to

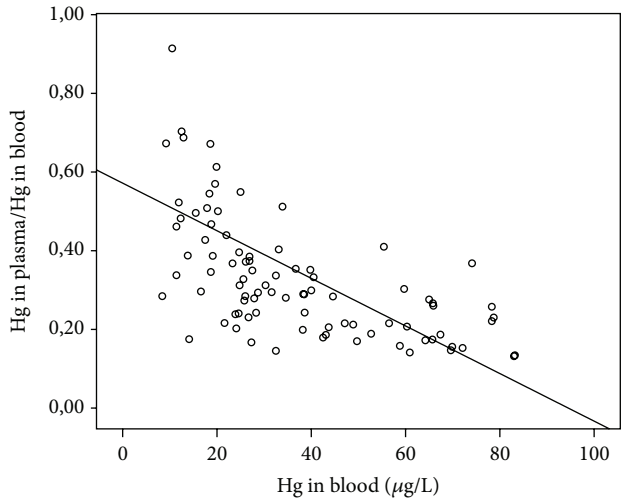

Figure 1: Correlation between total mercury in blood and the Hg in plasma/Hg in blood (Spearman's; r_s 0.71, $P < 0.0010$).

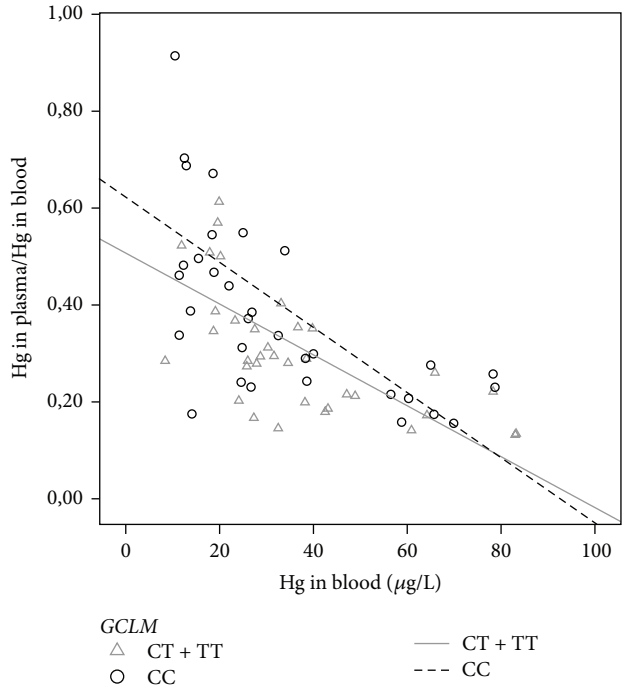

Figure 2: Hg in blood as a function of Hg in plasma/Hg in blood for *GCLM* genotypes. The regression lines do not reflect adjustments for age and gender as described in the text.

the metal and Hg species in plasma in a population highly exposed, via fish intake.

Correlations between fish intake and MeHgP were found, indicating that the populations are exposed predominantly to MeHg. However, significant correlations were not found between fish consumption and THgB, THgP, and IHgP. Accessing the association between the exposure to MeHg and retention requires estimates of both. The exposure to MeHg depends on both the intake of fish and the concentration of the metal in the fish. Here, only data about fish intake collected by questionnaire was used and therefore, the variation of Hg levels in the fish, which was not estimated in this study, can be seen in the differences found in the correlations between fish consumption and Hg biomarkers (Table 3). Our group has previously found that MeHgP are associated with fish intake, while IHgP is not; the increase of IHgP was attributed to age and it is supposed that other processes of demethylation may be also evolved (data not published). However, we believe that other variations, such as genetic effects, are also associated with Hg metabolism and may explain part of this scenario.

According to the World Health Organization [33], after the ingestion of fish contaminated, approximately 95% of Hg is absorbed in the gastrointestinal tract resulting in 5% of Hg in the blood compartment and the ratio between THgP and THgB is 1/20 [34]. However low, Hg in plasma is the bioavailable fraction and may be related to increase of adverse health effects. However, nothing has been explored considering the effects of chemical forms of Hg, mainly in the plasma compartment as well as their usefulness to assess toxicological risks.

We observed a negative correlation between THgB and THgP/THgB; that is, with increase of THgB, a decrease in the ratio THgP/THgB is observed, indicating that even with the increase of THgB, saturation effects of erythrocytes do not occur, and therefore, there is no Hg mobilization of erythrocytes to the plasma fraction. In blood, MeHg is predominantly bound to erythrocytes, while IHg is mostly in plasma. When the exposure is to IHg, the increase of THgP is independent of the concentration of THgB, since IHg binds weakly to red blood cells [15, 20, 22]; our data give further support to these previous findings, since we observed a strong correlation between THgB and THgP. Therefore, our results suggest that determination of Hg in total blood may not predict directly the toxicity in individuals predominantly exposed to MeHg and alternative approaches to assess the toxicological effects associated with MeHg exposure should be strongly encouraged.

As mentioned above, THgP levels are highly correlated to MeHgP; therefore, the changes in THgP probably are associated to the alterations in MeHgP. We found higher concentrations of MeHgP among *GSTM1* null participants, which may be related to lower MeHg-conjugating activity, lower MeHg excretion, and a higher MeHg retention.

Earlier findings of our group have also found associations between THgB and *GSTM1* polymorphisms [22, 23], which were not supported in the present study; these differences between our studies may be explained by the size of the sample, which is reduced here, but not limiting for gene-environment interactions studies. In studies of Swedish populations exposed to MeHg via fish intake and to IHg by gold mining activity, Custodio et al. [24, 25] found no associations between *GSTM1* and concentrations of Hg in blood. On the other hand, Lee et al. [27] evaluated 417 pregnant women of North Korea exposed to MeHg via fish consumption and observed that women who had homozygous deletion for *GSTM1* had higher Hg levels in blood, either during the early or late pregnancy (Hg in blood 3.7 and 3.3 μg/L, resp.), than persons with the gene.

Table 4: Total Hg in blood (THgB) and total Hg, methylmercury, and inorganic Hg in plasma (THgP, MeHgP, and IHgP, resp.) as well as the ratio THgP/THgB among the different genotypes.

Genotypes	THgB	THgP	MeHgP	IHgP	THgP/THgB
	Mean ± SD[d]	Mean ± SD	Mean ± SD	Mean ± SD	Mean ± SD
GSTM1	37 ± 21	10 ± 4.4	4.4 ± 2.5	5.9 ± 2.4	0.33 ± 0.16
Present	34 ± 18	9.6 ± 4.2	4.1 ± 2.8	5.5 ± 2.2	0.33 ± 0.14
Null	44 ± 24	12 ± 4.7*	5.1 ± 3.2	6.6 ± 2.5*	0.34 ± 0.18
GSTT1	37 ± 21	10 ± 4.4	4.4 ± 2.9	5.9 ± 2.4	0.33 ± 0.16
Present	35 ± 22	9.9 ± 4.6	4.1 ± 3.1	5.7 ± 2.4	0.34 ± 0.17
Null	40 ± 19	11 ± 4.1	5.0 ± 2.7	6.0 ± 2.3	0.31 ± 0.13
GSTPI[a]	38 ± 21	10 ± 4.0	4.3 ± 2.5	5.8 ± 2.3	0.32 ± 0.16
Ile/Ile	40 ± 22	11 ± 3.7	4.5 ± 2.3	6.1 ± 2.4	0.33 ± 0.15
Ile/Val + Val/Val	36 ± 20	9.8 ± 3.9	4.2 ± 2.6	5.6 ± 2.2	0.31 ± 0.16
GCLM[b]	35 ± 20	9.7 ± 3.7	4.2 ± 2.3	5.6 ± 2.2	0.34 ± 0.16
CC	33 ± 21	10 ± 4.1	4.5 ± 2.4	5.7 ± 2.6	0.38 ± 0.16
CT + TT	36 ± 19	9.4 ± 3.2	3.9 ± 2.3	5.5 ± 1.7	0.30 ± 0.13*
GCLC[c]	35 ± 19	9.9 ± 4.3	4.3 ± 3.0	5.6 ± 2.2	0.34 ± 0.15
CC	34 ± 20	9.7 ± 4.1	4.1 ± 2.9	5.5 ± 2.1	0.33 ± 0.16
CT + TT	42 ± 12	15 ± 6.2*	6.9 ± 3.2*	8.1 ± 3.1*	0.36 ± 0.13

[a]rs1695; [b]rs41307970; [c]rs17883901; [d]arithmetic mean ± standard deviation (SD).
*indicates significant difference between the wild genotypes and the polymorphic ones (Student's t-test; $P < 0.050$).

Table 5: Multivariate regression parameters for the associations between genotype and total Hg in blood (THgB) and total Hg, methylmercury, and inorganic Hg in plasma (THgP, MeHgP, and IHgP, resp.) as well as the ratio THgP/THgB.

Genotypes	THgB[d]		THgP[d]		MeHgP[d]		IHgP[d]		THgP/THgB[d]	
	β^e	P	β	P	β	P	β	P	β	P
GSTM1										
Present	—	—	—	—	—	—	—	—	—	—
Null	0.21	0.13	0.22	0.035	0.30	0.050	0.18	0.10	0.16	0.88
GSTT1										
Present	—	—	—	—	—	—	—	—	—	—
Null	0.14	0.31	0.10	0.34	0.18	0.24	0.090	0.45	−0.040	0.71
GSTPI[a]										
Ile/Ile	—	—	—	—	—	—	—	—	—	—
Ile/Val + Val/Val	−0.10	0.49	−0.12	0.27	−0.79	0.59	−0.11	0.36	−0.018	0.87
GCLM[b]										
CC	—	—	—	—	—	—	—	—	—	—
CT + TT	0.12	0.38	−0.08	0.41	−0.16	0.29	−0.020	0.88	−0.21	0.050
GCLC[c]										
CC	—	—	—	—	—	—	—	—	—	—
CT + TT	0.34	0.25	0.45	0.046	0.69	0.038	0.36	0.14	0.12	0.61

[a]rs1695; [b]rs41307970; [c]rs17883901; [d]Natural ln-transformed.
[e]Unstandardized beta (β) coefficients for the $\beta_1 \times$ genotype term (categorical) adjusted for covariates. The genotype denoted first is used as reference. Multivariate model: Hg biomarkers = $\alpha + \beta_1 \times$ genotype + $\beta_2 \times$ fish intake + $\beta_3 \times$ age + $\beta_4 \times$ gender.

The different results between the studies might be related to different levels of MeHg exposure. The studies of Gundacker et al. [35], Custodio et al. [24], and Engström et al. [28] were performed on study participants with lower MeHg exposure than the study carried by Lee et al. [27] and our earlier study [22, 23]. Another hypothesis is that the differences also may be explained, in some extent, to the biomarker used in the studies; however, as mentioned above, currently there is no data concerning assessment of genetic effects on Hg species in plasma.

We did not find association between *GSTT1* polymorphism and THgP, MeHgP, and IHgP levels. An earlier work showed the *GSTT1* null polymorphisms are associated with accumulation of Hg in individuals exposed to EtHg via vaccines [36]. According to Custodio et al. [24], the dealkylation of EtHg occurs faster than MeHg and therefore, the genetic effects may thus affect the elimination of IHg, a point which was not observed in a further study of the same group [25] and, also, in the present work. However, in a previous work, we observed an association between THgB and *GSTT1* polymorphisms [22] in the same studied population. Thus, these data bring some pieces of evidence that the genetic effects of *GSTT1* may be more associated with the bioavailable MeHg or other organic forms than the levels of exposure to Hg as well as the exposure to IHg.

Also, in the present work, association between polymorphism of *GSTP1* and Hg biomarkers was not found. Actually,

a recent experimental study demonstrated that the Ile allele is more sensitive to Hg exposure. Goodrich and Basu [37] evaluated the activity of allozymes of *GSTP1* towards IHg and MeHg and found that the *GSTP1* Val allozyme was less sensitive to inhibition induced by treatment of high doses of Hg than the Ile allozyme. In support of this data, previous *in vitro* studies have suggested that *105Val amino acid may confer protection against Hg-induced inhibition due to structural changes in cysteine residues which may impact the ability of Hg to bind and, consequently, inhibit the enzyme [38, 39].

GCLM polymorphism did not impact the concentrations of Hg biomarkers but altered the percentage of THgP in the blood stream (as seen in Figure 2). A previous work of our group [23] showed that polymorphic individuals for *GCLM* had lower THgB levels than those who carried at least one C-allele. However, although these polymorphic individuals had lower THgB levels, they tended to have more THgP, which may modulate the adverse health effects related to MeHg exposure. Moreover, variation in *GCLC* gene influences the levels of MeHgP. Here, we found that T-carriers for *GCLC* allele had significant higher levels of MeHgP than subjects with the nonvariant genotype. These data suggest that polymorphisms in *GCLs* may be related to biomarkers for Hg as well the species of the metal; also, interindividuals variations may be considered. For example, Engström et al. [28] found that Swedish persons with GCLM CC genotype had lower THgB concentrations than those who carried at least one T allele, whereas Custodio et al. [24] did not find any association at lower MeHg exposure, in same studied populations. Interestingly, in the same work, authors showed that carriers of T allele for *GCLC* had lower concentrations of Hg in erythrocytes than CC subjects, a contradictory result compared to our present.

To our knowledge, this work is the first to investigate the genetic effects of Hg species on plasma. Taken together, our results indicate that GSH-related polymorphisms may influence levels of Hg fractions in plasma, which may modulate Hg-induced toxicity. However, further studies concerning both Hg species in plasma as well as genetic effects are necessary for a better elucidation of the mechanisms evolved in Hg species metabolism.

Conflict of Interests

The authors declare that there is no conflict of interests regarding the publication of this paper.

Acknowledgments

We would like to thank São Paulo Foundation Research (FAPESP), National Counsel of Technological and Scientific Development (CNPq), and Coordination for the Improvement of Higher Level Education Personnel (CAPES) for financial support.

References

[1] S. A. Counter and L. H. Buchanan, "Mercury exposure in children: a review," *Toxicology and Applied Pharmacology*, vol. 198, no. 2, pp. 209–230, 2004.

[2] C. Johansson, A. F. Castoldi, N. Onishchenko, L. Manzo, M. Vahter, and S. Ceccatelli, "Neurobehavioural and molecular changes induced by methylmercury exposure during development," *Neurotoxicity Research*, vol. 11, no. 3-4, pp. 241–260, 2007.

[3] M. R. Karagas, A. L. Choi, E. Oken et al., "Evidence on the human health effects of low-level methylmercury exposure," *Environmental Health Perspectives*, vol. 120, pp. 799–806, 2012.

[4] M. Ni, X. Li, J. B. Rocha et al., "Glia and methylmercury neurotoxicity," *Journal of Toxicology and Environmental Health A*, vol. 75, no. 16-17, pp. 1091–1101, 2012.

[5] A. L. Choi, P. Weihe, E. Budtz-Jørgensen et al., "Methylmercury exposure and adverse cardiovascular effects in Faroese Whaling men," *Environmental Health Perspectives*, vol. 117, no. 3, pp. 367–372, 2009.

[6] M. C. Houston, "Role of mercury toxicity in hypertension, cardiovascular disease, and stroke," *Journal of Clinical Hypertension*, vol. 13, no. 8, pp. 621–627, 2011.

[7] Agency for Toxic Substances and Diseases Control (ATSDR), *Toxicological Profile for Mercury*, U.S. Department of Health and Human Services, Public Health Service, Washington, DC, USA, 1999.

[8] C. J. Passos and D. Mergler, "Human mercury exposure and adverse health effects in the Amazon: a review," *Cadernos de Saude Publica*, vol. 24, no. 4, pp. S503–S520, 2008.

[9] K. L. Caldwell, M. E. Mortensen, R. L. Jones, S. P. Caudill, and J. D. Osterloh, "Total blood mercury concentrations in the U.S. population: 1999–2006," *International Journal of Hygiene and Environmental Health*, vol. 212, no. 6, pp. 588–598, 2009.

[10] M. F. Carneiro, D. Grotto, B. L. Batista, C. R. Rhoden, and F. Barbosa Jr., "Background values for essential and toxic elements in children's nails and correlation with hair levels," *Biological Trace Element Research*, vol. 144, no. 1–3, pp. 339–350, 2011.

[11] J. F. Nyland, M. Fillion, F. Barbosa Jr. et al., "Biomarkers of methylmercury exposure immunotoxicity among fish consumers in amazonian Brazil," *Environmental Health Perspectives*, vol. 119, no. 12, pp. 1733–1738, 2011.

[12] S. M. Vieira, R. de Almeida, I. B. Holanda et al., "Total and methyl-mercury in hair and milk of mothers living in the city of Porto Velho and in villages along the Rio Madeira, Amazon, Brazil," *International Journal of Hygiene and Environmental Health*, vol. 216, no. 6, pp. 682–689, 2013.

[13] World Health Organization (WHO), *International Programme on Chemical Safety (IPCS)-Environmental Health Criteria 155: Biomarkers and Risk Assessment: Concepts and Principles*, World Health Organization, Geneva, Switzerland, 1993.

[14] F. L. Lorscheider, M. J. Vimy, and A. O. Summers, "Mercury exposure from "silver" tooth firings: emerging evidence questions a traditional dental paradigm," *FASEB Journal*, vol. 9, no. 7, pp. 504–508, 1995.

[15] T. W. Clarkson, J. B. Vyas, and N. Ballatori, "Mechanisms of mercury disposition in the body," *American Journal of Industrial Medicine*, vol. 50, no. 10, pp. 757–764, 2007.

[16] S. Ancora, R. Rossi, P. Di Simplicio, L. Lusini, and C. Leonzio, "*In Vitro* study of methylmercury in blood of bottlenose dolphins (*Tursiops truncatus*)," *Archives of Environmental Contamination and Toxicology*, vol. 42, no. 3, pp. 348–353, 2002.

[17] K. C. de Marco, G. U. Braga, and F. Barbosa Jr., "Determination of the effects of *eNOS* gene polymorphisms (T-786C and Glu^{298}Asp) on nitric oxide levels in a methylmercury-exposed population," *Journal of Toxicology and Environmental Health A*, vol. 74, no. 20, pp. 1323–1333, 2011.

[18] D. Grotto, J. Valentini, M. Fillion et al., "Mercury exposure and oxidative stress in communities of the Brazilian Amazon," *Science of the Total Environment*, vol. 408, no. 4, pp. 806–811, 2010.

[19] M. Berglund, B. Lind, K. A. Björnberg, B. Palm, Ö. Einarsson, and M. Vahter, "Inter-individual variations of human mercury exposure biomarkers: a cross-sectional assessment," *Environmental Health*, vol. 3, pp. 4–20, 2005.

[20] T. W. Clarkson and L. Magos, "The toxicology of mercury and its chemical compounds," *Critical Reviews in Toxicology*, vol. 36, no. 8, pp. 609–662, 2006.

[21] C. Gundacker, M. Gencik, and M. Hengstschläger, "The relevance of the individual genetic background for the toxicokinetics of two significant neurodevelopmental toxicants: mercury and lead," *Mutation Research*, vol. 705, no. 2, pp. 130–140, 2010.

[22] G. R. M. Barcelos, K. C. de Marco, D. Grotto et al., "Evaluation of glutathione S-transferase i and *GSTT1* polymorphisms and methylmercury metabolism in an exposed Amazon population," *Journal of Toxicology and Environmental Health A*, vol. 75, no. 16-17, pp. 960–970, 2013.

[23] G. R. M. Barcelos, D. Grotto, K. C. de Marco et al., "Polymorphisms in glutathione-related genes modify mercury concentrations and antioxidant status in subjects environmentally exposed to methylmercury," *Science of Total Evironment*, vol. 463-464, pp. 319–325, 2013.

[24] H. M. Custodio, K. Broberg, M. Wennberg et al., "Polymorphisms in glutathione-related genes affect methylmercury retention," *Archives of Environmental Health*, vol. 59, no. 11, pp. 588–595, 2004.

[25] H. M. Custodio, R. Harari, L. Gerhardsson, S. Skerfving, and K. Broberg, "Genetic influences on the retention of inorganic mercury," *Archives of Environmental and Occupational Health*, vol. 60, no. 1, pp. 17–23, 2005.

[26] C. Gundacker, K. J. Wittmann, M. Kukuckova et al., "Genetic background for mercury metabolism," *Toxicology Letters*, vol. 189, pp. S89–S90, 2009.

[27] B. Lee, Y. Hong, H. Park et al., "Interaction between *GSTM1*/*GSTT1* polymorphism and blood mercury on birth weight," *Environmental Health Perspectives*, vol. 118, no. 3, pp. 437–443, 2010.

[28] K. S. Engström, U. Strömberg, T. Lundh et al., "Genetic variation in glutathione-related genes and body burden of methylmercury," *Environmental Health Perspectives*, vol. 116, no. 6, pp. 734–739, 2008.

[29] C. J. Passos, D. Mergler, M. Fillion et al., "Epidemiologic confirmation that fruit consumption influences mercury exposure in riparian communities in the Brazilian Amazon," *Environmental Research*, vol. 105, no. 2, pp. 183–193, 2007.

[30] S. S. Souza, A. D. Campiglia, and F. Barbosa Jr., "A simple method for methylmercury, inorganic mercury and ethylmercury determination in plasma samples by high performance liquid chromatography-cold-vapor-inductively coupled plasma mass spectrometry," *Analytica Chimica Acta*, vol. 761, pp. 11–17, 2013.

[31] S. Z. Abdel-Rahman, R. A. El-Zein, W. A. Anwar, and W. W. Au, "A multiplex PCR procedure for polymorphic analysis of *GSTM1* and *GSTT1* genes in population studies," *Cancer Letters*, vol. 107, no. 2, pp. 229–233, 1996.

[32] Z. Mo, Y. Gao, Y. Cao, F. Gao, and L. Jian, "An updating meta-analysis of the GSTM1, GSTT1, and GSTP1 polymorphisms and prostate cancer: a HuGE review," *Prostate*, vol. 69, no. 6, pp. 662–688, 2009.

[33] World Health Organization (WHO), *Environmental Health Criteria 101: Methylmercury*, World Health Organization, Geneva, Switzerland, 1990.

[34] T. W. Clarkson, "The three modern faces of mercury," *Environmental Health Perspectives*, vol. 110, no. 1, pp. 11–23, 2002.

[35] C. Gundacker, G. Komarnicki, P. Jagiello et al., "Glutathione-S-transferase polymorphism, metallothionein expression, and mercury levels among students in Austria," *Science of the Total Environment*, vol. 385, no. 1–3, pp. 37–47, 2007.

[36] G. A. Westphal, A. Schnuch, T. G. Schulz et al., "Homozygous gene deletions of the glutathione S-transferases M1 and T1 are associated with thimerosal sensitization," *International Archives of Occupational and Environmental Health*, vol. 73, no. 6, pp. 384–388, 2000.

[37] J. M. Goodrich and N. Basu, "Variants of glutathione s-transferase pi 1 exhibit differential enzymatic activity and inhibition by heavy metals," *Toxicology in Vitro*, vol. 26, no. 4, pp. 630–635, 2012.

[38] M. M. Almar and P. J. Dierickx, "*In Vitro* interaction of mercury, copper (II) and cadmium with human glutathione transferase π," *Research Communications in Chemical Pathology and Pharmacology*, vol. 69, no. 1, pp. 99–102, 1990.

[39] P. J. Dierickx, "*In Vitro* inhibition of the soluble glutathione S-transferases from rat liver by heavy metals," *Enzyme*, vol. 27, no. 1, pp. 25–32, 1982.

Hindawi Publishing Corporation
BioMed Research International
Volume 2014, Article ID 181989, 24 pages
http://dx.doi.org/10.1155/2014/181989

Research Article

Unexpected Lack of Deleterious Effects of Uranium on Physiological Systems following a Chronic Oral Intake in Adult Rat

Isabelle Dublineau,[1] Maâmar Souidi,[1] Yann Gueguen,[1] Philippe Lestaevel,[1] Jean-Marc Bertho,[1] Line Manens,[1] Olivia Delissen,[2] Stéphane Grison,[1] Anaïs Paulard,[1] Audrey Monin,[1] Yseult Kern,[1] Caroline Rouas,[1] Jeanne Loyen,[3] Patrick Gourmelon,[4] and Jocelyne Aigueperse[4]

[1] *Institut de Radioprotection et de Sûreté Nucléaire (IRSN), PRP-HOM, SRBE, LRTOX, 31 avenue de la Division Leclerc, BP 17, 92262 Fontenay-aux-Roses Cedex, France*
[2] *Institut de Radioprotection et de Sûreté Nucléaire (IRSN), PRP-HOM, SRBE, LRTOX, BP 166, 26702 Pierrelatte Cedex, France*
[3] *Institut de Radioprotection et de Sûreté Nucléaire (IRSN), PRP-ENV, STEME, BP 40035, 78116 Le Vésinet Cedex, France*
[4] *Institut de Radioprotection et de Sûreté Nucléaire (IRSN), PRP-HOM, BP 17, 92262 Fontenay-aux-Roses Cedex, France*

Correspondence should be addressed to Isabelle Dublineau; isabelle.dublineau@irsn.fr

Received 19 September 2013; Revised 18 December 2013; Accepted 18 December 2013; Published 12 February 2014

Academic Editor: Fernando Barbosa Jr.

Uranium level in drinking water is usually in the range of microgram-per-liter, but this value may be as much as 100 to 1000 times higher in some areas, which may raise question about the health consequences for human populations living in these areas. Our purpose was to improve knowledge of chemical effects of uranium following chronic ingestion. Experiments were performed on rats contaminated for 9 months via drinking water containing depleted uranium (0.2, 2, 5, 10, 20, 40, or 120 mg/L). Blood biochemical and hematological indicators were measured and several different types of investigations (molecular, functional, and structural) were conducted in organs (intestine, liver, kidneys, hematopoietic cells, and brain). The specific sensitivity of the organs to uranium was deduced from nondeleterious biological effects, with the following thresholds (in mg/L): 0.2 for brain, >2 for liver, >10 for kidneys, and >20 for intestine, indicating a NOAEL (No-Observed-Adverse-Effect Level) threshold for uranium superior to 120 m g/L. Based on the chemical uranium toxicity, the tolerable daily intake calculation yields a guideline value for humans of 1350 μg/L. This value was higher than the WHO value of 30 μg/L, indicating that this WHO guideline for uranium content in drinking water is very protective and might be reconsidered.

1. Introduction

Uranium is a natural component of the earth crust. Its concentrations vary highly according to the location and the type of rocks [1]. In fact, it can vary from 3 to 4 g/t in granites and from 20 to 120 g/t in phosphate rocks [2], leading consequently to a great variability of the uranium content in drinking water. For instance, average uranium levels in drinking water are in microgram-per-liter range (0.4 μg/L throughout the world, [3]; 6.7 μg/L in USA, [4]; 4 μg/L in Canada [5]; 2.2 μg/L in China [6]; or 2.22 μg/L in France [7], but they may reach exceptionally the milligram-per-liter range in some specific areas, including some US states (2.5 mg/L [4]; 7.8 mg/L [8]) or southern Finland (9.2 mg/L [9]; 3.4 mg/L [10]). Anthropogenic utilization of uranium for civil, military, and nuclear fuel purposes leads to additional release of this radio element into environment, either around uranium mining sites [11, 12], uranium reprocessing plants [13], or following the use of depleted uranium (DU) in conflict zones [11, 14]. The persistent use of depleted uranium in weapon composition in the recent conflicts (Iraq in 1991 and 2001, Bosnia and Herzegovina in 1995, and Kosovo in 1999)

continues to keep the scientific and social queries concerning the environmental contamination by such metal, as well as subsequent human exposure and possible consequences on health.

The particularity of uranium is its dual toxicity, due to its radiological effects as an alpha emitter and its chemical effects due to its properties as metal. However, the chemical toxicity of this radionuclide was considered as predominant in case of depleted and natural uranium. The major biological effects of uranium on health concern renal function [15, 16]. According to these specific properties, most of guidelines concerning uranium levels were based on chemical effects of uranium on kidneys. As ingestion (by drinking water or alimentary chain) is the predominant way of human exposure for public in case of environmental exposure, guideline values concerning uranium level in drinking water were established by several national and international organizations. These guidelines were based on existing information about chemical effects of uranium, mainly in kidneys. Thus, the World Health Organization set a guideline value of 15 μg/L for uranium in drinking water [3], recently reevaluated at 30 μg/L [17]. This value, however, was provisional in view of several limitations pointed out by WHO [17] concerning the lack of extensive knowledge about the chronic effects of uranium in drinking water. These restrictions were in accordance with a recent review that claimed the need for more epidemiological and experimental studies [18]. Indeed, the existing epidemiological studies do not allow clearly demonstrating health effects of radionuclides at levels naturally encountered in drinking water due to methodological limitations (exposure assessment, possible confounders, and limited sample size). In addition, few experimental studies were performed with uranium levels close to real environmental situations. Considering the previous guideline of WHO [3], the value of 15 μg/L was derived from a single study of subchronic renal effects of uranium when administered to rats in drinking water for 3 months [19]. Moreover, several authors have since shown that the kidneys are not the only biological target of chronic exposure to low levels of uranium; for examples changes have been reported in the gastrointestinal system [20], in the central nervous system [21, 22], or in the liver [23].

These two points—the limitations of existing studies and necessity to take into consideration the recent concept that uranium affects multiple organs—led us to conduct new experimental studies of the results of chronic uranium exposure. The investigation of this present study focused on five organs/tissues: the small intestine, which is the entry route for uranium after ingestion [24]; the kidneys, traditionally considered the target organ of uranium following an acute contamination at high doses [16]; the hematopoietic cells that may be modified by uranium due to its accumulation in the bones and kidneys [25], and other organs described more recently as affected by chronic exposure at low levels: the liver [23] and the brain [22]. The objective was to evaluate the possible biological effects of uranium on the primary function of each organ/tissue. Concerning the intestines, we choose to investigate uranium effects on immune function of intestinal mucosa, because previous studies demonstrated a specific localization of uranium in immune cells of intestinal wall [26, 27]. The investigation of uranium effects on the kidneys and the liver was based on the different phases of the xenobiotic metabolism, since they are the major organs involved in detoxification processes of endo- and xenomolecules. In addition, cholesterol metabolism was studied in the liver, since this organ plays the central role in whole organism concerning this metabolism. The effects of uranium on the central nervous system were evaluated *via* two mechanisms, the uranium-induced oxidative stress and the cholinergic system. Indeed, a possible mechanism of uranium effects observed in cognitive functions may be due to the oxidative stress induced by reactive oxygen species imbalance.

In order to complete this investigation and to be sure to provide an extensive view of uranium effects in the present study, the analyses were performed at the several macroscopic and microscopic levels of organism (molecular, functional, structural, and pathological).

This study was performed in rats of a wide range of concentrations (0.2, 2, 5, 10, 20, 40, or 120 mg/L) of uranium in drinking water. These uranium levels include the uranium level of 0.2 mg/L close to values measured around mining areas [28], the uranium level of 1 mg/L close to the concentration of 0.96 mg/L that served to determine the previous WHO guideline of uranium level in drinking water [3], and the maximal concentration measured throughout the world (20 mg/L in Finland [29]). Duration of 9 months was chosen for the present study to mimic the chronic exposure of populations living on uranium-rich territories and to evaluate its long-term consequences.

2. Material and Methods

2.1. Animals. These experiments were conducted on 8-week old Sprague-Dawley male rats (Charles River, L'Arbresle, France) according to French regulations for animal experimentation (Ministry of Agriculture Act number 2001-464, 2001) and with the approval of IRSN animal welfare committee. Two rats were housed per cage at 21 ± 2°C and a 12 h : 12 h cycle with free access to normal rat food (105, CERJ, France) and water. Animals were contaminated for 9 months with drinking water containing uranium (uranyl nitrate hexahydrate ($UO_2(NO_3)_2{\cdot}6H_2O$)) dissolved in mineral water for final concentration at 0.2, 2, 5, 10, 20, 40, or 120 mg/L (AREVA, France) (10 rats per group). The group of 40 mg/L was added in this study to serve as the reference group, as several studies have been published with this uranium level in drinking water [20, 23, 30, 31]. Control animals drunk uncontaminated mineral water (which contains naturally uranium at 1.42 μg/L). Alpha spectrometry following chemical separation was performed to determine uranium isotope ratio in the contaminated water according the standard norm NF M 60-805-5. The $^{235}U/^{238}U$ ratio of 0.25% indicated depleted uranium (Table 1), which was used in this study to address the chemical toxicity of this radionuclide. At the end of contamination, after overnight fasting, the animals were anesthetized by inhalation of 5% isoflurane (Abbot France, Rungis, France) before being euthanized for tissue sampling. These experiments were conducted on male animals, since

Table 1: Determination of uranium radioisotopes present in drinking water contaminated with 40 mg/L.

Uranium		
^{234}U	Bq/L	93.4 ± 6.5
^{235}U	Bq/L	8.70 ± 1.13
^{238}U	Bq/L	531.5 ± 31.9
U total	mg/L	42.85 ± 2.57
Ratio ^{235}U/^{238}U	%	0.25

Uranium was analysed by alpha spectrometry following chemical separation. See Material and Methods section for more details.

a previous study demonstrated that this gender in rats is more sensitive to uranium than the female is [19].

2.2. Uranium Measurements in Biological Samples. Biological samples were prepared by adding 8 mL nitric acid 70% ultrapure (INSTRA-analyzed for trace metal analysis, Sodipro, Echirolles, France) and 2 mL of hydrogen peroxide. They were then mineralized using a 1000 W microwave (Ethos Touch, Milestone Microwave Laboratory Systems, Sorisole, Italy). Before measurement, samples were diluted between 1/5 and 1/500 depending on considered organ and administrated dose in 2% nitric acid. The samples were then analyzed for their uranium content by inductively coupled plasma mass spectrometry (ICP-MS) (XSERIE 2, Thermoelectron, France). Calibration was performed with a multielemental standard solution (Analab-STD-495, Analab, Bischheim, France). In all solutions likely to be analyzed (biological samples or calibration solutions), bismuth 209 was added as an internal standard. Further indications have been provided in a previous study [32]. For ^{238}U, the detection and quantification limits were, respectively, 0.5 ng/L and 1.5 ng/L, and for ^{235}U, 0.01 ng/L and 0.03. The limits for ^{238}U were applied to total uranium. Uranium was measured in kidney, bone (femur), liver, and brain (entorhinal cortex).

2.3. Biochemical Parameters in Blood. An automated spectrophotometric system (Konelab 20, Thermo Electron Corporation, Cergy-Pontoise, France) was used to measure these parameters, with biological chemistry reagents from the manufacturer or Diagam (Lille, France). Bilirubin was measured with the Thermo Electron Corporation kit. Kits from Diagam were used for measuring total cholesterol, low-density lipoprotein- (LDL-) cholesterol, high-density lipoprotein- (HDL-) cholesterol, triglycerides, alanine aminotransferase (ALT), aspartate aminotransferase (AST), creatinine, urea, iron, ferritin, transferrin, and ceruloplasmin. Phospholipids B were measured with a kit provided by Diagnostic Partners (Bougival, France).

2.4. Blood Cell Counts. Blood was harvested by intracardiac puncture into either EDTA coated tubes for plasma isolation or dry tubes for serum isolation. Blood cell counts were performed by means of an MS-9 vet automatic counter (Melet-Schlossing, Osny, France). The remaining blood was centrifuged at 400 g for 10 minutes and plasma or serum was frozen for later use.

2.5. Cytokine Measurements. Flt-3 ligand concentration, a biological indicator of bone marrow function [33], and IL-7, a biological indicator of T lymphocyte homeostasis [34], were measured in plasma samples using ELISA kits according to manufacturer's recommendation (R&D System, Abington, UK). Sensitivity was 7 pg/mL for Flt3-ligand ELISA test and 15 pg/mL for IL-7 ELISA test.

2.6. Colony-Forming Cell Assay. Femurs were flushed with 5 mL washing medium (MEM-α medium supplemented with 1% fetal calf serum (FCS) and antibiotics, both from Life Technologies, Cergy-Pontoise, France). Spleen cells were crushed in Tenbrock's Potter in the presence of 5 mL washing medium. After washing twice (8 min at 400 g), cells were numbered and viability assessed in the presence of Trypan Blue. Cells were then plated at 5×10^5 for spleen cells and 5×10^4 bone marrow cells in 1.1 mL of complete methylcellulose medium with cytokines (Stem Cell Technologies, Vancouver, Canada). Cultures were incubated at 37°C in 95% air/5% CO_2 in a humidified atmosphere. Colony-forming units-granulocyte macrophage (CFU-GM) and burst-forming units-erythroid (BFU-E) were scored on day 12 of culture.

2.7. Histology and Immunohistochemistry. After fixation in 4% formaldehyde solution (Carlo Erba, Rueil Malmaison, France), tissues were dehydrated, embedded in paraffin, and cut in sections 5 μm thick. Hematoxylin-eosin-saffron staining was then performed in sections of liver, kidney, and terminal ileum by an independent laboratory (Biodoxis, Romainville, France).

Determination of immune cells was also performed in terminal ileum by immunohistochemistry or histochemistry as previously reported in [20]. The tissue neutrophil infiltration was estimated on paraffin sections incubated with rabbit antibody directed against rat myeloperoxidase (IMG antibody, $d = 1/x00$, Clinisciences, Nanterre, France) and LSAB2 HRP kit (Dako, Trappes, France). The macrophages were visualized with mouse antibody against CD68 (Serotec, Cergy Saint Christophe, France) followed by histofine simple stain mouse MAX PO (Microm Microtech, Francheville, France). For mast cell coloration, the ileal segments were fixed in Carney solution. Histological slides were then stained with Alcan Blue method. Neutrophils and mast cells were quantified by determining the number of their respective cells per crypt-villus axis. The results were expressed as mean ± SD of 8 animals. A qualitative analysis was realized for macrophages with establishment of a scoring of macrophage density network in crypts and villi.

2.8. Gene Expression. The different genes measured in the different organs were indicated in the Table 2. Total RNA was prepared from tissues (~30 mg for liver, kidney, entorhinal cortex, and ileum) with the RNeasy Mini Kit (Qiagen,

Table 2: Primer sequences for rat genes studied in several organs following chronic ingestion of uranium.

Genes	Forward	Reverse
HPRT	5′-GCTCGAGATGTCATGAAGGAGA-3′	5′-TCAGCGCTTTAATGTAATCCAGC-3′
	Cytokines	
CCL-2	5′-CAGCCAGATGCAGTTAATGCC-3′	5′-AGCCGACTCATTGGGATCAT-3′
TNFα	5′-ATCCGAGATGTGGAACTGGC-3′	5′-CGATCACCCCGAAGTTCAGTA-3′
IFNγ	5′-CACGCCGCGTCTTGGT-3′	5′-TCTAGGCTTTCAATGAGTGTGCC-3′
TGFβ	5′-TCCCAAACGTCGAGGTGAC-3′	5′-CAGGTGTTGAGCCCTTTCCA-3′
IL-10	5′-GTTGCCAAGCCTTGTCAGAAA-3′	5′-TTTCTGGCCATGGTTCTCT-3′
	Xenobiotic metabolising enzymes	
CYP3A2	5′-AGTAGTGACGATTCCAACATAT-3′	5′-TCAGAGGTATCTGTGTTTCCT-3′
CYP2C11	5′-ATGGGATGCAATGGAAGGAG-3′	5′-TCTTGCCCATCCCAAAAGTC-3′
ST1A1	5′-AGGGTGGCAAGCTAGAGAAGTG-3′	5′-GAGGGAACCCCTGGACATTT-3′
GSTA2	5′-TTGACATGTATTCAGAGGGT-3′	5′-TTGTTTTGCATCCATGGCTG-3′
UGT1A1	5′-TGGCATCCCCAAAACGATCT-3′	5′-GGAACCGGAGTGTGTGATGAA-3′
UGT2B1	5′-TGGAGAACATGGTGTAGTGGT-3′	5′-TTGGCTTTTTCTTCAGTAGTCAGG-3′
MDR1	5′-ATCAACTCGCAAAAGCATCC-3′	5′-AATTCAACTTCAGGATCCGC-3′
MRP2	5′-TTCGAAGCTGGATGATGTGTTT-3′	5′-GCCATGCAGATCATGACAAGAG-3′
	Enzymes of cholesterol metabolism	
HMGR	5′-GGCGGGTCCTGCAAGTG-3′	5′-GCAGGTGAGCGGGTGAGA-3′
CYP27A1	5′-GGAAGGTGCCCCAGAACAA-3′	5′-GCGCAGGGTCTCCTTAATCA-3′
CYP7A1	5′-CCAAGTCAAGTGTCCCCCTCTA-3′	5′-GACTCTCAGCCGCCAAGTG-3′
CYP8B1	5′-GTACACATGGACCCCGACATC-3′	5′-GGGTGCCATCAGGGTTGAG-3′
CYP7B1	5′-TCAGATGCAAAGACGGTCAGA-3′	5′-TTCATGCCCGTAGTATTTTTTCAG-3′
ACAT2	5′-GCCCCAGCCGACATTTT-3′	5′-GTGCAGTGTGAAGCCTTGACTT-3′
ABCA1	5′-ATCTCATAGTATGGAAGAATGTGAAGCT-3′	5′-CGTACAACTATTGTATAACCATCTCCAAA-3′
ABCG5	5′-CGCAGGAACCGCATTGTAA-3′	5′-TGTCGAAGTGGTGGAAGAGCT-3′
LDL-r	5′-CAGCCGATGCATTCCTGACT-3′	5′-AGTTCATCCGAGCCATTTTCAC-3′
SR-B1	5′-GTTGGTCACCATGGGCCA-3′	5′-CGTAGCCCCACAGGATCTCA-3′
ApoA1	5′-AATGGGACAGGGTGAAGGA-3′	5′-TGAACCCAGAGTGTCCCAGTT-3′
ApoB	5′-TCCTAACATCATTGTGCCTTCAT-3′	5′-CCTTGAAATCTGGGAGGGAAAACT-3′
LXRα	5′-AGCAACAGTGTAACAGGCGCT-3′	5′-GTGCAATGGGCCAAGGC-3′
FXR	5′-TGACAAAGAAGCCGCGAAT-3′	5’-TGTAATGGTACCCAGAGGCCC-3′
RXRα	5′-CGCAAAGACCTGACCTACACC-3′	5′-TCCTCCTGCACGGCTTCCC-3′
SREBP2	5′-AGCTGGCAAATCAGAAAAACAAG-3′	5′-CGATCTTCAAGTCCACATCACTGT-3′
PPARα	5′-TCTCTTCCCAAAACTCCTTCA-3′	5′-GCACGAGCTGCGCATGCTC-3′
PPARγ	5′-TCA TGA CCA GGG AGT TCC TCA-3′	5′-TCATCTAATTCCAGTGCATTGAACTT-3′

Courtaboeuf, France) following the manufacturer's instructions. The NanoDrop apparatus (ThermoFisher Scientific, Cergy Pontoise, France) was used for determining the concentration of RNA in ng/μL. For the reverse transcription, 1 μg of total RNA was reverse transcribed at 37°C for 120 minutes using the High Capacity cDNA Reverse Transcription kit (Applied Biosystems, Courtaboeuf, France) according to the manufacturer's instructions. Real-time semiquantitative analysis was performed with the Abi PRISM 7900 sequence detection system (Applied Biosystems). The PCR amplification was performed using Syber PCR master mix (Qiagen) in a final volume of 25 μL. Sequences for the forward and reverse primers of different genes studied in the present study are listed in Table 2. The relative mRNA quantification of the target gene was made by using the comparative $\Delta\Delta$CT-method [35]. Data were first normalized to an endogenous reference (HPRT: hypoxanthine-guanine phophoribosyltransferase, a housekeeping gene) and expressed as the level relative to the uncontaminated controls (mean ± SD; $n = 10$).

2.9. Determination of Inflammatory Mediators in Intestine. Mucosal samples were obtained by scraping the rat terminal ileum at euthanasia and were kept at 80°C until analysis. Mucosal protein extracts were obtained from tissue homogenates performed using ribolyser (FastPrep 120, ThermoSavant, ThermoScientific, Cergy Pontoise, France) in phosphate buffer (pH = 7.4, PBS, Gibco, Invitrogen, Cergy Pontoise, France) containing a protease inhibitor cocktail (0.5 mL/100 mL, Sigma, L'Isle D'Abeau Chesnes, France).

This step was followed by a centrifugation step (10000 g, 10 minutes). Tissue levels of cytokines were measured by ELISA assays: TNFα, IFNγ, and IL-10 were measured using Duoset kit ELISA (R&D systems, Lille, France) and CCL-2 using the Kit rat MCP-1 (Clinisciences, Montrouge, France). To ensure a higher sensitivity and a much greater dynamic range than that of classical colorimetric revelation by tetramethylbenzidine (TMB) substrate, a chemiluminescent substrate (luminol/peroxide substrate) is added to the wells (Glo Substrate, R&D systems, Lille, France). The results were expressed per mg of protein determined with Bradford assay (Sigma, L'Isle D'Abeau Chesnes, France).

2.10. Expression of Enzymes of Xenobiotics Metabolism Measured by Western Blotting on Liver and Kidney Samples. Proteins from tissue homogenates (microsome or cytosol) were prepared as described in [23]. These proteins were loaded, separated by 10% SDS-polyacrylamide gel electrophoresis and transferred onto nitrocellulose membrane. The membranes were blocked for 1 h in 5% nonfat dry milk in TBS. The blots were incubated overnight with antibodies diluted in 2% nonfat dry milk in TBS at 4°C. Microsomal CYP3A1 and CYP3A2 were detected using rabbit polyclonal antibodies (Abcam, Paris, France). Microsomal CYP2C11 was detected using goat polyclonal antibodies (Daiichi Pure Chemicals, Tokyo, Japan). Measurements of microsomal (CYP3A1, CYP3A2, CYP2C11, and UGT2B1) and cytosolic (GST2a) enzymes were detected and measured as described [36]. Microsomal UGT2B1 was detected using goat polyclonal antibodies and rabbit polyclonal antibodies, respectively (Santa Cruz Biotechnology, Heidelberg, Germany). Cytosolic GST2a was detected using goat antibody (Oxford Biomedical Research, Oxford, USA). Immune complexes were revealed by rabbit anti-goat IgG and goat anti-rabbit IgG (Santa Cruz Biotechnology) coupled to horseradish peroxidase (HRP) and the luminol derivative of Immobilon Western (Millipore, Billerica, USA). Samples were normalized to glyceraldehyde 3-phosphate dehydrogenase (GAPDH) which was detected using rabbit anti-rat antibody (Santa Cruz Biotechnology). Reaction intensity was determined by computer-assisted densitometry (Fuji Las3000, Raytest, France). Samples were normalized to glyceraldehyde 3-phosphate dehydrogenase (GAPDH).

2.11. Xenobiotic Metabolism Enzyme Activity in the Liver. Freshly prepared microsomal fractions were used to measure testosterone hydroxylase activity [36]. The enzymatic activity of 2α-testosterone hydroxylase (CYP2C11) and 6β-testosterone hydroxylase (CYP3A1/2) was expressed as picomoles per minute per whole liver and normalized to that of the noncontaminated group.

2.12. Cholesterol Metabolism Enzyme Activity in the Liver. The specific activities of cytochromes P450 CYP27A1 and CYP7A1 were assessed, respectively, on hepatic mitochondrial and microsomal fractions, with a radioisotopic method [37]. Enzymatic activity was expressed as picomoles per minute per milligram. The results are expressed as mean ± SEM of 6 animals.

2.13. Antioxidant Status in the Brain. The tissues were prepared as described in [30]. Each cerebral sample was measured in duplicate. The tissues were homogenized in ice-cold 0.1 M phosphate-buffered saline (PBS, pH 7.4) containing 1 mM EDTA. The homogenates were centrifuged at 10000 g for 15 min at 4°C, and the supernatants were collected for analyses. Protein concentrations were determined by Bradford method using bovine serum albumin as a standard. The activity of CAT (catalase), SOD (superoxide dismutase), glutathione peroxidase (GPx), and total glutathione (GSH) was determined with commercial kits (Bertin Pharma, Montigny-le-Bretonneux, France).

For CAT activity, the method is based on the reaction of the enzyme with methanol in the presence of an optimal concentration of H_2O_2. The formaldehyde produced is measured spectrophotometrically with 4-amino-3-hydrazino-5-mercapto-1,2,4-triazole (Purpald) as the chromogen. The CAT activity was expressed in nmol of formaldehyde per min per mg protein.

SOD activity is assessed by using a tetrazolium salt for detection of superoxide radicals generated by xanthine oxidase and hypoxanthine. The SOD assay measures all three types of SOD (Cu/Zn-, Mn-, and Fe-SOD). One unit of SOD is defined as the amount of enzyme needed to exhibit 50% dismutation of the superoxide radical. The enzyme units were recorded as U per mg protein.

GPx activity was indirectly measured by a coupled reaction with glutathione reductase (GR). Oxidized glutathione (GSSH), produced upon reduction of hydroperoxyde by GPx, is recycled to its reduced state by GR and NADPH. The oxidation of NADPH to $NADP^+$ is accompanied by a decrease in absorbance at 340 nm, which is directly proportional to the GPx activity. The enzyme units were recorded as nmol NADPH oxidized per min per mg protein.

Cayman's GSH assay kit utilizes a carefully optimized enzymatic recycling method, using glutathione reductase for the quantification of GSH. The rate of TNB (5-thio-2-nitrobenzoic acid), produced by the reaction of the sulfhydryl group of GSH with DTNB, is directly proportional to the recycling reaction which in turn is directly proportional to the concentration of GSH. Measurement of the absorbance of TNB at 405 nm provides thus an accurate estimation of GSH. GSH is easily oxidized to the disulfide dimer GSSG. Both GSH and GSSG are measured in this assay kit and the assay reflects thus total glutathione.

2.14. Cholinergic Pathway in the Cerebral Cortex. Acetylcholine rates and acetylcholinesterase activity were measured in the entorhinal cortex with the Amplex Red Acetylcholine/Acetylcholinesterase Assay Kit (Molecular Probes, Invitrogen, Cergy Pontoise, France) as described in [38]. For both assays, samples of ~30 mg were diluted in Tris-HCl buffer (final volume of 100 μL). A 100 μL volume of 400 μM Amplex Red Reagent containing 2 U/mL of HRP, 0.2 U/mL of choline oxidase, and 1 U/mL acetylcholinesterase was

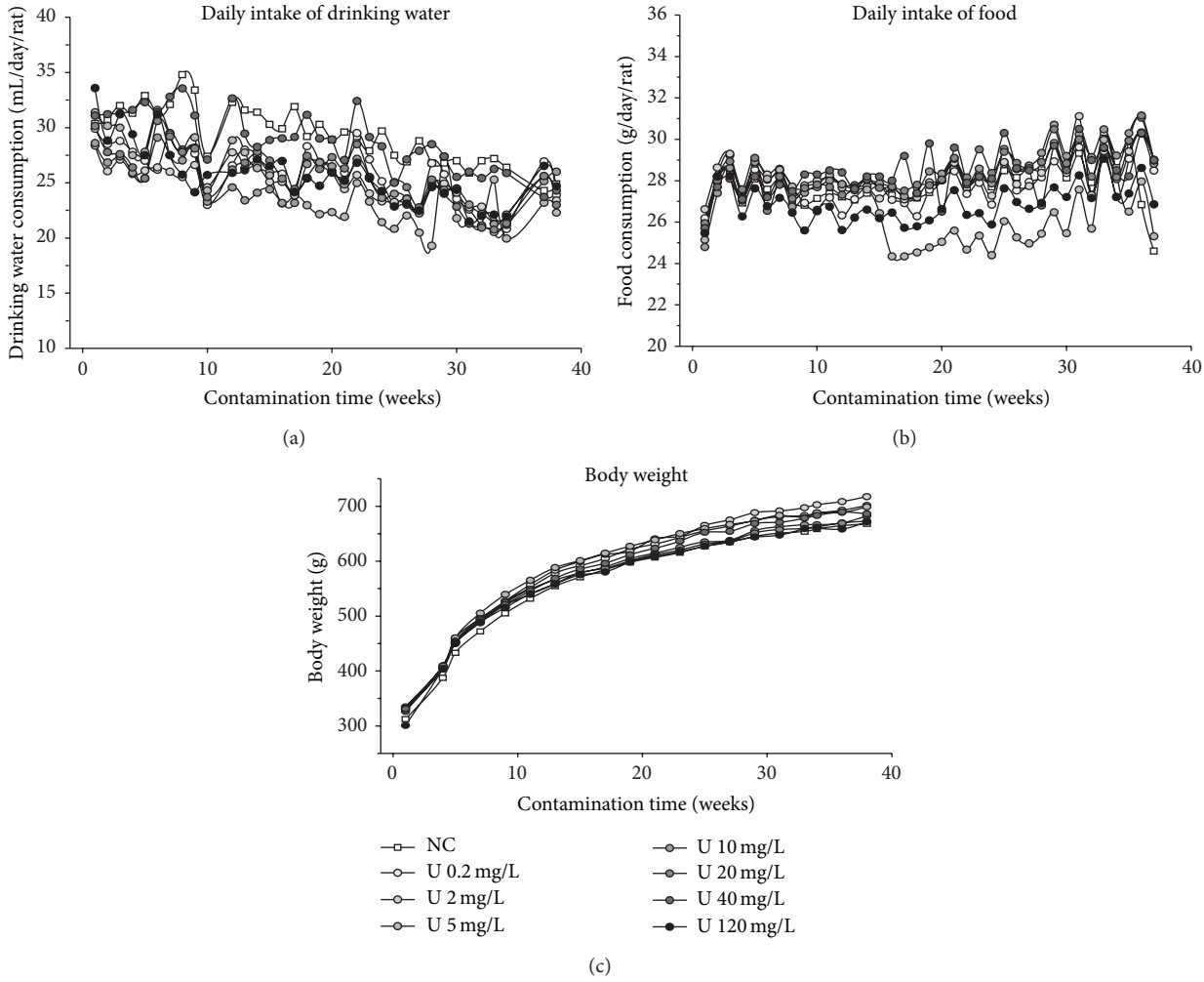

FIGURE 1: Effect of chronic ingestion of uranium on body weight, food, and drinking water intakes. Three parameters were recorded weekly in control group (open square) and in animals contaminated with uranium at 0.2, 2, 5, 10, 20, 40, or 120 mg/L (close circles). For standardization, drinking water consumption was expressed as mL per day per rat, food consumption was expressed as g per day per rat, and body weight was expressed by g. The indicated values are mean of $n = 10$ animals for body weight and $n = 5$ for daily intake of food and drinking water (two rats were housed per cage). For a clearer visualization, the SD of these values were not indicated in this figure: they were below 30% of mean values. There are no significant differences between control and contaminated groups.

added to samples. Results were expressed as μM/μg protein. Absorbance was measured at 595 nm following a 45 min incubation at room temperature. The acetylcholinesterase assay was performed with a working solution of 200 μM Amplex Red Reagent containing 2 U/mL of HRP, 0.2 U/mL of choline oxidase, and 100 μM of acetylcholine. Absorbance was measured at 595 nm after 30 minutes of incubation at room temperature. Results were expressed as μmole/mg protein/hour.

2.15. Statistical Analysis. Results are presented as mean ± SD from 5 to 10 animals, depending on the parameters measured. The control and each of the contaminated groups were compared with one-way ANOVA analysis and the post hoc Holm-Sidak method. Statistical significance was defined by a P value ≤0.05. All statistical analyses were performed with SigmaStat, Statistical Software (SPSS, Paris, France).

3. Results

3.1. Health Parameters: Body Weight Gain, Food Intake, and Water Consumption. Body weight as well as food and drinking water intakes following 9-month chronic ingestion of uranyl nitrate was given in Figure 1. For a better visualization of the different curves, only means were indicated in this figure. The mean ± SD of the control group (noncontaminated) was 24.7 ± 6.0 for drinking water intake (mL/day), 26.9 ± 2.7 for food intake (g/day), and 672 ± 73 for body weight (g), at the end of experiment (9-month contamination). The results show that these chronic contaminations did not affect general health parameters, whatever the uranium content in drinking water (from 0.2 to 120 mg/L) (one-way analysis ANOVA, NS), indicating that these different uranium levels were not toxic for animals following a chronic exposure. In addition, these values allow the calculation of daily intake of

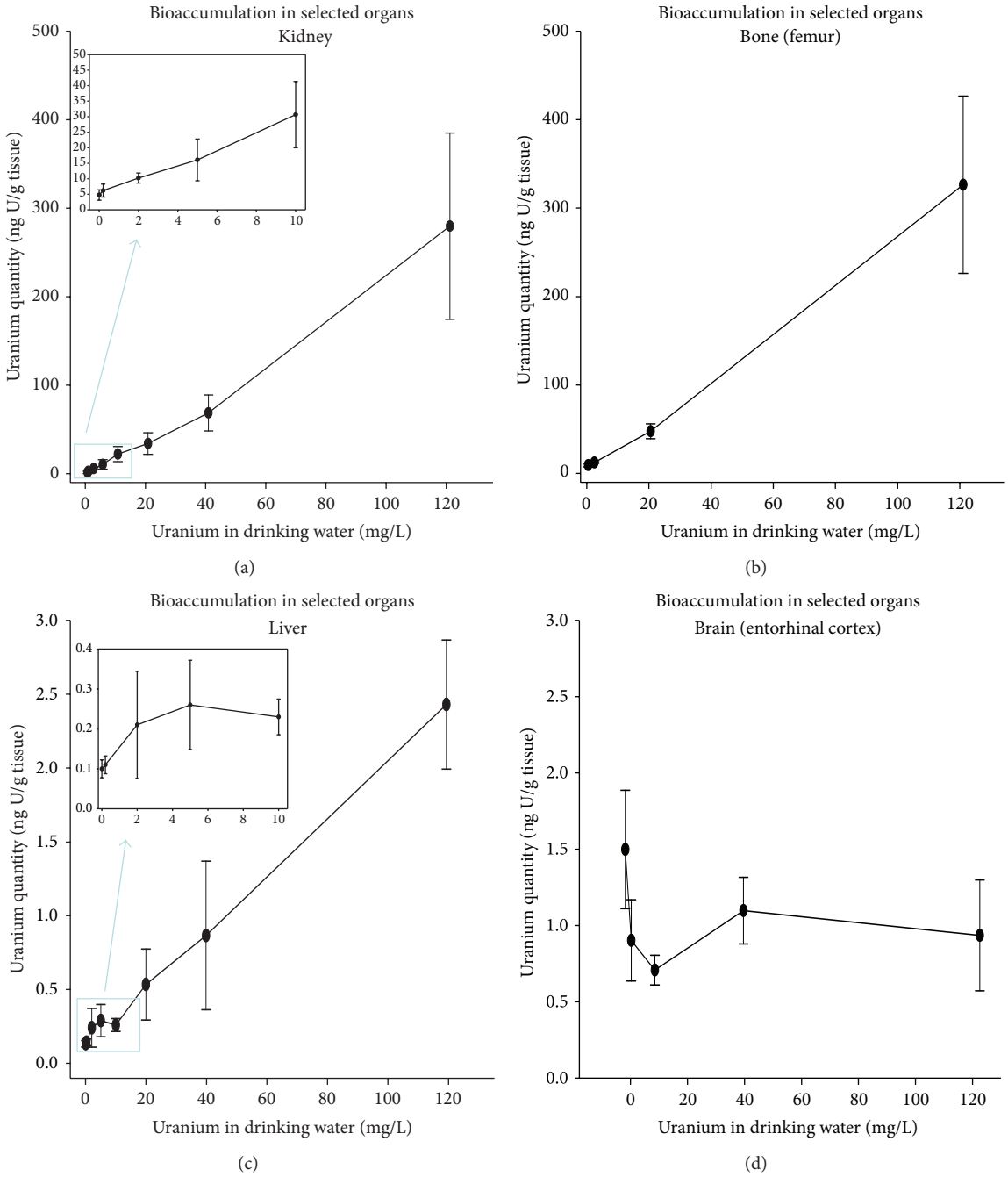

Figure 2: Bioaccumulation of uranium in organs after chronic ingestion for 9 months. Uranium was measured in organs (the kidney, femur, liver, and brain (entorhinal cortex)) by ICP-MS (see Material and Methods section for details). The results are expressed as ng/g tissue for 10 animals in the kidney and femur and for 4–6 in the liver and entorhinal cortex. The insets in the figures on the left (kidney and liver) show the increase in uranium accumulation for the lowest U levels (from 0.2 to 10 mg/L).

uranium throughout the experiment. Dependent on age and body weight, the daily intake of uranium was estimated to be between 10.8 at the beginning of experiment and 3.6 mg/kg body weight per day 9 months later (mean: 5.4 mg/kg/d) for the highest level (120 mg/L). The mean daily intake of uranium was estimated to be 0.009, 0.09, 0.23, 0.45, 0.9, 1.8, and 5.4 mg/kg/d for 0.2, 2, 5, 10, 20, 40, and 120 mg/L, respectively.

Furthermore, no changes in macroscopic appearance or weights of organs (kidney, liver, and spleen) were noted following chronic ingestion by uranium (data not shown).

3.2. Uranium Accumulation in Organs. Uranium accumulation was measured in different organs after 9-month chronic contamination by ingestion. These measurements

Table 3: Plasma parameters in rats contaminated to uranium in drinking water for 9 months.

Parameters	Noncontaminated	Uranium (mg/L)				
		0.2	10	20	40	120
Glycaemia						
Glucose (mM)	11.58 ± 1.14	11.1 ± 1.17	10.51 ± 1.36	11.74 ± 1.52	9.91 ± 0.95	10.63 ± 1.23
Lipids						
Cholesterol (mM)	1.99 ± 0.54	2.3 ± 0.63	2.33 ± 0.38	2.14 ± 0.89	2.40 ± 0.82	2.43 ± 0.76
LDL-cholesterol (mM)	0.38 ± 0.51	0.46 ± 0.22	0.48 ± 0.13	0.41 ± 0.73	0.50 ± 0.35	0.36 ± 0.38
HDL-cholesterol (mM)	1.40 ± 0.41	1.59 ± 0.38	1.65 ± 0.32	1.54 ± 0.63	1.62 ± 0.51	1.58 ± 0.89
Phospholipids B (g/L)	1.38 ± 0.25	1.54 ± 0.28	1.56 ± 0.16	1.59 ± 0.44	1.64 ± 0.38	1.72 ± 0.44
Triglycerides (mM)	1.27 ± 0.47	1.60 ± 0.73	1.53 ± 0.47	2.0 ± 0.92	1.59 ± 0.57	1.74 ± 0.54
Liver integrity						
ALAT (U/L)	43.4 ± 12.3	43.0 ± 16.1	37.6 ± 11.7	38.0 ± 10.75	37.8 ± 19.6	139.9 ± 183.0
ASAT (U/L)	118.1 ± 38.9	108.6 ± 35.4	93.1 ± 27.5	98.4 ± 26.9	96.1 ± 42.7	231.9 ± 225.0
Bilirubin (μM)	55.6 ± 4.74	60.7 ± 3.5	61.0 ± 7.6	63.2 ± 10.1	58.0 ± 4.4	60.9 ± 4.7
Renal function						
Creatinine (μM)	49.3 ± 3.32	50.2 ± 4.11	50.4 ± 4.74	52.0 ± 4.74	47.0 ± 4.4	48.9 ± 5.1
Urea (mM)	5.27 ± 0.82	5.22 ± 0.82	5.47 ± 0.89	5.81 ± 1.04	4.81 ± 0.82	5.30 ± 0.95
Iron metabolism						
Iron (μM)	31.5 ± 7.91	26.6 ± 3.16	33.4 ± 7.27	33.3 ± 5.7	27.6 ± 5.4	30.3 ± 8.5
Ferritin (ng/L)	31.1 ± 13.0	36.0 ± 21.5	39.3 ± 18.34	21.3 ± 11.4	20.3 ± 13.9	23.9 ± 18.3
Transferrin (g/L)	1.39 ± 0.13	1.49 ± 0.19	1.53 ± 0.16	1.55 ± 0.38	1.58 ± 0.22	1.60 ± 0.19
Ceruloplasmin (mg/L)	72.3 ± 8.5	70.2 ± 28.8	81.6 ± 13.6	63.5 ± 19.3	89.1 ± 17.4	90.4 ± 24.4
Red blood cells ($\times 10^{12}$/L)	9.04 ± 1.30	9.48 ± 1.9	9.28 ± 1.1	9.28 ± 2.0	9.74 ± 2.0	8.90 ± 4.6
Hematocrit (%)	43.9 ± 8.9	46.8 ± 14.2	46.4 ± 9.8	45.5 ± 8.2	47.8 ± 11.1	42.7 ± 20.6
Hemoglobin (g/L)	14.2 ± 2.21	14.7 ± 1.9	14.6 ± 2.53	14.7 ± 1.9	14.9 ± 1.9	13.8 ± 7.0

Mean ± SD, $n = 10$ per group. There are no significant differences between groups (one-way ANOVA with $P < 0.05$ significant).

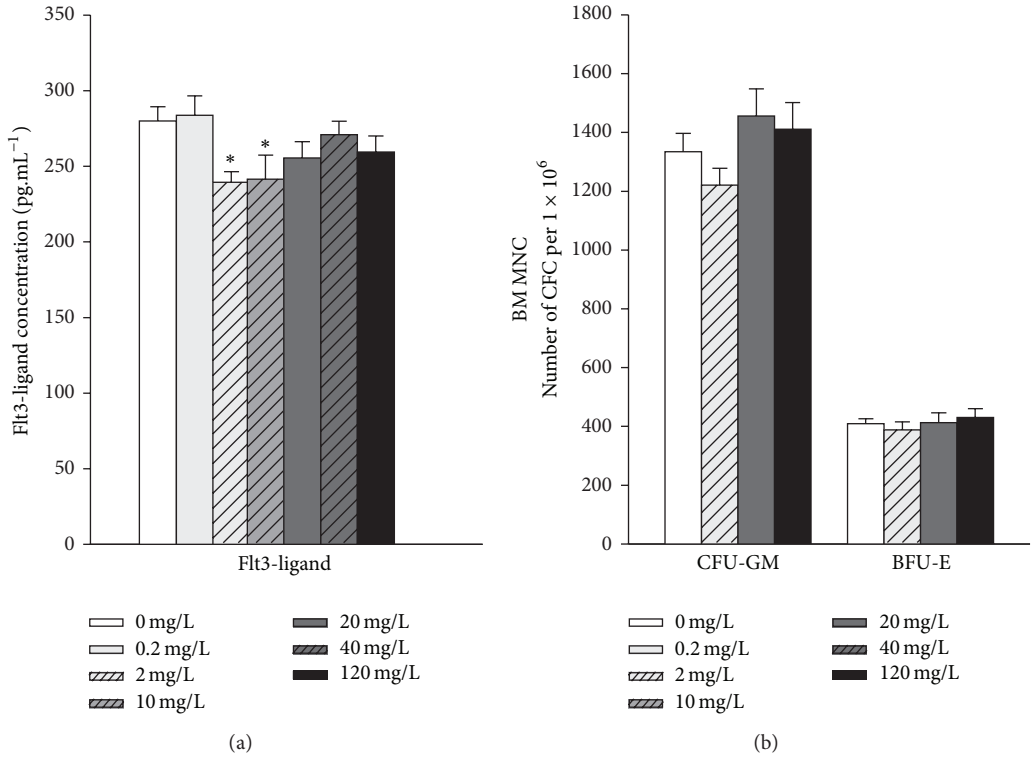

Figure 3: (a) Flt3-ligand in the plasma of animals contaminated through uranium ingestion. A significant difference was observed between 2 and 10 mg/L contaminated animals and control animals ($P < 0.05$, $n = 10$). (b) Progenitor frequency in the bone marrow of control and contaminated animals. Results did not show any significant difference between control and contaminated animals ($n = 5$ animals per group) both for burst forming units erythroid (BFU-E) and colony-forming units-granulocyte macrophages (CFU-GM).

were performed in selected organs, that is, the two storage organs of uranium, that is, kidney and bone (femur), as well as liver and brain (entorhinal cortex). Results are indicated in Figure 2. These results show an increasing accumulation of uranium in kidney and bone, depending on the ingested uranium level. These accumulations appeared to be similar in both organs at 120 mg/L. In kidney, the ingestion of the highest level of contamination (120 mg/L) led to a uranium concentration of 352 ng U/g tissue. Concerning the other organs, liver and brain, uranium accumulation was very low as compared to kidney, since the uranium quantity in these tissues was 100-fold less. Uranium quantity in liver is 2.45 ± 0.45 ng/g at 120 mg/L, 0.85 ± 0.51 ng/g at 40 mg/L, and 0.10 ± 0.02 in noncontaminated animals. The uranium accumulation at 120 mg/L corresponds to 2 orders of magnitude less than in the kidneys. The inset linked to the graph representative of uranium accumulation in liver indicates that concentration of 20 mg/L of uranium in drinking water corresponds to a threshold level for uranium accumulation in liver. In central nervous system, the quantities of uranium measured in central nervous system remained extremely low, even at the highest level of 120 mg/L. In fact, there is no dose-dependent accumulation of uranium in brain (0.98 ± 0.34 at 120 mg/L versus 1.5 ± 0.36 ng/g in control group).

3.3. Plasma Biochemical Parameters. Plasma biochemical parameters are shown in Table 3. In this table are reported various plasma parameters concerning lipid profile, liver integrity, renal function, and iron metabolism. The results show no changes following a chronic ingestion of uranium for any of these measures (one-way ANOVA analysis, NS). The absence of any difference in plasma concentrations of kidney function markers (creatinine and urea), even at the highest uranium level (120 mg/L), indicates that there was no nephrotoxicity after 9 months of chronic contamination. An increase in the ALAT (3 folds) and ASAT (2 folds) plasma concentrations reflecting liver integrity was noted in the highest group as compared with control group. However, this difference in liver function was not significant, mainly because of great variability in the 120 mg/L group.

3.4. Evaluation of Haematopoiesis. Blood cell counts were performed with differential for granulocytes, lymphocytes, monocytes, platelets, and red blood cells (RBC) (Tables 3 and 4). No significant differences were detected in circulating white blood cells, lymphocytes, granulocytes, or monocytes, regardless of the uranium exposure level. As well, there is no significant difference in RBC numbers, nor in haemoglobin concentration and in haematocrit (Table 3). Two cytokines were also measured in plasma samples, namely, Flt3-ligand and IL-7. The blood level of IL-7 did not vary significantly at any exposure level (data not shown). This indicates that uranium ingestion did not modify T lymphocyte homeostasis at the levels of uranium concentration studied. By contrast, the concentration of the Flt3-ligand was significantly lower in the plasma of animals ingesting 2 and 10 mg/L (Figure 3(a)).

Table 4: Blood cell counts and differential in rats ingesting uranium through drinking water during 9 months.

Cell lineage ($\times 10^9$ per L of blood)	Noncontaminated	Uranium (mg/L)				
		0.2	10	20	40	120
White blood cells	4.43 ± 1.58	6.19 ± 1.01	5.83 ± 2.72	5.40 ± 1.83	5.31 ± 1.64	6.20 ± 4.11
Lymphocytes	3.22 ± 1.23	3.20 ± 1.39	7.45 ± 1.33	5.85 ± 1.11	4.06 ± 1.33	3.70 ± 1.83
Granulocytes	1.07 ± 0.54	1.67 ± 0.35	1.52 ± 0.70	1.32 ± 0.28	1.15 ± 0.41	2.35 ± 2.43
Monocytes	0.08 ± 0.03	0.13 ± 0.03	0.12 ± 0.06	0.10 ± 0.03	0.10 ± 0.03	0.15 ± 0.13
Platelets	472 ± 484	603 ± 847	229 ± 351	177 ± 395	455 ± 496	165 ± 405

Mean SD, n = 9-10 per group. There are no significant differences between groups (one-way ANOVA with $P < 0.05$ significant).

This suggested that uranium ingestion induced an increase in haematopoietic activity in these animals, but only in specific contamination conditions, that is, 2 and 10 mg/L of uranium in drinking water. In order to confirm a possible effect of uranium ingestion on haematopoiesis, haematopoietic progenitor frequencies were determined both in the bone marrow and in the spleen of control animals and animals contaminated with 2, 20, and 120 mg/L. Results indicated that uranium ingestion did not induce a modification of progenitor frequency both in the bone marrow (Figure 3(b)) and in the spleen (data not shown). This suggested that the slight modifications in Flt3-ligand concentration observed in the plasma were not associated with a modification of haematopoiesis. Overall, these results suggest that whatever the uranium concentration in drinking water (including the highest uranium concentration of 120 mg/L), uranium ingestion did not modify significantly blood and bone marrow parameters.

3.5. Histological Studies. Histological analysis of intestine (ileum), liver, and kidney (renal cortex) was performed in control and contaminated animals. Figure 4 showed microphotographs of histological slides from these organs, and Table 5 reported the different microscopic evaluations for the three organs considered. Concerning the small intestine (terminal ileum), no epithelial injuries were noticed (Figure 4, compare part (a) to (b)). No microscopic anomalies were identified in muscular layers, in nervous structures, or in vessels. Small intestine wall never presented inflammatory alteration or fibrosis. Gut associated lymphoid tissue (GALT) displayed normal microscopic aspect, often with some activation signs (germinal centres). Such lack of histological lesions led to a score equal to zero for intestine regardless the uranium level in drinking water. Concerning kidney microscopic evaluation, glomerular (parts (c) and (d) of the Figure 4) and tubular (parts (e) and (f) of the Figure 4) aspects were analysed. Glomerular lesions were mostly absent (Figure 4, parts (c) and (d)). Only some scattered glomerular cysts could be noticed. Tubulointerstitial lesions remained limited, with minimal to rarely mild intensity when present (Figure 4, parts (e) and (f)). These lesions consisted of multifocal inflammatory cell infiltrates, mainly composed of lymphocytes, with few plasma cells, macrophages, and rare granulocytes. Some tubules were sometimes filled with proteinaceous, eosinophilic material (hyaline casts). Interstitial fibrosis was exceptionally noticed and remained minimal, with only narrow bands of fibrous tissue thickening rare tubular basement membranes and glomerular Bowman's capsules. Tubular necrosis was never observed, whatever the group including the highest level of uranium concentration (120 mg/L). In fact, all these features were recognized in rats of either control or contaminated groups. Tubular regeneration was slightly increased in 10 and 40 mg/L groups, in comparison to control group. Tubular inflammation was slightly increased in 0.2, 10, and 40 mg/L groups, in comparison to control group (Table 5). Surprisingly, this increase remained very limited and was not observed in 120 mg/L group (high dose).

Histological evaluation was also performed in liver (parts (g), (h), (i), and (j) of the Figure 4 and Table 5). Almost all the rats presented inflammatory cell infiltrates into hepatic parenchyma, which always remained minimal and were mainly composed of lymphocytes (mononuclear cells), with few plasma cells, some macrophages, and rare granulocytes. They could be localized in portal areas connective tissue (portal inflammation, Figure 4, part (g)) or appear as scattered and small cellular aggregates slightly distending sinusoids (intralobular inflammation, Figure 4, part (h)). These features were recognized in rats of either control or contaminated groups. Portal necrosis was never observed, whatever the group. Cytoplasmic macrovacuolation was quite regularly observed, with minimal to moderate intensity when present (Figure 4, parts (i) and (j)). Altered hepatocytes displayed in their cytoplasm small vacuoles about 3 to 5 μm in diameter, rounded, well-delimited, with empty lumen. Vacuoles were usually found in small numbers in hepatocytes. Cytoplasmic macrovacuolation was increased in contaminated groups in comparison to control group, particularly in 40 and 120 mg/L groups (Figure 4, part (j)), which suggests that it was related to uranium contamination (Table 5). One-way ANOVA analysis indicates a statistical significant difference between groups ($P < 0.05$).

3.6. Intestinal Immune System. Immune cell composition of lamina propria was investigated after a 9-month chronic ingestion of uranium. This study was performed on neutrophils, macrophages, and mast cells, all of them involved in innate immunity. Figure 5 shows the effects of uranium on the three selected immune cells after 0.2, 2, 20, and 120 mg/L, as compared with control group (NC: noncontaminated). These results indicated that number of immune cell populations did not vary after 9 months of uranium exposure, at any

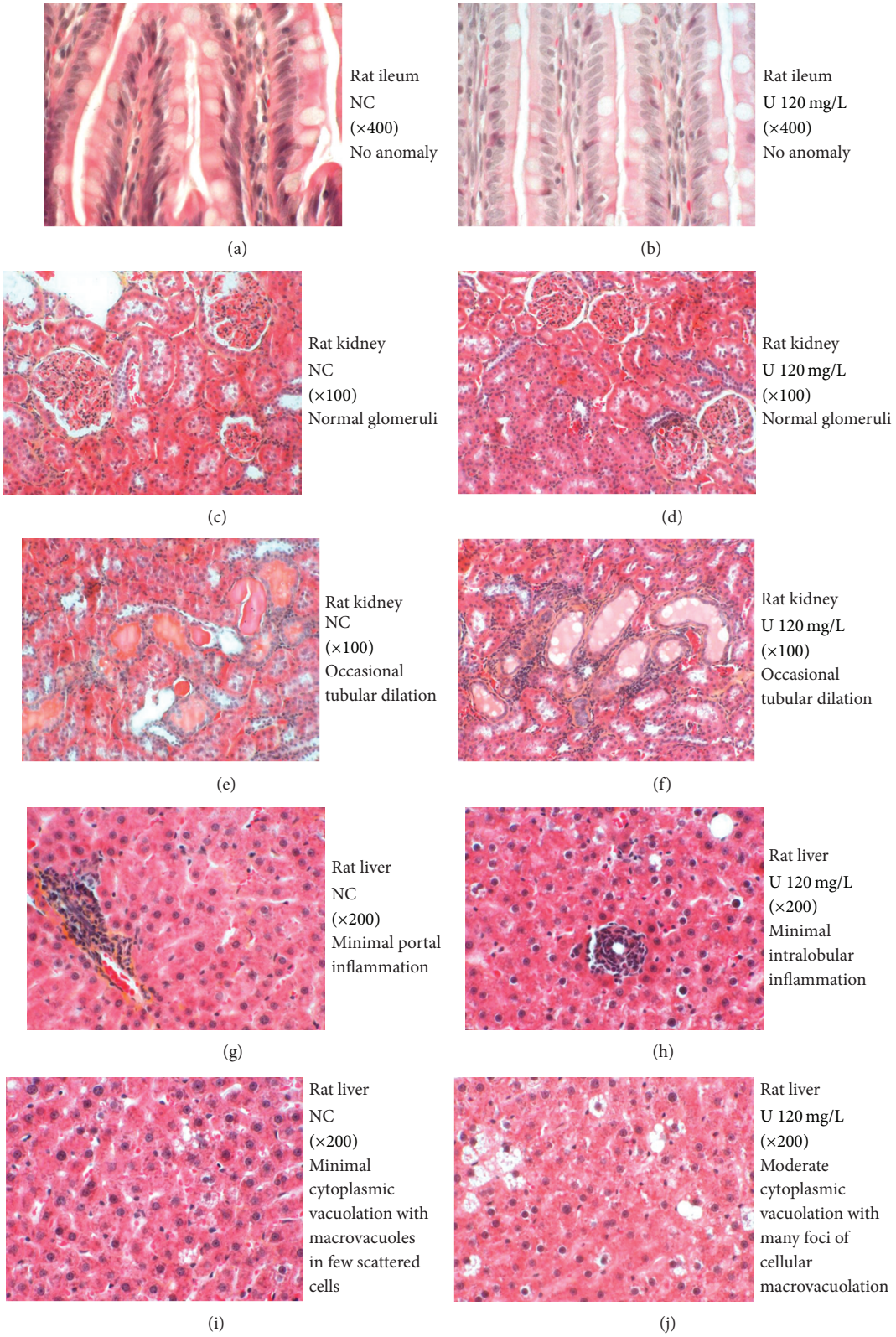

Figure 4: Histological alterations of intestinal, renal, and hepatic sections in rats receiving uranium at 120 mg/L in drinking water for 9 months. Microphotographs of rat tissues were obtained from control (NC: noncontaminated) and contaminated rat (120 mg/L uranium in drinking water). Sections were stained with hematoxylin-eosin-saffron. ((a), (b)) Intestinal longitudinal sections of rat ileum. ((c)–(f)) Histological sections of renal cortex. ((g)–(j)) Liver sections.

Table 5: Histological alterations in intestine, kidney, and liver from rats contaminated with uranium in drinking water for 9 months.

Parameters	Noncontaminated	Uranium (mg/L)			
		0.2	10	40	120
Intestine					
Villous epithelial injury	0	0	0	0	0
Villous atrophy	0	0	0	0	0
Crypt hyperplasia	0	0	0	0	0
Crypt distension	0	0	0	0	0
Goblet cell hyperplasia	0	0	0	0	0
Inflammation	0	0	0	0	0
Mucosal fibrosis	0	0	0	0	0
Kidney					
Mesangial proliferation/glomerulosclerosis	0	0	0	0	0
Glomerular cystic dilation	0.08	0	0.1	0	0
Tubular necrosis	0	0	0	0	0
Tubular regeneration	0.67	0.5	0.8	0.75	0.4
Tubular dilation	0.67	0.6	0.4	0.33	0.3
Tubular inflammation	0.83	1	0.9	1	1
Interstitial fibrosis	0.42	0.1	0.3	0.33	0
Liver					
Portal inflammation	1	1	1	1	1
Intralobular inflammation	0.92	0.9	1	0.67	0.9
Periportal necrosis	0	0	0	0	0
Intralobular necrosis	0	0	0	0	0
Cytoplasmic vacuolation	0.67	1.2	1.4	1.67*	2.2*
Fibrosis	0	0	0	0	0

Intestinal lesions scoring: group means (scores/3), with $n = 6$–8.
Renal lesions scoring: group means (scores/4), with $n = 5$-6.
Hepatic lesions scoring: group means (scores/4), with $n = 5$-6.
*$P < 0.05$ between groups (one-way ANOVA analysis).

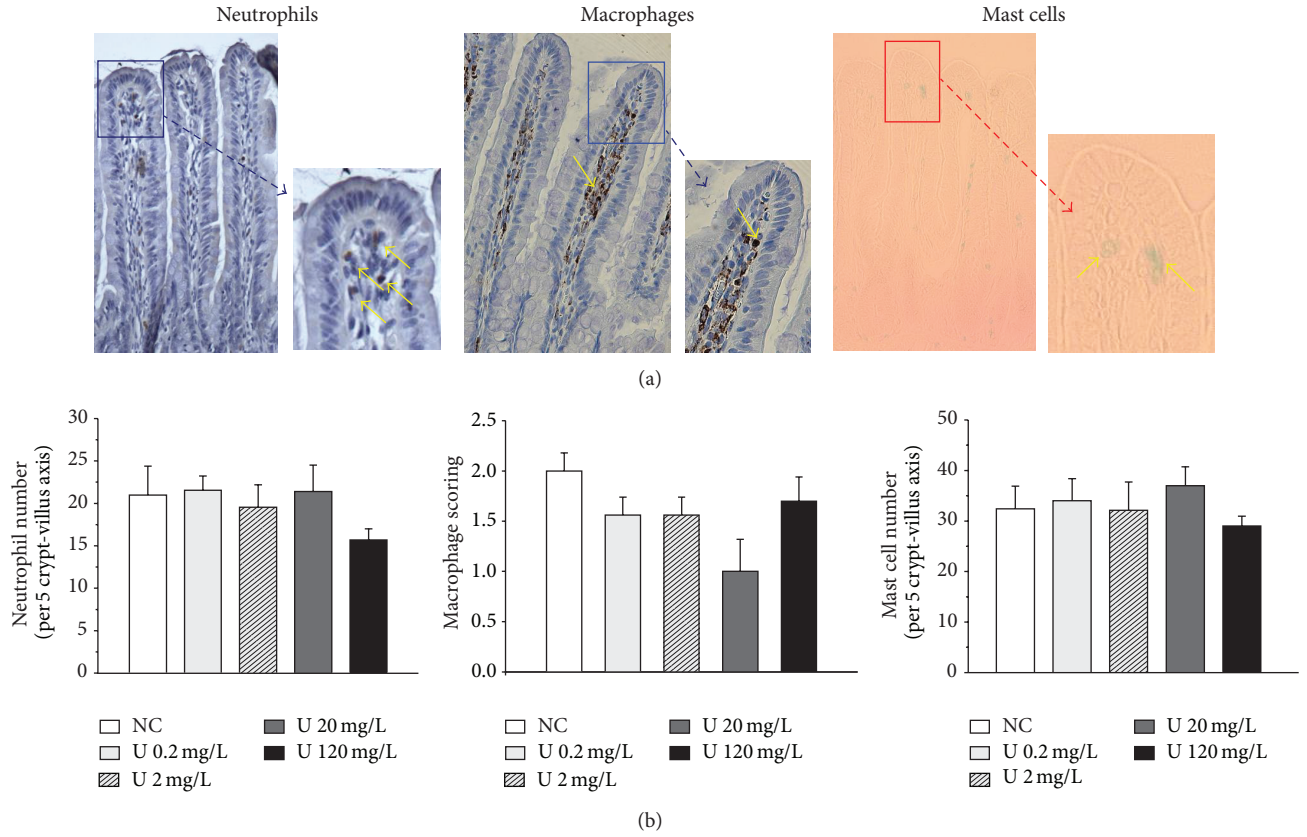

FIGURE 5: Effects of chronic uranium ingestion on immune cells in the intestinal mucosa in rats receiving contaminated drinking water during 9 months. Micrographs were obtained from control animals (objective ×20 and ×40). The brown staining indicates the cells positive for CD68 (macrophages) and for MPO (myeloperoxidase, neutrophils). Mast cells were stained with Alcian Blue technique. The positive cells were estimated per 5 villus-crypt axes, along the 60 measurements per animal, in control animals (NC: noncontaminated) and in animals contaminated with uranium (U) in their drinking water at various concentrations (0.2, 2, 20, or 120 mg/L). Data were mean ± SD of 8 rats. There is no significant difference between control and experimental groups.

exposure level (from 0.2 to 120 mg/L). The neutrophil and mast cells number in lamina propria remained constant, even at the highest level (120 mg/L). Concerning macrophages, a decrease in its network in lamina propria seemed to be induced by uranium exposure, with a diminution of 50% at 20 mg/L. However, this decrease was not significant ($P = 0.069$).

To complete this cellular study, effects of uranium were investigated on cytokine and chemokine content in small intestinal wall. The relative mRNA level of 5 cytokines (CCL-2, TNFα, IFNγ, TGFβ, and IL-10) was studied in intestinal mucosal extracts of control rats and in rats contaminated at 0.2, 2, 20, and 120 mg/L. The tissue protein level was also studied for CCL-2, TNFα, IFNγ, and IL-10. Figure 6 represents the results of gene (Figure 6, top) and protein expression (Figure 6, bottom) for CCL-2, TNFα, IFNγ, and IL-10. In the top part of Figure 6, we observe an increase in gene expression for the four cytokines studied, which was significant ($P < 0.05$) for uranium levels in drinking water 20 mg/L for IFNγ, IL-10, and CCL-2. Modification of TNFα gene expression was observed only at 120 mg/L. However, this activation is not general for all cytokines because no changes were observed in the mRNA levels of TGFβ (data not shown). Experiments were then performed to determine whether these differences in mRNA levels were associated with similar differences in protein levels. The results are indicated in the part (b) of Figure 6. Contrary to cytokine mRNA expression, which increased with uranium exposure, uranium seemed to induce an inhibition of protein levels for three cytokines studied (IFNγ, IL-10, and TNFα). These variations were also observed for uranium levels >20 mg/L. However, this inhibitory effect was not observed for the highest uranium level, for which a return to control values and even an overincrease were noted for three cytokines (IFNγ, CCL-2, and TNFα).

3.7. Xenobiotic Metabolism in Liver and Kidney. Xenobiotic metabolizing enzymes (XME) were studied in the liver and kidneys, the major organs involved in detoxification. The levels of major enzymes and proteins involved in the three phases of xenobiotic metabolism, phase I (CYP 3A2, CYP2C11), phase II (GSTA2, UGT2B1), and phase III (MRP2, MDR1), were studied in control and uranium-exposed rats. Figure 7 illustrates the effects of uranium exposure on

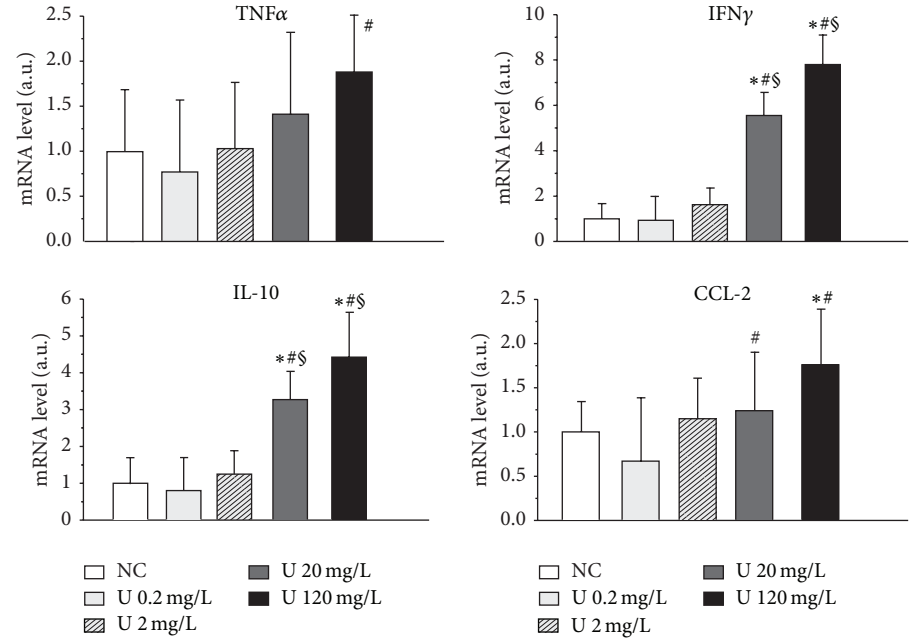

(a) Gene expression

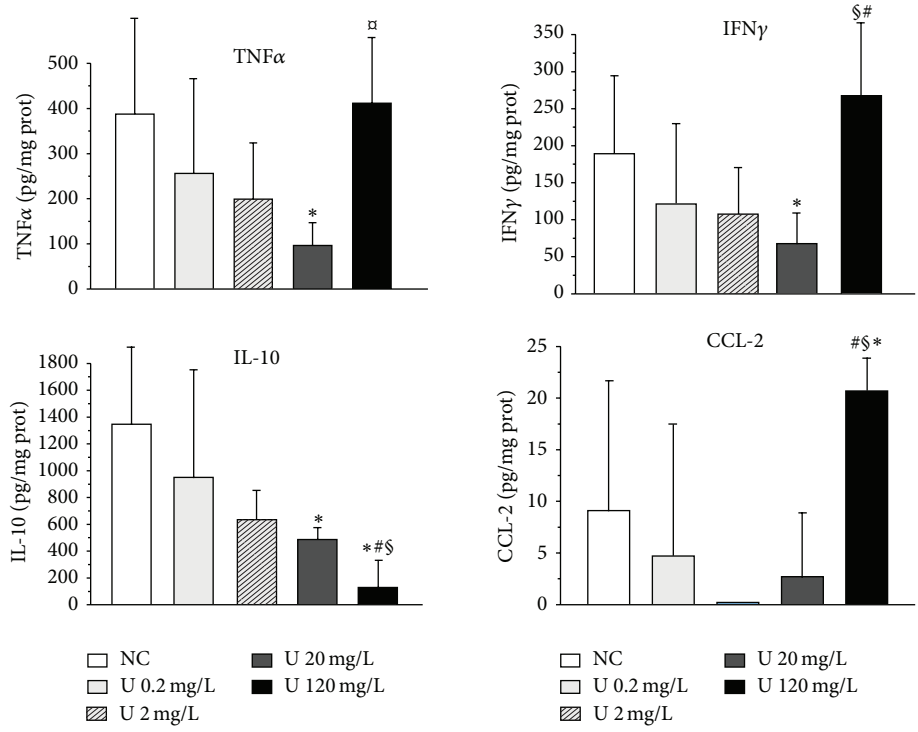

(b) Protein expression

Figure 6: Effects of uranium on cytokine gene and protein expression in rat intestine. Expression was measured in samples from control animals (NC: noncontaminated) and animals contaminated by uranium (U) in their drinking water at various concentrations (0.2, 2, 20, or 120 mg/L). Data are mean ± SD of 9-10 animals. (a) Gene expression: the mRNA levels are expressed as a ratio to the reference gene HPRT (hypoxanthine-guanine phophoribosyltransferase, a housekeeping gene). (b) Protein expression: tissue protein levels are expressed in pg/mg protein. $^{*}P < 0.05$: significantly different from control values. $^{\S}P < 0.05$: significantly different from the U 0.2 mg/L group. $^{\#}P < 0.05$: significantly different from the U 20 mg/L group.

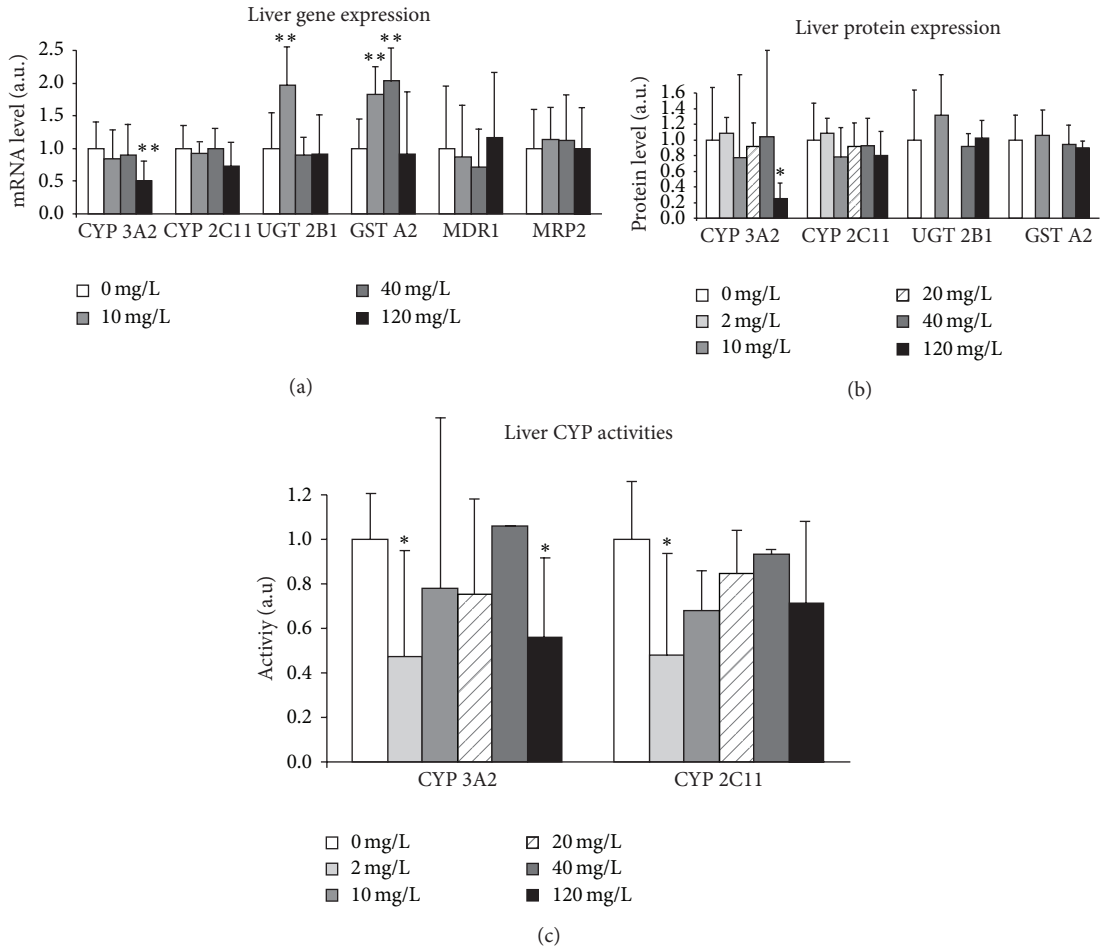

Figure 7: Effects of uranium on enzymes of xenobiotic metabolism in the liver. The molecules of phases I, II, and III of xenobiotic metabolism were measured in control animals (NC: noncontaminated) and in animals contaminated by uranium (U) in their drinking water at various concentrations (10, 40, or 120 mg/L). Gene expression: the mRNA levels are expressed as a ratio to the reference gene HPRT (hypoxanthine-guanine phophoribosyltransferase, a housekeeping gene). Data are mean ± SEM of 8 animals. Protein expression: protein levels are expressed as a ratio to the reference gene GAPDH (glyceraldehyde 3-phosphate dehydrogenase, a housekeeping gene). Data are mean ± SD of 8 animals. CYP activities: enzyme activities are expressed in picomoles per minute per whole liver and values are normalized to the noncontaminated group. Data are mean ± SD of 6 animals. $^{*}P < 0.05$: significantly different from control values. $^{**}P < 0.01$: significantly different from control values.

cytochrome P450, expressed mainly in the liver. Some variations of enzyme activity were observed starting from 2 mg/L of uranium in drinking water, that is, for CYP3A2 (−53%, $P < 0.05$) and CYP2C11 (−52%, $P < 0.05$) (Figure 7(c)), but these effects were not observed at the mRNA and protein levels. By contrast, gene expression of phase II enzymes was modified at 10 (GSTA2, UGT2B1) and 40 mg/L (GSTA2) (data not shown). It appears that 120 mg/L induced major effects, since a drastic decrease in CYP3A2 was observed concomitantly in the levels of mRNA (−50%, $P < 0.01$), protein (−75%, $P < 0.05$), and enzyme activity (−44%, $P < 0.05$) in the rat liver. This indicated that uranium exposure at this concentration altered a major enzyme of the xenobiotic system which could impact the detoxification function in the liver.

To determine if uranium also targets this detoxification system in the kidneys, the classical storage and target organ of this radionuclide, XME (CYP 3A2 and CYP2C11 for phase I, UGT2B1, GSTA2, and ST1A1 for phase II, and MDR1 and MRP2 for phase III), was studied in the renal cortex. Figure 8 shows that there was no effect on several phase I (CYP 3A2, CYP2C11) and II (UGT2B1, GSTA2) enzymes. Thus, in contrast to the results observed in liver, this figure indicates that renal mRNA (Figure 8(a)) and protein (Figure 8(b)) levels of CYP3A2 did not change in the kidneys of rats exposed to uranium, at any exposure level. Moreover, there were no changes in UGT2B1 and GSTA2 phase II enzymes, which are more abundant in the kidneys than phase I enzymes. Only an increase, apparently dose-dependent, in STA1 gene expression was observed from 10 mg/L.

3.8. Cholesterol Metabolism in Liver. To complete the evaluation of liver function, we investigated the different steps of cholesterol metabolism in the liver (biosynthesis, catabolism, storage, transport, and regulation). The gene expressions of enzymes and transcription factors involved

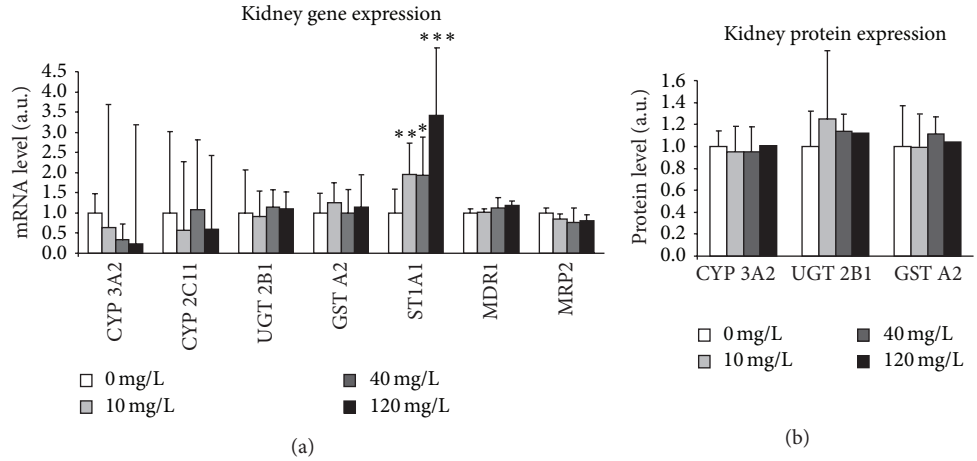

Figure 8: Effects of uranium on enzymes of xenobiotic metabolism in the kidneys. The molecules of phases I, II, and III of xenobiotic metabolism were measured in control animals (NC: noncontaminated) and in animals contaminated by uranium in their drinking water at various concentrations (10, 40, or 120 mg/L). Gene expression: the mRNA levels are expressed as a ratio to the reference gene HPRT (hypoxanthine-guanine phophoribosyltransferase, a housekeeping gene). Data are mean ± SD of 8 animals. Protein expression: protein levels are expressed as a ratio to the reference gene GAPDH (glyceraldehyde 3-phosphate dehydrogenase, a housekeeping gene). Data are mean ± SD of 6 animals. $^{*}P < 0.05$, $^{**}P < 0.01$: significantly different from control values. $^{***}P < 0.001$: significantly different from control values.

in this metabolism in the liver of control and contaminated animals with uranium at 0.2, 20, 40, and 120 mg/L were indicated in Figure 9. Any modification was noted for the biosynthesis step. Concerning the catabolism step of cholesterol metabolism, the results show that uranium affected the relative mRNA level of CYP27A1 in the 120 mg/L group (+31%, Figure 9). This highest level of uranium induces also an increase in gene expression of some molecules involved in storage (ACAT2, +70%), in storage (ABCA1, +70%), and in regulation (LXR, RXR, and SREBP2, between 30 and 40%) processes.

These results were completed by measurement of enzyme activity of the two major cytochrome P450 of type 27A1 (CYP27A1) and 7A1 (CYP7A1) (Figure 10). No change was observed for CYP27A1, but uranium affected the activity of CYP7A1 (by a multiple of 6.5, Figure 10).

3.9. Cholinergic Pathway in the Entorhinal Cortex. The cholinergic system in the brain (entorhinal cortex) was examined to investigate the molecular effects of uranium that might underlie central nervous system dysfunction. Figure 11 illustrates the results obtained after a 9-month contamination. Chronic ingestion of uranium did not modify acetylcholine content in the cortex at any exposure level. We did, however, note a dose-independent diminution of acetylcholinesterase activity after uranium contamination (−15%).

3.10. Antioxidant Enzymes in the Entorhinal Cortex. Because oxidative stress is a potential mechanism of uranium neurotoxicity, we investigated the effects of uranium on the brain by studying antioxidant defenses. Uranium affected each enzyme studied, but at different thresholds and in opposite directions (Figure 12). It induced a slight increase in catalase activity (+20% at 120 mg/L) and GSH content (+20% at 2 mg/L) and a dose-dependent activation effect on glutathione peroxidase (+68% at 2 mg/L and +90% at 120 mg/L). On the other hand, it inhibited superoxide dismutase activity at all uranium concentrations, in a dose-independent manner (~ −50%).

4. Discussion

The primary objective of this experimental study was to obtain new data to improve our knowledge of the long-term effects of uranium chronically ingested in drinking water. More specifically, the purpose of this work was to (i) determine the possible thresholds for functional (molecular or cellular) and for pathological (tissue and general health) effects of uranium and (ii) establish the differential sensitivity of the different organs to uranium. The strength of the present study lies in its combination of a wide range of uranium levels (0.2, 2, 5, 10, 20, 40, or 120 mg/L), a large panel of target organs (the small intestine, liver, kidneys, hematopoietic tissue, and brain), and complementary levels of biological analyses (molecular, functional, structural, and pathological).

Concerning the intestines, a uranium accumulation was previously demonstrated in the lamina propria of intestinal wall, near the immune cells [26] and in Peyer's patches [27], a site specialized in the immune response of the small intestine against pathogens. The objective of the present study was thus to investigate uranium effects on immune function of intestinal mucosa due to this specific localization of uranium. The kidneys and the liver are the major organs involved in detoxification processes of endo- and xenomolecules, which constitute in return the primary function of these organs. Thus, the present investigation of uranium effects on the kidneys and the liver was based on the different phases of the xenobiotic metabolism. In addition, cholesterol metabolism

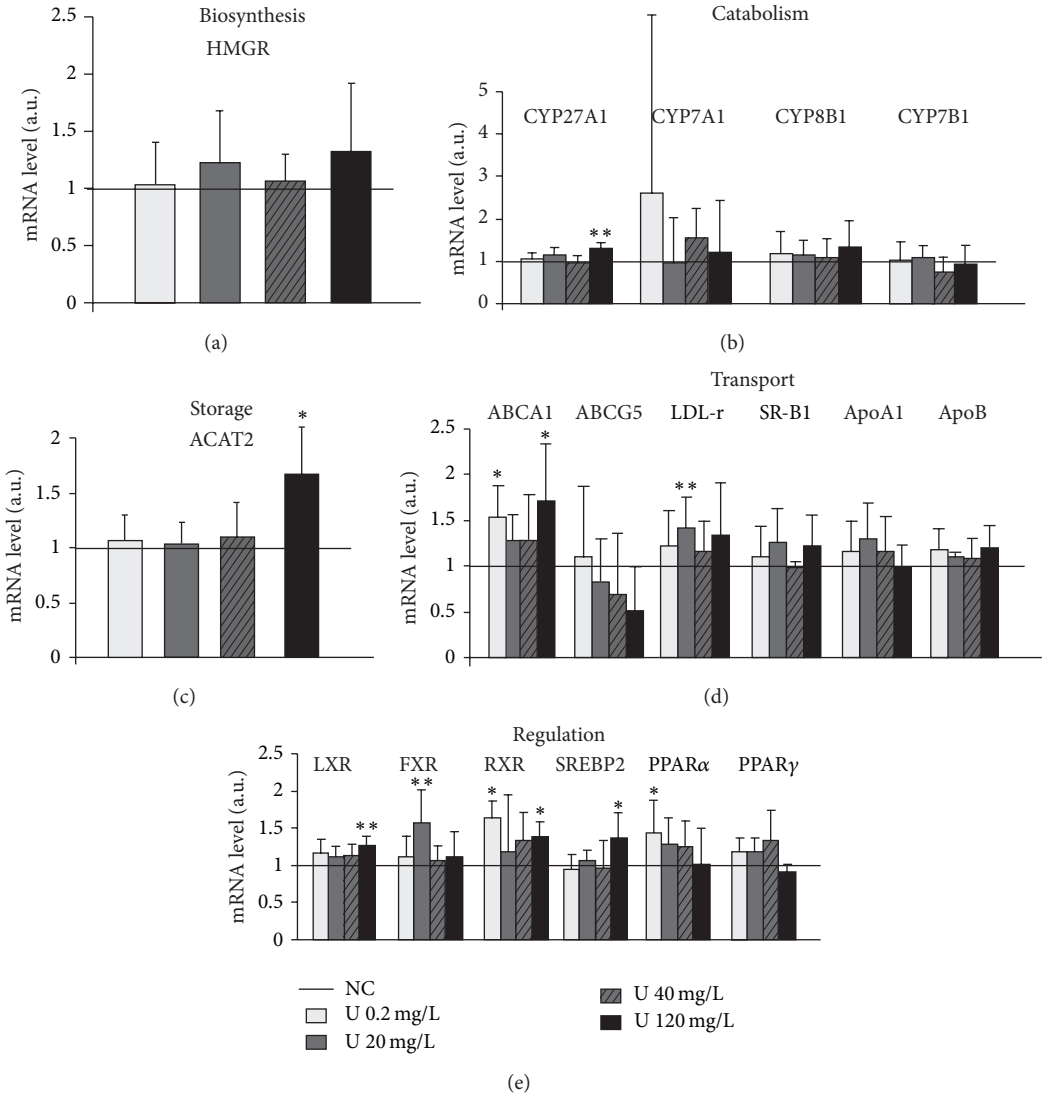

Figure 9: Effects of uranium on gene expression of enzymes of cholesterol metabolism in the liver. The gene expressions were measured in control animals (NC: noncontaminated) and in animals contaminated by uranium in their drinking water at various concentrations (0.2, 20, 40, and 120 mg/L). The mRNA levels are expressed as a ratio to the reference gene HPRT (hypoxanthine-guanine phophoribosyltransferase, a housekeeping gene). Data are mean ± SD of 8 animals. $^{*}P < 0.05$, $^{**}P < 0.01$: significantly different from control values.

was studied in the liver, since this organ plays the central role in whole organism concerning this metabolism. The effects of uranium on the central nervous system were evaluated *via* two mechanisms, the uranium-induced oxidative stress and the cholinergic system. Indeed, a possible mechanism of uranium effects observed in cognitive functions may be due to the oxidative stress induced by reactive oxygen species imbalance [30]. A uranium-induced chronic cerebral oxidative stress may have subsequent consequences on brain function, with possible development of neurological disorders [39]. Effects of uranium on cholinergic system may lead to impairment in learning and attention [40] or promote neurodegenerative pathologies such as Alzheimer's disease. Finally, effects induced by uranium were measured in hematopoietic cells, since uranium accumulated in the bones and kidneys following chronic contamination [25, 41].

As indicated above, this study investigated several parameters of specific function(s) of all organs considered, to ensure the absence of possible consequences of uranium exposure on them. The present study did demonstrate that uranium induces some effects at the molecular level on the five considered organs.

Investigation of cholesterol metabolism in the liver indicated variations of mRNA levels for the molecules involved, but most uranium-induced effects were noted at 120 mg/L and led to minor modifications in catabolism, storage, transport, and regulation processes. These results indicate that uranium targets cholesterol metabolism at mRNA level, as previously reported [42]. Nevertheless, these biological effects were not harmful as they had no impact on the plasma lipid profile. Concerning the liver xenobiotic metabolism, some slight effects on mRNA levels were reported at low

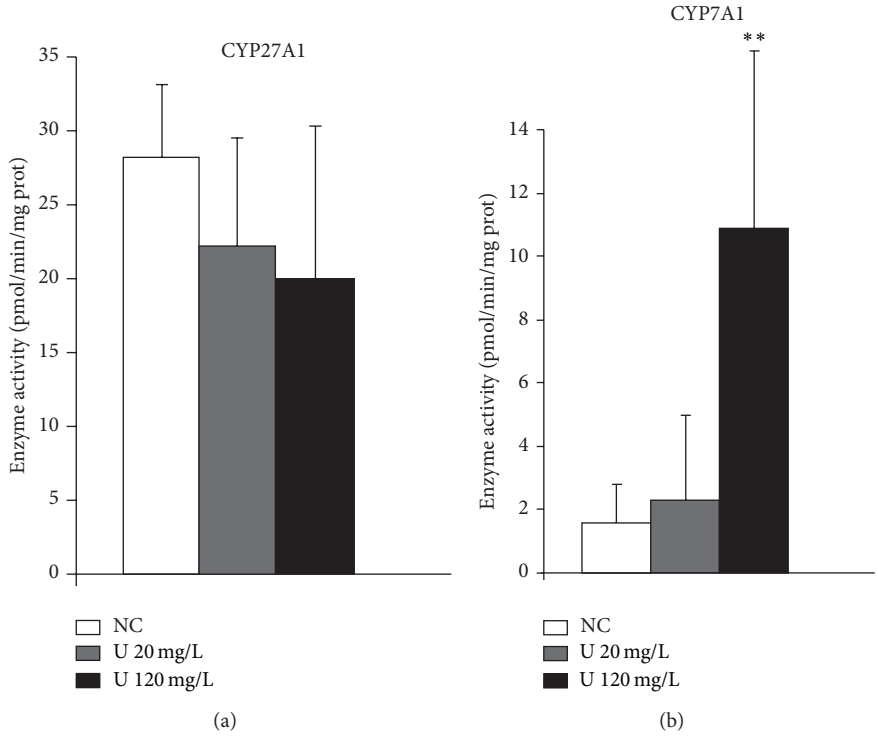

Figure 10: Effects of uranium on enzyme activity of enzymes of cholesterol metabolism in the liver. Enzyme activity is expressed as picomoles per minute per milligram total protein. Data are mean ± SEM of 6 animals. $^{**}P < 0.01$: significantly different from control values.

exposure (2 mg/L) and more important effects (mRNA, proteins, and activity) on a specific enzyme (CYP3A) with a greater variation at high exposure (120 mg/L). These results supplemented previous studies of xenobiotic metabolism in the liver [23, 36]. Surprisingly, the present study did not observe these effects on xenobiotic metabolism in the kidney, the organ considered most sensitive to uranium. This lack of molecular effects on the kidneys is in accordance with previous results obtained by Linares et al., which demonstrated induction of oxidative stress only at uranium levels above 400 mg/L [43]. In the small intestine, changes of protein and mRNA tissue levels of cytokines were observed for medium (20 mg/L) and high (120 mg/L) uranium levels, demonstrating effect of uranium on inflammatory mediators in the intestines, corroborating the hypothesis that the intestinal system may be a biological target of uranium following ingestion. However, these variations should not be considered adverse effects, given that the number of immune cells in the intestinal mucosa did not change significantly. The only change was a nonsignificant 50% diminution of macrophages, as mentioned previously [20]. Biological effects of uranium on the brain were estimated by investigating the cholinergic pathway and oxidative stress. For the former, a non-dose-dependent reduction in acetylcholinesterase activity began at 0.2 mg/L, the lowest exposure level. Such decreased acetylcholinesterase activity was already reported [38]. Modifications of the activity of antioxidant enzymes were also observed at that level. At higher exposures (2, 20, and 120 mg/L), the activity of 3 enzymes (of the 4 studied) was modified. Other recent studies have reached the same conclusions, reporting opposite effects by uranium on the antioxidant status of the brain, depending on radiological activity [30] and uranium levels [44]. As for the other organs, these modifications need not be considered deleterious, since both antioxidant enzyme activity and acetylcholine levels were not reduced in the brain. Finally, no real damages to hematopoiesis were observed. This finding suggests that the slight modifications of the Flt3-ligand concentration in the blood were not linked to a major modification of hematopoietic activity.

Overall, these results indicate that uranium ingestion is able to induce subtle but significant effects at the molecular level, mainly on mRNA expression, which does not have any deleterious consequences.

Different thresholds may be deduced on the basis of these observed molecular effects: 20 mg/L for the intestine, >10 mg/L for the kidneys, >2 mg/L for the liver, and only 0.2 mg/L for the brain. This indicates that the kidneys are not the organ the most sensitive to chronic contamination by uranium ingestion. The brain appears very sensitive, as several previous studies have shown [44–46]. At high doses, uranium may induce adverse effects including impairment of memory [47] and locomotion [45]. Surprisingly, these results demonstrated that there is no clear positive relationship between uranium accumulation and its biological effects. Indeed, this relation appeared to be an inverse one: the organs the most affected by uranium exposure were those that did not accumulate it (1 ng/g in brain, 2.5 ng/g in

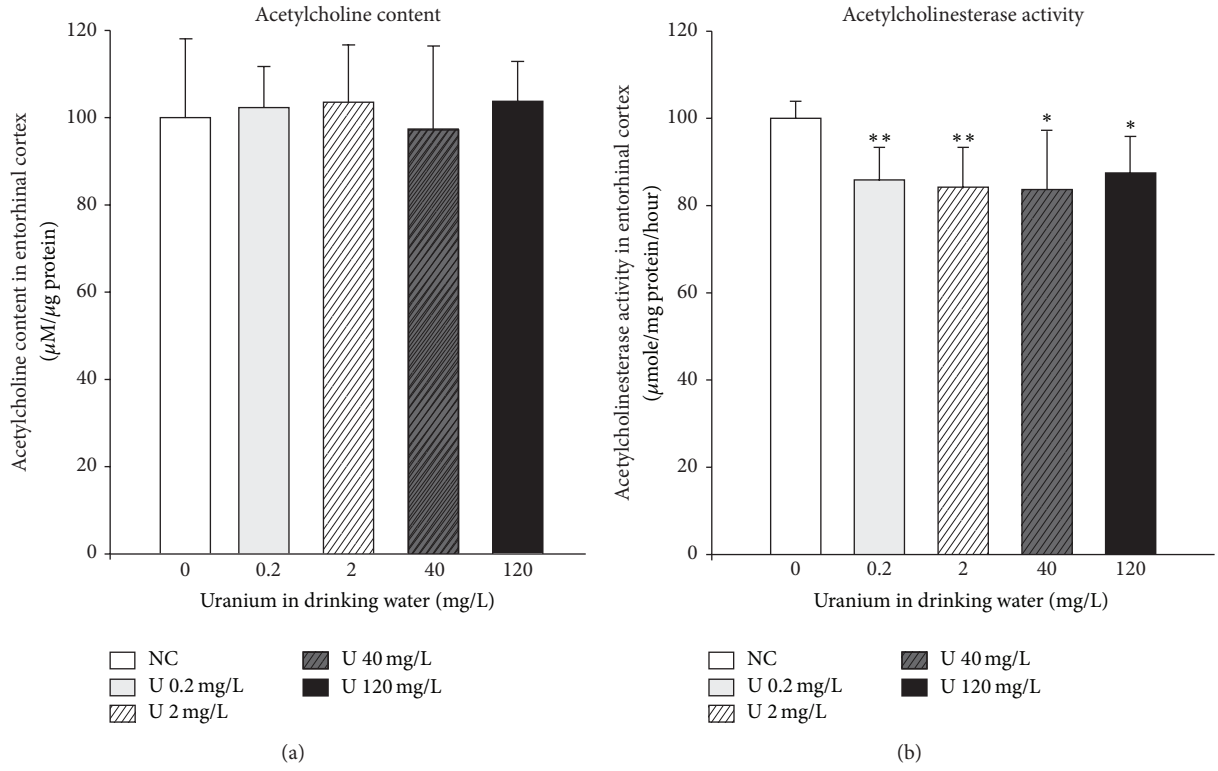

Figure 11: Effect of chronic ingestion of uranium on cholinergic pathway in the entorhinal cortex. The measurements were measured in control animals (NC: noncontaminated) and in animals contaminated by uranium in their drinking water at various concentrations (0.2, 2, 20, 40, and 120 mg/L). Results are expressed as mean ± SD (n = 8–10). $^{*}P < 0.05$, $^{**}P < 0.01$: significantly different from control values.

liver, and 350 ng/g in kidney, at 120 mg/L). These values are consistent with data of previous studies that indicated no real accumulation of uranium in central nervous system following chronic contamination with uranium [30, 48].

Such observation was confirmed in other organs, namely, gonads. Indeed, very low quantities of uranium were measured in ovaries [49, 50] and testis [43], when uranium effects were observed on reproductive function. This finding shows the special sensitivity of the brain or the gonads to chemical toxicity by metals, notably uranium [51].

Another noteworthy point about the observations in this study is the shape of the dose-response relations. Although we might have expected increased classical dose-response curves, we found also that uranium contamination elicited U-shaped or inverted U-shaped curves. Such nonmonotonic shapes have previously been described following chronic low-dose uranium contamination. A kinetic study performed during a chronic ingestion of uranium in drinking water showed successive waves of uranium accumulation and elimination depending on the time exposure [48]. Nonmonotonic curves were also observed with uterine parameters depending on uranium levels [52]. Two nonexclusive hypotheses may be proposed. Firstly, it can be assumed that uranium may inhibit or activate the concerned genes depending on the dose. Secondly, the number and the role of molecular targets for uranium may vary with exposure levels, modifying thus the whole response of the organ. Only the elucidation of the underlying mechanisms of uranium effects following a chronic exposure to low level could reply to these queries. Besides, the nonmonotonic form of these dose-response relations raises the problem of their use for the possible establishment of guidelines [53].

The second major information of the present study concerns the nondeleterious effects induced by uranium. This present study demonstrates clearly that chronic ingestion of uranium at environmental exposures (≤2 mg/L) and higher (up to 120 mg/L) did not produce harmful effects in rats, as evidenced by the absence of clinical signs and histological lesions in all the organs we studied. Our study observed only a trend toward minor uranium-induced histological impairment, specifically, increased cytoplasmic vacuolation in the liver. Gilman and his colleagues reported also this minor histological alteration in the kidneys and in the liver at all uranium exposure levels [19]. The lack of adverse histological lesions in the kidneys is in accordance with the absence of changes of urea and creatinine in blood, traditionally considered as bioindicators of a renal dysfunction. The primary site of accumulation and subsequent effects of uranium in the kidneys was the proximal tubule cells as observed with other metals [54]. Specific biomarkers of proximal tubule function were not analyzed in this study, but a recent study [36] failed to evidence a change of Kim-1, kallikrein, and osteopontin levels following a chronic exposure to uranium with a contamination protocol (9 months

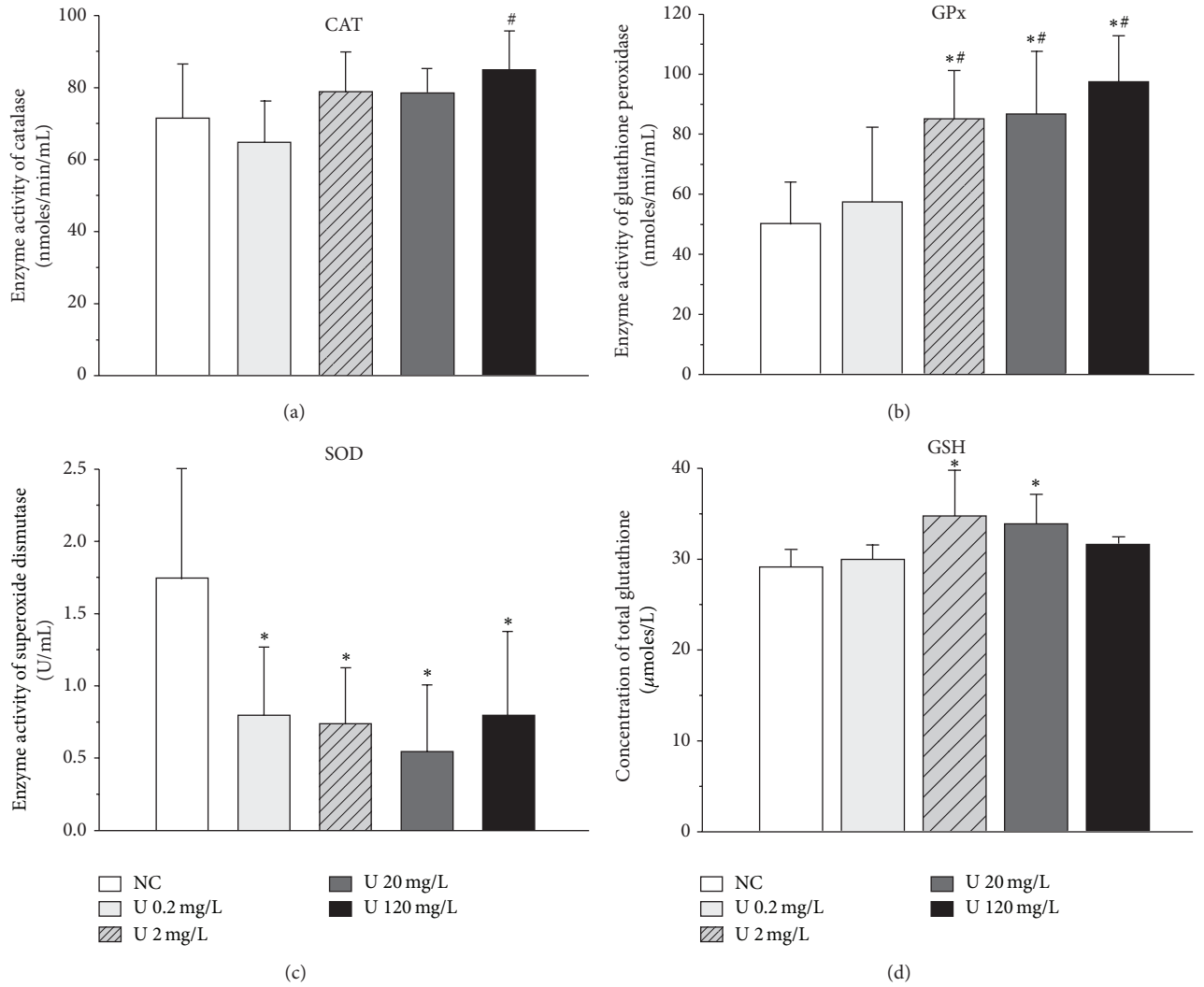

Figure 12: Effect of chronic ingestion of uranium on antioxidant enzyme activity in the entorhinal cortex. Three enzymes were measured, catalase (CAT), glutathione peroxidase (GPx), and superoxide dismutase (SOD), as well as total glutathione (GSH). NC: noncontaminated animal. Results are expressed as mean ± SEM ($n = 8$). $^{*}P < 0.05$, $^{**}P < 0.01$: significantly different from control values. $^{\#}P < 0.05$: significantly different from the U 0.2 mg/L group.

with 40 mg/L) similar to this used in the present study. This point strengthens the absence of marked uranium effects in the kidneys even at high level. In fact, the maximal uranium quantity measured in kidney of the present study following a chronic exposure at the highest level corresponded to 1/10 of the nephrotoxic threshold of 3 μg/g defined for an acute exposure [15], despite a high uranium level in drinking water. This may explained the absence of adverse effects in kidneys. Our conclusion is consistent with other reports, including the recent study by Linares et al. [43], which demonstrated only minor histological lesions for uranium exposure >200 mg/L. However, some studies are not in accordance with the present study and the studies cited above. For instance, these results are not concordant with those obtained by Gilman et al. in 1998 [19]. The objective of Gilman's study was to determine a NOAEL in rats by investigating kidney and liver after chronic ingestion of uranium-contaminated drinking water (from 0.96 to 600 mg/L). The authors reported adverse renal lesions on tubules and glomeruli. Surprisingly, these histological lesions were observed in all contaminated groups including the lowest exposure of 0.96 mg/L, independently of dose. It is noteworthy that no other experimental study has been performed at such low exposure levels. Other publications have noted histological lesions of rat kidneys, but at higher uranium exposure levels (200 mg/L, [43]; 30 mg/L, [55]). Recently, Homma-Takeda et al. published deleterious effects of uranium in different rat models (neonate, prepubertal, and adult) after subcutaneous administration of uranium acetate [56]. The discrepancy is very likely due to the difference of the administration mode. Indeed, previous study demonstrated that only 0.5% of uranium present in drinking water was absorbed into blood by the gastrointestinal system [57].

This lack of histopathological lesions and clinical signs was thus in accordance with the subtle biological effects

Table 6: Symopsis of uranium accumulation and effects in rats contaminated with uranium in drinking water for 9 months.

Uranium (mg/L)	0.2	2	5	10	20	40	120
Health	*Type equation here.*						
Body weight	=	=	=	=	=	=	=
Water consumption	=	=	=	=	=	=	=
Food consumption	=	=	=	=	=	=	=
Intestine							
Gene expression of cytokines	=	=			↑	=	↑
Protein expression of cytokines	=	=			↓	=	↑
Immune cell number	=	=			=	=	=
Histology	=	=		=	=	=	=
Kidney							
Uranium accumulation		↑	↑	↑	↑	↑	↑
Gene expression of EMX				↑		↑	↑
Protein expression of EMX				=		=	=
Histology	=	=	=	=	=	=	=
Plasma parameters	=	=	=	=	=	=	=
Liver							
Uranium accumulation	=	=	=	=	↑	↑	↑
Gene expression EMX				↑		↑	=
Protein expression EMX		=		=	=	=	↓
Enzyme activity EMX		↓		=	=	=	↓
Gene expression Chol Met	=				=	=	↑
Enzyme activity Chol Met					=		↑
Histology	=	=	=	=	=	↑	↑
Plasma parameters	=			=	=	=	=
Haematopoiesis							
Uranium accumulation in bone		=			↑		↑
Bone marrow progenitors	=				=		=
Spleen progenitors	=				=		=
Blood cell counts	=			=	=	=	=
Plasma cytokines	=	↓	=	↓	=	=	=
Brain							
Uranium accumulation		=		=		=	=
Antioxidant enzymes	↓	↓↑			↓↑		↓↑
Cholinergic pathway	=↓	=↓				=↓	=↓

EMX: enzymes and transcription factors of xenobiotic metabolism; Chol Met: enzymes and transcription factors of cholesterol metabolism.

observed in animals contaminated with uranium regardless the uranium level in drinking water. Table 6 summarizes the data obtained in the present study, biological effects and deleterious effects.

Thus, according to standard criteria, we conclude that the NOAEL (No-Observed-Adverse-Effect Level) threshold for uranium chronically ingested in drinking water is superior to 120 mg/L for male adult rats. The findings of the present study indicate thus that the NOAEL threshold based in the present study on the histological alterations was >125 times higher than the level determined in Gilman's study (>120 mg/L versus <0.96 mg/L, resp.).

The guideline issued by WHO (2005) [3] derived with a TDI (tolerable daily intake) approach from Gilman's study (1998) [19] and based on uranium's chemical toxicity to the kidneys assessed a LOAEL of 0.96 mg/L, equivalent to 0.06 mg/kg/day. This TDI, combined with a presumed uncertainty factor of 100 and a presumed 60 kg adult consuming 2 L of drinking water daily, yielded a guideline value of 15 μg/L (before July 2011). A similar calculation was applied to our results deduced from a 5.4 mg/kg/day dose ingested by a rat weighting between 300 and 700 g during the whole experiment and consuming between 20 and 30 mL of water contaminated at 120 mg/L (see Figure 1). This calculation leads to a guideline value of 1350 μg/L, a very high value compared with environmental levels and the WHO reference guideline. Indeed, WHO established a new guideline value in 2011 based on new epidemiological studies not able to demonstrate obvious effects of uranium below an exposure concentration of 30 μg/L [17]. In fact, changes of proximal tubular function of kidneys remained in the physiological range for the different published epidemiological studies for

uranium levels <30 μg/L [18]. Our results seem consistent with epidemiological studies that found no adverse effects in adults exposed to drinking-water containing naturally high uranium levels of 500 to 1000 μg/L [58–61]. Other studies have reported some slight effects on renal function for uranium exposure >300 μg/L [62, 63], effects that did not appear either deleterious or irreversible. The conjunction of experimental and epidemiological studies suggests thus that the threshold for induction of renal adverse effects should at least be above 300 μg/L for humans consuming uranium-contaminated drinking water. This value was 10-fold higher that the guideline value of 30 μg/L provided by WHO in 2011 [17].

5. Conclusions

In conclusion, TDI calculation leads to a guideline value of 1350 μg/L, a very high value compared with WHO reference guideline (30 μg/L). Our experimental results associated with published epidemiological studies suggest that adverse chemical effects of uranium on kidneys in humans should be expected only for values above 300 μg/L. In light of these new results, it appears that the current WHO reference guideline for uranium content in drinking water is very protective (×100) and might be reconsidered.

Abbreviations

DU: Depleted uranium
EMX: Enzymes of xenobiotic metabolism
NOAEL: No-Observed-Adverse-Effect Level
LOAEL: Low-Observed-Adverse-Effect Level
LOEL: Low-Observed-Effect Level
TDI: Tolerable daily intake
WHO: World Health Organization.

Conflict of Interests

The authors declare that there is no conflict of interests regarding the publication of this paper.

Acknowledgments

The authors thank T. Loiseau and F. Voyer for animal care and J. Briard for management of nuclear sources and wastes. This study was part of the ENVIRHOM research program supported by the "Institut de Radioprotection et de Sûreté Nucléaire (IRSN)" and was also partly funded by the "Delegation Generale de l'Armement" (DGA, France, CER 2006.94.0920).

References

[1] M. Cuney, "The extreme diversity of uranium deposits," *Mineralium Deposita*, vol. 44, no. 1, pp. 3–9, 2009.

[2] United Nations Scientific Committee on the Effects of Atomic Radiation (UNSCEAR), Sources and effects of ionizing radiation. Volume I: Sources; Volume II, "Effects. Report to the General Assembly, with scientific annexes. United Nations sales publications E.00.IX.3 and E.00.IX.4. United Nations", 2000.

[3] WHO (World Health Organization), "Uranium in drinking-water background document for development of WHO guidelines for drinking-water quality," Tech. Rep., 2005.

[4] B. C. Jurgens, M. S. Fram, K. Belitz, K. R. Burow, and M. K. Landon, "Effects of groundwater development on uranium: Central Valley, California, USA," *Ground Water*, vol. 48, no. 6, pp. 913–928, 2010.

[5] Province of British Columbia, "Variation in uranium and radioactivity levels in surface and ground water at selected sites in British Columbia, April 1980—March 1981," Tech. Rep., B.C. Ministry of Energy, Mines and Petroleum Resources and B.C. Ministry of Health, Victoria, Canada, 1981.

[6] Z. Pan and L. Senlin, *Radiation Level in China*, China Atomic Energy Publishing and Media, 2011.

[7] IRSN (Institut de Radioprotection et de Sûreté Nucléaire), "Bilan: la qualité radiologique de l'eau du robinet en France 2008-2009," Tech. Rep., 2011.

[8] K. G. Orloff, K. Mistry, P. Charp et al., "Human exposure to uranium in groundwater," *Environmental Research*, vol. 94, no. 3, pp. 319–326, 2004.

[9] M. Muikku, T. Heikkinen, M. Puhakainen, T. Rahola, and L. Salonen, "Assessment of occupational exposure to uranium by indirect methods needs information on natural background variations," *Radiation Protection Dosimetry*, vol. 125, no. 1–4, pp. 492–495, 2007.

[10] O. Prat, T. Vercouter, E. Ansoborlo et al., "Uranium speciation in drinking water from drilled wells in Southern Finland and its potential links to health effects," *Environmental Science and Technology*, vol. 43, no. 10, pp. 3941–3946, 2009.

[11] F. P. Carvalho and J. M. Oliveira, "Uranium isotopes in the Balkan's environment and foods following the use of depleted uranium in the war," *Environment International*, vol. 36, no. 4, pp. 352–360, 2010.

[12] A. Frostick, A. Bollhöfer, and D. Parry, "A study of radionuclides, metals and stable lead isotope ratios in sediments and soils in the vicinity of natural U-mineralisation areas in the Northern Territory," *Journal of Environmental Radioactivity*, vol. 102, no. 10, pp. 911–918, 2011.

[13] L. Pourcelot, B. Boulet, C. Le Corre et al., "Isotopic evidence of natural uranium and spent fuel uranium releases into the environment," *Journal of Environmental Monitoring*, vol. 13, no. 2, pp. 355–361, 2011.

[14] S. Handley-Sidhu, M. J. Keith-Roach, J. R. Lloyd, and D. J. Vaughan, "A review of the environmental corrosion, fate and bioavailability of munitions grade depleted uranium," *The Science of the Total Environment*, vol. 408, no. 23, pp. 5690–5700, 2010.

[15] G. L. Diamond, P. E. Morrow, B. J. Panner, R. M. Gelein, and R. B. Baggs, "Reversible uranyl fluoride nephrotoxicity in the Long Evans rat," *Fundamental and Applied Toxicology*, vol. 13, no. 1, pp. 65–78, 1989.

[16] J. L. Domingo, J. M. Llobet, J. M. Tomas, and J. Corbella, "Acute toxicity of uranium in rats and mice," *Bulletin of Environmental Contamination and Toxicology*, vol. 39, no. 1, pp. 168–174, 1987.

[17] WHO (World Health Organization), *Guidelines for Drinking-Water Quality*, 4th edition, 2011.

[18] I. G. Canu, O. Laurent, N. Pires, D. Laurier, and I. Dublineau, "Health effects of naturally radioactive water ingestion: the need for enhanced studies," *Environmental Health Perspectives*, vol. 119, no. 12, pp. 1676–1680, 2011.

[19] A. P. Gilman, D. C. Villeneuve, V. E. Secours et al., "Uranyl nitrate: 28-day and 91-day toxicity studies in the sprague-dawley rat," *Toxicological Sciences*, vol. 41, no. 1, pp. 117–128, 1998.

[20] I. Dublineau, L. Grandcolas, S. Grison et al., "Modifications of inflammatory pathways in rat intestine following chronic ingestion of depleted uranium," *Toxicological Sciences*, vol. 98, no. 2, pp. 458–468, 2007.

[21] P. Houpert, S. Frelon, P. Lestaevel, C. Bussy, P. Gourmelon, and F. Paquet, "Parental exposure to enriched uranium induced delayed hyperactivity in rat offspring," *NeuroToxicology*, vol. 28, no. 1, pp. 108–113, 2007.

[22] P. Lestaevel, C. Bussy, F. Paquet et al., "Changes in sleep-wake cycle after chronic exposure to uranium in rats," *Neurotoxicology and Teratology*, vol. 27, no. 6, pp. 835–840, 2005.

[23] M. Souidi, Y. Gueguen, C. Linard et al., "In vivo effects of chronic contamination with depleted uranium on CYP3A and associated nuclear receptors PXR and CAR in the rat," *Toxicology*, vol. 214, no. 1-2, pp. 113–122, 2005.

[24] I. Dubuneau, S. Grison, C. Baudelin et al., "Absorption of uranium through the entire gastrointestinal tract of the rat," *International Journal of Radiation Biology*, vol. 81, no. 6, pp. 473–482, 2005.

[25] H. Berradi, J.-M. Bertho, N. Dudoignon et al., "Renal anemia induced by chronic ingestion of depleted uranium in rats," *Toxicological Sciences*, vol. 103, no. 2, pp. 397–408, 2008.

[26] C. Floren, L. Tekaya, F. Escaig, L. Labejof, G. Mouthon, and P. Galle, "Analytical microscopy observations of rat enterocytes after oral administration of soluble salts of lanthanides, actinides and elements of group III-A of the periodic chart," *Cellular and Molecular Biology*, vol. 47, no. 3, pp. 419–425, 2001.

[27] I. Dublineau, S. Grison, L. Grandcolas et al., "Absorption, accumulation and biological effects of depleted uranium in Peyer's patches of rats," *Toxicology*, vol. 227, no. 3, pp. 227–239, 2006.

[28] K. M. Dias da Cunha, H. Henderson, B. M. Thomson, and A. A. Hecht, "Ground water contamination with 238U, 234U, 235U, 226Ra and 210Pb from past uranium mining: cove wash, Arizona," *Environmental Geochemistry and Health*, 2013.

[29] R. Juntunen, "Etelä-Suomen kallioporakaivojen uraani- ja radontukimukset (Uranium and radon in wells drilled into bedrock in southern Finland. Report of Investigation," *Geological Survey of Finland*, vol. 98, 1991.

[30] P. Lestaevel, E. Romero, B. Dhieux et al., "Different pattern of brain pro-/anti-oxidant activity between depleted and enriched uranium in chronically exposed rats," *Toxicology*, vol. 258, no. 1, pp. 1–9, 2009.

[31] C. Rouas, M. Souidi, L. Grandcolas et al., "Acetaminophen induces xenobiotic-metabolizing enzymes in rat: impact of a uranium chronic exposure," *Environmental Toxicology and Pharmacology*, vol. 28, no. 3, pp. 363–369, 2009.

[32] S. Grison, G. Favé, M. Maillot et al., "Metabolomics identifies a biological response to chronic low-dose natural uranium contamination in urine samples," *Metabolomics*, vol. 9, no. 6, pp. 1168–1180, 2013.

[33] M. Prat, C. Demarquay, J. Frick, N. Dudoignon, D. Thierry, and J. M. Bertho, "Use of Flt3 ligand to evaluate residual hematopoiesis after heterogeneous irradiation in mice," *Radiation Research*, vol. 166, no. 3, pp. 504–511, 2006.

[34] T. J. Fry and C. L. Mackall, "The many faces of IL-7: from lymphopoiesis to peripheral T cell maintenance," *Journal of Immunology*, vol. 174, no. 11, pp. 6571–6576, 2005.

[35] N. Brink, M. Szamel, A. R. Young, K. P. Wittern, and J. Bergemann, "Comparative quantification of IL-1β, IL-10, IL-10r, TNFα and IL-7 mRNA levels in UV-irradiated human skin in vivo," *Inflammation Research*, vol. 49, no. 6, pp. 290–296, 2000.

[36] C. Rouas, J. Stefani, S. Grison et al., "Effect of nephrotoxic treatment with gentamicin on rats chronically exposed to uranium," *Toxicology*, vol. 279, no. 1–3, pp. 27–35, 2011.

[37] M. Souidi, M. Parquet, J. Férézou, and C. Lutton, "Modulation of cholesterol 7α-hydroxylase and sterol 27-hydroxylase activities by steroids and physiological conditions in hamster," *Life Sciences*, vol. 64, no. 17, pp. 1585–1593, 1999.

[38] H. Bensoussan, L. Grandcolas, B. Dhieux-Lestaevel et al., "Heavy metal uranium affects the brain cholinergic system in rat following sub-chronic and chronic exposure," *Toxicology*, vol. 261, no. 1-2, pp. 59–67, 2009.

[39] K. Jomova, D. Vondrakova, M. Lawson, and M. Valko, "Metals, oxidative stress and neurodegenerative disorders," *Molecular and Cellular Biochemistry*, vol. 345, no. 1-2, pp. 91–104, 2010.

[40] I. Q. Whishaw, W. T. O'Connor, and S. B. Dunnett, "Disruption of central cholinergic systems in the rat by basal forebrain lesions or atropine: effects on feeding, sensorimotor behaviour, locomotor activity and spatial navigation," *Behavioural Brain Research*, vol. 17, no. 2, pp. 103–115, 1985.

[41] N. M. Wade-Gueye, O. Delissen, P. Gourmelon, J. Aigueperse, I. Dublineau I, and M. Souidi, "Chronic exposure to natural uranium via drinking water affects bone in growing rats," *Biochimica et Biophysica Acta*, vol. 1820, no. 7, pp. 1121–1127, 2012.

[42] R. Racine, L. Grandcolas, S. Grison et al., "Cholesterol 7α-hydroxylase (CYP7A1) activity is modified after chronic ingestion of depleted uranium in the rat," *The Journal of Steroid Biochemistry and Molecular Biology*, vol. 120, no. 1, pp. 60–66, 2010.

[43] V. Linares, M. Bellés, M. L. Albina, J. J. Sirvent, D. J. Sánchez, and J. L. Domingo, "Assessment of the pro-oxidant activity of uranium in kidney and testis of rats," *Toxicology Letters*, vol. 167, no. 2, pp. 152–161, 2006.

[44] V. Linares, D. J. Sánchez, M. Bellés, L. Albina, M. Gómez, and J. L. Domingo, "Pro-oxidant effects in the brain of rats concurrently exposed to uranium and stress," *Toxicology*, vol. 236, no. 1-2, pp. 82–91, 2007.

[45] W. Briner and J. Murray, "Effects of short-term and long-term depleted uranium exposure on open-field behavior and brain lipid oxidation in rats," *Neurotoxicology and Teratology*, vol. 27, no. 1, pp. 135–144, 2005.

[46] C. Bussy, P. Lestaevel, B. Dhieux et al., "Chronic ingestion of uranyl nitrate perturbs acetylcholinesterase activity and monoamine metabolism in male rat brain," *NeuroToxicology*, vol. 27, no. 2, pp. 245–252, 2006.

[47] M. L. Albina, M. Bellés, V. Linares, D. J. Sánchez, and J. L. Domingo, "Restraint stress does not enhance the uranium-induced developmental and behavioral effects in the offspring of uranium-exposed male rats," *Toxicology*, vol. 215, no. 1-2, pp. 69–79, 2005.

[48] F. Paquet, P. Houpert, E. Blanchardon et al., "Accumulation and distribution of uranium in rats after chronic exposure by ingestion," *Health Physics*, vol. 90, no. 2, pp. 139–147, 2006.

[49] É. Arnault, M. Doussau, A. Pesty et al., "Natural uranium disturbs mouse folliculogenesis in vivo and oocyte meiosis in vitro," *Toxicology*, vol. 247, no. 2-3, pp. 80–87, 2008.

[50] A. Feugier, S. Frelon, P. Gourmelon, and M. Claraz, "Alteration of mouse oocyte quality after a subchronic exposure to depleted

Uranium," *Reproductive Toxicology*, vol. 26, no. 3-4, pp. 273–277, 2008.

[51] P. Grandjean and P. Landrigan, "Developmental neurotoxicity of industrial chemicals," *The Lancet*, vol. 368, no. 9553, pp. 2167–2178, 2006.

[52] S. Raymond-Whish, L. P. Mayer, T. O'Neal et al., "Drinking water with uranium below the U.S. EPA water standard causes estrogen receptor-dependent responses in female mice," *Environmental Health Perspectives*, vol. 115, no. 12, pp. 1711–1716, 2007.

[53] J. P. Myers, R. T. Zoeller, and F. S. Vom Saal, "A clash of old and new scientific concepts in toxicity, with important implications for public health," *Environmental Health Perspectives*, vol. 117, no. 11, pp. 1652–1655, 2009.

[54] I. Sabolić, "Common mechanisms in nephropathy induced by toxic metals," *Nephron—Physiology*, vol. 104, no. 3, pp. p107–p114, 2006.

[55] A. Ortega, J. L. Domingo, J. M. Llobet, J. M. Tomas, and J. L. Paternain, "Evaluation of the oral toxicity of uranium in a 4-week drinking-water study in rats," *Bulletin of Environmental Contamination and Toxicology*, vol. 42, no. 6, pp. 935–941, 1989.

[56] S. Homma-Takeda, T. Kokubo, Y. Terada et al., "Uranium dynamics and developmental sensitivity in rat kidney," *Journal of Applied Toxicology*, vol. 33, no. 7, pp. 685–694, 2013.

[57] S. Frelon, P. Houpert, D. Lepetit, and F. Paquet, "The chemical speciation of uranium in water does not influence its absorption from the gastrointestinal tract of rats," *Chemical Research in Toxicology*, vol. 18, no. 7, pp. 1150–1154, 2005.

[58] P. Kurttio, A. Harmoinen, H. Saha et al., "Kidney toxicity of ingested uranium from drinking water," *American Journal of Kidney Diseases*, vol. 47, no. 6, pp. 972–982, 2006.

[59] A. I. Seldén, C. Lundholm, B. Edlund et al., "Nephrotoxicity of uranium in drinking water from private drilled wells," *Environmental Research*, vol. 109, no. 4, pp. 486–494, 2009.

[60] H. S. Magdo, J. Forman, N. Graber et al., "Grand rounds: nephrotoxicity in a young child exposed to uranium from contaminated well water," *Environmental Health Perspectives*, vol. 115, no. 8, pp. 1237–1241, 2007.

[61] P. Kurttio, A. Auvinen, L. Salonen et al., "Renal effects of uranium in drinking water," *Environmental Health Perspectives*, vol. 110, no. 4, pp. 337–342, 2002.

[62] M. Limson Zamora, B. L. Tracy, J. M. Zielinski, D. P. Meyerhof, and M. A. Moss, "Chronic ingestion of uranium in drinking water: a study of kidney bioeffects in humans," *Toxicological Sciences*, vol. 43, no. 1, pp. 68–77, 1998.

[63] M. L. L. Zamora, J. M. Zielinski, G. B. Moodie, R. A. F. Falcomer, W. C. Hunt, and K. Capello, "Uranium in drinking water: renal effects of long-term ingestion by an aboriginal community," *Archives of Environmental & Occupational Health*, vol. 64, no. 4, pp. 228–241, 2009.

Hindawi Publishing Corporation
BioMed Research International
Volume 2014, Article ID 165046, 13 pages
http://dx.doi.org/10.1155/2014/165046

Research Article

Effect of Mining Activities in Biotic Communities of Villa de la Paz, San Luis Potosi, Mexico

Guillermo Espinosa-Reyes,[1] Donaji J. González-Mille,[1] César A. Ilizaliturri-Hernández,[1] Jesús Mejía-Saavedra,[1] V. Gabriela Cilia-López,[1] Rogelio Costilla-Salazar,[2] and Fernando Díaz-Barriga[1]

[1] *CIACYT-Facultad de Medicina, Universidad Autónoma de San Luis Potosí, Avenida Sierra Leona No. 550, Lomas 2da Sección, 78210 México, SLP, Mexico*
[2] *Life Sciences Division, Universidad de Guanajuato, Campus Irapuato-Salamanca, Carretera Salamanca-Valle de Santiago Km. 3.5 + 1.8, Palo Blanco, 36885 Salamanca, GTO, Mexico*

Correspondence should be addressed to Donaji J. González-Mille; donaji.gonzalez@uaslp.mx

Received 20 October 2013; Revised 12 December 2013; Accepted 16 December 2013; Published 30 January 2014

Academic Editor: Fernando Barbosa Jr.

Mining is one of the most important industrial activities worldwide. During its different stages numerous impacts are generated to the environment. The activities in the region have generated a great amount of mining residues, which have caused severe pollution and health effects in both human population and biotic components. The aim of this paper was to assess the impact of mining activities on biotic communities within the district of Villa de la Paz. The results showed that the concentrations of As and Pb in soil were higher than the national regulations for urban or agricultural areas. The bioavailability of these metals was certified by the presence of them in the roots of species of plants and in kidneys and livers of wild rodents. In regard to the community analysis, the sites that were located close to the mining district of Villa de la Paz registered a lower biological diversity, in both plants and wild rodents, aside from showing a change in the species composition of plant communities. The results of this study are evidence of the impact of mining on biotic communities, and the need to take into account the wildlife in the assessment of contaminated sites.

1. Introduction

Mining is one of the most important industrial activities worldwide. It is estimated that there are at least 10,000 mining industries and more than 20,000 mining sites, mineral processing plants, and smelting [1]. Nevertheless, it is considered to be a productive activity with a high environmental impact because in its different stages (exploration, extraction, and processing) it generates numerous adverse effects, as well as a great amount of residues, which could cause water, soil, and sediment pollution [2, 3]. The generation of residues (tailing dams, deposits, and slag) is one of the most notorious environmental impacts in the mining activity, for they are considered to be the source of heavy metals such as cadmium (Cd), chromium (Cr), copper (Cu), lead (Pb), zinc (Zn), and metalloids such as arsenic (As) [4]. This pollution source represents in a major or minor way a risk, for both human population (health) and for biota (ecological) living in the study site [5, 6].

Mining brings as a consequence diverse types of impact that could affect the composition and structure of the biotic communities (richness, abundance, diversity, dominance, trophic relationships, etc.); among the most evident impacts we can find (1) elimination of vegetation, which alters the availability of food and shelter for wild animals and (2) the toxic effects in the health of organisms derived from the presence of heavy metals [7–10].

In Mexico around 5,036,836,611.54 tons per year of metals such as silver (Ag), gold (Au), Cu, Cd, lead, and Zn

are extracted, which represents 1.3% of the gross domestic product, showing that mining is an important economic activity in our country [11].

The mining district of Santa María de la Paz is located between the municipalities of Villa de la Paz and Matehuala in the state of San Luis Potosí. A skarn deposit of Pb-Zn-Ag (Cu-Au) (metamorphic rocks made of silicates of calcium (Ca), iron (Fe), and magnesium (Mg) derived from a protolith limestone and dolomite in which great quantities of aluminum (Al), Fe, and Mg have been introduced) is found in this district.

The main activity in Villa de la Paz is the extraction of fluorite, Zn, Ag, Cu, Pb, bentonite, Au, clay, silica, limestone, and salt. For the past few years 2007–2012 246,665.36 ton of Au, Ag, Cd, Cu, Pb, Zn has been extracted [11]. This activity has been taking place for the past 200 years, and it has generated a great amount of waste (tailings and deposits), which lies in open air and is exposed to environmental weathering; it represents a risk of environmental pollution.

Several studies have been done in that mining region to determine whether risk to human health and diverse biological components exists. Among the studies that have been done, there are those regarding environmental characterization [12–17]; in some of these, it has been proven that risk for the health of human populations in the area due to the exposure to heavy metals and As exists [18–24]. On the other hand studies regarding exposure and effects on diverse species of flora and fauna have also been done [25–27].

Heavy metal accumulation in plants has multiple direct and indirect effects on plant growth and alters many physiological functions by forming complexes with O, N, and S ligands. They interfere with membrane functioning, water relations, protein metabolism, and seed germination [28]. Impediment of proper absorption and essential element transport in plants, metabolic alterations, decrease and inhibition of adequate growth, reproductive alterations, wilting, chlorosis, dehydration, mortality, and photosynthesis inhibition are among the main reported effects on plants due to heavy metal exposure [29–31].

Regarding the effects of mining activities on plant communities, the presence of different concentration levels of metals such as Cd, Cu, Se, and Zn in soil and water has been reported and is known to reduce the diversity and abundance in plant communities [32, 33].

The study of diversity and abundance among species has been commonly used as an indicator of biotic integrity in different types of ecosystems [34, 35]. Some studies have used the diversity and structure of communities (plants and/or animals) to demonstrate the effect of exposure to a certain pollutant such as pest-control substances, metals, herbicides, chemical wastes, residual water discharge, to name a few [32, 36–41].

The study done on wild rodents and small mammals in polluted sites has been focused on evaluating the bioaccumulation and sublethal effects (DNA damage, oxidative stress, etc.) [25, 42–50]. These kinds of projects are important but are generally not very ecologically relevant. In what concerns studies in superior levels of biological organization in Rusia Kataev et al. [51] registered that the population densities of rodents that are found close to where the mining activity takes place are lower in comparison to the ones found farther away.

The objective of this study was to evaluate the impact of the mining activity on biotic communities in the mining district of Villa de la Paz. In order to do this the determination of the heavy metals and As was done in soil and roots of plants as well as the estimation of parameters in the communities of plants and rodents.

2. Materials and Methods

2.1. Study Site. The mining district of Santa Maria de la Paz is located on 23°41′ longitude N and 100°38′ latitude W. Within this district we can find Villa de la Paz, which has been exploited for over 200 years. The predominant weather in the region is mild semidry with rains in the summer [52]. The average annual temperature is between 12° and 18°C; the total annual precipitation varies from 400 to 600 mm [53]. Haplic and calcic xerosols are the dominant soils, which are the typical types of soil in semiarid regions [53]. The main types of vegetation are the xerophytic scrubland and the gypsophyllous grassland [54]. The main economic activities in the region are mining, agricultural production, livestock production, and tourism [53, 55].

2.2. Selection of Sampling Sites. The main types of dominant vegetation selected within the area of study were the microphyllous desert scrub (MDS) and the rosettophyllous desert scrub (RDS); a sampling site was chosen within in each of these, considering the areas with the highest arsenic and metal concentrations [15, 25]. Aside of this, two sites within a reference zone were selected (with similar exposure, relief, lithology, altitude, and condition) to make a comparison with the polluted zone. This zone is located, approximately 10 km south of the impacted zone (Figure 1).

Plant, root, and soil samplings took place in each of the selected sites during the months of May and June of 2004.

2.3. Environmental Monitoring. The quantification of As, Cu, Pb, and Zn was done in plant species, in order to measure the concentrations to which they were exposed. Fifty samples from the superficial soil were obtained (0 to 10 cm of depth) in each of the sampling sites, to obtain a total of 60 soil samples. The samples were collected using the same transects that were used for the plant sampling (see under), five points were established every 5 m within the sampling areas, starting from the origin of the line (0 m) and up to 20 m [56]. In each of the points, 10 cm^3 blocks of soil were extracted using a shovel and were put in polyethylene bags, so they could be transported and analyzed elsewhere.

2.4. Monitoring of Plant Species. The plant sampling was done through the point quadrats method [57] and three transects were traced perpendicularly to the slope in each of the sites (in a southeast-northeast direction, with an average length of 20 m) in order to obtain the frequency, the basal area, the density, and the value of importance of the plant species [58, 59].

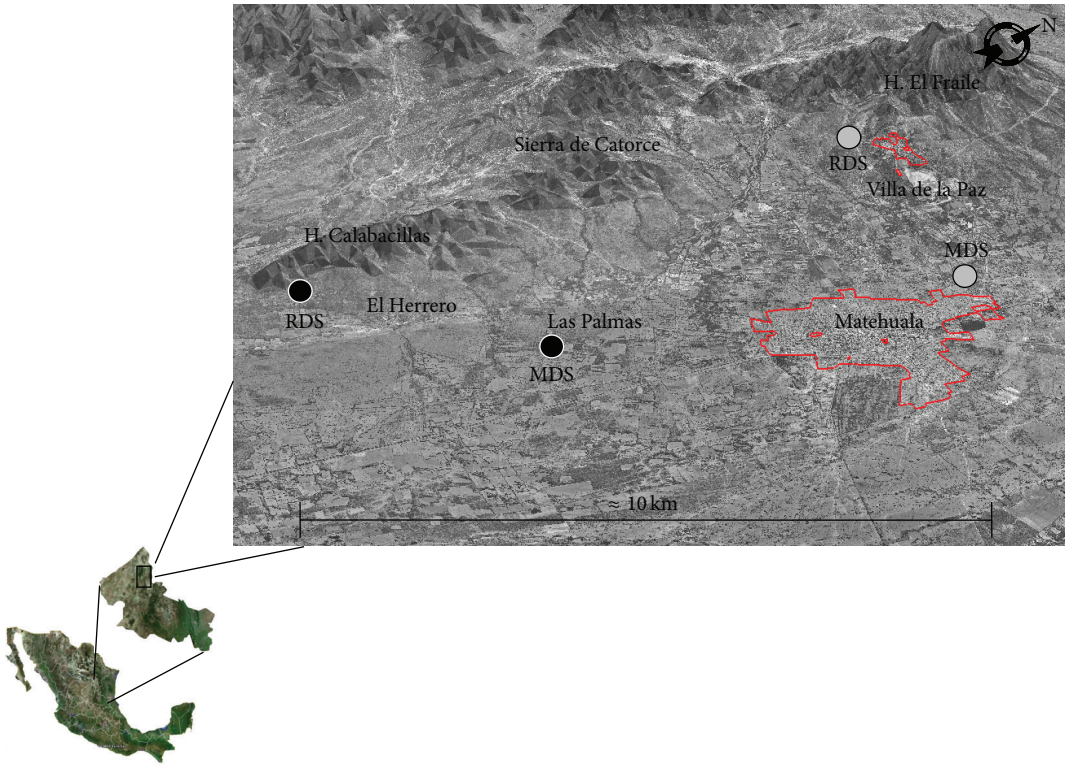

Figure 1: Location of the sampling sites in the mining region of Villa de la Paz, San Luis Potosi, Mexico. Contaminated sites (gray circles); reference sites (black circles). RDS: rosettophyllous desert scrub; MDS: microphyllous desert scrub.

In order to verify if absorption was happening in the roots, the quantification of As, Cu, Pb, and Zn had to be done. For this process, individuals were selected from the four dominant species of plants of each type of vegetation present in both the contaminated and the reference site. The selected species in the RDS were *Jatropha dioica* (Jadi), *Karwinskia mollis* (Kamo), *Agave lechuguilla* (Agle), and *Dyssodia acerosa* (Dyac). The ones on the MDS were *J. dioica* (Jadi), *Larrea tridentata* (Latr), *Parthenium incanum* (Pain), and *Zinnia acerosa* (Ziac). Five individuals of each of these species were collected, except for *D. acerosa*, for which 10 individuals had to be taken so a composite sample could be done, because its roots are very small. All the collected plants were fully extracted, the aerial part (foliage) was eliminated, and the roots were collected in polyethylene bags for easier transportation for analysis.

2.5. Rodent Monitoring. Rodents were captured alive using Sherman traps, only in the MDS. The capture was done two nights in a row, with two repetitions per plot of land, in six different outings, which totaled 960 night-traps. All six outings for the capture and recapture of rodents were done during the period between September 2005 and May 2007. During the period of study the existing assumptions established by Seber [60] where complied with for the study of open populations, as well as getting to know the biology of all the species of rodents within the area of study [59]. A mixture of oats and vanilla was used as bait. The species of the captured rodents were determined as well as different morphometric parameters such as total length, of the tail, the body, the back legs, and the ear. Their sex was recorded and all individuals captured were marked [61, 62]. For the collection of plants and the capture of rodents we have the scientific collector permit FAUT-262 issued by Secretaría de Medio Ambiente y Recursos Naturales (SEMARNAT).

2.6. Parameter Estimates at a Community Level. The Shannon-Wiener index (H') was used to determine the diversity of both plant and rodent species present on the sites: $H' = -\sum_{i=1}^{s}(Ni/N)\ln(Ni/N)$ [58, 63].

As for plant communities, all evaluated attributes were determined according to the vegetative stratus and for the total vegetation.

2.7. Analysis of As and Metals in Soil and Roots. The soil samples of roots and soil were put through a process of acid digestion for the quantification of As, Cu, Pb, and Zn. The digestion of the soil was done in a microwave oven (CEM MDS-2000) using nitric acid (HNO_3), and for the roots the digestion had to be done using a heating plate with HNO_3 and perchloric acid ($HClO_4$).

The quantification of heavy metals was done using spectrophotometry of atomic absorption (EAA). Standard Reference Materials (SRM) which were certified by the National Institute for Standards and Tests of the United States of America (NIST) were analyzed, as a strategy for quality

Table 1: Concentrations (mg/kg) of As, Cu, Pb, and Zn in soil by vegetation type.

Vegetation types	Site	As	Cu	Pb	Zn
RDS	Reference	46.8 (12.0–23.0)	16.3 (10.0–20.0)	16.8 (23.8–97.6)	57.7 (45.0–125.0)
	Contaminated	222.1* (125.8–329.3)	231.9* (155.0–382.5)	204.3* (117.9–487.1)	175.4* (125.0–275.0)
MDS	Reference	23 (18.3–38.5)	25.6 (22.5–30.0)	23.5 (15.9–31.2)	87.3 (57.5–280.0)
	Contaminated	7902.6* (502.0–17325.0)	703.7* (292.5–1080.0)	1228.2* (428.1–2226.8)	3513.5* (505.0–6325.0)
NOM-147-SEMARNAT/SSA1-2004 agricultural/residential land		22	—	400	—
CEQG agricultural land		12	63	70	200

The values represent the mean and range. RDS: rosettophyllous desert scrub; MDS: microphyllous desert scrub. *Statistically different concentrations ($P < 0.05$) in relation to the reference site; —: not mentioned.

control. The employed SRM were the SRM 2710 for trace analysis in soils and SRM 1547 for plants. The percentage of recovery for both ranged from 80 to 104%.

2.8. Statistical Analysis. A Chi Square test, using a contingency chart of 2 × 2, had to be done in order to evaluate the differences in the composition of flora on the sites [64]. A two-sample t-test was used in order to compare the diversity (Shannon-Wiener index) [65, 66]. For the comparison of metal concentrations, the Kruskal-Wallis test in soil and the Mann-Whitney U test in plants were used. The level of statistical significance was considered at $P < 0.05$ for all tests. Statistical analysis was performed with STATISTICA (version 12.0, StatSoft Inc.). Diversity-abundance models were done in order to extract patterns of relative species abundances without reducing information and to make a comparison between reference and contaminated sites [66].

3. Results and Discussion

3.1. Metals and As in Soil. In Table 1 the concentrations of the quantified metals in the superficial soil samples classified according to the type of vegetation are shown. For both types of vegetation, a statistically significant difference was found ($P < 0.05$) between the concentrations of the contaminated and reference site. In the case of RDS, As turned out to be five times higher, Cu 14 times, Pb 12 times, and Zn three times more than in the reference site. The decreasing order of concentration found in the contaminated site was Cu > As > Pb > Zn compared to the reference site which was Zn > As > Pb > Cu. For the MDS it was found that As was 344 times higher, Cu 27 times, Pb 52 times, and Zn 40 times more than the value from the reference site. The order of concentration on the contaminated site was As > Zn > Pb > Cu and for the reference site it was Zn > Cu > Pb > As.

In Table 1 the concentrations of As and Pb which surpass the maximum limits allowed according to the NOM-147-SEMARNAT-2004 are shown. Thresholds for Cu and Zn do not exist in Mexican regulations, which is the easy why the parameter established by the Canadian guides for environmental protection and human health had to be used as comparison; it was found that Cu exceeds the protection limits in both types of vegetation, while Zn was found to have exceeded the protection limits only in the MDS contaminated site [67]. This information concurs with reported results from other authors.

The registered differences in the concentrations of metals in soil among the contaminated and the reference sites confirm the impact of mining activity reported by Razo et al. [15]. In the contaminated sites, higher concentrations were found in the MDS than in the RDS; these differences can be attributed to the topographic location of the sites. The RDS site is found on the slope of the hill "El Fraile" which favors the movement of metals and As to lower areas due to run off. The MDS site is found in the valley, which probably explains why a higher concentration was reported. These results coincide with what was registered by Razo et al. [15], who reported lower concentrations in the hillside areas (As 731 mg/kg; Cu 206 mg/kg; Pb 433 mg/kg; and Zn 2351 mg/kg), compared to the ones in the valley (As 10459 mg/kg; Cu 1023 mg/kg; Pb 1560 mg/kg; and Zn 5205 mg/kg).

Regarding the concentrations that were registered in the reference area, these were found to be within the range of what some authors registered as being basal (As 1–40 mg/kg; Cu 1–140 mg/kg; Pb 10–70 mg/kg; and Zn 5–125 mg/kg) [32, 68, 69].

3.2. Metals and As in Roots. The quantification of the content of metals in the roots of plants was done for the purpose of determining if they could be absorbed by plants. The concentrations of As, Cu, Pb, and Zn, found in the roots of the selected species according to their vegetation type, are shown in Table 2. In the RDS, no differences were found between the contaminated and the reference site for any metal in the *K. mollis* specie ($P > 0.05$); however for the *A. lechuguilla* and *J. dioica* species differences were found ($P < 0.05$) (with the exception of Zn in *A. lechuguilla* and Pb in *J. dioica*). In the MDS a statistically significant difference was found ($P < 0.05$) between the concentrations of the four species from the contaminated and reference sites (with the exception of Zn en *J. dioica*). Zn was the element that was absorbed in the highest amounts (with the exception of *J. dioica* where it was Pb).

Table 2: Concentrations (mg/kg) of As, Cu, Pb, and Zn, in roots, by species and vegetation type.

Vegetation types	Site	Specie	As	Cu	Pb	Zn
RDS	Reference	**Kamo**	1.6 (1.4–1.9)	2.0 (1.5–2.8)	0.3 (0.2–0.4)	9.3 (5.0–14.1)
		Agle	0.5 (0.1–1.0)	2.8 (2.3–3.5)	0.5 (0.4–0.6)	8.9 (5.8–13.0)
		Jadi	0.7 (0.2–1.1)	3.2 (2.5–4.8)	0.5 (0.2–1.0)	11.2 (7.5–14.8)
		Dyac	0.7	10.0	22.3	1.0
	Contaminated	**Kamo**	1.8 (0.7–2.3)	1.8 (0.2–2.8)	0.4 (0.3–0.5)	5.6 (4.5–7.0)
		Agle	1.1* (0.8–1.6)	4.5* (3.3–6.1)	1.7* (0.7–3.6)	8.4 (6.4–13.0)
		Jadi	2.6* (1.1–4.7)	7.3* (3.0–10.5)	0.9 (0.3–2.0)	37.8* (13.5–52.0)
		Dyac	1.1	11.3	16.0	2.1
MDS	Reference	**Latr**	0.3 (0.1–0.7)	6.0 (3.9–7.4)	0.3 (0.2–0.5)	12.5 (8.9–20.5)
		Pain	0.3 (0.2–0.5)	3.3 (2.5–3.6)	0.6 (0.4–0.7)	14.0 (10.8–17.5)
		Jadi	1.1 (1.0–1.4)	1.8 (1.5–2.0)	0.1 (0.02–0.3)	6.0 (4.5–7.8)
		Ziac	1.6 (0.8–2.3)	2.8 (1.5–7.5)	4.5 (2.8–5.6)	6.7 (5.3–8.5)
	Contaminated	**Latr**	4.3* (1.4–14.1)	10.6* (8.0–18.1)	1.3* (0.4–4.1)	38.5* (12.8–129.3)
		Pain	5.1* (3.2–6.2)	14.0* (9.5–19.8)	2.2* (1.4–2.5)	23.1* (17.8–30.0)
		Jadi	22.0* (1.9–43.9)	13.4* (8.5–20.5)	2.3* (1.4–3.2)	5.4 (5.0–6.3)
		Ziac	15.2* (1.3–32.1)	12.0* (8.3–20.5)	365.5* (0.8–2.6)	1.7* (307.5–422.5)

The values represent the mean and range. RDS: rosettophyllous desert scrub; MDS: microphyllous desert scrub. The range is not shown for the *D. acerosa*, because there was only one analyzed compound sample. $^*P < 0.05$ with regard to the reference site for the same species and vegetation type. Kamo: *K. mollis,* Agle: *A. lechuguilla*, Jadi: *J. dioica*, Dyac: *D. acerosa*, Latr: *L. tridentata*, Pain: *P. incanum*, and Ziac*: Z. acerosa.*

According to these results, it can be stated that metals and As present in the area are available for the plant species; however, not all plants have the same method for absorption and/or translocation. It has been observed that plants develop different resistance mechanisms when exposed to high metal concentrations, which makes them absorb metals in a differential way [70–72]. In this regard Machado-Estrada et al. [27] did the evaluation of the translocation of metals and As in plant species (*A. lechuguilla, P. incanum,* and *Z. acerosa*) of the same sites that we evaluated in Villa de la Paz and the reference area. They state that there is more translocation towards stems and leafs in recollected plants in the polluted sites, which shows the bioavailability of the metals in these species of plants.

Added to this, the absorption of metals in plants depends mainly on bioavailability of metals and on the intrinsic characteristics of each species. Several authors have reported that bioavailability of metals depends on factors such as condition of soil, pH, and the chemical form [73–75]. According to them, the differences in the absorption by the plants of the region can be attributed to the possible development of resistance mechanisms towards metals (e.g., evasion) and to the presence of the different chemical forms of metals generated in the mining processes that have been reported in the area by Razo et al. [15].

3.3. Metals and As in Rodents. Jasso-Pineda et al. [25] evaluated the concentrations of As, Cd, and Pb in livers and kidneys of the rodents that were captured in the mining district of Villa de la Paz and in a reference site. Our study was done jointly (sampling sites and seasons) with the previously mentioned study. On that basis the concentrations of metals in the tissues of rodents registered in the article by Jasso-Pineda et al. [25] can be directly compared to the concentrations of metals in soil and the roots of plants. The levels of registered metals, in all cases, were significantly

Table 3: Richness, total diversity, and by stratus for the RDS and the MDS.

Vegetation types		Contaminated		Reference	
		Richness	Diversity	Richness	Diversity
RDS	Herbaceous	10	0.75	10	0.61
	Bushy	10	0.71*	9	0.51
	Total	**20**	**1.03**	**19**	**0.82**
MDS	Herbaceous	8	0.6*	17	1.04
	Bushy	5	0.55*	15	0.98
	Subarboreal	2	0.05*	1	0
	Total	**13***	**0.88***	**32**	**1.28**

* $P < 0.05$.

higher in the contaminated site compared to the reference site.

3.4. Plant Communities. As it is shown in Table 3, the richness of the species was similar between the contaminated and reference sites of the RDS (20 and 19 species, resp.) ($P > 0.05$); unlike the MDS in which the reference site showed a major richness (32 species) than the contaminated site (13 species) ($P < 0.05$).

Regarding the total diversity of the RDS (Table 3), a statistically significant difference was registered ($P < 0.05$), between the contaminated and the reference site. There was also a significant difference for the bushy stratus ($P < 0.05$), but not for the herbaceous one ($P > 0.05$).

Aside from this, it was determined that the contaminated site has a higher diversity than the reference site (Table 3), which is given by the highest abundance of individuals in the bushy stratus. The total diversity of the MDS, as well as the stratus (Table 3) of the contaminated site, was higher ($P < 0.05$) than the ones from the reference site.

The elements of diversity are richness and equity of species. In the case of RDS in both sites the richness was the same (Table 3); likewise the relative abundance (number of individuals per species) was similar in both communities, just not with the same species (Figure 2), which explains why communities do not show differences in the value of the diversity index. In the contaminated site, a larger diversity of species was found in the bushy stratus (Table 3), because the species present in this site had a greater abundance of individuals (Figure 2). This difference among the diversity of individuals could be attributed to the change in species, because this new species could have lower environmental requirements and/or less competition in comparison with the ones that were not registered, which allows them to have a greater number of individuals [66].

In the case of MDS the way communities responded to metals was by reducing the diversity of species (Table 3), which could be caused by a difference in sensibility towards pollutants among the plants species that are present; this way more sensitive species are replaced with tolerant species or are eliminated completely (Figure 3) [66, 76].

In the RDS regarding the composition of species in the sites, it was found that the contaminated and the reference sites share 9 species; 11 species are only present in the contaminated site and 10 only registered in the reference site. A statistically significant difference was found ($P < 0.05$) among the sites (Table 4).

In the case of MDS 11 species were registered and they were present in both sites, 3 species were registered only on the contaminated site and 21 of them only on the reference site. The difference regarding composition in both sites turned out to be statistically significant ($P < 0.05$) (Table 4).

The diversity-abundance models of the RDS are shown in Figure 2, where similarities in the behavior between the contaminated and the reference site can be seen, meaning that both sites had the same amount of both abundant species and not very abundant ones. In the case of MDS (Figure 3) it can be observed that the contaminated site behaves completely different compared to the reference site, because there were mostly abundant species. Abundant and not very abundant species were registered in the reference site.

In the RDS, a change between the floral composition of the communities in the contaminated and the reference zone was found (Table 4), although it kept the same richness (Table 3) and a relationship is still being maintained regarding the proportion among the abundance of species (Figure 2), which was not the case for the MDS where aside from the change in species (Table 4) the richness showed a contrast between both sites (Table 3). In the contaminated site a higher number of dominant species were present, and there was an absence of species with low abundance (Figure 3). With the results it became evident that the change in floral composition was one of the effects of metals in the communities of the area, which is similar to what has been reported in other environments [7–9].

Luoma [77] arguments that the presence of species tolerant to pollution in a community is a strong evidence that a pollutant is causing adverse effects over it. Some of the species that were only found in the contaminated zone of the RDS (*B. veronicaefolia, E. karvinskianus, L. tridentata,* and *P. laevigata*) have previously been registered as being accumulative and tolerant to metals [78–81].

The presence of tolerant species and the absence of sensitive ones, the increase or decrease in the abundance of species, the change in their composition are the main effects that were found in plant communities within the area of Villa de la Paz; these effects are causing a change in the structure of their communities, which could lead to

Table 4: Composition of species for the rosettophyllous desert scrub (RDS) and the microphyllous desert scrub (MDS).

Site	Species	Acronym	RDS		MDS	
			Contaminated	Reference	Contaminated	Reference
Both sites	*Dyssodia acerosa*	Dyac	X	X	X	X
	Prosopis laevigata	Prla	—	—	X	X
	Parthenium incanum	Pain	—	—	X	X
	Larrea tridentata	Latr	—	—	X	X
	Jatropha dioica	Jadi	X	X	X	X
	Zaluzania triloba	Zatr	—	—	X	X
	Senna wislizeni	Sewi	—	—	X	X
	Bahia absinthifolia	Baab	—	—	X	X
	Zinnia acerosa	Ziac	—	—	X	X
	Euphorbia prostrata	Eupo	—	—	X	X
	Tridens sp.	Trsp	—	—	X	X
	Buchloe dactyloides	Buda	X	X	—	—
	Agave lechuguilla	Agle	X	X	—	—
	Karwinskia mollis	Kamo	X	X	—	—
	Opuntia stenopetala	Opst	X	X	—	—
	Acalypha sp.	Acsp	X	X	—	—
	Mimosa biuncifera	Mibi	X	X	—	—
	Linum rupestre	Liru	X	X	—	—
Only impacted	*Loeselia coerulea*	Loco	X	—	—	—
	Menodora helianthemoides	Mehe	X	—	—	—
	Condalia fasciculata	Cofa	X	—	—	—
	Erigeron karvinskianus	Erka	X	—	—	—
	Euphorbia prostrata	Eupo	X	—	—	—
	Haplopappus spinulosus	Hasp	X	—	—	—
	Condalia sp.	Cosp	X	—	X	—
	Brickellia veronicaefolia	Brbe	X	—	—	—
	Lycium berlandieri	Lybe	X	—	—	—
	Scleropogon sp.	Scsp	X	—	—	—
	Tiquilia canescens	Tica	X	—	X	—
	Trixis angustifolia	Tran	—	—	X	—

Table 4: Continued.

Site	Species	Acronym	RDS		MDS	
			Contaminated	Reference	Contaminated	Reference
Only reference	*Bouteloua curtipendula*	Bocu	—	X	—	—
	Cenchrus ciliaris	Ceci	—	—	—	X
	Kalanchoe blossfeldiana	Kabl	—	—	—	X
	Conyza schiedeana	Cosh	—	—	—	X
	Lycium berlandieri	Lybe	—	—	—	X
	Opuntia lindheimeri	Opli	—	—	—	X
	Physalis sp.	Phsp	—	—	—	X
	Menodora helianthemoides	Mehe	—	—	—	X
	Celtis pallida	Cepa	—	—	—	X
	Dalea bicolor	Dabi	—	—	—	X
	Erigeron karvisnkianus	Erka	—	—	—	X
	Opuntia leptocaulis	Ople	—	—	—	X
	Agave salmiana	Agsa	—	—	—	X
	Mimosa biuncifera	Mibi	—	—	—	X
	Buddleja scordioides	Busc	—	—	—	X
	Lippia sp.	Lisp	—	—	—	X
	Acalypha sp.	Acsp	—	—	—	X
	Cenchrus altianus	Ceal	—	—	—	X
	Lantana sp.	Lasp	—	—	—	X
	Salvia ballotaeflora	Saba	—	X	—	X
	Strenandum sp.	Stsp	—	—	—	X
	Viola sp.	Visp	—	—	—	X
	Bacopa procumbens	Bapr	—	X	—	—
	Evolvulus alsinoides	Eval	—	X	—	—
	Sida absintipholia	Siab	—	X	—	—
	Amelanchier denticulata	Amde	—	X	—	—
	Condalia mexicana	Come	—	X	—	—
	Dichondra sericea	Dise	—	X	—	—
	Ferocactus pilosus	Fepi	—	X	—	—
	Scutellaria potosina	Scpo	—	X	—	—

Table 5: Captured species from the mining site in Villa de la Paz, San Luis Potosí.

Site	Family	Species	Acronym	Relative Abundance
Reference	Muridae	*Sigmodon hispidus*	Sihi	2.33
		Neotoma mexicana	Neme	2.33
		Peromyscus maniculatus	Pema	9.30
		P. eremicus	Peer	11.63
	Heteromyidae	*Chaetodipus nelsoni*	Chne	18.60
		Dipodomys merriami	Dime	55.81
Contaminated	Heteromyidae	*C. nelsoni*	Chne	47.06
		D. merriami	Dime	52.94

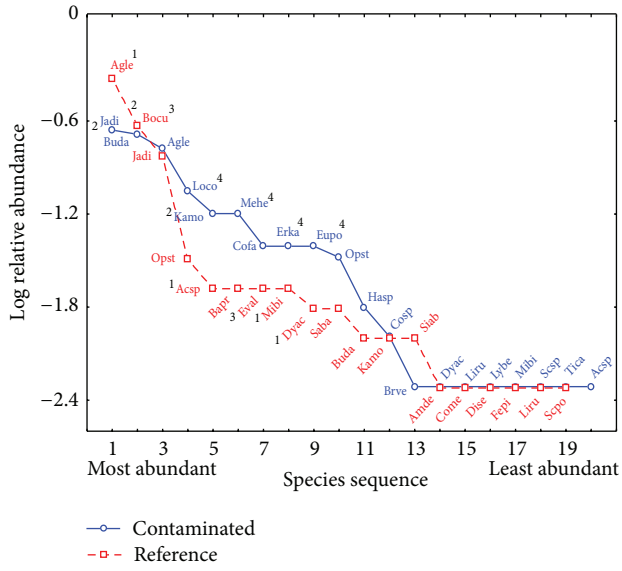

Figure 2: Abundance-diversity model from the rosettophyllous desert scrub (RDS). 1: species with the greatest abundance in the reference site, 2: species with a greater abundance in the impacted site, 3: species only present in the reference site, and 4: species only present in the impacted site (see Table 4 for the acronyms).

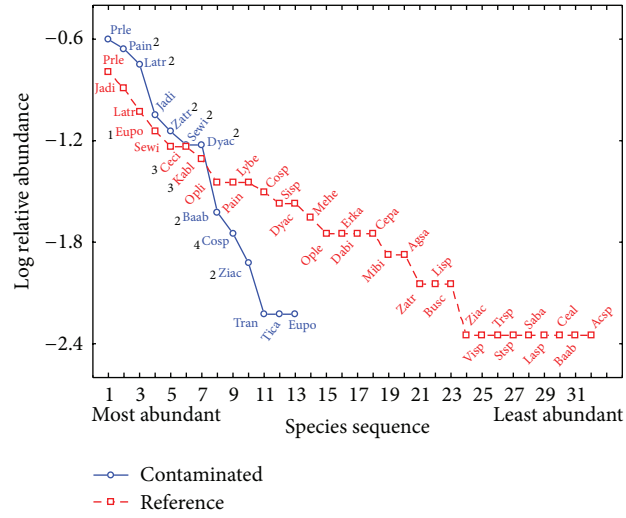

Figure 3: Abundance-diversity model from the microphyllous desert scrub (MDS). 1: species with the greatest abundance in the reference site, 2: species with a greater abundance in the impacted site, 3: species only present in the reference site, and 4: species only present in the impacted site (see Table 4 for the acronyms).

an imbalanced ecosystem, and it will be reflected in the alterations of its properties such as productivity and the biogeochemical cycles. The plant communities in the MDS are at higher risk than the communities in the RDS, because of the changes on their structure and the loss of diversity, which can lead to an imbalance of their ecosystem properties. Aside of this, if the impacts towards the environment continue, the communities from the RDS could present this same risk.

One of the first visible symptoms of the environmental stress due to contamination is the changes in vegetation, the latter being a component of an ecosystem which fully reflects the features of its site. The changes in the plant communities also represent a direct risk for the animal communities that depend on them. As a result, plant communities are a good indicator of the changes in the site. Hence, research on the changes in vegetation, as well as changes in the structure of plant communities and their dynamics, provides the necessary information not only for assessing the degree of contamination and degradation of the environment, but also for the measurement of the decrease in its production potential [82].

3.5. Wild Rodent Communities. During the six outings for the systemic capturing-recapturing of rodents, a total of 77 rodents were captured (43 from the reference site and 34 from the polluted site).

The sampling period took place from September 2005 to May 2007. In the reference site, six species belonging to two different families were captured, Heteromyidae and Muridae, and in the contaminated site two species belonging to the Heteromyidae family were found (Table 5).

Just like in the plant communities, diversity is made up of the number of species (richness) and the number of individuals of each species (equity). In Figure 4 how the rodent community diversity in the reference site ($H' = 1.28$) is greater than that in the contaminated site ($H' = 0.69$) is shown; it is likely that this decrease in the diversity is actually a response from communities towards metals, which could be

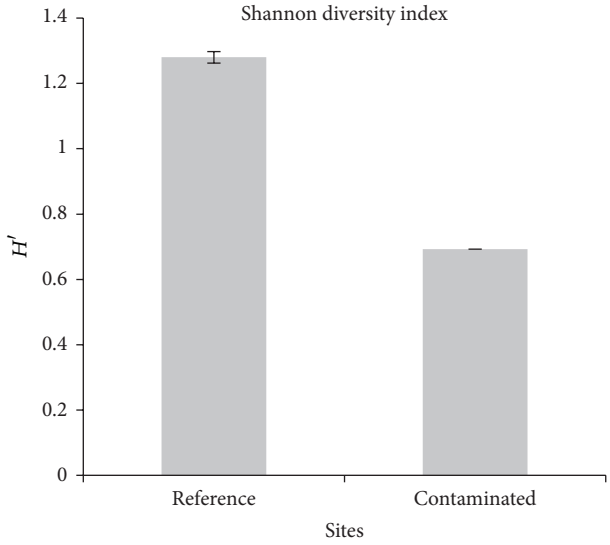

Figure 4: Diversity of rodents in the mining site of Villa de la Paz and the reference zone.

attributed to a difference in sensitivity towards contaminants among species. This way, sensitive species are replaced for tolerant species or they are definitely eliminated [66, 74].

One alternative is that the concentrations of metals can first of all affect the species of plants that are used as source of food for distinct species of rodents, and with the absence of species to feed upon, rodents will emigrate to other areas.

There are no similar studies in communities of rodents with which we can compare the obtained results on this research.

Species richness has been employed as indicator of ecological integrity (ecosystem distress syndrome); reduced species richness is one of the most consistent responses to assess effects of contaminants and also has high social relevance. Diversity indices provide important information about rarity and commonness of species in a community; they have been employed as integrative indicator. The ability to quantify diversity in this way is an important tool for biologists and ecotoxicologist trying to understand community structure and effects derivatives of anthropogenic activities in biomonitoring studies [66].

4. Conclusions

The concentrations of As and Pb exceed the maximum allowed limits established by the NOM-147-SEMARNAT-2004 and by the Canadian guides for environmental protection. Metals and As in the mining district of Villa de la Paz are bioavailable, because concentrations of them were found in roots and organs of wild rodents [25]. Regarding the community level analysis a change in the plant composition was registered, as well as a loss in diversity of the plant communities and rodents, high concentrations of metals present in plants, the tissues of rodents, and the roots of plant species, and the registered effects on a molecular level in rodents from the contaminated site [25], all strong evidence of the existent risk in the biotic communities of Villa de la Paz, San Luis Potosi, caused by the mining activities that take place there. However, there is also a possibility that this loss of diversity is due to the continuous fragmentation of the habitat and regional stressors (e.g., climatic change, desertification, and drought) in the municipalities of Villa de la Paz and Matehuala.

It is also important to mention that risk assessments are made in Mexico often neglects the assessment of biota (some components), which represents a severe problem because they are an essential part of the ecosystem and if the biotic components are affected at some time will be reflected in the health of the human population. In the northern part of Mexico and particularly in San Luis Potosi there are various mining areas (Villa de Ramos, Charcas, and Cedral), with similar characteristics as Villa de la Paz. The results of this study will allow the selection of sites and species in order to incorporate them in a medium and long range monitoring program on the effect of metals and As for the region.

Conflict of Interests

The authors declare that there is no conflict of interests regarding the publication of this paper.

Acknowledgments

This work was supported by a grant from the National Council for Science and Technology (SEP-CONACYT-Ciencia Basica-178778) and the Autonomous University of San Luis Potosi (UASLP) through the Fund for the support of research (C12-FAI-03-67.67). The authors thank the taxonomist José García Pérez from Instituto de Investigaciones de Zonas Desérticas de la UASLP for identifying the plant species. They also thank Laura Martínez Turrubiartes for the English language editing of the paper.

References

[1] PNUMA/IPCS, "Evaluación de los riesgos químicos: humanos, ambientales y ecológicos," Programa de las Naciones Unidad Para el Medio Ambiente (PNUMA), Programme for the Sound Management of Chemicals (IPCS), Geneva, Switzerland, 1999.

[2] J. O. Nriagu and J. M. Pacyna, "Quantitative assessment of worldwide contamination of air, water and soils by trace metals," *Nature*, vol. 333, no. 6169, pp. 134–139, 1988.

[3] N. Madhavan and V. Subramanian, "Sulphide mining as a source of arsenic in the environment," *Current Science*, vol. 78, no. 6, pp. 702–709, 2000.

[4] United Nations Environment Programme (UNEP), "Mining and sustainable development II: challenges and perspectives," *Industry and Environment*, vol. 23, p. 95, 2000.

[5] J. L. Fernández-Turiel, P. Aceñolaza, M. E. Medina, J. F. Llorens, and F. Sardi, "Assessment of a smelter impact area using surface soils and plants," *Environmental Geochemistry and Health*, vol. 23, no. 1, pp. 65–78, 2001.

[6] M. C. Jung, "Heavy metal contamination of soils and waters in and around the Imcheon Au-Ag mine, Korea," *Applied Geochemistry*, vol. 16, no. 11-12, pp. 1369–1375, 2001.

[7] D. R. Morrey, A. J. M. Baker, and J. A. Cooke, "Floristic variation in plant communities on metalliferous mining residues in the northern and southern Pennines, England," *Environmental Geochemistry and Health*, vol. 10, no. 1, pp. 11–20, 1988.

[8] M. Salemaa, I. Vanha-Majamaa, and J. Derome, "Understorey vegetation along a heavy-metal pollution gradient in SW Finland," *Environmental Pollution*, vol. 112, no. 3, pp. 339–350, 2001.

[9] S. Koptsik, G. Koptsik, S. Livantsova, L. Eruslankina, T. Zhmelkova, and Z. Vologdina, "Heavy metals in soils near the nickel smelter: chemistry, spatial variation, and impacts on plant diversity," *Journal of Environmental Monitoring*, vol. 5, no. 3, pp. 441–450, 2003.

[10] E. Taucer, "Mitigación de las amenazas a la biodiversidad por las actividades mineras en el corredor de conservación Vilcabamba-Amboró (Bolivia-Perú)," in *Artesanos del socavón: Pequeña minería y minería artesanal en América Latina*, M. Bernales and J. Valdivia, Eds., pp. 44–71, UNESCO: Fondo Editorial del Congreso del Perú: Futuro Sostenible, Lima, Peru, 2006.

[11] SGM, *Anuario Estadístico de la Minería Mexicana Ampliada 2011*, Servicio Geológico Mexicano y Secretaría de Economía, 2012.

[12] J. Castro-Larragoitia, U. Kramar, and H. Puchelt, "200 years of mining activities at La Paz/San Luis Potosí/Mexico—consequences for environment and geochemical exploration," *Journal of Geochemical Exploration*, vol. 58, no. 1, pp. 81–91, 1997.

[13] M. Monroy, M. F. Díaz-Barriga, I. Razo, and L. Carrizales, *Evaluación de la contaminación por arsénico y metales pesados (Pb, Cu, Zn) y análisis de riesgo en salud en Villa de la Paz-Matehuala, S.L.P. [M.S. thesis]*, Instituto de Metalurgia, Universidad Autónoma de San Luis Potosí, San Luis Potosí, Mexico, 2002.

[14] M. Monroy, M. F. Díaz-Barriga, I. Razo, and L. Carrizales, *Evidencias de contaminación de agua y sedimento por arsénico en el área de Cerrito Blanco, municipio de Matehuala, SLP [M.S. thesis]*, Instituto de Metalurgia, Universidad Autónoma de San Luis Potosí, San Luis Potosí, Mexico, 2002.

[15] I. Razo, L. Carrizales, J. Castro, F. Díaz-Barriga, and M. Monroy, "Arsenic and heavy metal pollution of soil, water and sediments in a semi-arid climate mining area in Mexico," *Water, Air, and Soil Pollution*, vol. 152, no. 1–4, pp. 129–152, 2004.

[16] J. A. Chiprés, J. C. Salinas, J. Castro-Larragoitia, and M. G. Monroy, "Geochemical mapping of major and trace elements in soils from the Altiplano Potosino, Mexico: a multi-scale comparison," *Geochemistry: Exploration, Environment, Analysis*, vol. 8, no. 3-4, pp. 279–290, 2008.

[17] J. A. Chiprés, J. Castro-Larragoitia, and M. G. Monroy, "Exploratory and spatial data analysis (EDA-SDA) for determining regional background levels and anomalies of potentially toxic elements in soils from Catorce-Matehuala, Mexico," *Applied Geochemistry*, vol. 24, no. 8, pp. 1579–1589, 2009.

[18] L. Yáñez, J. Calderón, L. Carrizales, and M. F. Díaz-Barriga, "Evaluación del riesgo en sitios contaminados por plomo aplicando un modelo de exposición integral (IEUBK)," in *Evaluación de riesgos para la salud en la población expuesta a metales en Bolivia*, F. Díaz-Barriga, Ed., p. 90, Centro Panamericano de Ecología Humana y Salud, División de Salud y Ambiente, Estado de México, Metepec, Mexico, 1997.

[19] J. Calderón, M. E. Navarro, M. E. Jiménez-Capdeville, and M. F. Díaz-Barriga, "Neurobehavioral effects among children exposed chronically to arsenic, cadmium and lead," in *Proceedings of the 3rd International Conference on Arsenic Exposure and Health Effect*, p. 8, San Diego, Calif, USA, 1998.

[20] L. Carrizales, L. Batres, M. Ortiz et al., "Efectos en salud asociados con la exposición a residuos peligrosos," *Scientiae Naturae*, vol. 2, no. 1, pp. 5–28, 1999.

[21] M. F. Díaz-Barriga, "Metodología identificación y evaluación de riesgos para la salud en sitios contaminados," Centro Panamericano de Ingeniería Sanitaria y Ciencias del Ambiente, Lima, Peru, 1999.

[22] J. Mejía, L. Yáñez, L. Carrizales, and M. F. Díaz-Barriga, "Evaluación integral del riesgo en sitios contaminados: una propuesta metodológica," *Scientiae Naturae*, vol. 4, pp. 25–42, 2001.

[23] L. Yáñez, E. García-Nieto, E. Rojas et al., "DNA damage in blood cells from children exposed to arsenic and lead in a mining area," *Environmental Research*, vol. 93, no. 3, pp. 231–240, 2003.

[24] S. P. Gamiño-Gutiérrez, C. I. González-Pérez, M. E. Gonsebatt, and M. G. Monroy-Fernández, "Arsenic and lead contamination in urban soils of Villa de la Paz (Mexico) affected by historical mine wastes and its effect on children's health studied by micronucleated exfoliated cells assay," *Environmental Geochemistry and Health*, vol. 35, no. 1, pp. 37–51, 2013.

[25] Y. Jasso-Pineda, G. Espinosa-Reyes, D. González-Mille et al., "An integrated health risk assessment approach to the study of mining sites contaminated with arsenic and lead," *Integrated Environmental Assessment and Management*, vol. 3, no. 3, pp. 344–350, 2007.

[26] L. Chapa-Vargas, J. J. Mejía-Saavedra, K. Monzalvo-Santos, and F. Puebla-Olivares, "Blood lead concentrations in wild birds from a polluted mining region at Villa de la Paz, San Luis Potosí, Mexico," *Journal of Environmental Science and Health A*, vol. 45, no. 1, pp. 90–98, 2010.

[27] B. Machado-Estrada, J. Calderón, R. Moreno-Sánchez, and J. S. Rodríguez-Zavala, "Accumulation of arsenic, lead, copper, and zinc, and synthesis of phytochelatins by indigenous plants of a mining impacted area," *Environmental Science and Pollution Research*, vol. 20, no. 6, pp. 3946–3955, 2013.

[28] S. A. Hasan, Q. Fariduddin, B. Ali, S. Hayat, and A. Ahmad, "Cadmium: toxicity and tolerance in plants," *Journal of Environmental Biology*, vol. 30, no. 2, pp. 165–174, 2009.

[29] R. Eisler, *Copper Hazards to Fish, Wildlife, and Invertebrates: A Synoptic Review*, Biological Science Report no. 33, U.S. Geological Survey, Biological Resources Division, 1998.

[30] R. A. Efroymson, M. E. Will, G. W. Suter II, and A. C. Wooten, *Toxicological Benchmarks for Screening Contaminants of Potential Concern for Effects on Terrestrial Plants: 1997 Revision*, U.S. Department of Energy, Oak Ridge, Tenn, USA, 1997.

[31] S. Cheng, "Heavy metals in plants and phytoremediation," *Environmental Science and Pollution Research*, vol. 10, no. 5, pp. 335–340, 2003.

[32] A. Kashem and B. R. Singh, "Heavy metal contamination of soil and vegetation in the vicinity of industries in Bangladesh," *Water, Air, and Soil Pollution*, vol. 115, no. 1–4, pp. 347–361, 1999.

[33] D. Peplow, "Environmental impacts of mining in eastern Washington," Center for Water and Watershed Studies, University of Washington, Seattle, Wash, USA, 1999.

[34] R. A. Medellín, M. Equihua, and M. A. Amin, "Bat diversity and abundance as indicators of disturbance in neotropical rainforest," *Conservation Biology*, vol. 14, no. 6, pp. 1666–1675, 2000.

[35] B. P. Mishra, O. P. Tripathi, R. S. Tripathi, and H. N. Pandey, "Effects of anthropogenic disturbance on plant diversity and community structure of a sacred grove in Meghalaya, northeast India," *Biodiversity and Conservation*, vol. 13, no. 2, pp. 421–436, 2004.

[36] J. A. Vásquez, J. M. A. Vega, B. Matsuhiro, and C. Urzúa, "The ecological effects of mining discharges on subtidal habitats dominated by macroalgae in northern Chile: population and community level studies," *Hydrobiologia*, vol. 398-399, pp. 217–229, 1999.

[37] D. K. Niyogi, W. M. Lewis Jr., and D. M. McKnight, "Effects of stress from mine drainage on diversity, biomass, and function of primary producers in mountain streams," *Ecosystems*, vol. 5, no. 6, pp. 554–567, 2002.

[38] A. A. Ramadan, "Heavy metal pollution and biomonitoring plants in Lake Manzala, Egypt," *Pakistan Journal of Biological Sciences*, vol. 6, no. 13, pp. 1108–1117, 2003.

[39] T. P. Sullivan and D. S. Sullivan, "Vegetation management and ecosystem disturbance: impact of glyphosate herbicide on plant and animal diversity in terrestrial systems," *Environmental Reviews*, vol. 11, no. 1, pp. 37–59, 2003.

[40] M. T. Fountain and S. P. Hopkin, "Biodiversity of collembola in urban soils and the use of *Folsomia candida* to assess soil 'quality'," *Ecotoxicology*, vol. 13, no. 6, pp. 555–572, 2004.

[41] H. Freitas, M. N. V. Prasad, and J. Pratas, "Plant community tolerant to trace elements growing on the degraded soils of São Domingos mine in the south east of Portugal: environmental implications," *Environment International*, vol. 30, no. 1, pp. 65–72, 2004.

[42] S. S. Talmage and B. T. Walton, "Small mammals as monitors of environmental contaminants," *Reviews of Environmental Contamination and Toxicology*, vol. 119, pp. 47–145, 1991.

[43] B. V. Erry, M. R. MacNair, A. A. Meharg, and R. F. Shore, "Arsenic contamination in wood mice (*Apodemus sylvaticus*) and bank voles (*Clethrionomys glareolus*) on abandoned mine sites in southwest Britain," *Environmental Pollution*, vol. 110, no. 1, pp. 179–187, 2000.

[44] K. C. Torres and M. L. Johnson, "Bioaccumulation of metals in plants, arthropods, and mice at a seasonal wetland," *Environmental Toxicology and Chemistry*, vol. 20, no. 11, pp. 2617–2626, 2001.

[45] A. Milton, J. A. Cooke, and M. S. Johnson, "Accumulation of lead, zinc, and cadmium in a wild population of *Clethrionomys glareolus* from an abandoned lead mine," *Archives of Environmental Contamination and Toxicology*, vol. 44, no. 3, pp. 405–411, 2003.

[46] L. A. Ieradi, J. Zima, F. Allegra et al., "Evaluation of genotoxic damage in wild rodents from a polluted area in the Czech Republic," *Folia Zoologica*, vol. 52, no. 1, pp. 57–66, 2003.

[47] R. Šumbera, V. Baruš, and F. Tenora, "Heavy metals in the silvery mole-rat, *Heliophobius argenteocinereus* (Bathyergidae, Rodentia) from Malawi," *Folia Zoologica*, vol. 52, no. 2, pp. 149–153, 2003.

[48] H. Reynolds, "The ecology of the Merriam kangaroo rat (*Dipodomys merriami* Mearns) on the grazing lands of southern Arizona," *Ecological Monographs*, vol. 28, no. 2, pp. 110–127, 1958.

[49] J. da Silva, T. R. O. de Freitas, J. R. Marinho, G. Speit, and B. Erdtmann, "An alkaline single-cell gel electrophoresis (comet) assay for environmental biomonitoring with native rodents," *Genetics and Molecular Biology*, vol. 23, no. 1, pp. 241–245, 2000.

[50] F. Festa, M. Cristaldi, L. A. Ieradi, S. Moreno, and R. Cozzi, "The comet assay for the detection of DNA damage in *Mus spretus* from Doñana National Park," *Environmental Research*, vol. 91, no. 1, pp. 54–61, 2003.

[51] G. D. Kataev, J. Suomela, and P. Palokangas, "Densities of microtine rodents along a pollution gradient from a copper-nickel smelter," *Oecologia*, vol. 97, no. 4, pp. 491–498, 1994.

[52] E. García, *Modificaciones al Sistema de Clasificación Climática de Köppen*, Instituto de Geografía, Universidad Nacional Autónoma de México, Coyoacán, Mexico, 2004.

[53] Instituto Nacional de Estadística, Geografía e Informática (INEGI), *Síntesis de información geográfica del estado de San Luis Potosí*, INEGI, Aguascalientes, Mexico, 2002.

[54] J. Rzedowski, *Vegetación de México*, Limusa, Mexico City, Mexico, 1978.

[55] Instituto Nacional de Estadística, Geografía e Informática (INEGI), *Anuario Estadístico: San Luis Potosí*, 2012, http://www.inegi.org.mx/est/contenidos/espanol/sistemas/aee12/estatal/slp/default.htm.

[56] M. C. Molina, M. E. García, R. R. Aguirre, and C. E. González, "La reserva de semillas de un pastizal de *Bouteloua gracilis*," *Agrociencia*, vol. 1, no. 3, pp. 93–103, 1991.

[57] D. Mueller-Dombois and H. Ellengerg, *Aims and Methods of Vegetation Ecology*, John Wiley & Sons, New York, NY, USA, 1974.

[58] L. J. Franco, G. A. de la Cruz, A. G. Cruz et al., *Manual de Ecología*, Trillas, Tlalnepantla de Baz, Mexico, 2nd edition, 1989.

[59] J. E. Brower, J. H. Zar, and C. N. von Ende, *Field and Laboratory Methods for General Ecology*, McGraw-Hill, Boston, Mass, USA, 4th edition, 1998.

[60] G. A. F. Seber, *The Estimation of Animal Abundance and Related Parameters*, Griffin, London, UK, 1973.

[61] L. Boitani and T. K. Fuller, *Research Techniques in Animal Ecology: Controversies and Consequences*, University Press Columbia, New York, NY, USA, 2000.

[62] M. Romero-Almaráz, C. Sánchez-Hernández, C. García-Estrada, and R. Owen, *Mamíferos pequeños: Manual de técnicas de captura, preparación, preservación y estudio*, UNAM, Coyoacán, Mexico, 2nd edition, 2007.

[63] A. E. Magurran, *Diversidad ecológica y su medición*, VEDRA, Barcelona, Spain, 1989.

[64] R. Margalef, *Ecología*, Planeta, Barcelona, Spain, 1981.

[65] K. Hutcheson, "A test for comparing diversities based on the Shannon formula," *Journal of Theoretical Biology*, vol. 29, no. 1, pp. 151–154, 1970.

[66] W. H. Clements and M. C. Newman, *Community Ecotoxicology*, John Wiley & Sons, London, UK, 2002.

[67] *Canadian Environmental Quality Guidelines* (CEQG), Canadian Council of Ministers of the Environment, 1999.

[68] C. Cervantes and S. R. Moreno, *Contaminación ambiental por metales pesados: impacto en los seres vivo*, AGT Editor, Mexico City, Mexico, 1999.

[69] A. Kabata-Pendias and H. Pendias, *Trace Elements in Soils and Plants*, CRC Press, Boca Raton, Fla, USA, 2001.

[70] S. E. Lorenz, R. E. Hamon, P. E. Holm et al., "Cadmium and zinc in plants and soil solutions from contaminated soils," *Plant and Soil*, vol. 189, no. 1, pp. 21–31, 1997.

[71] A. R. Memon, D. Aktoprakligil, A. Özdemir, and A. Vertii, "Heavy metal accumulation and detoxification mechanisms in plants," *Turkish Journal of Botany*, vol. 25, no. 3, pp. 111–121, 2001.

[72] M. Ghosh and S. P. Singh, "A review on phytoremediation of heavy metals and utilization of its byproducts," *Applied Ecology and Environmental Research*, vol. 3, no. 1, pp. 1–18, 2005.

[73] A. L. Youngman, T. L. Williams, and L. S. Tien, "Patterns of accumulation of heavy metals in non-woody vegetation established on zinc-lead smelter contaminated soils," in *Proceedings of the Conference on Hazardous Waste Research*, pp. 134–141, 1998.

[74] D. G. Lumsdon, J. C. L. Meeussen, E. Paterson, L. M. Garden, and P. Anderson, "Use of solid phase characterisation and'chemical modelling for assessing the behaviour of arsenic in contaminated soils," *Applied Geochemistry*, vol. 16, no. 6, pp. 571–581, 2001.

[75] Q.-R. Wang, Y.-S. Cui, X.-M. Liu, Y.-T. Dong, and P. Christie, "Soil contamination and plant uptake of heavy metals at polluted sites in China," *Journal of Environmental Science and Health A*, vol. 38, no. 5, pp. 823–838, 2003.

[76] F. Malaisse, A. Baker, and S. Ruell, "Diversity of plant communities and leaf heavy metal content at Luiswishi copper/cobalt mineralization, Upper Katanga, Dem. Rep. Congo," *Biotechnology Agronomy Society Environment*, vol. 3, no. 2, pp. 104–114, 1999.

[77] S. N. Luoma, "The dynamics of biologically available mercury in a small estuary," *Estuarine and Coastal Marine Science*, vol. 5, no. 5, pp. 643–652, 1977.

[78] H. W. Martin, T. R. Young, D. I. Kaplan, L. Simon, and D. C. Adriano, "Evaluation of three herbaceous index plant species for bioavailability of soil cadmium, chromium, nickel and vanadium," *Plant and Soil*, vol. 182, no. 2, pp. 199–207, 1996.

[79] J. L. Gardea-Torresdey, L. Polette, S. Arteaga, K. J. Tiemann, J. Bibb, and J. H. Gonzalez, "Determination of the content of hazardous heavy metals on Larrea tridentata grown around a contaminated area," in *Proceedings of the Conference on Hazardous Waste Research*, p. 10, 1998.

[80] J. L. Gardea-Torresdey, J. Bibb, K. J. Tiemann, J. H. González, and J. L. Arenas, "Adsorption of copper ions from solution by heavy metal stressed Larrea tridentate (creosote bush) biomass," in *Proceedings of the Conference on Hazardous Waste Research*, p. 11, 1998.

[81] A. H. Bu-Olayan and B. V. Thomas, "Biomonitoring studies on the lead levels in mesquite (*Prosopis juliflora*) in the arid ecosystem of Kuwait," *Kuwait Journal of Science and Engineering*, vol. 29, no. 1, pp. 65–73, 2002.

[82] J. Sienkiewicz, "Effect of heavy-metals industry on plant communities," *The Science of the Total Environment*, vol. 55, pp. 339–349, 1986.

Hindawi Publishing Corporation
BioMed Research International
Volume 2014, Article ID 143283, 7 pages
http://dx.doi.org/10.1155/2014/143283

Research Article

Differences of Cytotoxicity of Orthodontic Bands Assessed by Survival Tests in *Saccharomyces cerevisiae*

Tatiana Siqueira Gonçalves,[1] Luciane Macedo de Menezes,[1] Luciele Gonzaga Ribeiro,[2] Catieli Gobetti Lindholz,[2] and Renata Medina-Silva[2]

[1] *Department of Orthodontics, Dentistry Faculty, Pontifícia Universidade Católica do Rio Grande do Sul, Avenida Ipiranga 6681, Building 6, Room 209, 90619-900 Porto Alegre, RS, Brazil*
[2] *Immunology and Microbiology Laboratory, Biosciences Faculty, Pontifícia Universidade Católica do Rio Grande do Sul, Avenida Ipiranga 6681, Building 12, Lab 12D, 90619-900 Porto Alegre, RS, Brazil*

Correspondence should be addressed to Tatiana Siqueira Gonçalves; tatianasiqueiragoncalves@gmail.com

Received 19 October 2013; Revised 6 December 2013; Accepted 7 December 2013; Published 6 January 2014

Academic Editor: Susana Viegas

The aim of this study was to evaluate the cytotoxicity induced by orthodontic bands through survival tests on *Saccharomyces cerevisiae,* a microorganism that presents several genetic and biochemical characteristics similar to human cells. Three groups of bands were evaluated: silver soldered (SSB), laser soldered (LSB), and bands without any solder (WSB). Yeast cells were directly exposed to the bands and indirectly, when a previous elution of the metals in artificial saliva was performed. The negative control was composed of yeast cells or artificial saliva not exposed to any kind of metal. In the direct exposure experiments, all tested groups of bands induced a slight reduction in yeast viability compared to the control. This effect was more intense for the SSB, although not statistically significant. For the indirect exposure experiments, the SSB induced a statistically significant decrease in cell viability compared to the LSB. There were no significant differences between the survival rates of the negative control and the LSB group in both direct and saliva tests. SSBs were cytotoxic, whilst LSBs were not, confirming that laser soldering may be a more biocompatible alternative for use in connecting wires to orthodontic appliances.

1. Introduction

Biocompatibility refers to the ability of a biomaterial to perform its desired function with respect to a medical therapy, without eliciting any undesirable local or systemic effects in the recipient or beneficiary of that therapy but generating the most appropriate beneficial cellular or tissue response in that specific situation and optimizing the clinically relevant performance of that therapy [1]. Corrosion is the main concern when biocompatibility of orthodontic metallic materials is evaluated. The release of several metallic ions [2] may lead to hypersensitivity and allergic reactions, either locally as well as systemically [3].

In daily practice, it is usual to use orthodontic bands during interceptive and corrective treatments. The bands are generally made of stainless steel and are composed of nickel, iron and chromium, and it is considered a biocompatible alloy [4, 5]. However, in several clinical situations, it is necessary to connect orthodontic wires to the bands, especially when auxiliary appliances, such as lingual arches and maxillary expanders, are made. To connect the support wires to the appliances, silver solder is the alloy of choice, due to its proven effectiveness, low cost, and ease of use. However, the silver solder alloy contains silver, copper, and zinc. These ions present a major tendency to be released to the buccal cavity [6] and they may have cytotoxic effects, resulting in decrease of cell viability [5]. Cadmium used to be added to the composition of silver solder alloys some decades ago [7] and, due to the process of zinc obtaining from the ores, cadmium may appear as a zinc contaminant [8]. It is important to remember that cadmium exposure is responsible for hepatic, renal, and myocardial damage characterized by increased creatinine, total and direct bilirubin concentrations and increased ALT and lactate dehydrogenase (LDH) activities [9]. Besides this,

Figure 1: Silver soldered band (SSB).

Figure 2: Laser soldered band (LSB).

Figure 3: Band without any solder (as received—WSB).

cadmium has been considered a mutagen and may be related to the occurrence of cancer [10–12].

An alternative to soldering with silver solder can be the laser welding. In this method, the use of a third metal or alloy, such as the silver solder, can be avoided, as the stainless steel bands and orthodontic wires can be directly connected. With laser soldering, the energy generated promotes real fusion of the metals joined. It may be less susceptible to corrosion and consequently more biocompatible.

Nowadays, several *in vitro* cell culture tests can be used in order to assess the cytotoxicity of dental materials. Among these tests, some yield similar results, whereas some others reveal diverse or even opposing findings [5, 13–17]. The yeast *Saccharomyces cerevisiae* [18] can be used as a model organism for the *in vitro* cytotoxicity evaluation of several harmful agents as well [19–24], offering advantages once they are easy and inexpensive to manipulate. They can provide a large amount of quantitative data from well-controlled experiments with short-time results being phylogenetically very closely related to animals [25]. Biochemical and genetic similarities [26, 27] justify the use of yeast models to address a scientific question of clinical interest [18, 28–33]. However, few dental studies have used this microorganism for this purpose [34, 35], and only one was dedicated to efficiently evaluate orthodontic materials [4].

Taking into consideration the fact that silver solder may present cytotoxic effects, that laser soldering is still an emerging technique in orthodontics and has been scarcely evaluated and, mainly, considering the large scale use of orthodontic bands with silver soldered joints in orthodontic auxiliary appliance and the lack of studies evaluating the cytotoxicity of orthodontic bands, the aim of this study was to evaluate the induction of cytotoxicity by orthodontic bands with or without laser or silver solder using a wild-type *S. cerevisiae* strain as a model organism.

2. Materials and Methods

This study was approved by the ethics Committee from Pontifícia Universidade Católica do Rio Grande do Sul (Porto Alegre, Brazil). Stainless steel metallic orthodontic bands (Universal bands for upper molars Morelli, Sorocaba/SP, Brazil) were evaluated. The bands, according to the manufacturer's information, are composed of Cr: 17–20%; Ni: 8–10%; Mo: max. 0,60%; and Fe. Three groups were formed: silver soldered bands (SSB—Figure 1), laser soldered bands (LSB—Figure 2), and bands without any kind of solder (WSB—Figure 3). For the silver solder group, in each band, a segment of stainless steel 1.0 mm wire (Cr: 17–20%; Ni: 8–10%; Mo: max. 0,60%; and Fe) was soldered using silver solder alloy (Ag 55–57%, Cu 21–23%, Zn 15–19%, and Sn 4–6%) and solder flux (Morelli, Sorocaba/SP, Brazil) heated by a butane microtorch (GB 2001, Blazer, Farmingdale, NY, USA). For the laser soldered group, the same 1.0 mm stainless steel orthodontic wire was soldered to the band using *laser* Nd: Yag (250 V, 12 ms; Dentaurum, DL 2002-S, Germany). The third group was composed of bands without any solder and was evaluated as received.

2.1. S. cerevisiae Strain, Media, and Cultures. The *S. cerevisiae* strain used in this work was the wild-type strain FF18733. To cultivate this strain, YPD medium (1% yeast extract, 2% peptone, and 2% glucose) was used, either in broth or solid (with agar at 2%) form. In all survival experiments, *S. cerevisiae* precultures were prepared in 10 mL YPD broth

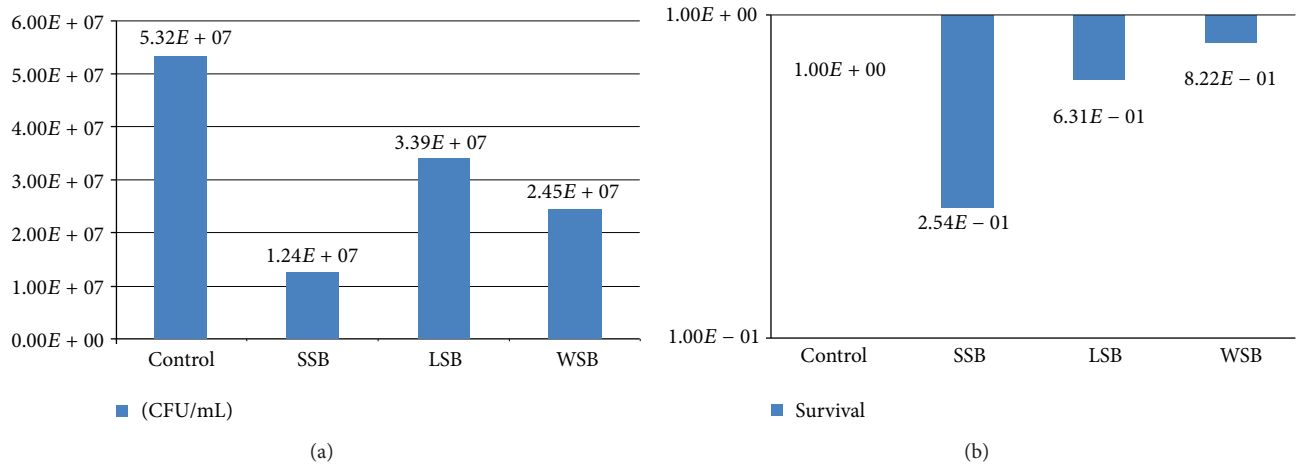

Figure 4: (a) Mean values of cell viability (CFU/mL) from three direct exposure experiments with *S. cerevisiae* strain FF18733 performed with bands bearing silver solder (SSB), laser solder (LSB), or without solder (WSB) in YPD agar. (b) Mean values of yeast survival from three direct exposure experiments with *S. cerevisiae* strain FF18733 performed with bands bearing silver solder (SSB), laser solder (LSB), or without solder (WSB) in YPD agar.

and grown overnight to exponential phase (~10^{-7} cells/mL) at 30°C.

2.2. Survival Experiments for Cytotoxicity Analysis. The cytotoxicity analysis was performed as already described [4] via two types of survival experiments: (1) direct exposure of *S. cerevisiae* cells to the bands and (2) previous elution of the bands in artificial commercial saliva (Salivan, Apsen Farmacêutica SA, Brazil), followed by exposure of *S. cerevisiae* cells to the artificial saliva containing the metals' elutes. The negative control in the direct exposure was composed of yeast cells that were not exposed to any kind of metal. In the saliva exposure test, the artificial saliva was the negative control. The experiments were performed in triplicate.

Direct Exposure Experiments. New inocula were made, each one containing one band either with silver solder (SSB), laser solder (LSB), or without any solder (WSB) and were incubated at 30°C to exponential phase (~10^{-7} cells/mL). Aliquots from each culture were diluted in 0.9% sterile saline solution and 5 μL drops from each dilution (from 10^{-2} to 10^{-5}) were plated on YPD agar and incubated at 30°C for two days for the emergence of small colonies, which allowed an initial qualitative approach. For the final quantitative analyses, 100 μL of the final dilutions were plated on YPD agar (two plates for each dilution) for colony counting and CFU/mL estimative after two days at 30°C.

Saliva Exposure Experiments. Each band was immersed in 500 μL of artificial saliva for 7 days. A total of 500 μL of the preinoculum was used for each treatment, which was centrifuged (2 min at 2000 g) and resuspended at 100% with the saliva preexposed to the different bands. The cells were then treated for 60 minutes, diluted, and plated in YPD agar as described above, for both qualitative and quantitative analyses. A negative control was performed with the artificial saliva not exposed to any kind of metal and the tests were performed in triplicate.

2.3. Data Analyses. The mean and standard deviation of the colony forming units per mL (CFU/mL) counts from three independent repeats of each treatment were compared to their specific controls to verify the occurrence of significant survival differences. If there was at least one log of difference in terms of CFU/mL in treatments in relation to controls, it was assumed a significant difference, which was an indication of cellular toxicity in *S. cerevisiae*.

3. Results

The results from survival experiments are shown in Figures 4 and 5. Regarding the direct experiments, it is possible to observe that the three groups (SSB, LSB, and WSB) induced a decrease in cell viability of *S. cerevisiae* in terms of CFU/mL compared to the control. This effect was more intense with the SSB group, which can be viewed in terms of viable cells (Figure 4(a)). Nevertheless, there was no significant difference in terms of survival, since it was below one log of difference for all samples, but SSB, the one that bear more metal alloys, achieved the higher value (Figure 4(b)). The experiments of saliva exposure showed that the saliva elutes from the three different groups are also able to induce a decrease in *S. cerevisiae* cell viability (Figure 5(a)). The SSB samples were also those that most induced cytotoxicity and, in this case, with a significant difference in terms of survival compared to the control, which did not occur with the LSB or the WSB samples (Figure 5(b)). It is important to notice that the data shows no significant differences between the survival results from the LSB (as well as from WSB) in relation to controls in both direct and saliva tests. Moreover, in saliva experiments the difference between the SSB and the LSB in terms of survival percent is considered significant. These

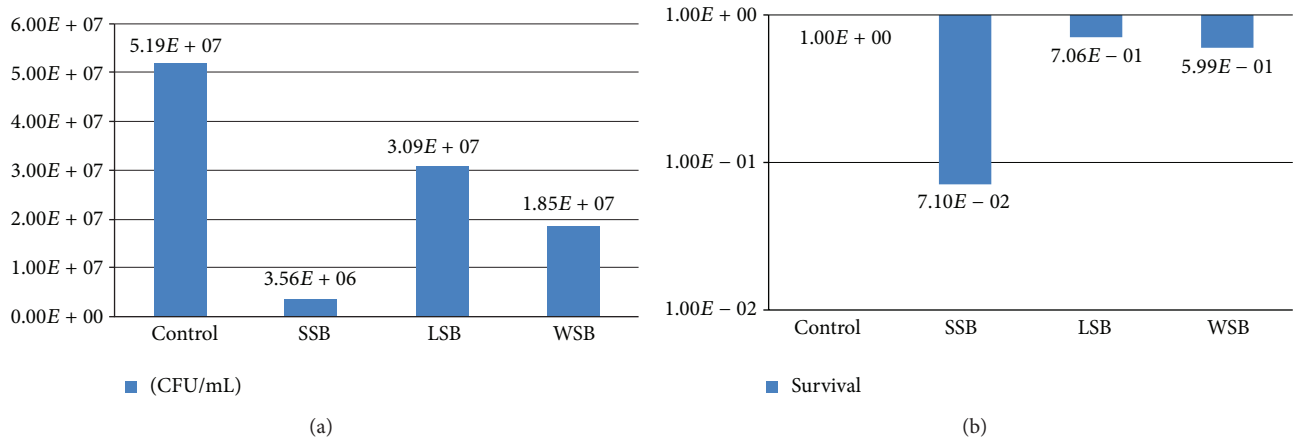

Figure 5: (a) Mean values of cell viability (CFU/mL) from three experiments with saliva elutes in *S. cerevisiae* strain FF18733 performed with bands bearing silver solder bands (SSB), laser solder (LSB), or without solder (WSB) in YPD agar. (b) Mean values of yeast survival from three experiments with saliva elutes in *S. cerevisiae* strain FF18733 performed with bands bearing silver solder (SSB), laser solder (LSB), or without solder (WSB) in YPD agar.

results indicate an important difference in terms of cytotoxicity induction between these two kinds of orthodontic joints and thus an indication of higher biocompatible properties of LSB compared to the most used worldwide, the SSB.

4. Discussion

An important part of the population undergoes orthodontic treatments during their lives. Orthodontic bands, composed of iron, nickel, and chromium, are frequently joined to orthodontic wires for the making of auxiliary appliances and, for this, it is usually employed a filling material such as the silver solder alloy. This alloy contains silver, copper, and zinc and may even contain a little amount of cadmium. These ions, together with nickel and chromium, may illicit several undesirable reactions. Specifically, when these metals are heated, the corrosion process may be increased, leading to the elution of ions to the buccal cavity, with local and systemic effects [2, 4, 5, 15, 16, 36–41]. In recent years, the use of laser solder has increased, especially for implant-based prosthesis and it can be used for orthodontic purposes as well [42]. It is a very interesting alternative to connect thick wires such as those used in auxiliary orthodontic appliances. The main advantage is that the energy generated by the laser produces a real fusion between the metals connected, avoiding the need of an additional filling material such as the silver alloy. Consequently, the variety of metallic ions is reduced and the corrosion process is lower. However, its cost is still high since there is the need of a very specific equipment to perform it [42].

The experimental model *S. cerevisiae* has been widely used in biomedical research studies, with very diverse objectives and applications, from cellular biology involved in genetic and neurological diseases [43] to toxicological surveys [44]. The broad applicability of this yeast species as a model organism is based on its easy cell cycle control, great facility of biochemical and genetic manipulation, short time, and inexpensive reproducible experiments [45] as well as biochemical and genetic similarity to animal cells [26, 27]. These *S. cerevisiae* properties' enables the achievement of results compatible with other experimental models such as cultured animal cell, such as fibroblasts, osteoblasts, and keratinocytes [15, 39, 40]. Moreover, it proved to be effective to evaluate the cytotoxicity induction of several orthodontic materials [4].

Based on the wide advantages of the biological model described above, the experiments were conducted using both direct exposure of *S. cerevisiae* cells to the bands and also the exposure of these yeast cells to artificial saliva containing the bands' elutes. This second group of experiments was performed in order to simulate the oral cavity chemistry and its effects over the materials tested.

Auxiliary orthodontic appliances with orthodontic bands may stay in the patient's mouth for a long period of time. For patients subject to maxillary expansion and protraction, at least 13 months with the appliance are necessary. When lingual arches are used as space maintainers, it may be used from as early as six years, until the end of the orthodontic treatment, what may occur only at 13-14 years old. For this reason, it is important to investigate cellular effects of the orthodontic bands, as well as their joins, mainly due to the lack of information in the literature concerning specifically this material. The current available reports evaluated mainly orthodontic wires with soldered connections [39–41].

In the SSB group, the bands tested contained silver flux and suffered the effects of the heat and the high temperatures achieved which are necessary to melt the silver alloy. The objective was to reproduce what actually occurs when auxiliary appliances are made, instead of testing the cytotoxic effects of silver solder alloy alone [4, 15]. Lower cell viability was observed in both experiments and with significant differences (higher than 1 log—Figure 5(b)) in relation to the control in the experiments of exposure to saliva elutes, in accordance with a previous study [4]. Possibly, when the bands were in contact with the artificial saliva, corrosion occurred, leading to the elution of toxic ions. Specifically,

nickel, a major component of stainless steel bands, may be easily released [46] leading to toxic effects [38, 47, 48]. The components of silver solder alloy may release toxic ions as well [49]. It has been stated that one of the mechanisms involved in the silver solder toxicity is the occurrence of oxidative stress [4].

Solmi et al. [40] evaluated the reaction of fibroblasts cultured *in vitro* in direct contact with samples of soldered and laser-welded joints from orthodontic lingual arches. Adhesion, morphology, and proliferation of the cells were evaluated under contrast phase light microscopy and scanning electron microscopy and it was concluded that laser-welded joints were superior in terms of biocompatibility. The results of Solmi et al. [40] are in accordance with the findings of the present study; however, the authors evaluated the fibroblast's reaction to the soldered surface only, not considering the whole band. It is important to consider that the oxidation process occurs at the whole surface of the band which is in contact with saliva during clinical use, suffering the effects of the corrosion all over the band, involving not only the silver solder metals but the stainless steel components as well. It seems that evaluating the cell survival after an elution time of the materials in artificial saliva, as performed in the present study, is a good alternative to simulate the effects of a liquid immersion media in corrosion of the bands.

Sestini et al. [39] evaluated orthodontic wires and their effects on osteoblasts, fibroblasts, and keratinocytes through several *in vitro* cytotoxicity tests. They found high cytotoxicity of silver soldered joints, whereas laser soldered joints were considered the only joining process well tolerated by all cell types. Again, the findings of Sestini et al. [39] agree with the findings of the present study; however, similar to Solmi et al. [38], the authors evaluated only the wires and did not consider the joining process that occurs in orthodontic bands, which presents a higher area of soldering. The authors used the wires in direct contact with the cells not considering a previous corrosion process, as reported in the present study for the indirect experiments.

As done by Sestini et al. [39], Vande Vannet et al. [41] also evaluated orthodontic wires but used three-dimensional oral mucosal cell. The authors revealed that silver soldered wires led to higher loss of viability than laser welded and electric welded joints. They also tested stainless steel wires alone, as we did with the WSB, assuring the biocompatibility of stainless steel alone. The same good performance was observed for the laser soldered wires, in accordance with the LSB group in our work with the bands. Vande Vannet et al. [41] also found lower cell viability with the silver soldered wires, however, with no statistical differences when compared to the control and to the other tested groups, such as laser solder and stainless steel alone.

In the present study no significant differences were observed between the results of cell survival from the LSB and those from the control, in both direct and indirect evaluations. This indicates that laser soldering was not cytotoxic to *S. cerevisiae* cells. Additionally, there was a significant difference from the levels of cytotoxicity induced by the SSB group in saliva experiments when compared to the LSB, which confirms laser soldering as an interesting alternative for clinical use in orthodontic bands and for the making of auxiliary appliances that are extensively used in clinical practice.

The present study clearly indicated that silver solder actually presents cytotoxic effects and that laser solder is certainly a more biocompatible option for the connection of wires and for auxiliary appliances. However, more studies are necessary using yeast cells or other experimental models to observe not only the cytotoxic effects of silver solder but also if this material actually increases the occurrence of oxidative stress and if that mechanism may lead to possible genotoxic effects.

5. Conclusions

Silver soldered bands were cytotoxic to *S. cerevisiae* cells. There was significant difference between the laser soldering and the silver soldering groups, indicating the use of laser soldering as a more biocompatible alternative for clinical use in orthodontic appliances.

Conflict of Interests

The authors have no conflict of interest to disclose.

Acknowledgments

This study is based on a thesis submitted to the Dentistry Faculty, Pontifícia Universidade Católica do Rio Grande do Sul, Brazil, in partial fulfillment of the requirements for an Orthodontics Ph.D. degree. The authors thank Coordenação de Aperfeiçoamento de Pessoal de Nível Superior (CAPES), Brazil, for funding this research.

References

[1] D. F. Williams, "On the mechanisms of biocompatibility," *Biomaterials*, vol. 29, no. 20, pp. 2941–2953, 2008.

[2] L. M. Menezes and C. C. A. Quintão, "The release of ions from metallic orthodontic appliances," *Seminars in Orthodontics*, vol. 16, pp. 282–292, 2010.

[3] L. M. Menezes, L. C. Campos, C. C. Quintão, and A. M. Bolognese, "Hypersensitivity to metals in orthodontics," *American Journal of Orthodontics and Dentofacial Orthopedics*, vol. 126, no. 1, pp. 58–64, 2004.

[4] K. M. Limberger, G. H. Westphalen, L. M. Menezes, and R. Medina-Silva, "Cytotoxicity of orthodontic materials assessed by survival tests in Saccharomyces cerevisiae," *Dental Materials*, vol. 27, no. 5, pp. e81–e86, 2011.

[5] O. Mockers, D. Deroze, and J. Camps, "Cytotoxicity of orthodontic bands, brackets and archwires in vitro," *Dental Materials*, vol. 18, no. 4, pp. 311–317, 2002.

[6] N. Shigeto, T. Yanagihara, T. Hamada, and E. Budtz-Jørgensen, "Corrosion properties of soldered joints. Part I: electrochemical action of dental solder and dental nickel-chromium alloy," *The Journal of Prosthetic Dentistry*, vol. 62, no. 5, pp. 512–515, 1989.

[7] M. Berge, N. R. Gjerdet, and E. S. Erichsen, "Corrosion of silver soldered orthodontic wires," *Acta Odontologica Scandinavica*, vol. 40, pp. 75–79, 1982.

[8] M. Fleischer, A. F. Sarofim, and D. W. Fassett, "Environmental impact of cadmium: a review by the panel on hazardous trace substances," *Environmental Health Perspectives*, vol. 7, pp. 253–323, 1974.

[9] E. L. B. Novelli, R. T. Hernandes, J. L. V. B. Novelli Filho, and L. L. Barbosa, "Differential/combined effect of water contamination with cadmium and nickel on tissues of rats," *Environmental Pollution*, vol. 103, no. 2-3, pp. 295–300, 1998.

[10] Y. H. Jin, A. B. Clark, R. J. C. Slebos et al., "Cadmium is a mutagen that acts by inhibiting mismatch repair," *Nature Genetics*, vol. 34, no. 3, pp. 326–329, 2003.

[11] J. Xie and Z. A. Shaikh, "Cadmium induces cell cycle arrest in rat kidney epithelial cells in G2/M phase," *Toxicology*, vol. 224, no. 1-2, pp. 56–65, 2006.

[12] J. Huff, R. M. Lunn, M. P. Waalkes, L. Tomatis, and P. F. Infante, "Cadmium-induced cancers in animals and in humans," *International Journal of Occupational and Environmental Health*, vol. 13, no. 2, pp. 202–212, 2007.

[13] M. Assad, A. Chernyshov, M. A. Leroux, and C. H. Rivard, "A new porous titanium-nickel alloy—part 2. Sensitization, irritation and acute systemic toxicity evaluation," *Bio-Medical Materials and Engineering*, vol. 12, no. 4, pp. 339–346, 2002.

[14] M. Assad, A. Chernyshov, M. A. Leroux, and C. H. Rivard, "A new porous titanium-nickel alloy—part 1. Cytotoxicity and genotoxicity evaluation," *Bio-Medical Materials and Engineering*, vol. 12, no. 3, pp. 225–237, 2002.

[15] M. P. M. Freitasa, H. M. S. Oshima, L. M. Menezes, D. C. Machado, and C. Viezzer, "Cytotoxicity of silver solder employed in orthodontics," *Angle Orthodontist*, vol. 79, no. 5, pp. 939–944, 2009.

[16] C. T. Kao, S. J. Ding, Y. Min, T. C. Hsu, M. Y. Chou, and T.-H. Huang, "The cytotoxicity of orthodontic metal bracket immersion media," *European Journal of Orthodontics*, vol. 29, no. 2, pp. 198–203, 2007.

[17] D. J. Wever, A. G. Veldhuizen, M. M. Sanders, J. M. Schakenraad, and J. R. van Horn, "Cytotoxic, allergic and genotoxic activity of a nickel-titanium alloy," *Biomaterials*, vol. 18, no. 16, pp. 1115–1120, 1997.

[18] J. E. Galagan, M. R. Henn, L.-J. Ma, C. A. Cuomo, and B. Birren, "Genomics of the fungal kingdom: insights into eukaryotic biology," *Genome Research*, vol. 15, no. 12, pp. 1620–1631, 2005.

[19] S. V. Avery, "Metal toxicity in yeasts and the role of oxidative stress," *Advances in Applied Microbiology*, vol. 49, pp. 111–142, 2001.

[20] J. de Freitas, H. Wintz, J. H. Kim, H. Poynton, T. Fox, and C. Vulpe, "Yeast, a model organism for iron and copper metabolism studies," *BioMetals*, vol. 16, no. 1, pp. 185–197, 2003.

[21] P. Perego and S. B. Howell, "Molecular mechanisms controlling sensitivity to toxic metal ions in yeast," *Toxicology and Applied Pharmacology*, vol. 147, no. 2, pp. 312–318, 1997.

[22] A. V. Pinto, E. L. Deodato, J. S. Cardoso et al., "Enzymatic recognition of DNA damage induced by UVB-photosensitized titanium dioxide and biological consequences in Saccharomyces cerevisiae: evidence for oxidatively DNA damage generation," *Mutation Research*, vol. 688, pp. 3–11, 2010.

[23] N. P. Poletto, J. O. Rosado, and D. Bonatto, "Evaluation of cytotoxic and cytostatic effects in Saccharomyces cerevisiae by poissoner quantitative drop test," *Basic and Clinical Pharmacology and Toxicology*, vol. 104, no. 1, pp. 71–75, 2009.

[24] C. Xu, J. Wang, Y. Gao et al., "The anthracenedione compound bostrycin induces mitochondria-mediated apoptosis in the yeast Saccharomyces cerevisiae," *FEMS Yeast Research*, vol. 10, no. 3, pp. 297–308, 2010.

[25] W. Marande, P. López-García, and D. Moreira, "Eukaryotic diversity and phylogeny using small- and large-subunit ribosomal RNA genes from environmental samples," *Environmental Microbiology*, vol. 11, no. 12, pp. 3179–3188, 2009.

[26] D. E. Bassett Jr., M. S. Boguski, and P. Hieter, "Yeast genes and human disease," *Nature*, vol. 379, no. 6566, pp. 589–590, 1996.

[27] D. Botstein, S. A. Chervitz, and J. M. Cherry, "Yeast as a model organism," *Science*, vol. 277, no. 5330, pp. 1259–1260, 1997.

[28] V. Khurana and S. Lindquist, "Modelling neurodegeneration in Saccharomyces cerevisiae: why cook with baker's yeast?" *Nature Reviews Neuroscience*, vol. 11, no. 6, pp. 436–449, 2010.

[29] K. Liang, L. Yang, C. Yin et al., "Estrogen stimulates degradation of β-amyloid peptide by up-regulating Neprilysin," *Journal of Biological Chemistry*, vol. 285, no. 2, pp. 935–942, 2010.

[30] I. G. Macreadie, "Copper transport and Alzheimer's disease," *European Biophysics Journal*, vol. 37, no. 3, pp. 295–300, 2008.

[31] L. J. Su, P. K. Auluck, T. F. Outeiro et al., "Compounds from an unbiased chemical screen reverse both ER-to-Golgi trafficking defects and mitochondrial dysfunction in Parkinson's disease models," *DMM Disease Models and Mechanisms*, vol. 3, no. 3-4, pp. 194–208, 2010.

[32] J. Winderickx, C. Delay, A. de Vos et al., "Protein folding diseases and neurodegeneration: lessons learned from yeast," *Biochimica et Biophysica Acta*, vol. 1783, no. 7, pp. 1381–1395, 2008.

[33] V. Yeh, J. M. Broering, A. Romanyuk, B. Chen, Y. O. Chernoff, and A. S. Bommarius, "The Hofmeister effect on amyloid formation using yeast prion protein," *Protein Science*, vol. 19, no. 1, pp. 47–56, 2010.

[34] H. Tanaka, S. Ebara, A. Sugawara, M. Nishiyama, and K. Hayashi, "Basic properties of an alginate impression material supplemented with chlorhexidine. I. Disinfectant effects on oral microbes," *The Journal of Nihon University School of Dentistry*, vol. 36, no. 2, pp. 135–138, 1994.

[35] D. W. Williams, M. G. J. Waters, A. J. C. Potts, and M. A. O. Lewis, "A novel technique for assessment of adherence of Candida albicans to solid surfaces," *Journal of Clinical Pathology*, vol. 51, no. 5, pp. 390–391, 1998.

[36] T. S. Gonçalves, L. M. de Menezes, and L. E. A. Silva, "Residual monomer of autopolymerized acrylic resin according to different manipulation and polishing methods," *Angle Orthodontist*, vol. 78, no. 4, pp. 722–727, 2008.

[37] T. S. Gonçalves, V. M. Schmitt, M. Thomas, M. A. L. de Souza, and L. M. de Menezes, "Cytotoxicity of two autopolymerized acrylic resins used in orthodontics," *Angle Orthodontist*, vol. 78, no. 5, pp. 926–930, 2008.

[38] T. Eliades, H. Pratsinis, D. Kletsas, G. Eliades, and M. Makou, "Characterization and cytotoxicity of ions released from stainless steel and nickel-titanium orthodontic alloys," *American Journal of Orthodontics and Dentofacial Orthopedics*, vol. 125, no. 1, pp. 24–29, 2004.

[39] S. Sestini, L. Notarantonio, B. Cerboni et al., "In vitro toxicity evaluation of silver soldering, electrical resistance, and laser welding of orthodontic wires," *European Journal of Orthodontics*, vol. 28, no. 6, pp. 567–572, 2006.

[40] R. Solmi, D. Martini, M. Zanarini et al., "Interactions of fibroblasts with soldered and laser-welded joints," *Biomaterials*, vol. 25, no. 4, pp. 735–740, 2004.

[41] B. Vande Vannet, J.-L. Hanssens, and H. Wehrbein, "The use of three-dimensional oral mucosa cell cultures to assess the toxicity of soldered and welded wires," *European Journal of Orthodontics*, vol. 29, no. 1, pp. 60–66, 2007.

[42] J. J. Bock, W. Fraenzel, J. Bailly, C. R. Gernhardt, and R. A. W. Fuhrmann, "Influence of different brazing and welding methods on tensile strength and microhardness of orthodontic stainless steel wire," *European Journal of Orthodontics*, vol. 30, no. 4, pp. 396–400, 2008.

[43] V. Franssens, T. Bynens, J. van den Brande, K. Vandermeeren, M. Verduyckt, and J. Winderickx, "The benefits of humanized yeast models to study Parkinson's disease," *Oxidative Medicine and Cellular Longevity*, vol. 2013, Article ID 760629, 9 pages, 2013.

[44] J. S. van Leeuwen, N. P. Vermeulen, and J. Chris Vos, "Yeast as a humanized model organism for biotransformation-related toxicity," *Current Drug Metabolism*, vol. 13, pp. 1464–1475, 2012.

[45] F. Sherman, "Getting started with yeast," *Methods in Enzymology*, vol. 350, pp. 3–41, 2002.

[46] C. T. Hanks, J. C. Wataha, and Z. Sun, "In vitro models of biocompatibility: a review," *Dental Materials*, vol. 12, no. 3, pp. 186–193, 1996.

[47] E. C. Rose, I. E. Jonas, and H. F. Kappert, "In vitro investigation into the biological assessment of orthodontic wires," *Journal of Orofacial Orthopedics*, vol. 59, pp. 253–2264, 1998.

[48] J. C. Wataha, P. E. Lockwood, and A. Schedle, "Effect of silver, copper, mercury, and nickel ions on cellular proliferation during extended, low-dose exposures," *Journal of Biomedical Materials Research*, vol. 52, pp. 360–364, 2000.

[49] M. R. Grimsdottir, A. Hensten-Pettersen, and A. Kullmann, "Cytotoxic effect of orthodontic appliances," *European Journal of Orthodontics*, vol. 14, no. 1, pp. 47–53, 1992.

Hindawi Publishing Corporation
BioMed Research International
Volume 2013, Article ID 983821, 12 pages
http://dx.doi.org/10.1155/2013/983821

Research Article

Effects of Diphenyl Diselenide on Methylmercury Toxicity in Rats

Cristiane L. Dalla Corte,[1] Caroline Wagner,[2] Jéssie H. Sudati,[2] Bruna Comparsi,[3] Gerlania O. Leite,[4] Alcindo Busanello,[1] Félix A. A. Soares,[1] Michael Aschner,[5,6] and João B. T. Rocha[1]

[1] *Biochemistry and Molecular Biology Department, Graduation Program in Biological Sciences: Toxicological Biochemistry, Natural and Exact Sciences Center, Federal University of Santa Maria, 97105-900 Santa Maria, RS, Brazil*
[2] *Federal University of Pampa—Caçapava do Sul Campus, Avenida Pedro Anunciação, Vila Batista, 96570-000 Caçapava do Sul, RS, Brazil*
[3] *Higher Education Cenecista Institute of Santo Ângelo—IESA, Rua Dr. João Augusto Rodrigues 471, 98801-015 Santo Ângelo, RS, Brazil*
[4] *Regional University of Cariri, Pharmacology and Molecular Chemistry Laboratory, Rua Cel. Antônio Luís 1161, 63100-000 Crato, CE, Brazil*
[5] *Department of Pharmacology, Vanderbilt University Medical Center, Nashville, TN 37232, USA*
[6] *Department of Pediatrics, Vanderbilt University Medical Center, Nashville, TN 37232, USA*

Correspondence should be addressed to Cristiane L. Dalla Corte; crisbioq@yahoo.com.br and João B. T. Rocha; jbtrocha@yahoo.com.br

Received 19 September 2013; Revised 25 November 2013; Accepted 25 November 2013

Academic Editor: Fernando Barbosa Jr.

This study investigates the efficacy of diphenyl diselenide [$(PhSe)_2$] in attenuating methylmercury- (MeHg-)induced toxicity in rats. Adult rats were treated with MeHg [5 mg/kg/day, intragastrically (i.g.)] and/ or $(PhSe)_2$ [1 mg/kg/day, intraperitoneally (i.p.)] for 21 days. Body weight gain and motor deficits were evaluated prior to treatment, on treatment days 11 and 21. In addition, hepatic and cerebral mitochondrial function (reactive oxygen species (ROS) formation, total and nonprotein thiol levels, membrane potential ($\Delta\Psi m$), metabolic function, and swelling), hepatic, cerebral, and muscular mercury levels, and hepatic, cerebral, and renal thioredoxin reductase (TrxR) activity were evaluated. MeHg caused hepatic and cerebral mitochondrial dysfunction and inhibited TrxR activity in liver (38,9%), brain (64,3%), and kidney (73,8%). Cotreatment with $(PhSe)_2$ protected hepatic and cerebral mitochondrial thiols from depletion by MeHg but failed to completely reverse MeHg's effect on hepatic and cerebral mitochondrial dysfunction or hepatic, cerebral, and renal inhibition of TrxR activity. Additionally, the cotreatment with $(PhSe)_2$ increased Hg accumulation in the liver (50,5%) and brain (49,4%) and increased the MeHg-induced motor deficits and body-weight loss. In conclusion, these results indicate that $(PhSe)_2$ can increase Hg body burden as well as the neurotoxic effects induced by MeHg exposure in rats.

1. Introduction

MeHg is one of the most poisonous environmental contaminants, causing toxic effects in humans and experimental animals [1, 2]. Environmental MeHg is largely derived from inorganic mercury biomethylation carried out primarily by aquatic microorganisms [3] with subsequent accumulation in the aquatic food chain and human consumption [4]. MeHg causes acute and chronic damage to multiple organs, most profoundly to the central nervous system (CNS), in particular when exposures occur during the neurodevelopmental period [1, 5, 6].

The events that mediate MeHg toxicity are largely dependent upon its electrophilic properties, which allow for its

interaction with soft nucleophilic groups (mainly thiols and selenols) from either low- or high-molecular-weight biomolecules [7]. The interaction of MeHg with soft nucleophilic groups from biomolecules is responsible, at least in part, for decreased antioxidant capacity and increased ROS generation [7, 8]. Notably, MeHg can disrupt the activity of thiol- and selenol-containing proteins, such as glutathione peroxidase (GPx), thioredoxin (Trx), and TrxR [1, 9–11]. These proteins are important components of the cellular antioxidant system, and their inhibition contributes to the disruption of the normal redox balance of cells [7].

In addition, MeHg can disrupt mitochondrial function by targeting specific thiol-containing proteins, including respiratory chain complexes [12, 13]. The inhibition of these complexes or enzymes can contribute to mitochondrial depolarization and swelling upon MeHg exposure. Mitochondrial targeting by MeHg has also been associated with increased mitochondrial ROS generation, which can further exacerbate the toxicity of MeHg by attacking additional nucleophilic centers in mitochondria and in other subcellular compartments [7, 10, 12–14], leading to a vicious cycle of cell demise.

Several studies demonstrated that organic and inorganic selenium (Se) compounds influence the deposition and toxicity of MeHg [13, 15, 16]. Se is an essential trace element for a wide range of living organisms, including humans [17]. Se is necessary for the expression of approximately 25 Se-dependent proteins, including GPx, TrxR, and several other enzymes and proteins, which can modulate the cellular redox and antioxidant status [17].

In addition to inorganic and naturally occurring organoselenium compounds, synthetic organoselenium compounds can also exhibit protective effects against MeHg. For example, ebselen and $(PhSe)_2$ have been shown to exert beneficial effects against *in vitro* and *in vivo* MeHg-induced toxicity [18–21]. $(PhSe)_2$ (which is the simplest of the diaryl diselenides [22]) protected against an array of toxic effects of MeHg and lowered the Hg burden in the brain, liver, and kidneys of adult mice [21]. The molecular mechanism(s) which underlie(s) the protective effects of $(PhSe)_2$ in mice likely reflect the direct interaction of MeHg with "selenol intermediate" of $(PhSe)_2$ after its reaction with thiols, or indirectly, by modulating oxidative stress levels [21, 23]. In short, the protective effects of $(PhSe)_2$ against MeHg-induced toxicity are likely related to its antioxidant properties and its ability to form stable complexes with MeHg, which can increase Hg excretion and decrease the MeHg body burden.

Of particular pharmacological significance, the toxicity and pharmacokinetics of MeHg [24] are different in mice and rat which can be explained by the higher binding affinity of rat hemoglobin, which contains more cysteinyl residues than mice protein, for MeHg when compared to the mice hemoglobin [25]. $(PhSe)_2$ toxicity and pharmacokinetics differences between mice and rat also exist and could be explained by a faster metabolization of $(PhSe)_2$ in mice [26–28].

Therefore, the aim of the present study was to investigate the potential protective effects of $(PhSe)_2$ against MeHg-induced toxicity and mitochondrial dysfunction in rats. To accomplish this goal, the effects of $(PhSe)_2$ on Hg deposition in liver and brain and on behavioral and biochemical parameters were studied in rats.

2. Materials and Methods

2.1. Chemicals. Chemicals, including ethylene glycol-bis(β-aminoethylether)-*N,N,N′,N′*-tetraacetic acid (EGTA), 4-(2-hydroxyethyl)-1-piperazineethanesulfonic acid (HEPES), 2,4 dinitrophenol (2,4 DNP), 3-(4,5-dimethylthiazol-2-yl)-2,5-diphenyltetrazolium bromide (MTT), glutamic acid, safranin O, 2′,7′-dichlorofluorescin diacetate (H_2-DCFDA), and methylmercury chloride were obtained from Sigma Aldrich (St. Louis, MO, USA). $(PhSe)_2$ was synthesized according to the method by Paulmier [29]. All other chemicals were of analytical reagent grade and purchased from local commercial suppliers.

2.2. Animals. Male Wistar rats, weighing 250–310 g and with age from 3 to 3.5 months, from our own breeding colony were kept in cages (four animals in each). Rats were placed in a room with controlled temperature (22 ± 3°C) on a 12 h light/dark cycle (lights on at 7:00 a.m.) and had continuous access to food and water. All experiments were conducted in accordance with the Committee on Care and Use of Experimental Animal Resources of the Federal University of Santa Maria, Brazil.

2.3. Treatment. Sixteen rats were equally divided into four experimental groups as follows: (1) control (10 mL/Kg of water i.g. and 1 mL/Kg of soybean oil i.p.); (2) $(PhSe)_2$ (10 mL/Kg of water i.g. and 1 mg/Kg of $(PhSe)_2$ i.p.); (3) MeHg (5 mg/Kg of MeHg i.g. and 1 mL/Kg of soybean oil i.p.); and (4) $(PhSe)_2$ + MeHg (5 mg/Kg of MeHg i.g. and 1 mg/Kg of $(PhSe)_2$ i.p.). Based on previous studies, exposures were performed daily over a 21-day period [21, 30, 31]. Twenty-four hours after the last exposure, the animals were sacrificed and the livers, brains, kidneys, and skeletal muscle were quickly removed, placed on ice and homogenized.

2.4. Determination of Hg Levels. Tissue levels of total Hg were measured in liver, brain, and skeletal muscle collected at the time of euthanasia [32]. Approximately 0.4 g (wet weight) of the tissues was weighed and digested with 5 mL of HNO_3 acid (65%). Digested samples were diluted to 50 mL with ultrapure water before analysis using a Multitype ICP Emission Spectrometer (ICPE-9000, Shimadzu). Calibration standard curve was prepared freshly using mercury stock standard solution.

2.5. Motor Coordination Tests

2.5.1. Open Field Test. General locomotor activity was evaluated as previously described [33]. The number of line crossings (number of segments crossed with the four paws) and rearings was measured over 5 min and taken as an indicator of locomotor activity. The test was carried out at 3 time points: 24 hours prior to treatment (basal), and on treatment days 11 and 21.

2.5.2. Rotarod Test. Motor coordination was tested on the rotarod apparatus as described previously [34, 35]. The latency to fall and the number of falls from the apparatus were recorded for 120 s. The tests were conducted 3 times: 24 hours prior to treatment (basal), and on treatment days 11 and 21.

2.6. TrxR

2.6.1. TrxR Purification. TrxR was partially purified by a modification of the method by Holmgren and Bjornstedt [36]. Tissues were homogenized in buffered saline (137 mM NaCl, 2.7 mM KCl, 4.3 mM Na_2HPO_4, and 1.4 mM KH_2PO_4, pH 7.3). Livers, brains, and kidneys (0.5 g) were homogenized in 10, 3, and 5 volumes of buffered saline, respectively. Homogenates were centrifuged at 13,000 g for 30 min. The protein concentration in the supernatant was measured and adjusted to 10 mg/mL. The supernatant was dialyzed against buffered saline for 16 h to remove endogenous glutathione (GSH) and Trx. The dialysate was heated at 55°C for 10 min, cooled, and centrifuged at 13,000 g for 30 min to remove denatured protein.

2.6.2. TrxR Activity. TrxR activity was measured by the method of Holmgren and Bjornstedt [36]. The reaction mixture consisted of the following: 0.24 mM NADPH, 10 mM EDTA, 100 mM potassium phosphate buffer (pH 7.0), 2 mg/mL 5,5′ dithiobis-2-nitrobenzoic acid (DTNB), and 0.2 mg/mL of BSA. The partially purified TrxR was added (to final concentration of 6–8 μg of protein) to the cuvette containing the reaction mixture, and the absorbance was followed at 412 nm for a maximum of 4 min.

2.7. Isolation of Rat Brain and Liver Mitochondria. Rat brain and liver mitochondria were isolated as previously described by Brustovetsky and Dubinsky [37], with some modifications. Brain and liver were rapidly weighed and homogenized in 1 : 5 (w/v) ice-cold "isolation buffer I" containing 225 mM mannitol, 75 mM sucrose, 1 mM K^+-EGTA, 0.1% bovine serum albumin (BSA), and 10 mM K^+-HEPES, pH 7.2. The tissue was then manually homogenized with a potter glass. The resulting suspension was centrifuged for 7 min at 2,000 g. After centrifugation the supernatant was recentrifuged for 10 min at 12,000 g. The pellet was resuspended in "isolation buffer II" containing 225 mM mannitol, 75 mM sucrose, 1 mM K^+-EGTA, and 10 mM K^+-HEPES pH 7.2 and recentrifuged at 12,000 g for 10 min. The supernatant was discarded and the final pellet gently washed and resuspended in "isolation buffer II" without EGTA.

2.8. Mitochondrial Nonprotein and Total Thiol Content. Mitochondrial nonprotein and total thiol content were measured according to the method of Ellman [38]. To determine total thiol groups, mitochondria (0.3 mg protein) were added to the reaction medium containing 10 mM Tris-HCl pH 7.2, 1% SDS, and 10 mM DTNB. Nonprotein thiol content was measured by adding 50 μL 10% TCA to 50 μL of the mitochondria (0.3 mg protein). After centrifugation (4,000 ×g at 4°C for 10 min), the protein pellet was discarded and an aliquot of the clear supernatant, neutralized with 0.1 M NaOH, was added to the medium containing 10 mM Tris-HCl pH 7.2 and 10 mM DTNB. The samples absorbance was measured spectrophotometrically at a wavelength of 412 nm.

2.9. Measurements of Mitochondrial $\Delta\Psi m$. Mitochondrial $\Delta\Psi$m was estimated by fluorescence changes in safranin O (3 mM) recorded by RF-5301 Shimadzu spectrofluorometer (Kyoto, Japan) operating at excitation and emission wavelengths of 495 and 535 nm, with slit widths of 1.5 nm [39]. Data on $\Delta\Psi$m in the figures is presented in Arbitrary Fluorescence Units (AFU).

2.10. Estimation of ROS Production. The mitochondrial generation of ROS was determined spectrofluorimetrically, using the membrane permeable fluorescent dye H_2-DCFDA recorded by RF-5301 Shimadzu spectrofluorometer (Kyoto, Japan) operating at excitation and emission wavelengths of 488 and 525 nm, with slit widths of 3 nm [40]. Data of ROS production in the figures is presented as Arbitrary Fluorescence Units (AFU).

2.11. Assessment of Mitochondrial Metabolic Function. The mitochondrial metabolic function was assessed by the conversion of MTT to a dark violet formazan product by mitochondrial dehydrogenases [41]. The rate of MTT reduction was measured spectrophotometrically at a wavelength of 570 nm. Results were expressed as the percentage of MTT reduction relative to control values.

2.12. Assessment of Mitochondrial Swelling. Measurement of mitochondrial swelling was performed in a RF-5301 Shimadzu spectrofluorometer at 600 nm (slit 1.5 nm for excitation and emission) [42]. Data for mitochondrial swelling are expressed as Arbitrary Absorbance Units (AAU). The difference (ΔA) between the initial absorbance reading and the final absorbance reading was used for statistical analysis.

2.13. Protein Measurement. Protein was assayed by the method of Bradford [43] with bovine serum albumin as standard.

2.14. Statistical Analysis. Normality assumption was tested with Kolmogorov-Smirnov test and the distribution of the majority of results is not normal. Data were analyzed statistically by Mann-Whitney or Kruskal-Wallis, followed by Dunn's post-hoc tests when appropriate. The results were considered statistically significant at $P < 0.05$. All statistical analyses were conducted using GraphPad Prism 5 (Version 5.01, GraphPad Software, Inc., USA).

3. Results

3.1. Effects of $(PhSe)_2$ and MeHg on Body Weight. Treatment with MeHg led to body-weight loss from the second week until the end of the treatment compared to controls ($P < 0.05$, Figure 1). Rats cotreated with $(PhSe)_2$ and MeHg also

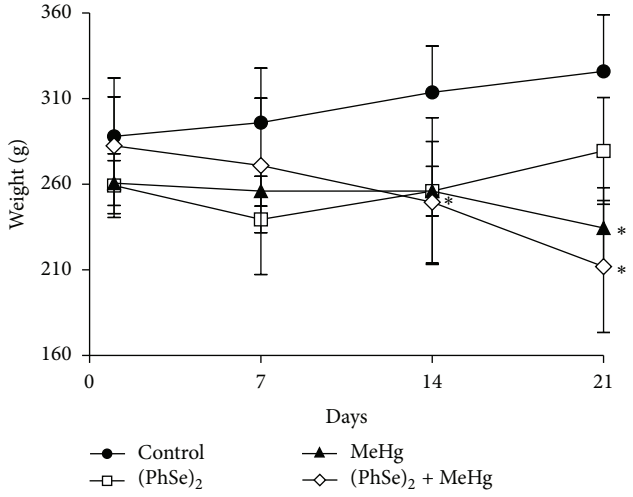

FIGURE 1: Effect of MeHg and/or $(PhSe)_2$ on the body weight gain in adult rats. Data are expressed as mean ± S.D., $n = 4$. (∗) represents $P < 0.05$ as compared to controls by Mann-Whitney test.

showed a decrease in the body weight when compared to the control group ($P < 0.05$, Figure 1). Rats treated with $(PhSe)_2$ lost weight after the first week of treatment ($P < 0.05$) but showed a trend towards a recovery and were statistically indistinguishable from the controls at the end of the treatment (Figure 1).

3.2. Effects of $(PhSe)_2$ and MeHg on Hg Deposition. Treatment with MeHg increased the levels of Hg in liver, brain, and skeletal muscle compared with controls ($P < 0.05$, Figure 2). The cotreatment with $(PhSe)_2$ caused a greater increase in brain Hg deposition when compared to MeHg alone treatment, both in brain (Figure 2(b)) and liver (Figure 2(a)), and showed a trend towards increased deposition in skeletal muscle (Figure 2(c)).

3.3. Effects of $(PhSe)_2$ and MeHg on Motor Coordination and Spontaneous Locomotor Activity. The effects of MeHg and/or $(PhSe)_2$ on locomotion and motor coordination were assessed by the open-field and rotarod tests, respectively. After 11 days, rats treated with MeHg showed increased number of falls on the rotarod and decreased latency to the first fall when compared to controls ($P < 0.05$, Figures 3(a) and 3(b)). Rats treated with $(PhSe)_2$ did not show statistically significant differences on the rotarod test when compared to controls; however, rats cotreated with $(PhSe)_2$ and MeHg showed increased loss of motor coordination as evidenced by increased number of falls and reduced latency to the first fall ($P < 0.05$, Figures 3(a) and 3(b)). The rotarod test could not be performed at the end of the treatment in rats receiving MeHg since they were unable to remain in the apparatus due to severe motor impairment caused by MeHg.

Rats treated with MeHg showed a decrease in the number of crossings and rearings in the open-field at the end of the treatment compared to the control rats ($P < 0.05$, Figures 3(c) and 3(d)). Rats cotreated with MeHg and $(PhSe)_2$ also showed a significant decrease in the number of crossings after 11 days of treatment and a decrease in the number of rearings at the end of the treatment ($P < 0.05$, Figure 3(d)). Treatment with $(PhSe)_2$ did not affect the rats' performance in the open-field. The decrease in the number of crossings and rearings observed in all groups on treatment days 11 and 21 was expected given that the animals habituate to the open-field arena [44].

3.4. Effects of $(PhSe)_2$ and MeHg on Mitochondrial Dysfunction

3.4.1. Mitochondrial Metabolic Function. The hepatic mitochondrial metabolic integrity (MTT reduction) was not affected by MeHg and/or $(PhSe)_2$ (Figure 4(a)). Treatment with MeHg or cotreatment with MeHg and $(PhSe)_2$ decreased the capacity of brain mitochondrial dehydrogenases to reduce MTT compared to controls ($P < 0.05$, Figure 4(b)). Treatment with $(PhSe)_2$ alone did not affect the cerebral mitochondrial metabolic function.

3.4.2. Mitochondrial Total and Nonprotein Thiols. MeHg treatment decreased the total mitochondrial thiol levels in brain and liver when compared to controls ($P < 0.05$, Figure 5). Treatment with $(PhSe)_2$ alone did not alter the mitochondrial total thiol levels in liver and brain (Figure 5). The cotreatment with $(PhSe)_2$ blunted the MeHg-induced mitochondrial total thiol level depletion in rats' liver and brain ($P < 0.05$, Figure 5). Rats treated with MeHg showed decreased mitochondrial nonprotein thiol levels in the liver compared to controls, and coadministration of $(PhSe)_2$ blunted the MeHg-induced decrease in hepatic nonprotein thiol content ($P < 0.05$, Figure 5(a)). Brain mitochondrial nonprotein thiol levels were not affected by any of the treatments (Figure 5(b)).

3.4.3. Mitochondrial Swelling. Treatment with MeHg significantly increased hepatic mitochondrial swelling when compared to controls ($P < 0.05$, Figure 6(a)). Cotreatment with $(PhSe)_2$ partially prevented the MeHg-induced mitochondrial swelling in liver (Figure 6(a)). Similarly, treatment with MeHg showed a trend towards increased mitochondrial swelling in brain (Figure 6(b)). The cotreatment with MeHg and $(PhSe)_2$ significantly increased cerebral mitochondrial swelling when compared to controls ($P < 0.05$, Figure 6(b)). Treatment with $(PhSe)_2$ alone did not alter the mitochondrial swelling in brain or liver compared to the controls (Figures 6(a) and 6(b)).

3.4.4. Mitochondrial ROS Production. Mitochondrial ROS production (DCFH oxidation) was significantly increased in livers of rats treated with MeHg or cotreated with MeHg and $(PhSe)_2$ ($P < 0.05$, Figure 7(a)). Rats treated with $(PhSe)_2$ showed hepatic mitochondrial ROS levels indistinguishable from controls. ROS production in cerebral mitochondria was not affected by any of the treatments (Figure 7(b)).

3.4.5. Mitochondrial $\Delta\Psi m$. Polarization ($\Delta\Psi$m) of mitochondria from liver of rats cotreated with MeHg and $(PhSe)_2$

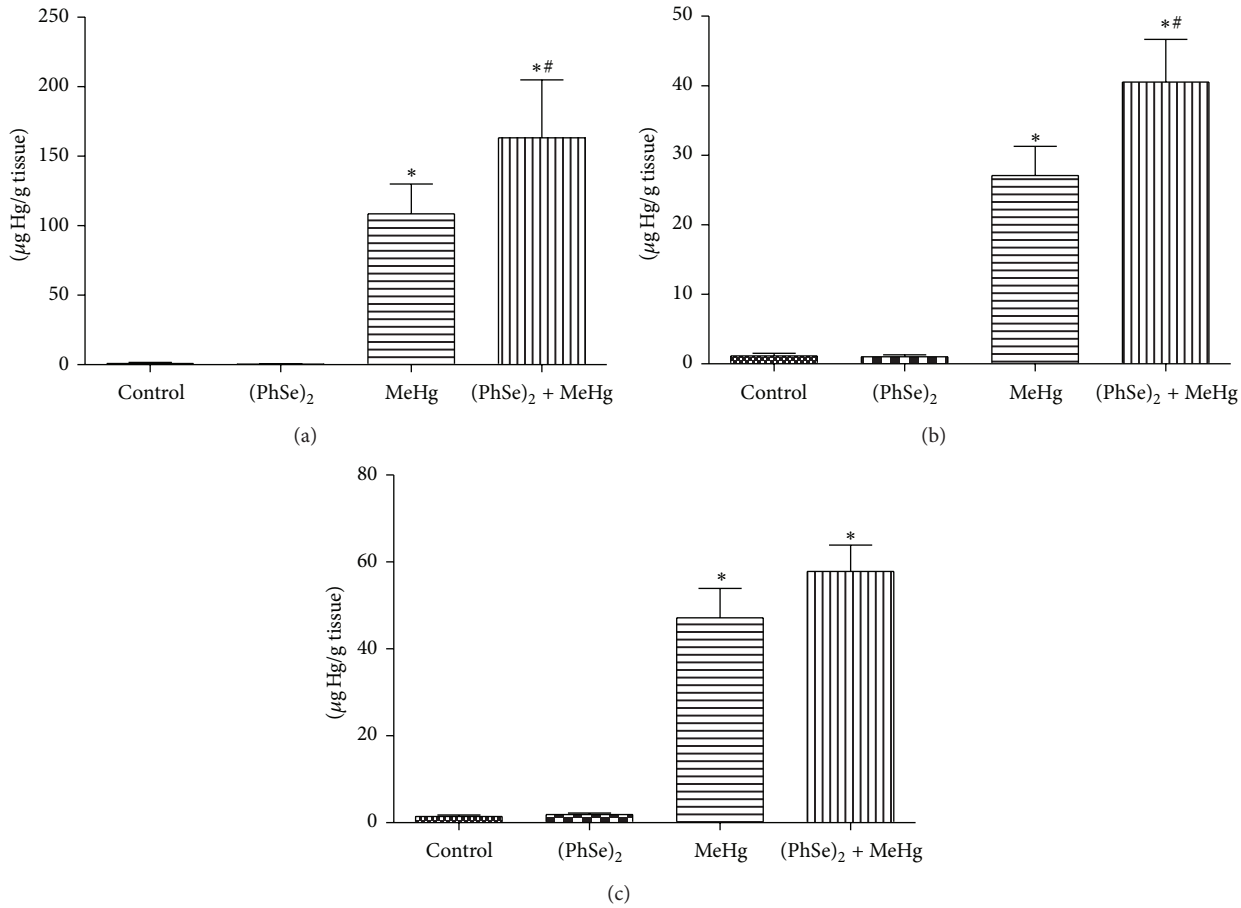

Figure 2: Hg content in liver (a), brain (b), and muscle (c) of rats exposed to MeHg and/or $(PhSe)_2$. Data are expressed as mean ± S.D., $n = 4$. (∗) represents $P < 0.05$ as compared to controls by Mann-Whitney test. (#) represents $P < 0.05$ as compared to MeHg by Mann-Whitney test.

showed only a trend towards decreased (Figures 8(a) and 8(c)). Treatment with $(PhSe)_2$ and MeHg alone did not cause mitochondrial depolarization in liver of rats (Figures 8(a) and 8(c)). Treatment with $(PhSe)_2$ and/or MeHg had no effect on mitochondrial $\Delta\Psi m$ in brain of rats (Figures 8(b) and 8(d)).

3.5. Effects of $(PhSe)_2$ and MeHg on TrxR Activity. MeHg is known to inhibit TrxR activity both *in vitro* and *in vivo* [1, 9, 11]. $(PhSe)_2$ treatment significantly increased renal TrxR activities when compared to controls ($P < 0.05$, Figures 9(a) and 9(b)). Hepatic and cerebral TrxR activity showed a trend towards increased in rats treated with $(PhSe)_2$ (Figure 9(c)). MeHg treatment also led to significant inhibition of TrxR in liver, kidney, and brain compared to controls ($P < 0.05$, Figure 9). Cotreatment with $(PhSe)_2$ failed to significantly attenuate the MeHg-induced inhibition of TrxR activity in the liver, kidney, or brain (Figure 9).

4. Discussion

The present study investigated the efficacy of $(PhSe)_2$, an organoselenium compound, in attenuating MeHg-induced toxicity in rats. Our results established that MeHg decreased body weight (Figure 1) and induced motor deficits (Figure 3) as well hepatic and cerebral mitochondrial dysfunction (Figures 4(b), 5, 6(a), and 7(a)) and inhibited TrxR activity in liver, brain, and kidney (Figure 9) in the rat. The cotreatment with $(PhSe)_2$ and MeHg increased Hg accumulation in the liver and brain (Figure 2). Furthermore, the cotreatment with $(PhSe)_2$ protected hepatic and cerebral mitochondrial thiols from depletion by MeHg (Figure 5) but did not prevent hepatic and cerebral mitochondrial dysfunction (Figures 4(b), 6(b), and 7(a)) nor did it reverse the MeHg-induced motor deficits (Figure 3), body-weight loss (Figure 1), and the MeHg-induced inhibition of TrxR activity in liver, brain, and kidney (Figure 9).

Cotreatment with $(PhSe)_2$ and MeHg increased Hg deposition in the brain and liver of exposed rats (Figure 2). These results differ from those of de Freitas et al. [21] where $(PhSe)_2$ led to a significant reduction in Hg concentrations in brain, liver, and kidney of MeHg-exposed mice. The discrepancies between the 2 studies may be attributed to metabolic differences between the species and the route of administration. The toxicity and pharmacokinetics of MeHg [24] are different in mice and rat which can be explained

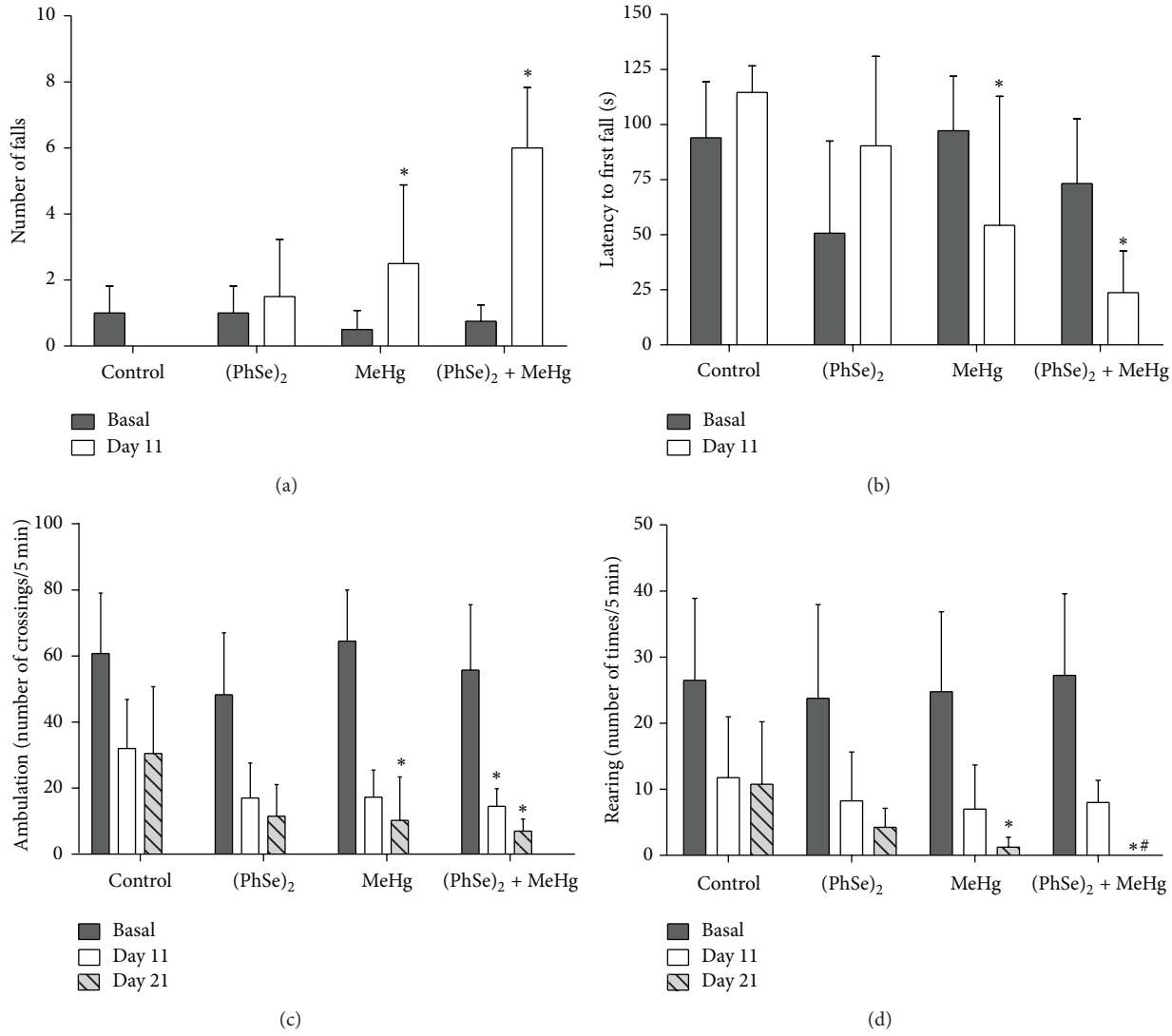

FIGURE 3: Rotarod and open field tests in rats exposed to MeHg and/or $(PhSe)_2$. The number of falls (a) and latency for the first fall (b) ambulation (crossing) (a) and rearing (b) were recorded. Data are expressed as mean ± S.D., $n = 4$. (∗) represents $P < 0.05$ as compared to controls by Kruskal-Wallis test followed by multiple comparison test. (#) represents $P < 0.05$ as compared to $(PhSe)_2$ by Kruskal-Wallis test followed by multiple comparison test.

by the higher binding affinity of rat hemoglobin, containing more cysteinyl residues, for MeHg when compared to the mice hemoglobin [25]. $(PhSe)_2$ toxicity and pharmacokinetics differences between mice and rat also exist and could be explained by a faster metabolization of $(PhSe)_2$ in mice [26–28]. Notably, herein rats were administered $(PhSe)_2$ i.p., whilst in the study by de Freitas et al. [21] $(PhSe)_2$ was subcutaneously (s.c.) administered to the mice. Another difference between the two works is in relation to the dose of MeHg: in our study we used a dose 2.5 times higher than in the study of de Freitas et al. (2 mg/Kg). However, the duration of the treatment was shorter in our study, 21 versus 35 days. On the other hand, the dose of $(PhSe)_2$ was similar between the two studies. The higher dose of MeHg used in our study may have contributed to the discrepancies since it could generate a more severe toxicity which could not be prevented by $(PhSe)_2$. However, we realize that the differences in the pharmacokinetics between rats and mice for the $(PhSe)_2$ is the major factor involved in the discrepancies found here [28].

In the study by de Freitas et al. [21] the proposed mechanism for the reduction Hg's organ burden by $(PhSe)_2$ was the formation of a selenol/selenolate ($PhSeH/PhSe^-$) intermediate, which could interact with MeHg, generating the readily excretable PhSeHgMe complex. One possible explanation for the increase in hepatic and cerebral Hg deposition (Figures 2(a) and 2(b), resp.) by the cotreatment with $(PhSe)_2$ observed herein may be the conversion of $(PhSe)_2$ to inorganic selenium, which is subsequently metabolized to selenhidric acid (HSe^-). HSe^- could bind to MeHg to form a less soluble complex [45], which can be degraded to HgSe [46, 47]. In addition, Palmer and Parkin [48] showed

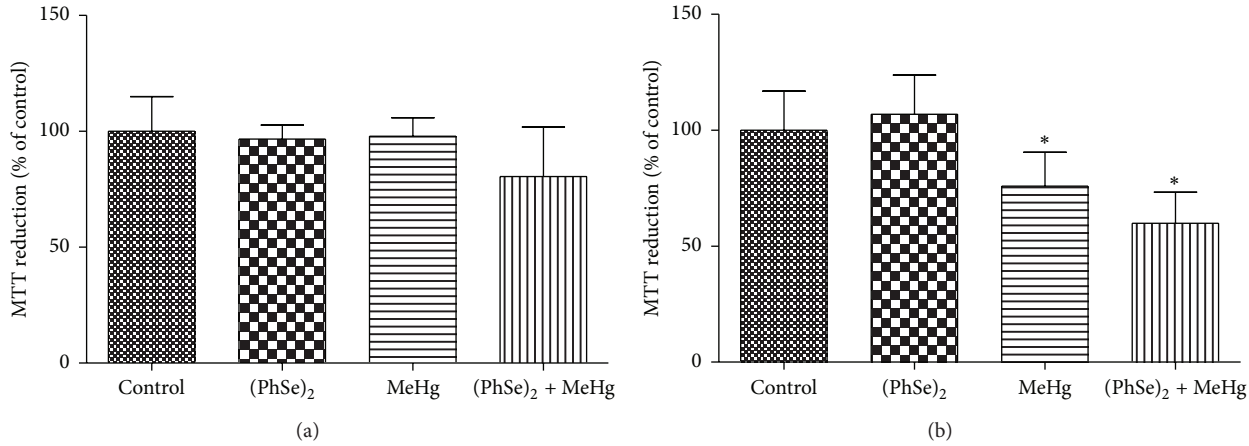

Figure 4: MTT reduction in liver (a) and brain (b) mitochondria of rats exposed to MeHg and/or $(PhSe)_2$. Data are expressed as mean ± S.D., $n = 4$. (∗) represents $P < 0.05$ as compared to controls by Mann-Whitney test.

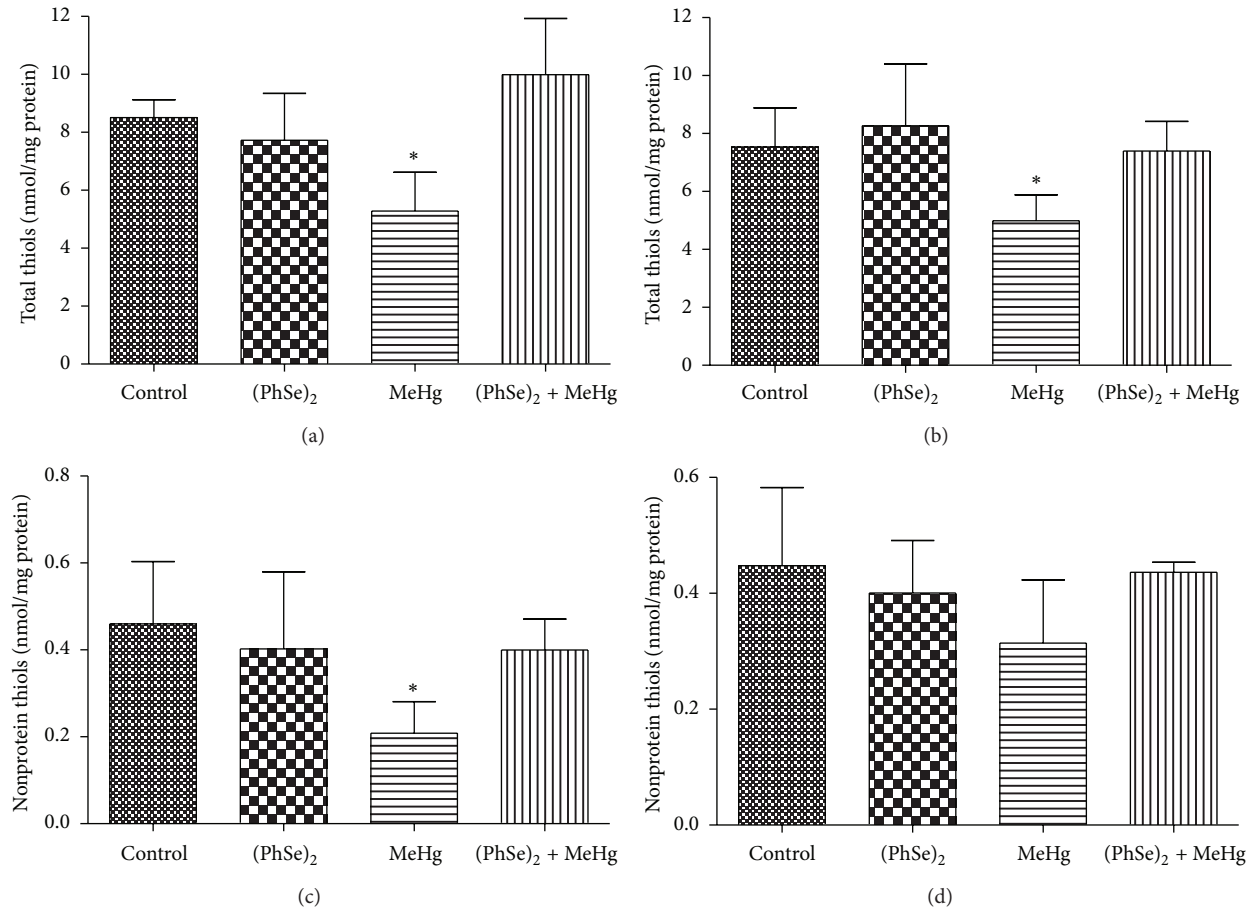

Figure 5: Total and nonprotein thiol content in liver (a), (c) and brain (b), (d) mitochondria of rats exposed to MeHg and/or $(PhSe)_2$. Data are expressed as mean ± S.D., $n = 4$. (∗) represents $P < 0.05$ as compared to controls by Mann-Whitney test.

that organoselenium can also form a complex with mercury. Thus the increase in hepatic and cerebral Hg deposition by the cotreatment with $(PhSe)_2$ possibly involves Hg:Se interactions and the formation of a less excretable compound that accumulates in these organs [45]. These results are in agreement with other studies that showed elevated deposition of Hg in key brain regions upon oral Se administration [49, 50]. It has been speculated that the formation of insoluble HgSe salt could reduce the toxicity of MeHg. However, experimental evidence supporting this assumption has yet to be

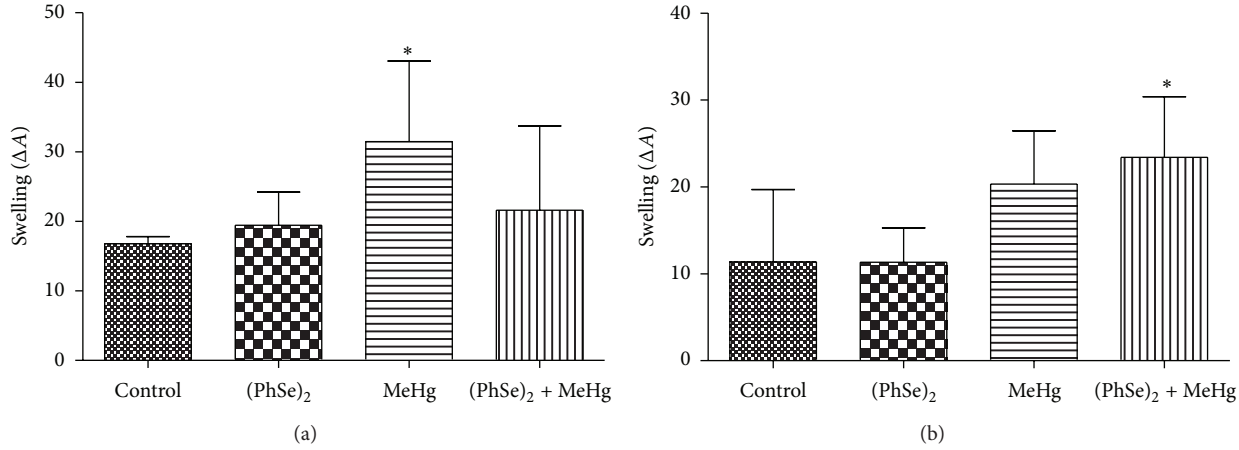

FIGURE 6: Mitochondrial swelling in liver (a) and brain (b) of rats exposed to MeHg and/or $(PhSe)_2$. Data are expressed as mean ± S.D., $n = 4$. (∗) represents $P < 0.05$ as compared to controls by Mann-Whitney test.

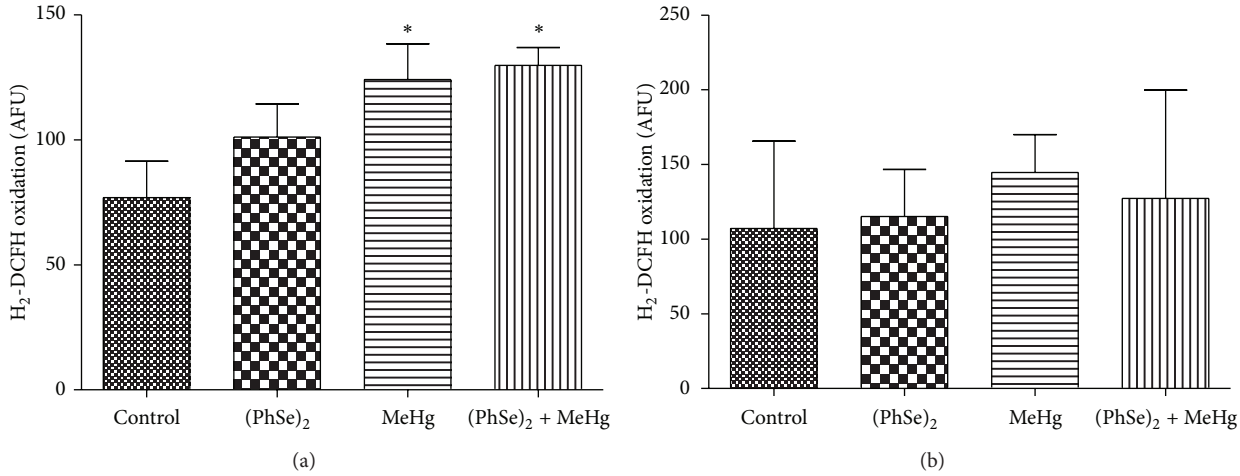

FIGURE 7: ROS production (H_2-DCFH oxidation) in liver (a) and brain (b) mitochondria of rats exposed to MeHg and/or $(PhSe)_2$. Data are expressed as mean ± S.D., $n = 4$. (∗) represents $P < 0.05$ as compared to controls by Mann-Whitney test.

generated. Although the cotreatment with $(PhSe)_2$ increased Hg levels in brain and liver, these were accompanied by a partial protection against MeHg-induced mitochondrial dysfunction. We suggest that the formation of an insoluble and inert complex between Hg and Se could decrease the availability of MeHg that could react with important cellular components decreasing its toxicity.

Decreased weight gain and weight loss are prominent and readily observed features of severe MeHg toxicity. In this study, rats treated with MeHg showed body-weight loss (Figure 1). Notably, the most severe effect on weight loss occurred in rats cotreated with $(PhSe)_2$ and MeHg (Figure 1). In addition, rats treated with MeHg showed decreased locomotor activity (Figure 3). Cotreatment with $(PhSe)_2$ and MeHg increased the severity of motor dysfunction (rotarod test) (Figure 3), likely as a result of increased Hg deposition in the brain (Figure 2(b)). Motor deficits are the most apparent neurological effects following MeHg exposure [51]. *In vivo* studies in rodents point to impairment in intracellular calcium homeostasis, alteration in glutamate homeostasis, and oxidative stress as critical mediators of MeHg-induced neurotoxicity [52]. The overactivation of N-methyl-D-aspartate- (NMDA-) type glutamate receptors increases Ca^{2+} influx into neurons, thereby leading to cell death [53]. Alternatively, Ca^{2+} taken up by mitochondria may stimulate the generation of ROS [54].

Several studies corroborate MeHg's ability to induce mitochondrial dysfunction and ROS generation [14, 18, 55]. The high affinity binding of MeHg to thiol groups inactivates enzymes, including respiratory chain complexes [7, 13, 55], decreasing mitochondrial dehydrogenases activity. Inhibition of these complexes may contribute to mitochondrial swelling and ROS production after MeHg exposure (Figures 6 and 7). However, in brain, the MeHg-induced decrease in mitochondrial dehydrogenases activity (MTT reduction) was not accompanied by an increase in ROS production. These

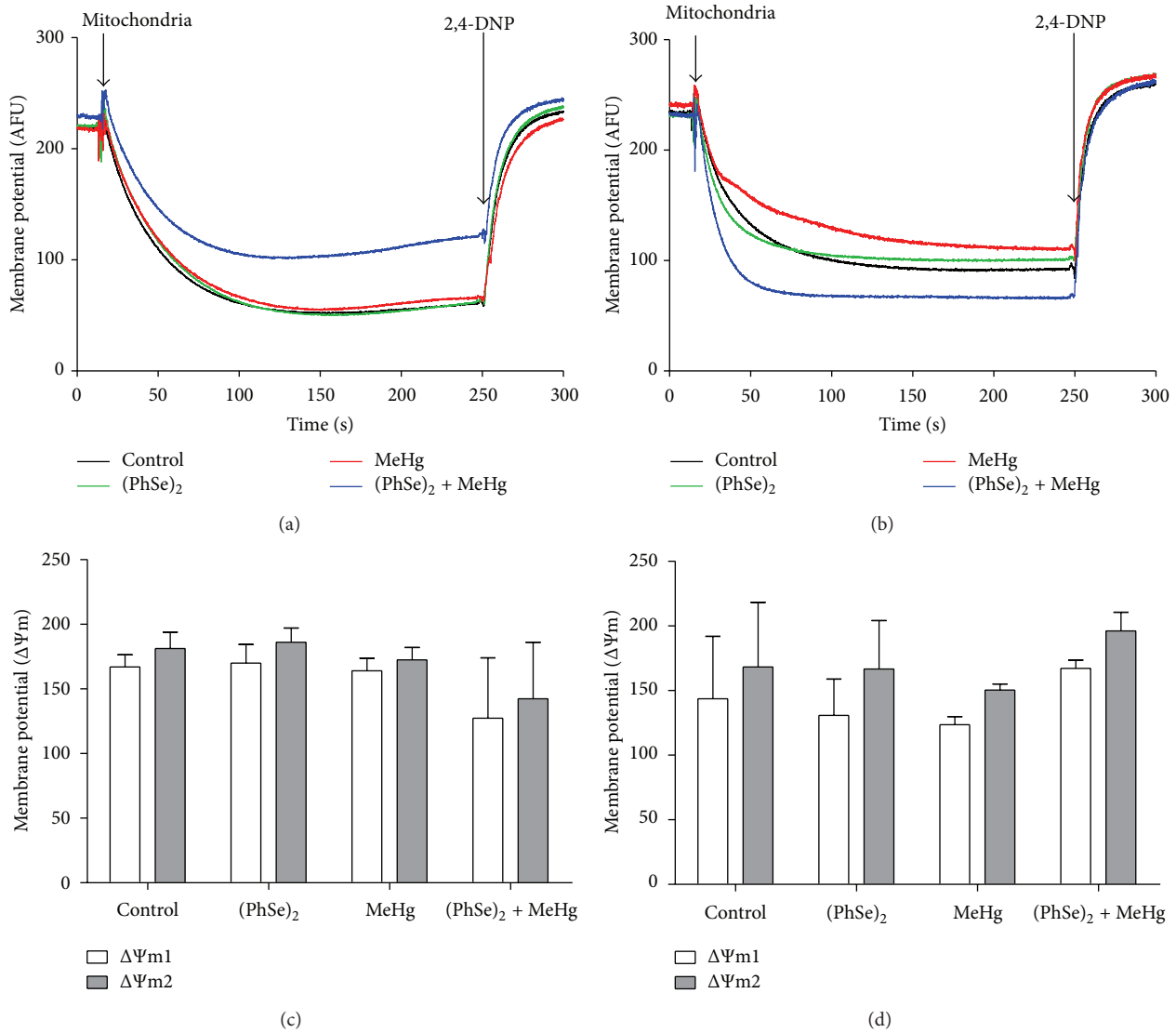

Figure 8: Mitochondrial depolarization in liver (a), (c) and brain (b), (d) of rats exposed to MeHg and/or $(PhSe)_2$. Figures (a) and (b) show mitochondrial membrane potential (AFU). Figures (c) and (d) show mitochondrial ΔΨm. ΔΨm1 = delta of fluorescence before (time 0) and after addition of mitochondria (time 150 seconds) and ΔΨm2 = delta of fluorescence before (time 150 seconds) and after addition of 2,4 DNP (time 300 seconds). Data are expressed as mean ± S.D., $n = 4$.

results are corroborated by the fact that MeHg affected total thiols but not nonprotein thiol levels in brain mitochondria. MeHg caused a decrease in the total mitochondrial thiol levels in brain, which is related mainly with protein thiols, and is in agreement with the inhibition of mitochondrial dehydrogenases activity in this tissue. On the other hand, MeHg did not affect nonprotein thiol levels (mainly GSH) in brain mitochondria, which can explain the normal ROS production, since GSH is the main antioxidant in brain.

The cotreatment with $(PhSe)_2$ prevented the MeHg-induced mitochondrial total and nonprotein thiol groups depletion in the brain and liver (Figure 4). The efficacy of $(PhSe)_2$ in preventing thiol depletion may reside in its ability to form a complex with MeHg, thus effectively reducing MeHg binding to protein and free thiols. Treatment with $(PhSe)_2$ also partially protected the liver from mitochondrial MeHg-induced swelling (Figure 6(a)). However, the cotreatment with $(PhSe)_2$ failed to reverse the MeHg-induced mitochondrial swelling (Figure 6(b)) and decreased mitochondrial metabolic function (Figure 3(b)) in the brain as well as increased mitochondrial ROS production (Figure 7(a)) in the liver. These results indicate that mechanisms other than the interaction with important free and protein thiols are likely involved in the MeHg-induced mitochondrial dysfunction. Thus, the preferential affinity of MeHg for specific, and as of yet unidentified, mitochondrial protein targets may have a critical role in MeHg's toxicity.

Previous studies have demonstrated that MeHg can directly inhibit TrxR activity both *in vitro* and *in vivo* [1, 9, 11]. Mammalian TrxR is a selenoenzyme containing a

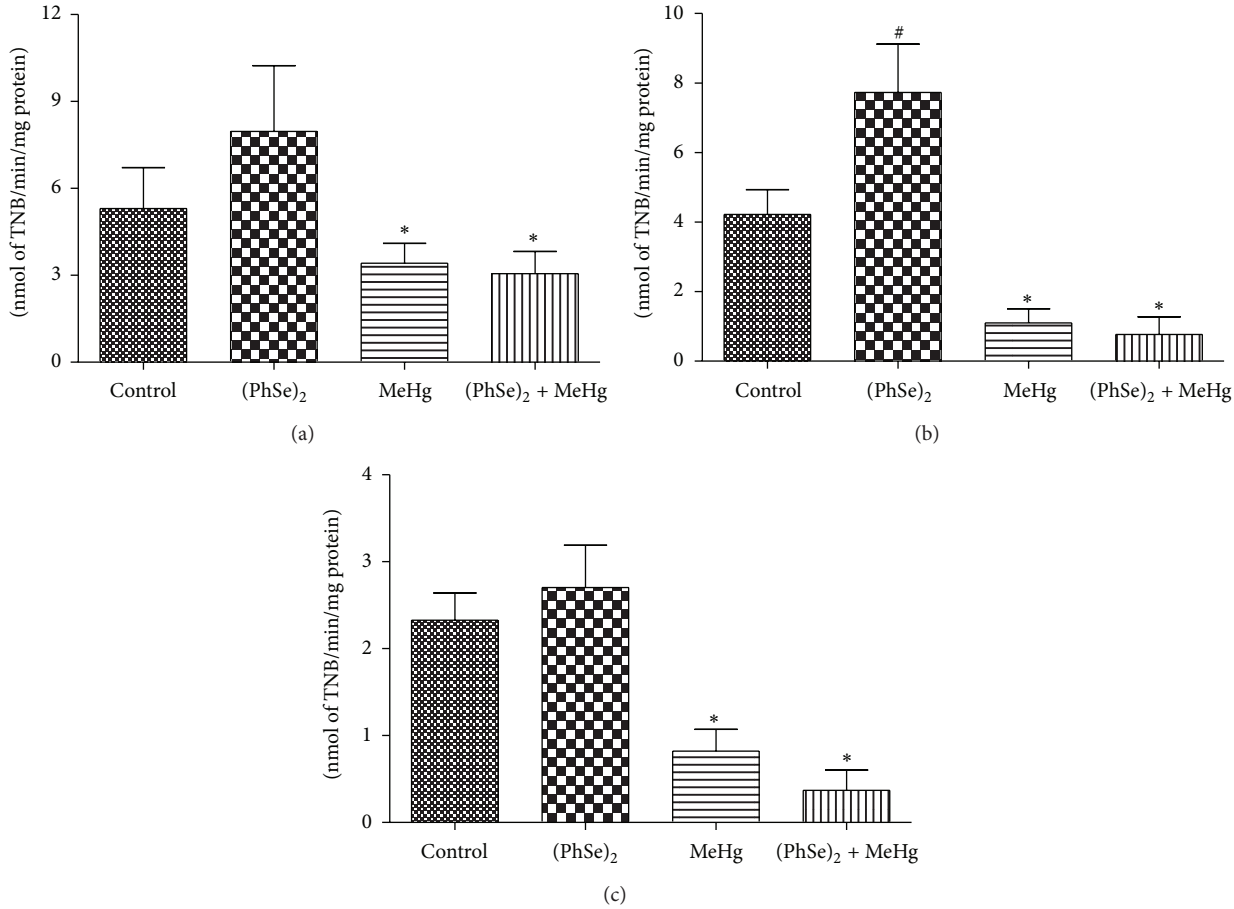

FIGURE 9: TrxR activity in liver (a), kidney (b), and brain (c) of rats exposed to MeHg and/or $(PhSe)_2$. Data are expressed as mean ± S.D., $n = 4$. (∗) represents $P < 0.05$ as compared to controls by Mann-Whitney test. (#) represents $P < 0.05$ as compared to controls by Mann-Whitney test.

unique, catalytically active selenolthiol/selenenylsulfide in the conserved C-terminal sequence (-Gly-Cys-Sec-Gly) [56]. Three mammalian TrxR selenoenzymes have been identified, the cytosolic enzyme TrxR1, the mitochondrial enzyme TrxR2, and a testis-specific enzyme thioredoxin-glutathione reductase (TGR/TrxR3) [56]. Here, we show that MeHg treatment inhibited rat TrxR activity in brain, liver, and kidney (Figure 9). MeHg forms covalent bonds between its Hg moiety and the Se of the selenocysteine of the enzyme, thus directly inhibiting the activity of TrxR [1]. Since TrxR is critical for cellular antioxidant defense system the inhibition of this enzyme likely has a central role in mediating the toxicity of MeHg.

Recently, diphenyl diselenide was demonstrated to be a substrate for cerebral and hepatic rat TrxR, which could account, at least in part, for the antioxidant properties of $(PhSe)_2$ [23]. Herein, rats treated solely with (PhSe) showed an increase in the activity of renal TrxR (Figures 9(a) and 9(b), resp.). The formation of selenhidric acid from $(PhSe)_2$ could also explain the increase in TrxR activity, since this inorganic form of Se can be converted to selenocysteine and incorporated to selenoenzymes, such as TrxR [45, 57]. Accordingly, Zhang et al. [58] have demonstrated that organoselenium compounds (including diselenide) increase the expression of TrxR in white blood cells lines in culture. The cotreatment with $(PhSe)_2$ and MeHg was ineffective in attenuating the inhibition of MeHg-induced TrxR in liver, kidney, and brain (Figure 9). Similarly, studies *in vitro* and *in vivo* have previously corroborated that selenite was able to recover the activity of $HgCl_2$-induced TrxR inhibition but not in response to MeHg. The effect of Se (as selenide) was attributed to the displacement of Hg from the active site, giving rise to mercury selenide and regenerating the TrxR selenol [1, 9].

5. Conclusions

In conclusion, the results of this study established that $(PhSe)_2$ can increase Hg body burden (likely associated with release of inorganic Se from $(PhSe)_2$) and MeHg neurotoxicity in rats despite the fact that $(PhSe)_2$ blunted the deleterious effects of MeHg on thiol levels. The results presented herein also reinforce the central role of mitochondrial dysfunction in mediating the aberrant effects of MeHg *in vivo*, as well as the role of TrxR as a molecular target for MeHg in the rat. Further research into MeHg-$(PhSe)_2$ interactions will be helpful in characterizing the consequences concomitant exposures to these and related compounds.

Conflict of Interests

The authors declare that there is no conflict of interests regarding the publication of this paper.

Acknowledgments

This work was supported by Fundação de Amparo a Pesquisa do Estado do Rio Grande do Sul (FAPERGS), CAPES (Coordenação de Aperfeiçoamento de Pessoal de Nível Superior), CNPq (Conselho Nacional de Desenvolvimento Científico e Tecnológico), FINEP (Rede Instituto Brasileiro de Neurociência (IBN-Net) no. 01.06.0842-00), FAPERGS-PRONEX-CNPQ, and INCT-EN (Instituto Nacional de Ciência e Tecnologia em Excitotoxicidade e Neuroproteção). Cristiane L. Dalla Corte is recipient of CAPES fellowship. Félix A. A. Soares and João B. T. Rocha are recipients of CNPq fellowships. Michael Aschner was partially supported by grants from the US PHS, R01 ES007331 and R01 ES020852.

References

[1] C. M. L. Carvalho, J. Lu, X. Zhang, E. S. J. Arnér, and A. Holmgren, "Effects of selenite and chelating agents on mammalian thioredoxin reductase inhibited by mercury: implications for treatment of mercury poisoning," *The FASEB Journal*, vol. 25, no. 1, pp. 370–381, 2011.

[2] T. W. Clarkson, L. Magos, and G. J. Myers, "The toxicology of mercury—current exposures and clinical manifestations," *The New England Journal of Medicine*, vol. 349, no. 18, pp. 1731–1737, 2003.

[3] G. C. Compeau and R. Bartha, "Sulfate-reducing bacteria: principal methylators of mercury in anoxic estuarine sediment," *Applied and Environmental Microbiology*, vol. 50, no. 2, pp. 498–502, 1985.

[4] J. G. Dórea, "Persistent, bioaccumulative and toxic substances in fish: human health considerations," *Science of the Total Environment*, vol. 400, no. 1–3, pp. 93–114, 2008.

[5] P. Grandjean and K. T. Herz, "Methylmercury and brain development: imprecision and underestimation of developmental neurotoxicity in humans," *Mount Sinai Journal of Medicine*, vol. 78, no. 1, pp. 107–118, 2011.

[6] C. Johansson, A. F. Castoldi, N. Onishchenko, L. Manzo, M. Vahter, and S. Ceccatelli, "Neurobehavioural and molecular changes induced by methylmercury exposure during development," *Neurotoxicity Research*, vol. 11, no. 3-4, pp. 241–260, 2007.

[7] M. Farina, M. Aschner, and J. B. T. Rocha, "Oxidative stress in MeHg-induced neurotoxicity," *Toxicology and Applied Pharmacology*, vol. 256, no. 3, pp. 405–417, 2011.

[8] J. L. Franco, H. C. Braga, J. Stringari et al., "Mercurial-induced hydrogen peroxide generation in mouse brain mitochondria: protective effects of quercetin," *Chemical Research in Toxicology*, vol. 20, no. 12, pp. 1919–1926, 2007.

[9] V. Branco, J. Canário, A. Holmgren, and C. Carvalho, "Inhibition of the thioredoxin system in the brain and liver of zebra-seabreams exposed to waterborne methylmercury," *Toxicology and Applied Pharmacology*, vol. 251, no. 2, pp. 95–103, 2011.

[10] J. L. Franco, T. Posser, P. R. Dunkley et al., "Methylmercury neurotoxicity is associated with inhibition of the antioxidant enzyme glutathione peroxidase," *Free Radical Biology and Medicine*, vol. 47, no. 4, pp. 449–457, 2009.

[11] C. Wagner, J. H. Sudati, C. W. Nogueira, and J. B. T. Rocha, "In vivo and in vitro inhibition of mice thioredoxin reductase by methylmercury," *BioMetals*, vol. 23, no. 6, pp. 1171–1177, 2010.

[12] A. Dreiem and R. F. Seegal, "Methylmercury-induced changes in mitochondrial function in striatal synaptosomes are calcium-dependent and ROS-independent," *NeuroToxicology*, vol. 28, no. 4, pp. 720–726, 2007.

[13] V. Glaser, E. M. Nazari, Y. M. R. Müller et al., "Effects of inorganic selenium administration in methylmercury-induced neurotoxicity in mouse cerebral cortex," *International Journal of Developmental Neuroscience*, vol. 28, no. 7, pp. 631–637, 2010.

[14] D. H. Roos, R. L. Puntel, M. Farina et al., "Modulation of methylmercury uptake by methionine: prevention of mitochondrial dysfunction in rat liver slices by a mimicry mechanism," *Toxicology and Applied Pharmacology*, vol. 252, no. 1, pp. 28–35, 2011.

[15] A. L. Choi, E. Budtz-Jørgensen, P. J. Jørgensen et al., "Selenium as a potential protective factor against mercury developmental neurotoxicity," *Environmental Research*, vol. 107, no. 1, pp. 45–52, 2008.

[16] A. Fredriksson, A. Teiling Gardlund, K. Bergman et al., "Effects of maternal dietary supplementation with selenite on the postnatal development of rat offspring exposed to methyl mercury in utero," *Pharmacology and Toxicology*, vol. 72, no. 6, pp. 377–382, 1993.

[17] D. L. Hatfield and V. N. Gladyshev, "How selenium has altered our understanding of the genetic code," *Molecular and Cellular Biology*, vol. 22, no. 11, pp. 3565–3576, 2002.

[18] C. L. Dalla Corte, F. A. A. Soares, M. Aschner, and J. B. T. Rocha, "Diphenyl diselenide prevents methylmercury-induced mitochondrial dysfunction in rat liver slices," *Tetrahedron*, vol. 68, no. 51, pp. 10437–10443, 2012.

[19] D. H. Roos, R. L. Puntel, M. M. Santos et al., "Guanosine and synthetic organoselenium compounds modulate methylmercury-induced oxidative stress in rat brain cortical slices: involvement of oxidative stress and glutamatergic system," *Toxicology in Vitro*, vol. 23, no. 2, pp. 302–307, 2009.

[20] Z. Yin, E. Lee, M. Ni et al., "Methylmercury-induced alterations in astrocyte functions are attenuated by ebselen," *NeuroToxicology*, vol. 32, no. 3, pp. 291–299, 2011.

[21] A. S. de Freitas, V. R. Funck, M. D. S. Rotta et al., "Diphenyl diselenide, a simple organoselenium compound, decreases methylmercury-induced cerebral, hepatic and renal oxidative stress and mercury deposition in adult mice," *Brain Research Bulletin*, vol. 79, no. 1, pp. 77–84, 2009.

[22] C. W. Nogueira and J. B. T. Rocha, "Diphenyl diselenide a janus-faced molecule," *Journal of the Brazilian Chemical Society*, vol. 21, no. 11, pp. 2055–2071, 2010.

[23] A. S. de Freitas, A. de Souza Prestes, C. Wagner et al., "Reduction of diphenyl diselenide and analogs by mammalian thioredoxin reductase is independent of their gluthathione peroxidase-like activity: a possible novel pathway for their antioxidant activity," *Molecules*, vol. 15, no. 11, pp. 7699–7714, 2010.

[24] L. Magos, "The absorption, distribution, and excretion of methylmercury," in *The Toxicity of Methylmercury*, C. U. Edccles and Z. Annau, Eds., pp. 24–44, John Hopkins University Press, Baltimore, Md, USA, 1987.

[25] R. Doi and M. Tagawa, "A study on the biochemical and biological behavior of methylmercury," *Toxicology and Applied Pharmacology*, vol. 69, no. 3, pp. 407–416, 1983.

[26] V. B. Brito, V. Folmer, G. O. Puntel et al., "Diphenyl diselenide and 2,3-dimercaptopropanol increase the PTZ-induced chemical seizure and mortality in mice," *Brain Research Bulletin*, vol. 68, no. 6, pp. 414–418, 2006.

[27] C. W. Nogueira and J. B. T. Rocha, "Toxicology and pharmacology of selenium: emphasis on synthetic organoselenium compounds," *Archives of Toxicology*, vol. 85, no. 11, pp. 1313–1359, 2011.

[28] M. Prigol, R. F. Schumacher, C. WayneNogueira, and G. Zeni, "Convulsant effect of diphenyl diselenide in rats and mice and its relationship to plasma levels," *Toxicology Letters*, vol. 189, no. 1, pp. 35–39, 2009.

[29] C. Paulmier, "Selenoorganic functional groups," in *Selenium Reagents and Intermediates in Organic Synthesis*, pp. 25–51, Pergamon Press, Oxford, UK, 1 edition, 1986.

[30] J. Christinal and T. Sumathi, "Effect of *Bacopa monniera* extract on methylmercury-induced behavioral and histopathological changes in rats," *Biological Trace Element Research*, vol. 155, no. 1, pp. 56–64, 2013.

[31] T. Sumathi, C. Shobana, J. Christinal, and C. Anusha, "Protective effect of *Bacopa monniera* on methyl mercury-induced oxidative stress in cerebellum of rats," *Cellular and Molecular Neurobiology*, vol. 2, no. 6, pp. 979–987, 2012.

[32] G. R. Bhagure and S. R. Mirgane, "Heavy metal concentrations in groundwaters and soils of Thane Region of Maharashtra, India," *Environmental Monitoring and Assessment*, vol. 173, no. 1–4, pp. 643–652, 2011.

[33] P. L. Broadhurst, "The place of animal psychology in the development of psychosomatic research," *Fortschritte der Psychosomatischen Medizin*, vol. 1, pp. 63–69, 1960.

[34] R. Lalonde, T. L. Lewis, C. Strazielle, H. Kim, and K. Fukuchi, "Transgenic mice expressing the βAPP695SWE mutation: effects on exploratory activity, anxiety, and motor coordination," *Brain Research*, vol. 977, no. 1, pp. 38–45, 2003.

[35] R. Lalonde, H. D. Kim, and K. Fukuchi, "Exploratory activity, anxiety, and motor coordination in bigenic APPswe + PS1/ΔE9 mice," *Neuroscience Letters*, vol. 369, no. 2, pp. 156–161, 2004.

[36] A. Holmgren and M. Bjornstedt, "Thioredoxin and thioredoxin reductase," *Methods in Enzymology*, vol. 252, pp. 199–208, 1995.

[37] N. Brustovetsky and J. M. Dubinsky, "Dual responses of CNS mitochondria to elevated calcium," *Journal of Neuroscience*, vol. 20, no. 1, pp. 103–113, 2000.

[38] G. L. Ellman, "Tissue sulfhydryl groups," *Archives of Biochemistry and Biophysics*, vol. 82, no. 1, pp. 70–77, 1959.

[39] Q. Guo, S. Christakos, N. Robinson, and M. P. Mattson, "Calbindin D28K blocks the proapoptotic actions of mutant presenilin 1: reduced oxidative stress and preserved mitochondrial function," *Proceedings of the National Academy of Sciences of the United States of America*, vol. 95, no. 6, pp. 3227–3232, 1998.

[40] C. García-Ruiz, A. Colell, M. Marí, A. Morales, and J. C. Fernández-Checa, "Direct effect of ceramide on the mitochondrial electron transport chain leads to generation of reactive oxygen species: role of mitochondrial glutathione," *Journal of Biological Chemistry*, vol. 272, no. 17, pp. 11369–11377, 1997.

[41] T. Mosmann, "Rapid colorimetric assay for cellular growth and survival: application to proliferation and cytotoxicity assays," *Journal of Immunological Methods*, vol. 65, no. 1-2, pp. 55–63, 1983.

[42] T. V. Votyakova and I. J. Reynolds, "Ca^{2+}-induced permeabilization promotes free radical release from rat brain mitochondria with partially inhibited complex I," *Journal of Neurochemistry*, vol. 93, no. 3, pp. 526–537, 2005.

[43] M. M. Bradford, "A rapid and sensitive method for the quantitation of microgram quantities of protein utilizing the principle of protein dye binding," *Analytical Biochemistry*, vol. 72, no. 1-2, pp. 248–254, 1976.

[44] P. B. Mello, F. Benetti, M. Cammarota, and I. Izquierdo, "Effects of acute and chronic physical exercise and stress on different types of memory in rats," *Anais da Academia Brasileira de Ciencias*, vol. 80, no. 2, pp. 301–309, 2008.

[45] C. Pinheiro, J. L. M. Do Nascimento, L. C. L. Silveira, J. B. T. Rocha, and M. Aschner, "Mercury and selenium—a review on aspects related to the health of human populations in the Amazon," *Environmental Bioindicators*, vol. 4, no. 3, pp. 222–245, 2009.

[46] F. E. Huggins, S. A. Raverty, O. S. Nielsen, N. E. Sharp, J. D. Robertson, and N. V. C. Ralston, "An XAFS investigation of mercury and selenium in Beluga whale tissues," *Environmental Bioindicators*, vol. 4, no. 4, pp. 291–302, 2009.

[47] H. Iwata, T. Masukawa, H. Kito, and M. Hayashi, "Degradation of methylmercury by selenium," *Life Sciences*, vol. 31, no. 9, pp. 859–866, 1982.

[48] J. H. Palmer and G. Parkin, "2-Seleno-1-alkylbenzimidazoles and their diselenides: synthesis and structural characterization of a 2-seleno-1-methylbenzimidazole complex of mercury," *Polyhedron*, vol. 52, pp. 658–668, 2013.

[49] B. Moller-Madsen and G. Danscher, "Localization of mercury in CNS of the rat: IV. The effect of selenium on orally administered organic and inorganic mercury," *Toxicology and Applied Pharmacology*, vol. 108, no. 3, pp. 457–473, 1991.

[50] J. R. Prohaska and H. E. Ganther, "Interactions between selenium and methylmercury in rat brain," *Chemico-Biological Interactions*, vol. 16, no. 2, pp. 155–167, 1977.

[51] M. O. Dietrich, C. E. Mantese, G. D. Anjos, D. O. Souza, and M. Farina, "Motor impairment induced by oral exposure to methylmercury in adult mice," *Environmental Toxicology and Pharmacology*, vol. 19, no. 1, pp. 169–175, 2005.

[52] M. Aschner, T. Syversen, D. O. Souza, J. B. T. Rocha, and M. Farina, "Involvement of glutamate and reactive oxygen species in methylmercury neurotoxicity," *Brazilian Journal of Medical and Biological Research*, vol. 40, no. 3, pp. 285–291, 2007.

[53] D. W. Choi, "Excitotoxic cell death," *Journal of Neurobiology*, vol. 23, no. 9, pp. 1261–1276, 1992.

[54] S. Ceccatelli, E. Daré, and M. Moors, "Methylmercury-induced neurotoxicity and apoptosis," *Chemico-Biological Interactions*, vol. 188, no. 2, pp. 301–308, 2010.

[55] N. Mori, A. Yasutake, and K. Hirayama, "Comparative study of activities in reactive oxygen species production/defense system in mitochondria of rat brain and liver, and their susceptibility to methylmercury toxicity," *Archives of Toxicology*, vol. 81, no. 11, pp. 769–776, 2007.

[56] L. V. Papp, A. Holmgren, and K. K. Khanna, "Selenium and selenoproteins in health and disease," *Antioxidants and Redox Signaling*, vol. 12, no. 7, pp. 793–795, 2010.

[57] W. J. Adams Jr., J. J. Kocsis, and R. Snyder, "Acute toxicity and urinary excretion of diphenyldiselenide," *Toxicology Letters*, vol. 48, no. 3, pp. 301–310, 1989.

[58] G. Zhang, V. Nitteranon, S. Guo et al., "Organoselenium compounds modulate extracellular redox by induction of extracellular cysteine and cell surface thioredoxin reductase," *Chemical Research in Toxicology*, vol. 26, no. 3, pp. 456–464, 2013.

Hindawi Publishing Corporation
BioMed Research International
Volume 2013, Article ID 324830, 9 pages
http://dx.doi.org/10.1155/2013/324830

Research Article

Cadmium Phytoremediation by *Arundo donax* L. from Contaminated Soil and Water

Maria Sabeen,[1] Qaisar Mahmood,[1] Muhammad Irshad,[1] Iftikhar Fareed,[2] Afsar Khan,[3] Farid Ullah,[1] Jamshaid Hussain,[1] Yousaf Hayat,[4] and Sobia Tabassum[5]

[1] *Department of Environmental Sciences, COMSATS Institute of Information Technology, Abbottabad 22060, Pakistan*
[2] *Department of Natural Resource Engineering and Management, University of Kurdistan Hewlêr, Kurdistan, Iraq*
[3] *Department of Chemistry, COMSATS Institute of Information Technology, Abbottabad, Pakistan*
[4] *Department of Mathematics, Statistics and Computer Sciences, KPK Agricultural University, Peshawar, Pakistan*
[5] *Interdisciplinary Research Centre in Biomedical Materials, COMSATS Institute of Information Technology, Defence Road, Off Raiwind Road, Lahore, Pakistan*

Correspondence should be addressed to Qaisar Mahmood; mahmoodzju@gmail.com

Received 14 November 2013; Revised 8 December 2013; Accepted 8 December 2013

Academic Editor: Fernando Barbosa Jr.

The potential of *Arundo donax* L. for phytoextraction of cadmium (Cd) from contaminated soil and water was probed. The plants were grown under greenhouse conditions in pots containing a nutrient solution or soil with increasing doses of Cd (0, 50, 100, 250, 500, 750, and 1000 $\mu g\,L^{-1}$) for 21 days. The growth and physiology of plants were evaluated at the end of the experiment. The maximum Cd content in root was 300 $\mu g\,g^{-1}$ during hydroponics experiments over 230 $\mu g\,g^{-1}$ in soil experiment. Cd concentration in stem was 262 $\mu g\,g^{-1}$ at 750 $\mu g\,L^{-1}$ supplied Cd in hydroponics over 191.2 $\mu g\,g^{-1}$ at 1000 in soil experiment. The maximum Cd concentration in leaves from hydroponics was 187 $\mu g\,g^{-1}$. Relatively low Cd uptake occurred during soil experiment with low translocation factor (TF) values. Both Bioaccumulation Factor (BF) and TF values for hydroponics were greater than 1. The IC_{50} values of ABTS and DPPH showed that both time and increasing Cd concentrations affected the production of antioxidants with lower half maximal inhibitory concentration (IC_{50}) value on the 21st days. *A. donax* showed better potential for Cd remediation of aquatic environments.

1. Introduction

Consequent to global industrialization, heavy metal pollution is a widespread problem which has become a major environmental concern due to hazardous effects on human and environmental health. In industrialized societies, heavy metals are the world over environmental contaminants. Air or water pollution by metals varies from soil pollution, because heavy metals persevere in soil for a longer time period as compared with the other compartment of the biosphere [1]. In the latest decades, the yearly global release of heavy metals attained 22,000 t (metric ton) for cadmium, 939,000 t for copper, 783,000 t for lead, and 1,350,000 t for zinc [2]. Cadmium (Cd), a highly toxic metal pollutant of soils, inhibits root and shoot growth and yield production, affects nutrient uptake and homeostasis, is frequently accumulated by agriculturally important crops, and then enters the food chain with a significant potential to impair animal and human health [3]. The mutagenic aptitude of toxic heavy metals causes DNA damage and probably causes carcinogenic effects in animals and humans [4]. The prime health perils coupled with Cd are damage to the neurological system, having indications like uncontrollable shaking, muscle wasting, partial blindness, and deformities in children exposed in the womb [5].

Many phytoremediation technologies have been used for the remediation of polluted soils and water throughout the World [6]. Phytoremediation costs almost one-fourth of the other physical and chemical methods of pollutant treatment. The major advantages of the process include: improvement of the soil quality, as it is driven by solar energy thus suitable

to most regions and climates, cost effective and technically feasible process, plants serve as sufficient biomass for rapid remediation; promote high rhizosphere activity and finally restoration in a reasonable time frame of 2 to 3 years.

The use of low cost, fast growing indigenous plants with efficient biomass producing plant species such as *Arundo donax* L. is highly desirable for phytoremediation of metal contaminated sites and waters. It is cultivable throughout Asia, Southern Europe, North Africa, and the Middle East for thousands of years with local names of "Giant Reed," "Nurr," "Nurru," or "Nurro" [7–9]. It is considered as one of the most biologically productive of all communities [10]. Previous experiments on giant reed suggested that the stem height and diameter, number of nodes, fresh and dry weight of leaves, and net photosynthesis were not affected, indicating that plants tolerated the high concentrations of Cd and Ni [11]. As giant reed plants are very promising energy plants, they can be cultivated in contaminated soils to provide biomass for energy production purposes [11]. Our research group is exploring the potential of this plant in environmental remediation of various heavy metals at high concentrations. The plant showed some potential against arsenic [7–9] and chromium [10] remediation. The specific objective of the current study was to investigate the phytoremediation ability of *A. donax* for cadmium remediation and to compare the Cd removal from contaminated soil and water.

2. Materials and Methods

2.1. Plant Material. The plant material used for the present study was *A. donax* L. with the aim to evaluate its responses to cadmium added to liquid medium. The plant material was collected near PMA road Abbottabad, Khyber Pakhtunkhwa, Pakistan. Plants were collected for the heavy metal analysis. The soil-grown plants used for hydroponics tests were taken from growth of young meristematic buds grown in sterile aqueous medium [8]. The young plants were transplanted in plastic trays containing 1/2 strength basal nutrient solutions.

2.2. Experimental Design. The phytoremediation ability of *A. donax* was compared in Cd contaminated soil and aqueous solution. The Cd containing aqueous solution was prepared by dissolving cadmium chloride salt in the double distilled water. Various Cd treatments were given in triplicates to experimental plants (both in hydroponics and soil). Cd treatments included 0 (control), 50, 100, 250, 500, 750, and 1000 $\mu g\,L^{-1}$. Each pot contained 4 *A. donax* L. plants with an average 250 g biomass on fresh weight basis. Two kinds of experiments were performed in randomized complete block design (RCBD) with three replications for plants grown in Hoagland solution [12] and in soil. Plants with healthy and uniform shoots of almost equal morphological characteristics were immersed in nutrient solution for three weeks. Plants were grown under greenhouse conditions in the laboratory with Hoagland solution continuously aerated and renewed after every 2-3 days with an addition of 100–200 mL of nutrient solution. Table 1 shows the average values of various plant characteristics.

Table 1: Average values of various morphological parameters before cadmium treatment.

Parameters	Values
Plant height (cm)	55 ± 12
No. of leaves per plant	87 ± 18
No. of nodes per plant	33 ± 22
Average root length per plant (cm)	8 ± 2
Toxicity symptoms	Leaf burning

2.3. Growth Parameters. Various growth parameters of *A. donax* were studied under cadmium stress including plant height (cm), number of leaves per plant, number of nodes per plant, dry weight, average root length (cm), and toxicity symptoms prior to and after the cadmium treatments.

2.4. Physiological Parameters. The physiological parameters of the plants included photosynthetic pigments, and the determination of antioxidants.

2.4.1. Photosynthetic Pigments. At the time of harvest, fresh leaves of both of various treatments from both kinds of experiments were collected for the determination of chlorophyll a, chlorophyll b, and carotene contents. Leaves were cut into small pieces and 0.5 g of the sample was put into the glass test tubes. Then 10 mL of 80% acetone was added to the tubes and kept overnight for complete extraction. Photosynthetic pigments were determined spectrophotometrically using the visible wavelengths of 663, 645, and 480 nm for chlorophyll a, chlorophyll b and carotene, respectively [12].

2.4.2. Antioxidant Determination. To determine antioxidant activity another parallel set of experiment was conducted. In this experiment four replicates each of 250 gm against each treatment was planted in a pot. Each pot was given Hoagland's solution and the respective treatment of cadmium above mentioned. After each week, one set was taken out and new leaves were counted. These plants were placed outside for shade dry.

All the plants were ground until uniform size. Now this sample was dipped in methanol for 4 to 5 days. The plant extract was filtered and methanol was recovered by passing it through rotary. The thick left over extract was taken out in Petri dishes and placed in fume hood. The thick jelly like extract was stored in sample bottles for further analysis.

DPPH Free Radical Scavenging Assay. 2,2-diphenyl-1-picrylhydrazyl free radical (DPPH) scavenging activity of crude extract and various fractions were estimated by standard DPPH assay protocol with certain modifications [13]. The reaction mixture contains 0.5 mL of test samples and 2.5 mL of DPPH in methanol. Concentration of DPPH was 100 μM in the reaction mixture. These reaction mixtures were incubated for 30 min. at 37°C. The absorbance was measured at 517 nm using spectrophotometer (5000, Irmeco GmbH D-21496 Geesthacht, Germany). Percent radical scavenging activity or percent antioxidant index (AI%)

by sample treatment was determined by comparison with methanol treated control group. An IC_{50} value denotes the concentration of sample, which is required to scavenge 50% DPPH free radicals. Propyl gallate was used as positive controls.

$ABTS^+$ Assay. Total antioxidant activity was evaluated applying an improved 2,2′-azinobis-3-ethyl-benzothiazoline-6-sulfonic acid cation (ABTS) decolorization assay by Re et al. [14]. $ABTS^+$ radical cation ($ABTS^+$) was produced by reacting ABTS stock solution (7 mM) with 2.45 mM potassium persulphate and allowing the solution to stand in the dark at room temperature for 12–14 hours before use. For the study of total antioxidant activity, the solution was diluted with ethanol to an absorbance of 0.70 (±0.02) at 374 nm. Percentage inhibition was calculated by using the following equation:

$$\text{Percentage inhibition} = \left[1 - \frac{\text{absorbance}_{\text{sample}}}{\text{absorbance}_{\text{control}}}\right] \times 100. \quad (1)$$

IC_{50} values were calculated based on various determinations of these antioxidants by supposing that reduced IC_{50} values would indicate a greater oxidative stress in the plant caused by absorbed metal content.

2.5. Bioaccumulation Factors. The phytoextraction ability of *A. donax* L. plants was assessed using both the translocation factor (TF) and the bioaccumulation factor (BF) as follows.

(1) Translocation factor:

$$\text{TF} = \frac{[\text{Cd}]_{\text{shoot}}}{[\text{Cd}]_{\text{root}}}. \quad (2)$$

(2) Bioaccumulation factor:

$$\text{BF} = \frac{[\text{Cd}]_{\text{shoot}}}{[\text{Cd}]_{\text{solution}}}. \quad (3)$$

2.6. Analytical Procedure. The harvested plants were separated into stems, leaves, and branches and the fresh weight was recorded. For dry weight determination, plant material was oven-dried at 70°C for 24 h, weighed, ground with pestle and mortar, and sieved at 0.1 mm nylon sieve. Plant samples were digested through wet digestion for metals determination using the $HNO_3/HClO_4$. A 0.5 g sample was taken in 100 mL conical flask and 10 mL of Perchloric and Nitric acid mixture (1 : 2 ratios) was added to each conical flask and left overnight. Next day, glass funnels were placed at the mouth of each flask in such a way that funnel stem stayed at least one inch above the surface of liquid. The flasks were then placed on hot plate and the temperature was gradually increased to allow for effective digestion. It took about 15 to 20 minutes when HNO_3 volatilized as nitrous oxide fumes, and then white fumes of Perchloric acid came out from the flask. The solution in flask was white in color at that stage. After digestion, the flasks were removed from the hot plate allowed to cool and few milliliters of distilled water was added. The digested material was then transferred to 50 mL volumetric flask and the volume was made up to 50 mL with deionized water. The readings were measured on Perkin Elmer Atomic Absorption Spectrometer-700 [15].

Table 2: Physicochemical properties of the soil used in experiment.

Characteristic	Value
pH	6.8
Available nitrogen (mg kg^{-1})	75.4
Available potassium (mg kg^{-1})	62.1
Available phosphorus (mg kg^{-1})	7.8
Total nitrogen (g kg^{-1})	0.86
Total phosphorus (g kg^{-1})	0.7
Total potassium (g kg^{-1})	17.3
Organic matter (g kg^{-1})	21.4

2.7. Soil Analysis. The soil used in the experiment was collected from an experimental field in COMSATS Institute of Information Technology, Abbottabad. The soil was sieved to remove roots, pebbles, and other unwanted materials. The soil was analyzed for various physic-chemical parameters according to [8] and presented in Table 2.

At the end of growing periods, soil samples from two replicates were oven-dried at 70°C. Soil sample (1 g) was digested on a hot plate with 15 mL nitric acid and 10 mL hydrogen peroxide. The digests were brought to 50 mL with deionized distilled water and the impurities were removed by filtration. A total Cd content was analyzed by Perkin Elmer Atomic Absorption Spectrometer-700.

2.8. Statistical Analysis. All determinations were performed in triplicate and mean values are presented in the results. One-way analysis of variance (ANOVA) was carried out for both the experiments separately using SAS 8.3 software (SAS Ins. Inc., Cary, USA). Treatment means were portioned using Least Significant Difference (LSD) at appropriates α value (0.05).

3. Results

3.1. Cadmium Content of Plant. The results of the cadmium concentration in the different plant parts grown in contaminated water were presented in Figure 1(a). In root, the cadmium uptake had linear relation to the increasing supplied cadmium concentration. Root Cd contents at various treatments significantly ($P < 0.05$) differed. The maximum cadmium uptake in stem was noted at 750 μg L^{-1} (262.8 μg g^{-1}). However, the cadmium concentration at 1000 μg L^{-1} was significantly ($P < 0.05$) different from all other treatments except 750 μg L^{-1}. Cd accumulation in leaves was the maximum at 1000 μg L^{-1} (187.5 μg L^{-1}) and was significantly ($P < 0.05$) different from the rest of the treatments. For the treatments 50 to 500 μg L^{-1}, the leaf cadmium content was in the range of 4.8 to 129.83 μg g^{-1}. Overall, the Cd accumulation pattern in various plant organs was as follows: root > stem >

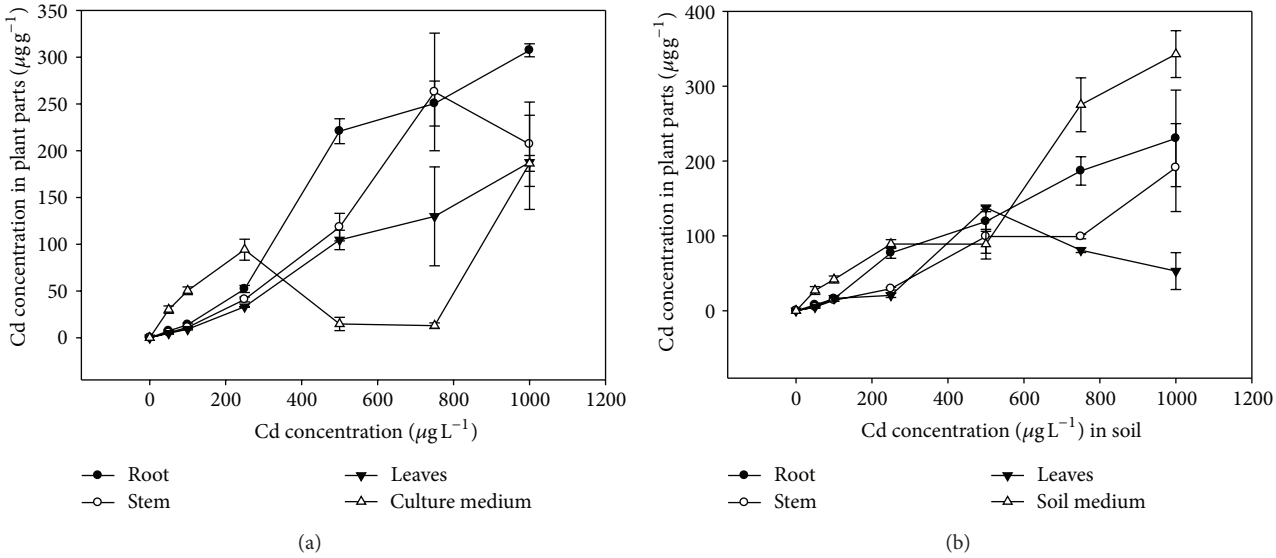

Figure 1: (a) The accumulation of cadmium in various plant parts in hydroponics experiment. (b) The accumulation of cadmium in various plant parts during soil experiment.

leaf (Figure 1(a)). The left over Cd content in the aqueous medium was in the range of 12 to 186.4 μg L^{-1} for various treatments. The maximum left over cadmium concentration (186.4 μg L^{-1}) was noted for 1000 μg L^{-1} supplied cadmium (Figure 1(a)).

The results of the cadmium concentration in plant parts grown in contaminated soil were presented in Figure 1(b). The maximum Cd concentration in roots of soil grown plants was 230 μg g^{-1} at 1000 μg g^{-1} supplied Cd content. The plant root Cd content was significantly ($P < 0.05$) different from supplied Cd contents of 500 μg g^{-1} and below. For stem, the maximum cadmium uptake occurred at 1000 μg g^{-1} which was 191 μg g^{-1} which was significantly ($P < 0.05$). The stem cadmium concentration at 750 μg L^{-1} was 99 μg g^{-1}, significantly ($P < 0.05$) different from the values at 250 μg g^{-1} and lower supplied Cd treatments (Figure 1(b)). The maximum uptake in leaves of soil grown plants occurred at 500 μg g^{-1} treatment which was 138 μg g^{-1} and was significantly ($P < 0.05$) different from the rest of treatments. At higher treatments (750 to 1000 μg L^{-1}), the leaf cadmium contents were 81 and 53 μg g^{-1}, respectively, and were nonsignificantly different ($P > 0.05$). Like hydroponics, the accumulation pattern of cadmium in various plant organs was as follows: root > stem > leaf (Figure 1(b)). The left over cadmium concentration in the soil medium was in the range of 27 to 343 μg g^{-1} soil for various supplied cadmium concentrations.

3.2. Effect of Cadmium on Photosynthetic Pigments. The effects of cadmium on the photosynthetic pigments that is chlorophyll a, chlorophyll b, and carotenes of plants grown in hydroponics were presented in Figure 2(a). The maximum chlorophyll a content was observed at Cd treatment of 250 μg L^{-1} (Figure 2(a)). The amount of chlorophyll b had similar trend like chlorophyll a with the maximum value (0.96 mg g^{-1}) at 250 μg L^{-1} supplied Cd (Figure 2(a)). As far as carotene content was concerned, its amount was the maximum (1.55 mg g^{-1}) at 100 μg L^{-1}. Further increase in the supplied Cd did not cause any significant ($P < 0.05$) increase in carotene content. However, the amount of carotene was significantly ($P < 0.05$) different than control and 50 μg L^{-1} (Figure 2(a)).

The effects of cadmium on the photosynthetic pigments in soil grown plants were presented in Figure 2(b). The chlorophyll a content was the maximum at Cd treatment of 1000 μg g^{-1}. The amount of chlorophyll b increased up to 250 μg g^{-1} where its value was 0.21 mg g^{-1} and then it showed a decline towards the maximum Cd content in soil. As far as carotene content was concerned, amount was the maximum (0.74 mg g^{-1}) at 100 μg g^{-1} supplied Cd in soil. Further increase in the supplied cadmium did not cause any increase in carotene content (Figure 2(b)).

3.3. Effect of Cadmium on Bioconcentration Factors. The results of bioconcentration factors for plants grown in hydroponics were presented in Figure 3(a). The translocation and bioaccumulation factors increased up to 750 μg L^{-1} Cd in the hydroponics culture (Figure 3(a)). Overall, BF and TF values were in the range of 0.3 to 30 and 1 to 2.28, respectively, for various Cd treatments. The highest values were TF = 1.6 and BF = 30.00 for 750 μg L^{-1} Cd treatment. However, both TF and BF decreased at 1000 μg L^{-1} and some toxicity symptoms appeared in the plants receiving that Cd treatment (Figure 3(a)). Both bioconcentration factor values for soil grown plants were presented in Figure 3(b). The translocation and bioaccumulation factors increased as a function of Cd concentration up to 500 μg g^{-1} supplied Cd; however, it decreased a little at higher Cd content in soil (Figure 3(b)). Overall, the values of BF and TF were in the range of 0.7 to 0.67 and 1.2 to 1.3, respectively, for various Cd treatments.

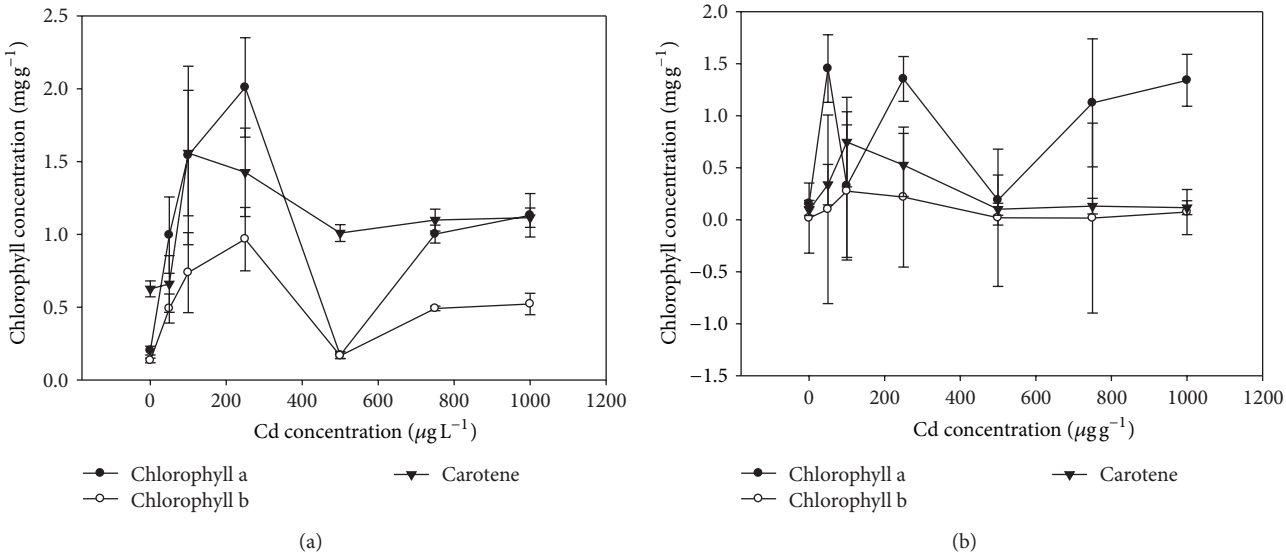

Figure 2: (a) The effect of cadmium concentrations on chlorophyll content in hydroponics experiment. (b) The effect of cadmium concentrations on chlorophyll content during soil experiment.

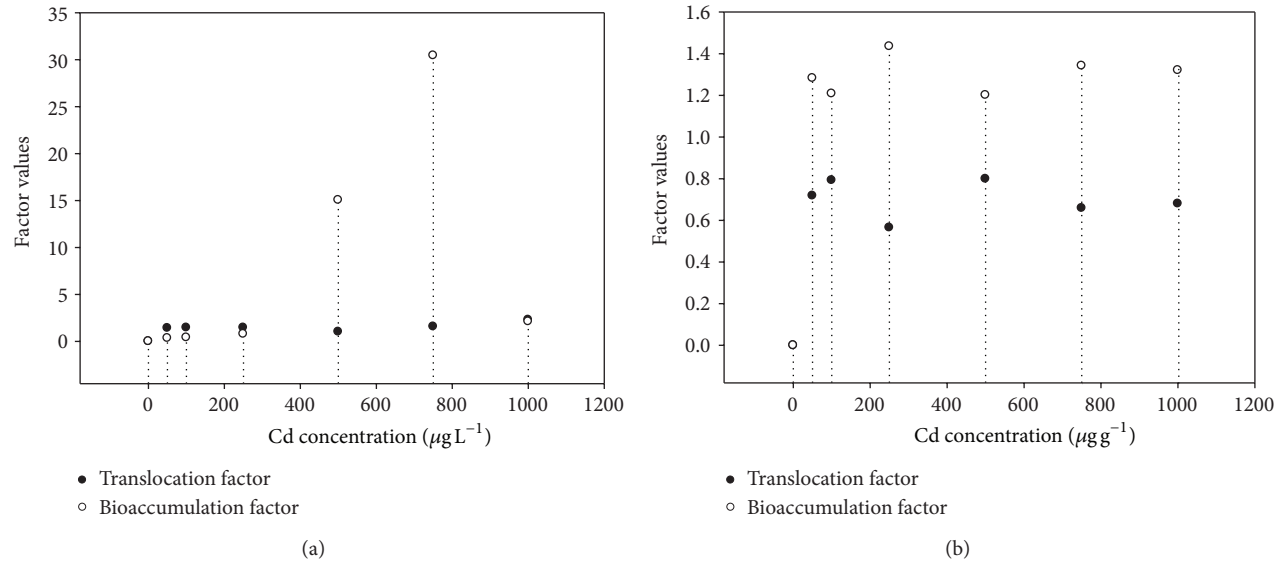

Figure 3: (a) Relative bioconcentration factors at various cadmium treatments in hydroponics. (b) Relative bioconcentration factors at various cadmium treatments in soil.

The highest values were TF = 1.3 and BF = 0.71 for the Cd treatment of 500 μg g^{-1}. Translocation factors were above the reference value (1.0) for hyperaccumulation; however, BF values were below 1 (Figure 3(b)).

3.4. Effects of Cadmium on Growth Characteristics. Growth performance of the plant in reference to plant height, nodes, internodes, tillers, fresh weight, and number of leaves of plants from hydroponics is depicted in Figure 4(a). The results showed that there was no significant ($P < 0.05$) increase in plant height, root length, nodes and internodes of treated plants at all levels of Cd treatments. However some increase in the fresh weight, leaves, and tillers of the treated plants was observed. For leaves, the number significantly increased up to 100 μg L^{-1} supplied Cd. The number was significantly different at all other treatments except 250 and 500 μg L^{-1} supplied Cd level. It implied that Cd initially enhanced the growth of plants up to the concentration of 300 μg L^{-1} in hydroponics culture; however, at higher concentrations, the growth of the plant was reduced (Figure 4(a)). Growth performance of the plant in reference to plant height, tillers, fresh weight, and number of leaves during the soil experiment is depicted in Figure 4(b). A trend of growth similar to hydroponics experiment was observed.

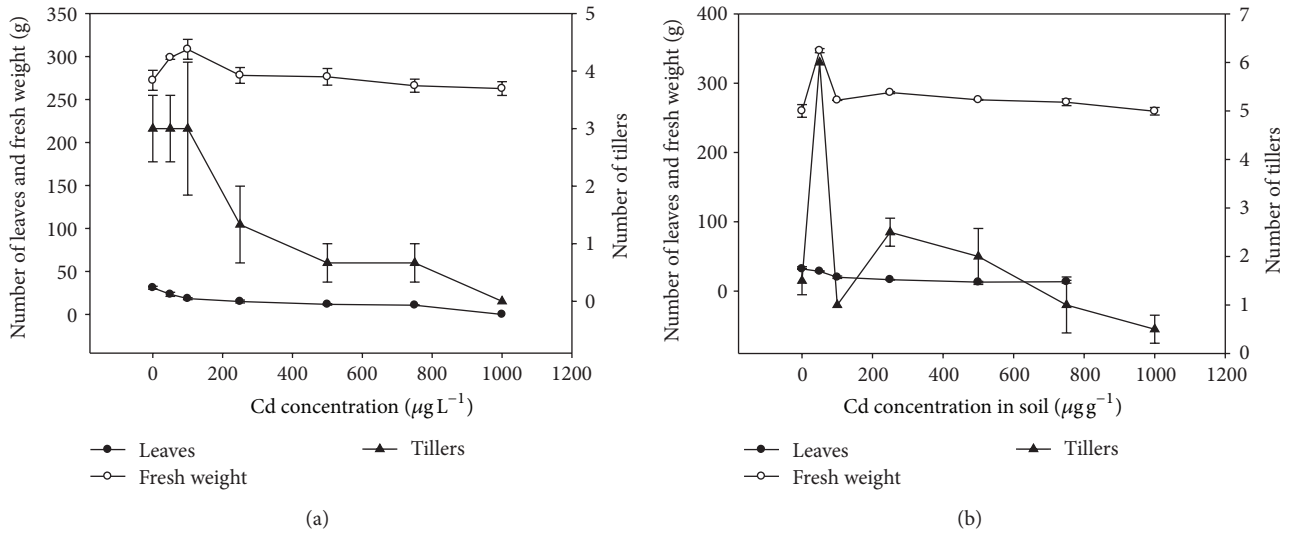

Figure 4: (a) Effect of cadmium on fresh weight, number of leaves, and tillers of treated plants growth in hydroponics culture. (b) Effect of cadmium on fresh weight, number of leaves, and tillers of treated plants growth in in soil.

The observation that increase in number of tillers without increase in plant height (stunted growth) indicated Cd stress.

3.5. Antioxidant Assays. Antioxidants are chemical compounds that can bind to free oxygen radicals preventing these radicals from damaging healthy cells. The present study involved the determination of one of the most commonly used organic radicals for the evaluation of antioxidant efficiency of pure compounds and complex mixtures is the radical cations derived from ABTS and DPPH. These radical cations could be generated by enzymatic, chemical, and electrochemical means. The IC_{50} measured at 7th, 14th, and 21st days of the experiment were presented in Figures 5 and 6. The IC_{50} values of ABTS showed that both time and increasing Cd concentrations strongly inhibited the production of ABTS (Figure 5) which was indicated by lower IC_{50} value on 21st day. A similar trend was obvious for DPPH up to 500 μg L^{-1} supplied Cd (Figure 6). However, a relative increase in IC_{50} was observed at higher supplied Cd contents (>500 μg L^{-1}) showing that the concentration of these antioxidants might be greater with increasingly higher Cd exposure.

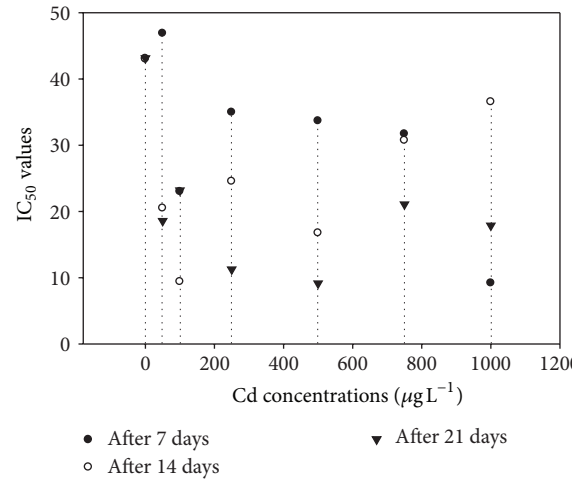

Figure 5: The effect of cadmium concentrations on the IC_{50} values against antioxidant activity of ABTS.

4. Discussion

The present study employed the use of *A. donax* to treat Cd metal in hydroponics and soil contaminated environments. Overall, the results indicated that the plant is useful for the treatment of Cd contaminated wastewaters. However, better uptake was observed in hydroponics cultures as compared with soil environment. The maximum plant root Cd content was 300 μg g^{-1} in hydroponics experiment as compared with 230 μg g^{-1} in soil experiment. Likewise, Cd concentration in stem for hydroponics culture was 262 μg g^{-1} at 750 μg L^{-1} supplied Cd over 191.2 μg g^{-1} at 1000 in soil experiment. In case of leaves, the maximum Cd concentration for hydroponics was 187 μg g^{-1} at 1000 μg L^{-1} supplied Cd. In soil experiment, the Cd concentration in leaves was 137 μg g^{-1} at 500 μg L^{-1}. Relatively low Cd uptake occurred during soil experiment which consequently resulted in low TF values. It was opposite in case of hydroponics where BF and TF values were always greater than 1. Both factors values were above the reference value (1.0) for hyperaccumulation.

A. donax L. (giant reed, Poaceae) is a potentially high-yielding nonfood crop, which can be used for the production of energy, paper pulp, and wooden building materials [11]. It is a robust invasive perennial grass, wild growing in southern European regions and other Mediterranean countries [16]. It is also very common in Pakistan. Giant reed can easily adapt

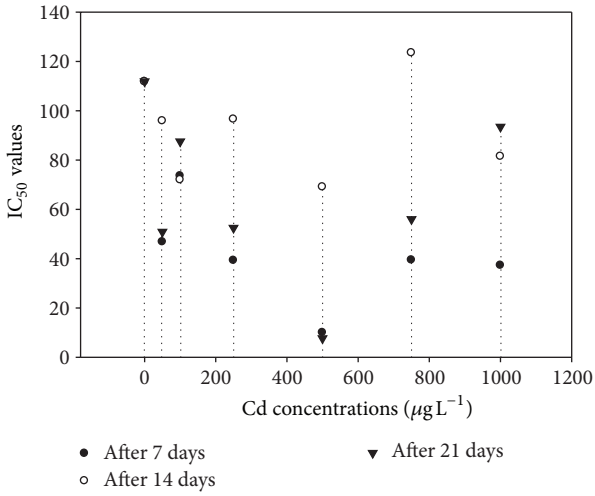

FIGURE 6: The effect of cadmium concentrations on the IC_{50} values against antioxidant activity of DPPH.

to different ecological conditions and grow in all types of soils [17]. The plant has been evaluated for the phytoremediation ability towards arsenic contamination [7]. It was suggested that *A. donax* plants may be employed to treat water containing arsenic concentrations up to 600 $\mu g\,L^{-1}$ [7].

Increasing metal concentrations in the wastewaters and soils adjacent to industrial regions of the world are a serious threat to the natural environmental sustainability. Among the heavy metals, cadmium is of special concern due to its potential toxicity to biota at low concentrations [18]. The use of indigenous plants like *A. donax* is very promising to combat metal toxicity in soils and wastewaters. Different plant species have different capacities for uptaking and tolerating the heavy metals like cadmium and others [19, 20]. The metal hyperaccumulators show an extra aptitude for accumulating the large quantity of metals in their aerial parts [21]. This special characteristic of the metal hyperaccumulators make them extremely appropriate for phytoremediation, that is, to use plants for cleaning up the polluted soils. In the preceding decade many studies have been accomplished to explore the mechanisms liable for the better metal uptake and tolerance via natural hyperaccumulators as model plant species [22]. In general the metal hyperaccumulation in plants is acknowledged as a mishmash of high metal uptake coupled with an improved tissue tolerance against the detrimental effects of higher metal concentrations through a better antioxidative response and sequestration at the cellular level [23]. Remediation of heavy metals contaminated that soil may possibly be carried out using physicochemicals processes such as ion-exchange, precipitation, reverse osmosis, evaporation, and chemical reduction; however, the procedures requisite external man-made resources and expensive [1].

Plants absorb toxic metals, translocate and accumulate them in roots and shoots; and finally resist to metal contamination, thus remediate contaminated environments [24]. Phytoremediation is a growing field of research in environmental studies because of the advantages of its environmental friendliness, safe, cost effectiveness, and the possibility of harvesting the plants for the extraction of absorbed contaminants such as metals that cannot be easily biodegraded for recycling among others [7]. Moreover, it is based on the ecological engineering principles. The most effective phytoremediation plants are those classified as hyperaccumulators [25] and accumulators. Hyperaccumulators are characterized based on four features. First, the concentration in the shoots (stems or leaves) of a hyperaccumulator should be 10,000 $\mu g\,g^{-1}$ for Zn and Mn; above 1000 $\mu g\,g^{-1}$ dry mass for As, Pb, Cu, Ni, and Co; 100 $\mu g\,g^{-1}$ for 1 Cd and 1 $\mu g\,g^{-1}$ for Au [7, 8, 26]. Second is translocation factor (concentration in shoots/roots >1), metal concentrations in the shoots of a plant should be higher than those in the roots [7]. Third is bioaccumulation factor (concentration in plant/habitat >1) [7] and lastly it is tolerance ability, a hyperaccumulator should have high tolerance to toxic contaminants. *A. donax* L. can tolerate arsenic concentrations up to 600 $\mu g\,L^{-1}$ without toxicity symptoms appeared on the plant. The appearance of some toxicity symptoms in the leaves, roots, and slow growth at 1000 $\mu g\,L^{-1}$ revealed that although *A. donax* L. cannot tolerate but still accumulate and volatilize as concentration above 600 $\mu g\,L^{-1}$ [7–9].

The results suggested that Cd contamination affected the photosynthetic pigments to some extent. Detailed studies indicate that heavy metals have effects on photosynthetic pigments in plants. Heavy metals are known to interfere with chlorophyll synthesis either through direct inhibition of an enzymatic step or by inducing deficiency of an essential nutrient [27]. An important indicator which determines photosynthesis intensity is chlorophyll content in plant leaves. Cadmium markedly suppresses chlorophyll accumulation in leaves [28]. Carotenoid actively participates in photosynthesis as well and it was shown that content and ratio of carotenoids are strictly changed under impact of different stresses [29]. However, it has been determined that carotenoids are less sensitive to the impact of cadmium as compared to chlorophylls [30]. The success of phytoextraction is inherently dependent on several plant characteristics, the two most important being the ability to accumulate large quantities of biomass rapidly and the capacity to accumulate large quantities of environmentally important metals in the shoot tissue [31]. Effective phytoextraction requires both plant genetic ability and the development of optimal agronomic practices, including (1) soil management practices to improve the efficiency of phytoextraction and (2) crop management practices to develop a commercial cropping system. The present study showed that *A. donax* has potential to remediate the Cd contaminated environments as indicated by its high tissue Cd concentrations and BF and TF values higher than 1 especially for hydroponics experiment. The reason behind less Cd uptake in soil experiment may be that it may have been adsorbed in soil particles or it is leaching from rhizosphere as the experiment was conducted in sandy soil.

The IC_{50} value was defined as the concentration of the sample necessary to cause 50% inhibition, which was obtained by interpolation from linear regression analysis [32]. A lower IC_{50} value is associated with a higher radical scavenging activity. The IC_{50} values of ABTS showed that both time

and increasing Cd concentrations affected the production of ABTS which was indicated by lower IC_{50} value on 21st days. A similar trend was obvious for DPPH upto 500 $\mu g\,L^{-1}$ supplied Cd. However, a relative increase in IC_{50} was observed at higher supplied Cd contents (>500 $\mu g\,L^{-1}$) showing that the concentration of these antioxidants might be greater with increasingly higher Cd exposure. One of the most commonly used organic radicals for the evaluation of antioxidant efficiency of pure compounds and complex mixtures is the radical cation derived from 2,2′-azinobis-3-ethyl-benzothiazoline-6-sulfonic acid (ABTS) [33]. The differences among all studied morphological parameters were statistically nonsignificant; likewise, the fresh and dry weights of control and experimental plants were also nonsignificant. Reduced growth was noted in control plants which may possibly be due to the fact that the plants were grown in pots and not in the field. *A. donax* is a grass with C3 photosynthetic pathway unlike other grasses (e.g., switchgrass and miscanthus) with C4 pathway [34]. Physiological processes, such as photosynthesis and water status, are sensitive to heavy metals [35] in several plant species. Heavy metals have been found to inhibit electron transport in photosynthetic systems [36]. Photosynthetic rates of *A. donax* were unaffected by the treatments, indicating that the photosynthetic system was not harmed and showed a strong tolerance of this plant to the increased heavy metal concentrations in the soil. The mean values of giant reed Pn rates found in this study were higher than those usual for C3 plants (18–20 $\mu mol\ CO_2\ m^{-2}\ s^{-1}$) [37]. Rossa et al. [38], in a comparative study on photosynthesis of five C3 and three C4 grasses, found that *A. donax* had high Pn rates, higher than the other grasses (37.0 $\mu mol\ CO_2\ m^{-2}\ s^{-1}$) under similar environmental conditions.

5. Conclusions

The phytoremediation ability of *Arundo donax* to treat cadmium contamination was compared in hydroponics and soil environments. The plant is useful for the treatment of Cd contaminated wastewaters both in hydroponics and in soil environments. However, better uptake was observed in hydroponics cultures as compared with soil environment. Both BF and TF values for hydroponics were greater than 1 which confirmed its suitability for aquatic contaminated environments. At higher Cd exposure, plant showed some antioxidative stress as the concentration of antioxidants was greater with increasing Cd exposure.

Conflict of Interests

The authors have neither any conflict of interests nor any financial gain from the present work.

References

[1] M. M. Lasat, "Phytoextraction of toxic metals: a review of biological mechanisms," *Journal of Environmental Quality*, vol. 31, no. 1, pp. 109–120, 2002.

[2] O. V. Singh, S. Labana, G. Pandey, R. Budhiraja, and R. K. Jain, "Phytoremediation: an overview of metallic ion decontamination from soil," *Applied Microbiology and Biotechnology*, vol. 61, no. 5-6, pp. 405–412, 2003.

[3] L. S. Di Toppi and R. Gabbrielli, "Response to cadmium in higher plants," *Environmental and Experimental Botany*, vol. 41, no. 2, pp. 105–130, 1999.

[4] C. Baudouin, M. Charveron, R. Tarroux, and Y. Gall, "Environmental pollutants and skin cancer," *Cell Biology and Toxicology*, vol. 18, no. 5, pp. 341–348, 2002.

[5] WHO, "Health and environment in sustainable development," Report, WHO, Geneva, Switzerland, 1997.

[6] M. A. Kamran, Amna, R. Mufti et al., "The potential of the flora from different regions of Pakistan in phytoremediation: a review," *Environmental Science and Pollution Research*, 2013.

[7] N. Mirza, Q. Mahmood, A. Pervez et al., "Phytoremediation potential of *Arundo donax* in arsenic-contaminated synthetic wastewater," *Bioresource Technology*, vol. 101, no. 15, pp. 5815–5819, 2010.

[8] N. Mirza, A. Pervez, Q. Mahmood, and S. S. Ahmad, "Phytoremediation of arsenic (As) and mercury (Hg) contaminated soil," *World Applied Sciences Journal*, vol. 8, pp. 113–118, 2010.

[9] N. Mirza, A. Pervez, Q. Mahmood, M. M. Shah, and M. N. Shafqat, "Ecological restoration of arsenic contaminated soil by *Arundo donax* L," *Ecological Engineering*, vol. 37, no. 12, pp. 1949–1956, 2011.

[10] S. Kausar, Q. Mahmood, I. A. Raja et al., "Potential of *Arundo donax* to treat chromium contamination," *Ecological Engineering*, vol. 42, pp. 256–259, 2012.

[11] E. G. Papazoglou, G. A. Karantounias, S. N. Vemmos, and D. L. Bouranis, "Photosynthesis and growth responses of giant reed (*Arundo donax* L.) to the heavy metals Cd and Ni," *Environment International*, vol. 31, no. 2, pp. 243–249, 2005.

[12] D. Liu, T. Q. Li, X. F. Jin, X. E. Yang, E. Islam, and Q. Mahmood, "Lead induced changes in the growth and antioxidant metabolism of the lead accumulating and non-accumulating ecotypes of *Sedum alfredii*," *Journal of Integrative Plant Biology*, vol. 50, no. 2, pp. 129–140, 2008.

[13] M. S. Blois, "Antioxidant determinations by the use of a stable free radical," *Nature*, vol. 181, no. 4617, pp. 1199–1200, 1958.

[14] R. Re, N. Pellegrini, A. Proteggente, A. Pannala, M. Yang, and C. Rice-Evans, "Antioxidant activity applying an improved ABTS radical cation decolorization assay," *Free Radical Biology and Medicine*, vol. 26, no. 9-10, pp. 1231–1237, 1999.

[15] R. John, P. Ahmad, K. Gadgil, and S. Sharma, "Heavy metal toxicity: effect on plant growth, biochemical parameters and metal accumulation by *Brassica juncea* L.," *International Journal of Plant Production*, vol. 3, no. 3, pp. 65–75, 2009.

[16] N. El Bassam, *Energy Plant Species: Their Use and Impact on Environment and Development*, Earthscan LLC, Washington, DC, USA, 1998.

[17] R. E. Perdue, "*Arundo donax*—source of musical reeds and industrial cellulose," *Economic Botany*, vol. 12, no. 4, pp. 368–404, 1958.

[18] P. Das, S. Samantaray, and G. R. Rout, "Studies on cadmium toxicity in plants: a review," *Environmental Pollution*, vol. 98, no. 1, pp. 29–36, 1997.

[19] V. Bert, I. Bonnin, P. Saumitou-Laprade, P. de Laguérie, and D. Petit, "Do *Arabidopsis halleri* from nonmetallicolous populations accumulate zinc and cadmium more effectively than those from metallicolous populations?" *New Phytologist*, vol. 155, no. 1, pp. 47–57, 2002.

[20] N. Roosens, N. Verbruggen, P. Meerts, P. Ximénez-Embún, and J. A. C. Smith, "Natural variation in cadmium tolerance and its relationship to metal hyperaccumulation for seven populations of *Thlaspi caerulescens* from western Europe," *Plant, Cell and Environment*, vol. 26, no. 10, pp. 1657–1672, 2003.

[21] A. J. M. Baker and P. L. Walker, "Ecophysiology of metal uptake by tolerant plants," in *Heavy Metal Tolerance in Plants: Evolutionary Aspects*, A. J. Shaw, Ed., pp. 155–177, CRC Press, Boca Raton, Fla, USA, 1999.

[22] E. Lombi, F. J. Zhao, S. P. McGrath, S. D. Young, and G. A. Sacchi, "Physiological evidence for a high-affinity cadmium transporter highly expressed in a *Thlaspi caerulescens* ecotype," *New Phytologist*, vol. 149, no. 1, pp. 53–60, 2001.

[23] B. P. Shaw, S. K. Sahu, and R. K. Mishra, "Heavy metal induced oxidative damage in terrestrial plants," in *Heavy Metal Stress in Plants—from Biomolecules to Ecosystems*, M. N. V. Prasad, Ed., pp. 84–126, Springer, New York, NY, USA, 2nd edition, 2004.

[24] V. Mudhal, N. Madaan, and A. Mudhal, "Heavy metals in plants: phytoremediation: plants used to remediate heavy metal pollution," *Agricultural and Biological Journal of North America*, vol. 1, pp. 40–46, 2010.

[25] C. Y. Wei and T. B. Chen, "Arsenic accumulation by two brake ferns growing on an arsenic mine and their potential in phytoremediation," *Chemosphere*, vol. 63, no. 6, pp. 1048–1053, 2006.

[26] M. Srivastava, L. Q. Ma, and J. A. G. Santos, "Three new arsenic hyperaccumulating ferns," *Science of the Total Environment*, vol. 364, no. 1–3, pp. 24–31, 2006.

[27] F. van Assche and H. Clijsters, "Effect of metals on enzyme activity in plants," *Plant, Cell and Environment*, vol. 13, no. 3, pp. 195–206, 1990.

[28] J. Moreno-Caselles, R. Moral, A. Pérez-Espinosa, and M. D. Pérez-Murcia, "Cadmium accumulation and distribution in cucumber plant," *Journal of Plant Nutrition*, vol. 23, no. 2, pp. 243–250, 2000.

[29] B. Demmig-Adams and W. W. Adams III, "The role of xanthophyll cycle carotenoids in the protection of photosynthesis," *Trends in Plant Science*, vol. 1, no. 1, pp. 21–26, 1996.

[30] N. Neelu, M. Kumar, M. Tomar, and A. K. Bhatnagar, "Influence of cadmium on growth and development of *Vicia faba* Linn," *Indian Journal of Experimental Biology*, vol. 38, no. 8, pp. 819–823, 2000.

[31] E. A. Pilon-Smits, "Phytoremediation," *Annual Review of Plant Biology*, vol. 56, pp. 15–39, 2005.

[32] Y. Qingming, P. Xianhui, K. Weibao et al., "Antioxidant activities of malt extract from barley (*Hordeum vulgare* L.) toward various oxidative stress in vitro and in vivo," *Food Chemistry*, vol. 118, no. 1, pp. 84–89, 2010.

[33] C. A. Rice-Evans and N. J. Miller, "Total antioxidant status in plasma and body fluids," *Methods in Enzymology*, vol. 234, pp. 279–293, 1994.

[34] I. Lewandowski, J. M. O. Scurlock, E. Lindvall, and M. Christou, "The development and current status of perennial rhizomatous grasses as energy crops in the US and Europe," *Biomass and Bioenergy*, vol. 25, no. 4, pp. 335–361, 2003.

[35] S. Monni, C. Uhlig, O. Junttila, E. Hansen, and J. Hynynen, "Chemical composition and ecophysiological responses of *Empetrum nigrum* to aboveground element application," *Environmental Pollution*, vol. 112, no. 3, pp. 417–426, 2001.

[36] J. M. Becerril, A. Munoz-Rueda, P. Aparicio-Tejo, and C. Gonzalez-Murua, "The effects of cadmium and lead on photosynthetic electron transport in clover and lucerne," *Plant Physiology and Biochemistry*, vol. 26, pp. 913–918, 1989.

[37] H. Mohr and P. Schopfer, *Plant Physiology C4 and CAM Plants*, Springer, Berlin, Germany, 1995.

[38] B. Rossa, A. V. Tüffers, G. Naidoo, and D. J. von Willert, "*Arundo donax* L. (Poaceae)—a C3 species with unusually high photosynthetic capacity," *Botanica Acta*, vol. 111, no. 3, pp. 216–221, 1998.

Hindawi Publishing Corporation
BioMed Research International
Volume 2013, Article ID 769295, 12 pages
http://dx.doi.org/10.1155/2013/769295

Research Article

In Vitro Manganese Exposure Disrupts MAPK Signaling Pathways in Striatal and Hippocampal Slices from Immature Rats

Tanara Vieira Peres,[1] Daniela Zótico Pedro,[1] Fabiano Mendes de Cordova,[2] Mark William Lopes,[1] Filipe Marques Gonçalves,[1] Cláudia Beatriz Nedel Mendes-de-Aguiar,[3] Roger Walz,[4] Marcelo Farina,[1] Michael Aschner,[5] and Rodrigo Bainy Leal[1]

[1] *Departamento de Bioquímica, Centro de Ciências Biológicas, Universidade Federal de Santa Catarina, Campus Universitário, 88040-900 Florianópolis, SC, Brazil*
[2] *Escola de Medicina Veterinária e Zootecnia, Universidade Federal do Tocantins, 77804-970 Araguaína, TO, Brazil*
[3] *Departamento de Biologia Celular, Embriologia e Genética, Centro de Ciências Biológicas, Universidade Federal de Santa Catarina, Campus Universitário, 88040-900 Florianópolis, SC, Brazil*
[4] *Departamento de Clínica Médica, Centro de Ciências da Saúde, Universidade Federal de Santa Catarina, Hospital Universitário (HU), 88036-800 Florianópolis, SC, Brazil*
[5] *Department of Pediatrics, Vanderbilt University Medical Center, Nashville, TN 37232, USA*

Correspondence should be addressed to Rodrigo Bainy Leal; rbleal@gmail.com

Received 31 July 2013; Accepted 7 October 2013

Academic Editor: Wilma De Grava Kempinas

The molecular mechanisms mediating manganese (Mn)-induced neurotoxicity, particularly in the immature central nervous system, have yet to be completely understood. In this study, we investigated whether mitogen-activated protein kinases (MAPKs) and tyrosine hydroxylase (TH) could represent potential targets of Mn in striatal and hippocampal slices obtained from immature rats (14 days old). The aim of this study was to evaluate if the MAPK pathways are modulated after subtoxic Mn exposure, which do not significantly affect cell viability. The concentrations of manganese chloride ($MnCl_2$; 10–1,000 μM) caused no change in cell viability in slices exposed for 3 or 6 hours. However, Mn exposure significantly increased extracellular signal-regulated kinase (ERK) 1/2, as well as c-Jun N-terminal kinase (JNK) 1/2/3 phosphorylation at both 3 and 6 hours incubations, in both brain structures. Furthermore, Mn exposure did not change the total content or phosphorylation of TH at the serine 40 site in striatal slices. Thus, Mn at concentrations that do not disrupt cell viability causes activation of MAPKs (ERK1/2 and JNK1/2/3) in immature hippocampal and striatal slices. These findings suggest that altered intracellular MAPKs signaling pathways may represent an early event concerning the effects of Mn in the immature brain.

1. Introduction

Manganese (Mn) is an essential metal for humans and animals. Its essentiality is due to its requirement as a cofactor in chemical reactions catalyzed by several enzymes involved in cellular homeostasis, such as mitochondrial superoxide dismutase and glutamine synthetase. However, exposure to high Mn levels may cause a neurological syndrome referred to as manganism, which shares multiple analogous symptoms with Parkinson's disease (PD) [1].

Within the central nervous system (CNS), Mn accumulates predominantly in structures of the basal ganglia, such as the striatum (caudate, putamen, and nucleus accumbens), globus pallidus, and substantia nigra, consistent with

dystonia, bradykinesia and rigidity secondary to damage to dopaminergic neurons and gliosis [2, 3]. Nonmotor symptoms have also been reported in Mn-exposed individuals, such as loss of attention and neuropsychological symptoms, suggesting that not only the basal ganglia are affected in manganism [1, 4].

Neonatal and developing brains are more susceptible to Mn toxicity. The uptake of metal in the intestine is usually elevated in the first week of life, followed by a steady decrease with age. These factors contribute to the increased risk for neurotoxicity in newborns when exposed to excess Mn [5]. In addition, increased hair Mn levels (a useful analytical biomarker of Mn exposure in humans) has been associated with learning disabilities, hyperactivity, and attention deficit disorder [5]. In rats, exposure to Mn during development has been shown to affect the dopaminergic system and induce lasting motor impairment and astrocyte activation [6]. Nevertheless, despite evidence suggesting that precocious Mn exposure may impair neurological function later in life [6, 7], studies on the molecular targets of Mn during critical periods of brain development have yet to be systematically addressed.

Although the molecular mechanisms that mediate Mn-induced neurotoxicity have yet to be fully understood, evidence points to mitochondrial dysfunction with formation of reactive oxygen species (ROS) and oxidative stress as critical mediators of neurotoxicity [8–11]. Increased striatal levels of F2 isoprostanes as consequence of oxidative stress have been reported in response to Mn treatment in rats during development, with concomitant activation of the mitogen-activated protein kinase (MAPK) ERK1/2 [12, 13]. Of particular importance, studies in cell culture models have shown that Mn-induced oxidative stress is related, at least in part, to the activation of MAPK pathways [14–17]. MAPKs are a family of serine-threonine kinases which play critical roles in neurodevelopment and neuroplasticity. They mediate various cellular responses, such as proliferation, differentiation, cell survival, death, and cell transformation. The three major MAPKs are extracellular signal-regulated kinases (ERK1/2), c-Jun N-terminal kinases (JNKs), and $p38^{MAPK}$ [18, 19].

Neurotransmission dyshomeostasis has been implicated in Mn neurotoxicity, and deregulated dopamine (DA) signaling has been a major focus of research (reviewed by Aschner et al. [1]). Due to similarities between manganism and PD and the accumulation of Mn in regions rich in dopaminergic (DAergic) neurons, altered DA metabolism has been considered an important aspect of the molecular actions of Mn [20]. Motor disturbances have been observed in children undergoing prolonged parenteral nutrition, where Mn is present at high concentrations [21]. *In vitro* evidence has shown that Mn decreases DA levels in the striatum due to direct oxidation of this monoamine [22]. Furthermore, Posser et al. [23] demonstrated that in PC12 cells low levels of Mn can induce sustained phosphorylation at serine (Ser) 40 of tyrosine hydroxylase (TH), the rate limiting enzyme for the synthesis of DA, leading to prolonged activation of the enzyme.

As noted above, activation of MAPK pathways has been linked to Mn-induced neurotoxicity [12, 14, 15, 17]. However, it is difficult to affirm whether MAPK activation is a cause or consequence of Mn-induced neurotoxicity. No reports were located to ascertain whether MAPK activation represents a primary event (that could trigger Mn toxicity) or if it occurs secondary to Mn-induced cellular dyshomeostasis/damage (triggered via other mechanisms, i.e., oxidative or metabolic changes). Accordingly, the aim of this study was to evaluate if MAPK pathways are modulated after Mn exposure when this metal is present at *subtoxic* concentrations, which are unable to change cell viability. In addition, the potential activation of TH was also investigated since it is important in maintaining homeostasis in DAergic neurons (targeted by Mn). To meet these objectives, fresh striatal and hippocampal slices from rats in a critical neurodevelopmental period (postnatal day 14/PND14) were acutely exposed to Mn (for 3–6 h). Our study indicates that disturbances in ERK and JNK activity in response to Mn may represent an early event. The occurrence of changes in ERK activity and JNK activity after Mn exposure, added to the absence of cell viability loss, suggests that the modulation of MAPK signaling pathway represents a primary event induced by Mn.

2. Methods

2.1. Chemicals. Anti-phospho-ERK1/2, anti-phospho-JNK1/2/3 antibodies, and LumiGLO chemiluminescent substrate were purchased from Cell Signaling (Beverly, MA, USA). Anti-phospho-$p38^{MAPK}$, anti-total-$p38^{MAPK}$, anti-total-ERK1/2, and anti-total-JNK1/2 antibodies and manganese chloride ($MnCl_2$) and Dulbecco's modified Eagle's medium (DMEM) were obtained from Sigma (St. Louis, MO, USA). Anti-phospho-TH, anti-total-TH, and goat anti-rabbit IgG HRP (horseradish peroxidase) conjugate secondary antibodies were purchased from Millipore (Billerica, MA, USA). Tris and β-mercaptoethanol were obtained from Amresco (Solon, OH, USA). 3-(4,5-dimethylthiazol-. 2-yl)-2,5-diphenyl tetrazolium bromide (MTT), SDS, and bis-acrylamide were from USB (Cleveland, OH, USA). Acrylamide and Hybond nitrocellulose were purchased from GE Healthcare Life Sciences (Piscataway, NJ, USA). All other reagents were of the highest analytical grade.

2.2. Animals. All animal studies were carried out in accordance with the "Principles of Laboratory Animal Care" (NIH publication number 80-23, revised 1996) and approved by the local Ethical Committee for Animal Research. Wistar rats of both genders at postnatal day 14 (PND14) were obtained from our own breeding colony at the Universidade Federal de Santa Catarina (UFSC), Brazil. At this developmental stage (PND14), female and male rats do not display differences in hormonal activity, since sexual maturity is not yet reached [24]. Rats were maintained in an air-conditioned room (22–25°C) on a 12-h light/dark cycle with water and food *ad libitum*.

2.3. Striatal and Hippocampal Slice Preparation and Treatments. Preparation and treatment of striatal and hippocampal slices were performed as previously described [25–27].

Briefly, a total of 32 animals were euthanized by decapitation; their encephala were extracted and the striata and hippocampi were immediately dissected (4°C) in HEPES-saline buffer (124 mM NaCl, 4 mM KCl, 1.2 mM $MgSO_4$, 12 mM D-glucose, 1 mM $CaCl_2$, and 25 mM HEPES; pH 7.4), which was previously oxygenated for 30 min. Slices of 400 μm thickness were prepared using a McIlwain Tissue Chopper. In order to obtain a sufficient number of slices, two immature rats (PND14) were used for each of the experiments. The hippocampal slices obtained were pooled and subsequently three slices for each treatment were carefully separated with a brush. The slices were individually preincubated with HEPES-saline buffer (300 μL/slice) for 30 min at room temperature (RT). For the treatments, the HEPES-saline buffer was replaced by fresh buffer in the absence (control) or presence of $MnCl_2$ (1–1,000 μM) and incubated for 3 h at 37°C. These concentrations were chosen based on previous reports, which have used similar concentrations *in vitro* [22]. The concentrations chosen encompass the physiological (10 μM), threshold of toxicity (100 μM), and toxic (1,000 μM) spectrum based on reports by Suzuki et al. [28] performed in monkeys.

The extended incubations (6 h) required different buffers similar to the conditions used for maintenance of organotypic slice cultures. The maintenance of cell viability under this experimental condition has been previously described [27]. Dissection (4°C) and preincubation (30 min, RT) were performed in Krebs-Ringer bicarbonate buffer (KRB) (122 mM NaCl, 3 mM KCl, 1.2 mM $MgSO_4$, 1.3 mM $CaCl_2$, 0.4 mM KH_2PO_4, 25 mM $NaHCO_3$, and 10 mM D-glucose). The buffer was bubbled with 95% O_2–5% CO_2 to pH 7.4. For the treatments, the medium was replaced by a nutritive incubation medium composed of 50% KRB, 50% Dulbecco's modified Eagle's medium (DMEM), 20 mM of HEPES, and 100 μg/mL of gentamicin, at 37°C in a 95% O_2/5% CO_2 atmosphere, in the absence (control) or presence of $MnCl_2$ (1–1,000 μM), and the slices were incubated for 6 h [26, 27].

2.4. Cell Viability. Slice viability was analyzed by the colorimetric MTT [3′-(4,5-dimethylthiazol-2yl) 2,5-diphenyltetrazolium bromide] reduction assay [29]. At the end of the treatments, the medium was removed and the slices (in triplicates) were incubated with 0.5 mg/mL MTT (200 μL) in HEPES-saline buffer (in the case of 3 h treatments) or KRB (6 h treatments). The slices were incubated for 20 minutes at 37°C. Mitochondrial dehydrogenases in viable cells reduce MTT to formazan crystals, which are dissolved in dimethylsulfoxide (DMSO). The absorbance was quantified spectrophotometrically using a microplate reader (λ = 540 nm). Results are expressed as a percentage of the control (absence of $MnCl_2$).

2.5. Western Blotting Analysis. To access MAPK activation, western blot analysis of slices samples was performed as previously described [25, 30, 31]. Briefly, the slices were solubilized with SDS-stopping solution (4% SDS, 2 mM EDTA, 50 mM Tris, 5% β-mercaptoethanol, pH 6.8) for 5 minutes at 100°C. Aliquots for protein concentration determination were collected before β-mercaptoethanol addition and protein concentration was later determined by the Peterson method [32]. Next, 25 : 100 (v/v) of sample dilution was added (40% glicerol, 25 mM Tris, bromophenol blue, and pH 6.8). Sixty μg of total protein/track were separated by sodium dodecyl sulfate polyacrylamide gel electrophoresis (SDS-PAGE) using 10% gels (miniVE Vertical Electrophoresis System, GE Healthcare Life Sciences, Piscataway, NJ, USA), followed by transfer to nitrocellulose membranes using a semidry blotting apparatus (TE 70 SemiPhor Unit, GE Healthcare Life Sciences, Piscataway, NJ, USA) (1.2 mA/cm^2; 1 h 30 min) as described by Bjerrum and Heegaard (1988). After blocking with 5% skim milk in Tris buffered saline (TBS) (Tris 10 mM, NaCl 150 mM, pH 7.5) for 1 hour, membranes were incubated overnight (4°C) with primary antibodies to detect the phosphorylated forms of ERK1/2, JNK1/2/3, p38^{MAPK}, and TH, in the dilutions recommended by the manufacturer. Subsequently, membranes were incubated for 1 h at RT with anti-Rabbit IgG HRP conjugate secondary antibodies. All steps were followed by three 5 minutes washing with TBS-T (TBS with the addition of Tween-20 0.1% and pH 7.5). The blots were developed by chemiluminescent reaction. Subsequently, membranes were stripped of the antibodies using a solution of NaOH 0.2 N and then reprobed to detect the total forms (phosphorylated plus nonphosphorylated form) of the target proteins. The bands were quantified using the Scion Image software (Frederick, MD, USA). The ratio of the optic density (OD) of the phosphorylated protein band over the OD of the total protein band was calculated and the phosphorylation level of each protein was determined as a percentage of the control (considered 100%).

The antibody against ERK1/2 detected two bands, one at approximately 44 kDa and the second at approximately 42 kDa, corresponding, respectively, to the two ERK isoforms, ERK1 and ERK2. Anti-p38^{MAPK} detected a single band of approximately 38 kDa; anti-JNK 1/2/3 detected two bands, one at approximately 54 kDa and the second at approximately 46 kDa, corresponding, respectively, to the three JNK isoforms, JNK2/3 and JNK1.

2.6. Statistical Analyses. Statistical analyses were performed by one-way analysis of variance (ANOVA) followed by Duncan's *post hoc* test when appropriate using STATISTICA 5.1 software (SS Inc., Tulsa, OK, USA). Differences were considered to be significant when $P < 0.05$. The values were expressed as mean ± S.E.M.

3. Results

3.1. Assessment of Cell Viability in Striatal and Hippocampal Slices Exposed to Mn. Previous studies show selective neurotoxicity of Mn toward basal ganglia structures, such as the striatum (caudate, putamen, and nucleus accumbens), globus pallidus, and substantia nigra [1]. In this study, *in vitro* Mn exposure (10–1,000 μM) for 3 or 6 hours did not

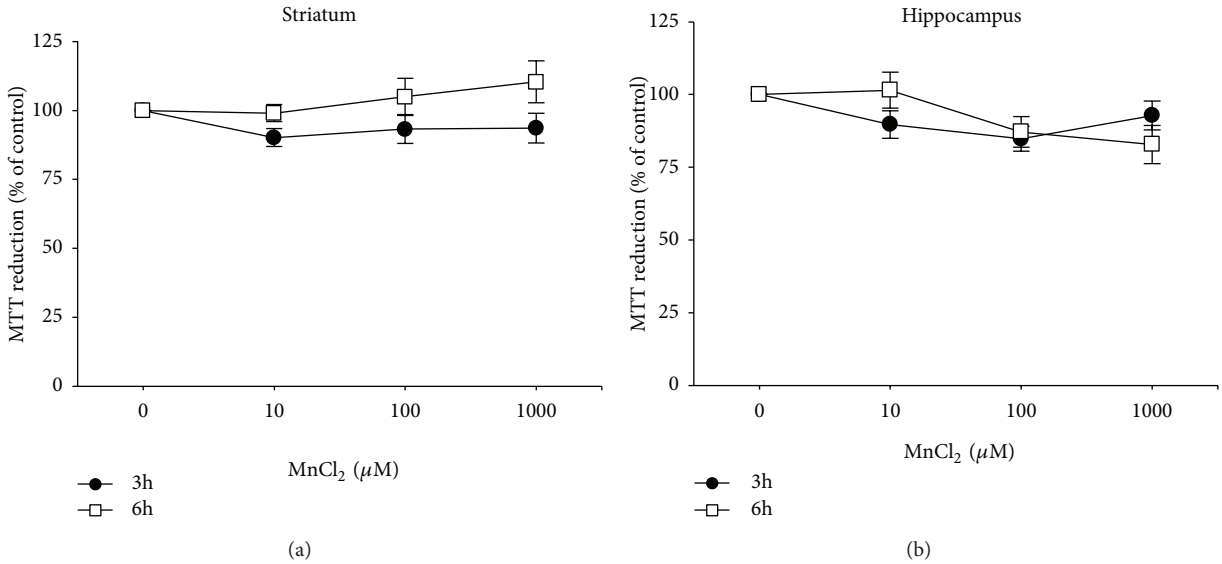

Figure 1: Effect of $MnCl_2$ on cell viability in striatal (a) and hippocampal (b) slices from immature rats. Slices were incubated for 3 h or 6 h in the absence (control) or presence of $MnCl_2$ (10–1000 μM). Cell viability was assessed by analysis of MTT reduction. The data represent the percentage of MTT reduction compared to control (considered as 100%) and express the mean ± SEM derived from 4 independent experiments.

significantly affect cell viability in either striatal (Figure 1(a)) or hippocampal slices (Figure 1(b)) assessed by MTT. The results for 3 and 6 hours incubations were obtained separately and are expressed as percentage relative to the control.

3.2. MAPKs Modulation in Striatal Slices Exposed to Mn. The phosphorylation levels of ERK1/2, JNK1/2/3, and $p38^{MAPK}$ were assessed in striatal or hippocampal slices isolated from immature rats (PND14) in response to *in vitro* Mn exposure. Slices were exposed for 3 or 6 h to Mn at concentrations ranging from 10–1,000 μM and then analyzed by western blotting.

Figures 2(a) and 2(b) show that Mn exposure (10 μM, 3 h) significantly increased ERK1 and ERK2 phosphorylation (49.81±7.66%) ($F(3, 12) = 3.53$, $P = 0.048$) and 54.96±6.43% ($F(3, 12) = 3.64$, $P = 0.045$), respectively, in striatal slices. JNK1/2/3 (Figures 2(c) and 2(d)), and $p38^{MAPK}$ (Figures 2(e) and 2(f)) phosphorylation were not significantly different from controls after 3 h exposure to Mn.

When striatal slices were exposed to 1,000 μM Mn for 6 h, significant increases in ERK1 (42.96 ± 4.48%) ($F(3, 12) = 19.79$, $P = 0.000465$), ERK2 (22.65±2.84%) ($F(3, 12) = 23.25$, $P = 0.000264$) (Figures 3(a) and 3(b)), JNK1 (33.29 ± 6.60%) ($F(3, 19) = 3.88$, $P = 0.025$), and JNK2/3 (30.65 ± 7.29%) ($F(3, 19) = 5.11$, $P = 0.00922$) (Figure 3(d)) phosphorylation were observed. However, only JNK1 (21.00 ± 6.16%) ($F(3, 19) = 3.88$ $P = 0.025$) and JNK2/3 (20.65±4.59%) ($F(3, 19) = 5.11$, $P = 0.00922$) phosphorylation (Figures 3(c) and 3(d)) were significantly increased after exposures to 100 μM Mn and no significant changes were observed in $p38^{MAPK}$ phosphorylation under the same experimental conditions (Figures 3(e) and 3(f)).

3.3. MAPKs Modulation in Hippocampal Slices Exposed to Mn. Hippocampal slices exposed to Mn for 3 h showed a significant increase of ERK1 (50.44 ± 6.47%) ($F(3, 19) = 3.23$, $P = 0.046$) and ERK2 phosphorylation (29.02 ± 5.45%) ($F(3, 19) = 3.48$, $P = 0.042$) at 100 μM Mn (Figures 4(a) and 4(b)). Moreover, ERK2 phosphorylation was also significantly increased (30.62 ± 7.80%) ($F(3, 19) = 3.48$, $P = 0.042$) at the highest Mn concentration tested (1,000 μM). JNK1/2/3 (Figures 4(c) and 4(d)) and $p38^{MAPK}$ (Figures 4(e) and 4(f)) phosphorylation were not modified in the hippocampal slices after 3 h exposure to Mn.

When hippocampal slices were exposed to Mn for 6 h, a significant increase in the phosphorylation of ERK1 (19.04 ± 4.48%) ($F(3, 19) = 3.21$, $P = 0.046$) and ERK2 (13.34±4.46%) ($F(3, 19) = 3.02$, $P = 0.049$) (Figures 5(a) and 5(b)), JNK1 (22.58 ± 5.41%) ($F(3, 19) = 5.22$, $P = 0.008$), and JNK2/3 (67.97 ± 24.94%) ($F(3, 19) = 3.11$, $P = 0.048$) (Figures 5(c) and 5(d)) were observed at the highest Mn concentration (1,000 μM). No significant changes were observed in $p38^{MAPK}$ phosphorylation under the same experimental conditions (Figures 5(e) and 5(f)).

3.4. Phosphorylation of TH at Ser^{40} in Striatal Slices Exposed to Mn. TH is the rate-limiting enzyme for dopamine (DA) synthesis. Medium- and long-term modulation of TH activity occurs by regulation of gene expression and in the short-term by regulation of enzyme activity. Phosphorylation on serine residues, by several enzymes, is the primary mechanism of short-term TH activity regulation [33, 34]. Previous studies in PC12 cells demonstrated increased Ser^{40} phosphorylation and activation of TH in response to Mn [23]. However, in our experimental protocol (with tissue slices) no significant

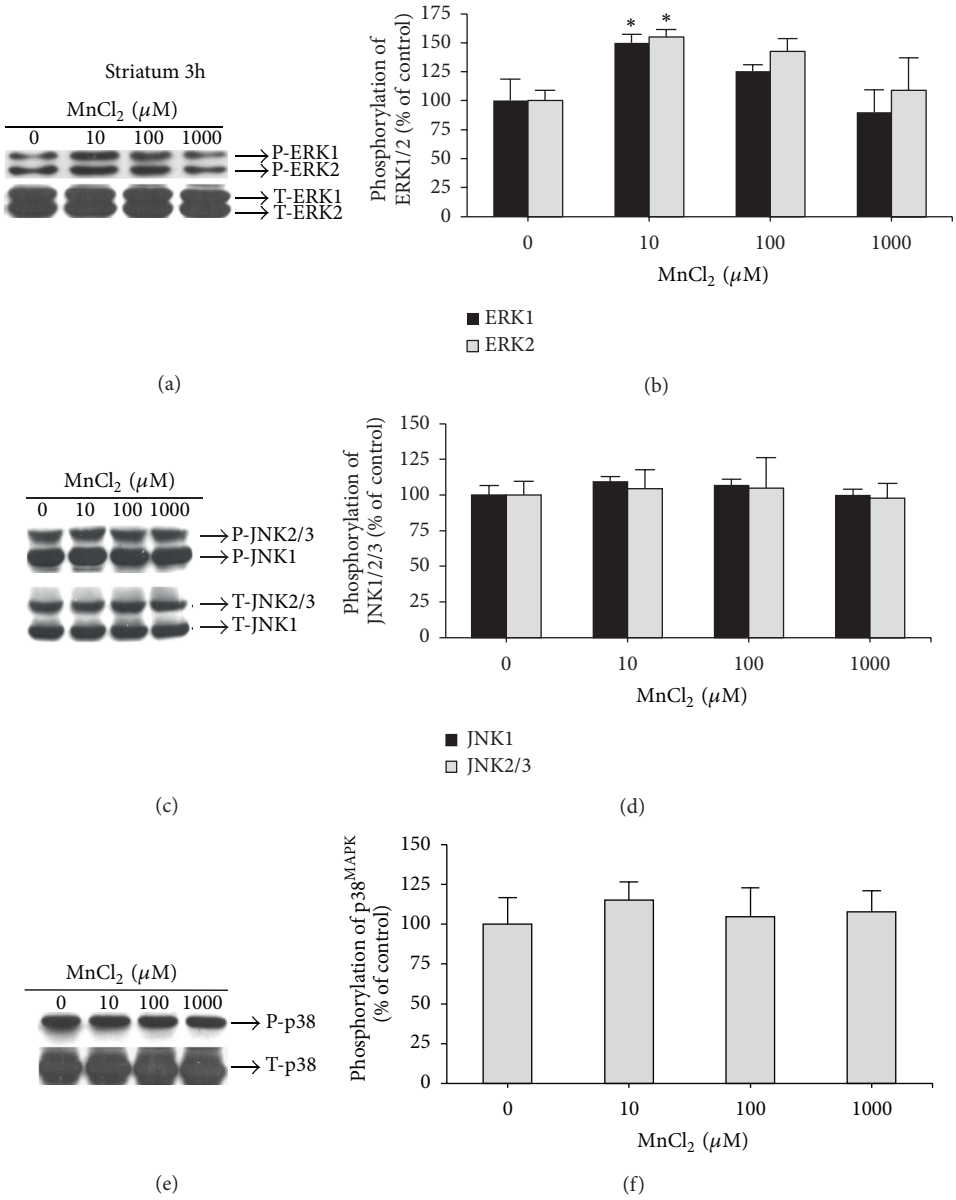

Figure 2: Effect of $MnCl_2$ on MAPKs phosphorylation (ERK1/2, JNK1/2/3 and $p38^{MAPK}$) in striatal slices from immature rats (PND14). Slices were incubated for 3 h in the absence (control) or presence of $MnCl_2$ (10–1000 μM). The panels (a), (c), and (e) show a representative blot of striatal immunoreactivity of the phospho (P)-ERK; and total (T)-ERK, P-JNK, and T-JNK; and $P\text{-}p38^{MAPK}$; and $T\text{-}p38^{MAPK}$, respectively. The panels (b), (d), and (f) show the striatal quantification of P-ERK, P-JNK, and $P\text{-}p38^{MAPK}$, respectively. The phosphorylation level of each protein was determined by computer-assisted densitometry as a ratio of the O.D. of the phosphorylated (P) band over the O.D. of the total (T) band, and the data are expressed as percentage of the control. The values are presented as mean ± S.E.M derived from 4 independent experiments. $^*P < 0.05$.

changes in TH-Ser^{40} phosphorylation in response to Mn (10–1,000 μM) exposure were observed (Figure 6).

4. Discussion

Recent data from our group demonstrated that developmental Mn exposure from postnatal days 8–12 (PND8–12) altered the activity of key cell signaling elements, causing increased phosphorylation of DARPP-32-Thr-34, ERK1/2, and AKT in the striatum of rats on PND14 [12]. Additionally, in the same experimental protocol, Mn impaired motor coordination later at the 3rd, 4th, and 5th week of life. These results were in line with recent evidence indicating that MAPK pathways might be involved in the neurotoxicity induced by Mn in various experimental models, such as mesencephalic cells [16], PC12 cells [15, 23, 35], microglial cells [36, 37], primary astrocyte culture [17], and *in vivo* developmental exposure

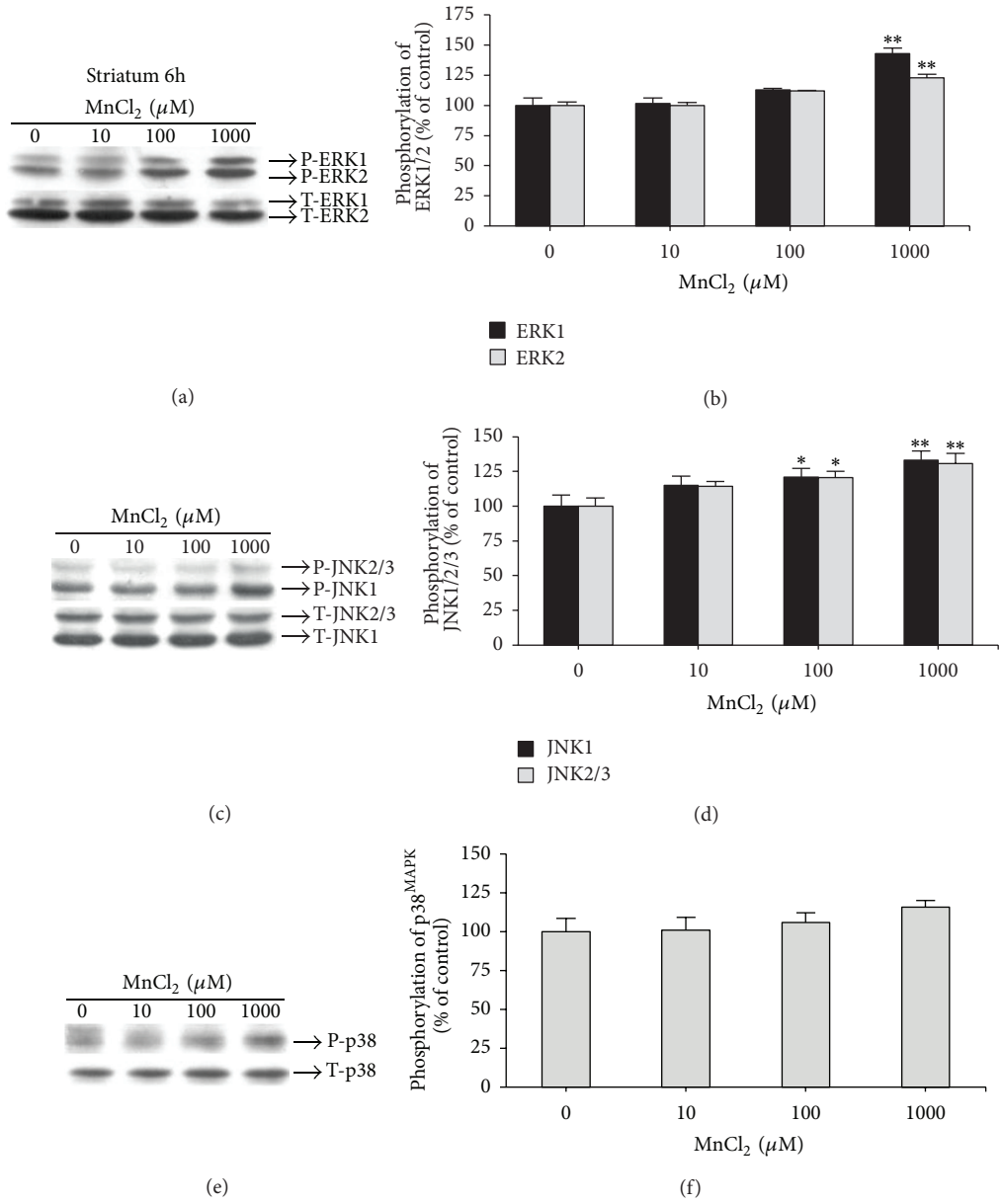

FIGURE 3: Effect of $MnCl_2$ on MAPKs phosphorylation (ERK1/2, JNK1/2/3, and $p38^{MAPK}$) in striatal slices from immature rats (PND14). Slices were incubated for 6 h in the absence (control) or presence of $MnCl_2$ (10–1000 μM). The panels (a), (c), and (e) show a representative blot of striatal immunoreactivity of the phospho (P)-ERK; and total (T)-ERK, P-JNK, and T-JNK; and P-$p38^{MAPK}$; and T-$p38^{MAPK}$, respectively. The panels (b), (d), and (f) show the striatal quantification of P-ERK, P-JNK, and P-$p38^{MAPK}$, respectively. The phosphorylation level of each protein was determined by computer-assisted densitometry as a ratio of the O.D. of the phosphorylated (P) band over the O.D. of the total (T) band, and the data are expressed as percentage of the control. The values are presented as mean ± S.E.M derived from 4 independent experiments. $^{**}P < 0.01$ and $^{*}P < 0.05$.

[12, 13]. However, the current knowledge on Mn-induced neurotoxicity does not allow for stating whether changes in MAPK signaling pathways represent cause or consequence of Mn-induced cell toxicity. In an attempt to investigate if Mn can modulate MAPK signaling pathways in conditions where cells are still completely viable, we took advantage of a slice-based model to evaluate Mn-induced effects *in vitro* with particular emphasis on striatal and hippocampal tissues. Employing experimental conditions (Mn concentration and exposure time) that do not cause significant cell death (evaluated by the MTT assay; Figure 1), we observed that both striatal and hippocampal slices showed significant changes in MAPKs phosphorylation.

Our results showed that slice incubation with $MnCl_2$ did not induce significant changes in cell viability (Figure 1). This finding corroborates findings by Sistrunk et al. [22], who failed to observe Mn-induced cell death in an *in vitro* model of rat striatal slices exposed to $MnCl_2$ (10–1,000 μM)

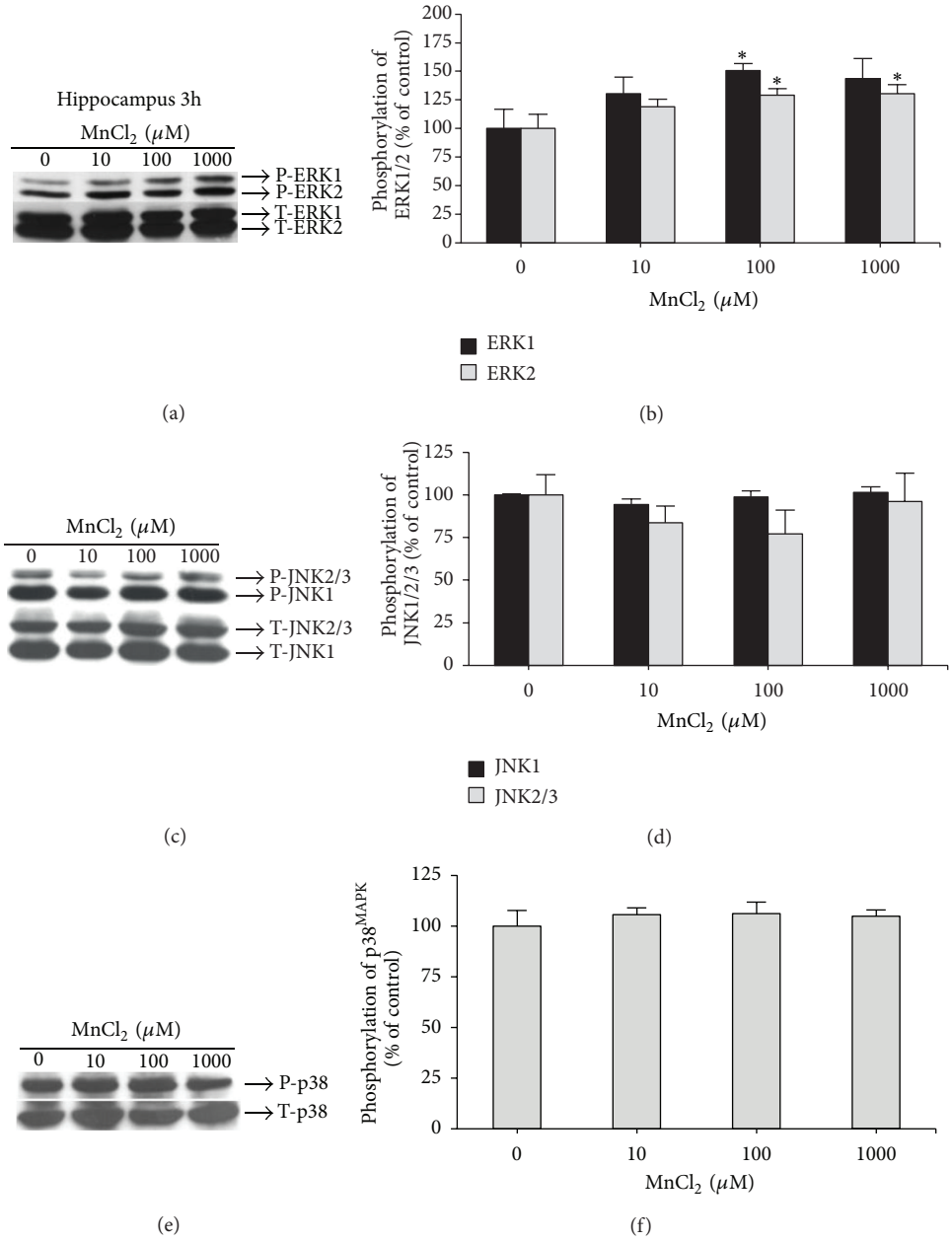

Figure 4: Effect of $MnCl_2$ on MAPKs phosphorylation (ERK1/2, JNK1/2/3, and $p38^{MAPK}$) in hippocampal slices from immature rats (PND14). Slices were incubated for 3 h in the absence (control) or presence of $MnCl_2$ (10–1000 μM). The panels (a), (c), and (e) show a representative blot of hippocampal immunoreactivity of the phospho (P)-ERK; and total (T)-ERK, P-JNK, and T-JNK, and P-$p38^{MAPK}$; and T-$p38^{MAPK}$, respectively. The panels (b), (d), and (f) show the hippocampal quantification of P-ERK, P-JNK, and P-$p38^{MAPK}$, respectively. The phosphorylation level of each protein was determined by computer-assisted densitometry as a ratio of the O.D. of the phosphorylated (P) band over the O.D. of the total (T) band, and the data are expressed as percentage of the control. The values are presented as mean ± S.E.M derived from 4 independent experiments. $^*P < 0.05$.

for 4 hours. However, a decrease in cell viability *in vitro* was demonstrated in DAergic PC12 cells [14, 23] after exposure to high Mn concentrations for extended periods (24–48 h). It needs to be taken into account that the cell viability in the present work was assessed only by the MTT test. Other methods such as lactate dehydrogenase (LDH) or neutral red could be tested in future works. Nevertheless, as mentioned above, it needs to be considered that studies in pure PC12 cultures are void of glial cells, which are known modulators of Mn CNS homeostasis. Astrocytes accumulate higher levels of Mn than neurons and may be an initial site for Mn-induced damage, thus, lowering the neuronal burden of Mn [8]. Furthermore, the slice model provides only a short time window for metal exposure (in our case

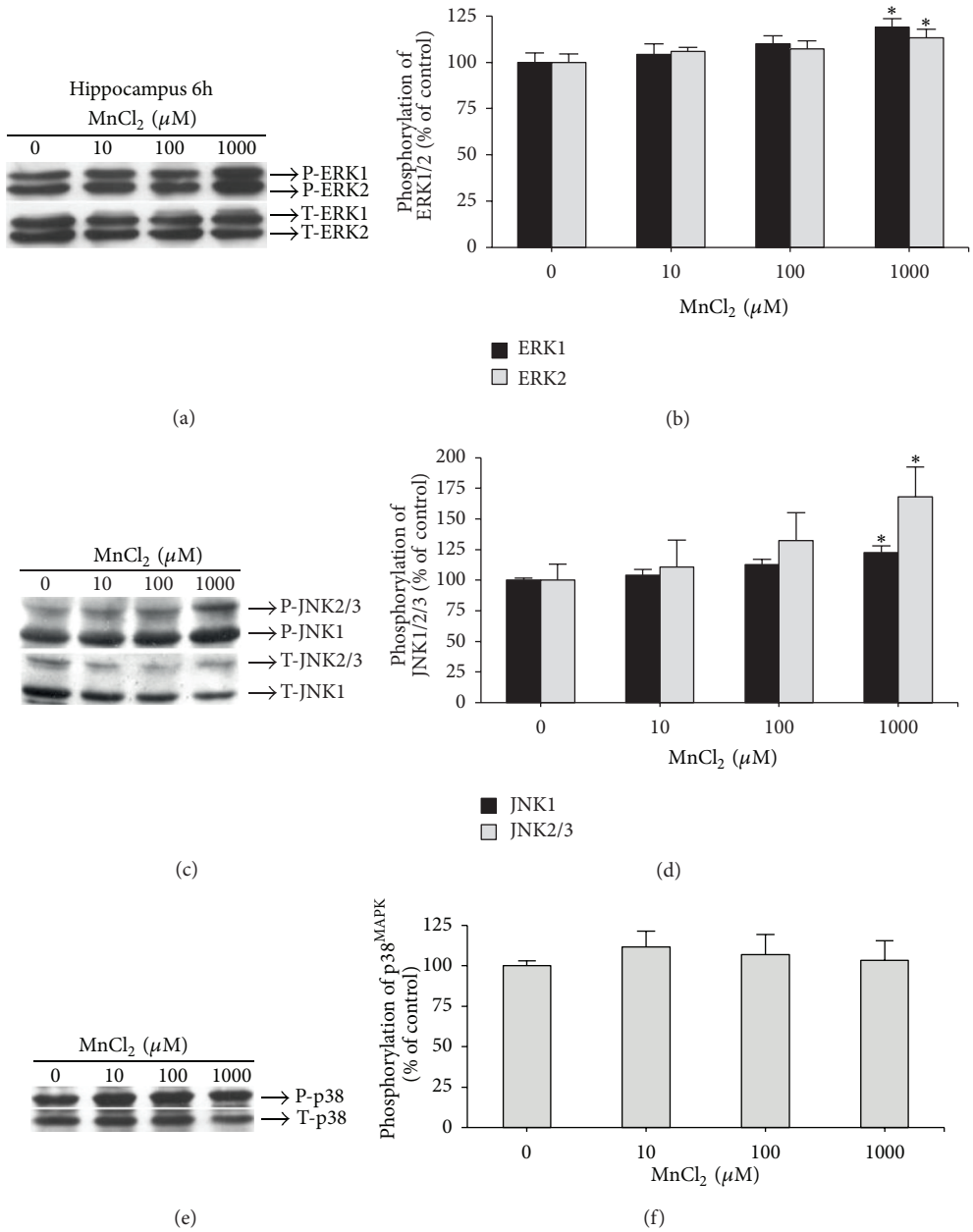

Figure 5: Effect of $MnCl_2$ on MAPKs phosphorylation (ERK1/2, JNK1/2/3, and $p38^{MAPK}$) in hippocampal slices from immature rats (PND14). Slices were incubated for 6 h in the absence (control) or presence of $MnCl_2$ (10–1000 μM). The panels (a), (c), and (e) show a representative blot of hippocampal immunoreactivity of the phospho (P)-ERK; and total (T)-ERK, P-JNK, and T-JNK; and $P\text{-}p38^{MAPK}$; and $T\text{-}p38^{MAPK}$, respectively. The panels (b), (d), and (f) show the hippocampal quantification of P-ERK, P-JNK, and $P\text{-}p38^{MAPK}$, respectively. The phosphorylation level of each protein was determined by computer-assisted densitometry as a ratio of the O.D. of the phosphorylated (P) band over the O.D. of the total (T) band, and the data are expressed as percentage of the control. The values are presented as mean ± S.E.M derived from 4 independent experiments. $^*P < 0.05$.

a maximum of 6 hours) beyond which the cell viability is compromised [27]. Lead (Pb), another metal widely recognized as a neurotoxicant [38], has also been evaluated in the slices model [25]. No changes in cell viability were observed after the treatment of hippocampal slices from PND14 rats with Pb acetate. However, phosphorylation levels of ERK and $p38^{MAPK}$ were increased. These results indicate that even though cell viability is not compromised, toxic metals may still cause changes in cells signaling pathways *in vitro* that may disturb cellular function [25].

Our results showed an increase in ERK phosphorylation in striatal slices exposed to a low Mn concentration (10 μM) for 3 hours (Figure 2(b)). ERK and JNK phosphorylation also increased in striatal slices exposed to 100 and 1,000 μM Mn

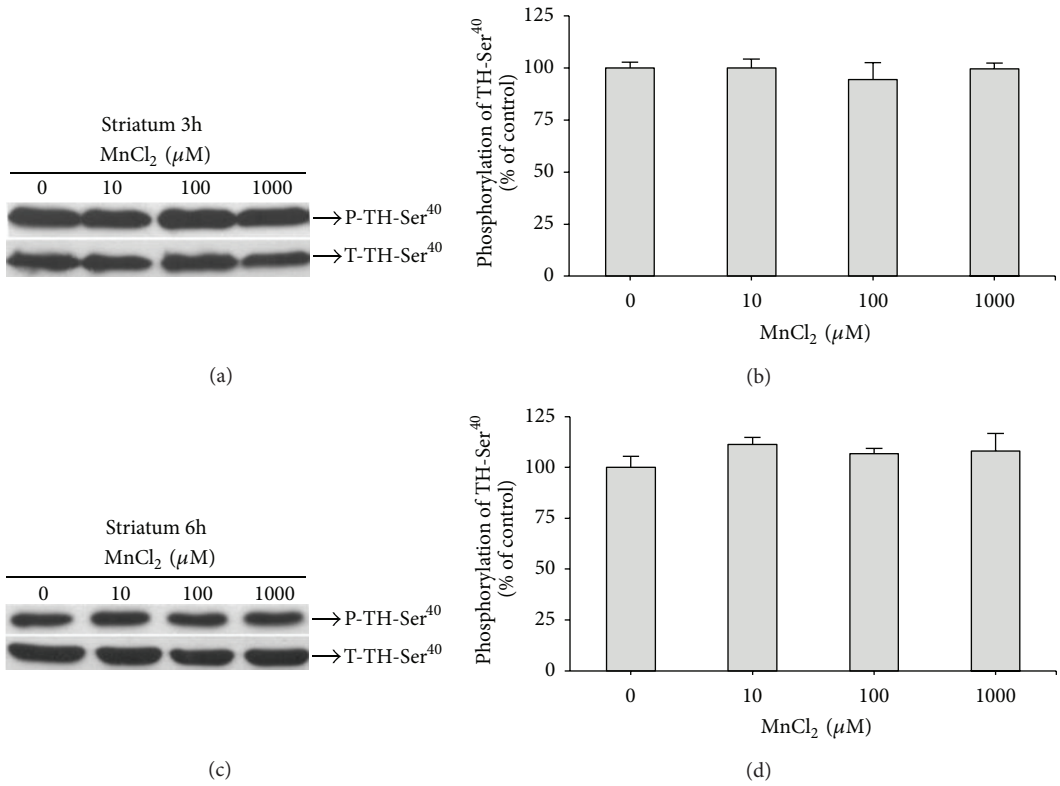

FIGURE 6: Effect of $MnCl_2$ on phosphorylation of tyrosine hydroxylase at serine 40 (TH-Ser^{40}) in striatal slices from immature rats (PND14). Slices were incubated for 3 and 6 h in the absence (control) or presence of $MnCl_2$ (10–1000 μM). The panel (a) shows a representative blot of striatal immunoreactivity of the phospho (P)-TH-Ser^{40} and total (T)-TH of the slices exposed for 3 h. The panel (b) shows the striatal quantification of P-TH-Ser^{40} of the slices exposed for 3 h. The panel (c) shows a representative blot of striatal immunoreactivity of the P-TH-Ser^{40} and T-TH of the slices exposed for 6 h. The panel (d) shows the striatal quantification of P-TH-Ser^{40} of the slices exposed for 6 h. The phosphorylation level of each protein was determined by computer-assisted densitometry as a ratio of the O.D. of the phosphorylated (P) band over the O.D. of the total (T) band, and the data are expressed as percentage of the control. The values are presented as mean ± S.E.M derived from 4 independent experiments.

for 6 hours (Figures 3(b) and 3(d), resp.). Of note, these changes in MAPK signaling pathways were observed in slices completely viable (no changes in the MTT assay), indicating that altered intracellular MAPKs signaling pathways may represent an early event of Mn action in the slices. ERK1/2 activation has also been observed in the striatum of immature rats (PND14) developmentally exposed to Mn (PND8–12) [12]. Therefore, it appears that activation of ERK1/2 by Mn may be an early and conserved mechanism observed both *in vitro* and *in vivo*.

The majority of *in vitro* studies concerning the effects of Mn on cell signaling pathways were conducted in cell culture models [23, 39]. However, neuroglial interactions may play important roles in the modulation of neurotoxic processes, including those triggered by metals [40, 41]. Thus, *in vitro* studies, which in general are focused on single cell type (e.g., neuron or astrocyte alone), fail to take into account toxic events that are dependent upon neuronal and glial interactions. In contrast, tissue slices from rat brain maintain the natural extracellular matrix, neuronal connectivity, and neuroglial interactions, providing an appropriate experimental model for studies on acute neurotoxic events [42, 43]. The model of 400 μm thick brain slices is well established [42, 44] and has been used for *in vitro* studies on the neurotoxicity of metals, such as cadmium (Cd) [30] and Pb [25].

Striatal slices are rich in DAergic neurons, in contrast to hippocampal slices. Of particular importance, Mn shows selective neurotoxicity to DAergic neurons by mechanisms that have yet to be fully defined but possibly involve interaction with DA, leading to its oxidation forming toxic quinones and consequent oxidative stress [45–47]. A recent study in *Caenorhabditis elegans* showed that extracellular and not intracellular DA is responsible for Mn-induced DAergic neurodegeneration [48]. Moreover, it is known that the striatum expresses higher levels of DMT-1, which is the predominant transporter for divalent Mn into cells [49]. Therefore, the presence of DAergic neurons and DMT1 in striatal slices may explain, at least in part, the significant modulation of MAPKs by a relative low Mn concentration in striatal tissue as compared to hippocampus.

With respect to the susceptibility of hippocampal slices to Mn, we noted increased ERK1/2 phosphorylation following exposure of hippocampal slices to 100 and 1,000 μM Mn for 3 hours (Figure 4(b)). ERK and JNK also showed increased

phosphorylation in hippocampal slices exposed to 1,000 μM Mn for 6 h (Figures 5(b) and 5(d), resp.). In a recent study, the hippocampus was studied as a site for Mn neurotoxicity *in vivo*, since Mn exposure increased the levels of thiobarbituric acid reactive species (TBARS), diminished total thiol content, and increased superoxide dismutase and catalase activity, indicating oxidative stress within this structure [50]. Therefore, although the basal ganglia are the most susceptible sites to Mn neurotoxicity, it is also evident that Mn may cause broad spectrum neuropathological changes in both neurons and glia in other brain regions, which may account for some of the nonmotor symptoms associated with this disorder [1].

Given the (1) importance of TH in controlling DA levels in neurons, (2) the involvement of DA metabolism in Mn neurotoxicity, as well as (3) a plethora of studies showing TH activity modulation and Ser^{40} phosphorylation by Mn [23, 39], we investigated Mn's effects on TH Ser^{40} phosphorylation in striatal slices from immature rats. This site is phosphorylated by protein kinase A (PKA) and protein kinase C (PKC), increasing TH activity. Ser^{40}dephosphorylation by protein phosphatase 2A (PP2A) results in decreased TH activity [33]. Our results showed no significant alteration in TH phosphorylation at Ser^{40} (Figure 6). This result indicates that in immature striatal slices Mn does not act in an analogous way to PC12 cells exposed to Mn (100 μM). In the latter study, a sustained TH-Ser^{40} phosphorylation (6–24 h) was observed, independent from H_2O_2 production and in the absence of significant changes in cell viability [23].

Thus, based on our and previous studies, it can be inferred that Mn requires longer exposure periods to induce cell death in slices. However, important molecular changes were observed within short periods after Mn exposure, such as the activation of ERK1/2 and JNK1/2/3 signaling pathway (Figures 2–5). These findings are in agreement with those previously reported by our group in a model of developmentally exposed rats where ERK1/2 activation but not JNK1/2/3 was noted [12]. Thus, striatal slices of immature rats exposed *in vitro* to Mn reproduce (at least in part) the changes observed *in vivo*.

5. Conclusions

A key finding in this study is the Mn-dependent activation of ERK1/2 and JNK1/2/3 in striatal and hippocampal slices with no significant changes in cell viability. This finding indicates that MAPKs activation may represent an important primary event that precedes the deleterious effects of Mn on the cellular viability. Extrapolating our data to *in vivo* conditions, one would posit that Mn is able to modulate the activation of MAPKs in tissues that maintain their metabolic competence and viability. The physiological significance of such activation represents a research topic that needs further attention.

Conflict of Interests

None of the authors has a known or perceived conflict of interests with the contents of this paper.

Acknowledgments

This work was supported by the Conselho Nacional de Desenvolvimento Científico e Tecnológico (CNPq) Brazil (no. 305194/2010-0); the Coordenação de Aperfeiçoamento de Pessoal de Nível Superior (CAPES)/PROCAD; the National Institute of Science and Technology (INCT) for Excitotoxicity and Neuroprotection; the Fundação de Amparo a Pesquisa de Santa Catarina (FAPESC); FAPESC/PRONEX—Núcleo de Excelência em Neurociências Aplicadas de Santa Catarina (NENASC); and IBN.Net/CNPq. Marcelo Farina, Roger Walz, and Rodrigo Bainy Leal are recipient of Research Scholarship from CNPq. Michael Aschner was supported in part by Grants from the National Institutes of Health ES R01 10563 and ES P30 00267. The funding agencies had no role in study design, data collection and analysis, decision to publish, or preparation of the paper.

References

[1] M. Aschner, K. M. Erikson, E. H. Hernández, and R. Tjalkens, "Manganese and its role in Parkinson's disease: from transport to neuropathology," *NeuroMolecular Medicine*, vol. 11, no. 4, pp. 252–266, 2009.

[2] T. R. Guilarte, "Manganese and Parkinson's disease: a critical review and new findings," *Environmental Health Perspectives*, vol. 118, no. 8, pp. 1071–1080, 2010.

[3] T. E. Gunter, C. E. Gavin, M. Aschner, and K. K. Gunter, "Speciation of manganese in cells and mitochondria: a search for the proximal cause of manganese neurotoxicity," *NeuroToxicology*, vol. 27, no. 5, pp. 765–776, 2006.

[4] T. R. Guilarte, N. C. Burton, T. Verina et al., "Increased APLP1 expression and neurodegeneration in the frontal cortex of manganese-exposed non-human primates," *Journal of Neurochemistry*, vol. 105, no. 5, pp. 1948–1959, 2008.

[5] R. M. Molina, S. Phattanarudee, J. Kim et al., "Ingestion of Mn and Pb by rats during and after pregnancy alters iron metabolism and behavior in offspring," *NeuroToxicology*, vol. 32, no. 4, pp. 413–422, 2011.

[6] C. H. Kern and D. R. Smith, "Preweaning Mn exposure leads to prolonged astrocyte activation and lasting effects on the dopaminergic system in adult male rats," *Synapse*, vol. 65, no. 6, pp. 532–544, 2011.

[7] J. A. Moreno, E. C. Yeomans, K. M. Streifel, B. L. Brattin, R. J. Taylor, and R. B. Tjalkens, "Age-dependent susceptibility to manganese-induced neurological dysfunction," *Toxicological Sciences*, vol. 112, no. 2, pp. 394–404, 2009.

[8] L. E. Gonzalez, A. A. Juknat, A. J. Venosa, N. Verrengia, and M. L. Kotler, "Manganese activates the mitochondrial apoptotic pathway in rat astrocytes by modulating the expression of proteins of the Bcl-2 family," *Neurochemistry International*, vol. 53, no. 6–8, pp. 408–415, 2008.

[9] Y. Liu, D. S. Barber, P. Zhang, and B. Liu, "Complex II of the mitochondrial respiratory chain is the key mediator of divalent manganese-induced hydrogen peroxide production in microglia," *Toxicological Sciences*, vol. 132, no. 2, pp. 298–306, 2013.

[10] H. Yoon, D.-S. Kim, G.-H. Lee, K.-W. Kim, H.-R. Kim, and H.-J. Chae, "Apoptosis induced by manganese on neuronal SK-N-MC cell line: Endoplasmic Reticulum (ER) stress and

mitochondria dysfunction," *Environmental Health and Toxicology*, vol. 26, Article ID e2011017, 2011.

[11] D. Milatovic, S. Zaja-Milatovic, R. C. Gupta, Y. Yu, and M. Aschner, "Oxidative damage and neurodegeneration in manganese-induced neurotoxicity," *Toxicology and Applied Pharmacology*, vol. 240, no. 2, pp. 219–225, 2009.

[12] F. M. Cordova, A. S. Aguiar Jr., T. V. Peres et al., "*In vivo* manganese exposure modulates Erk, Akt and Darpp-32 in the striatum of developing rats, and impairs their motor function," *PLoS ONE*, vol. 7, no. 3, Article ID e33057, 2012.

[13] F. M. Cordova, A. S. Aguiar Jr., T. V. Peres et al., "Manganese-exposed developing rats display motor deficits and striatal oxidative stress that are reversed by Trolox," vol. 87, no. 7, pp. 1231–1244, 2013.

[14] Y. Hirata, T. Meguro, and K. Kiuchi, "Differential effect of nerve growth factor on dopaminergic neurotoxin-induced apoptosis," *Journal of Neurochemistry*, vol. 99, no. 2, pp. 416–425, 2006.

[15] Y. Ito, K. Oh-hashi, K. Kiuchi, and Y. Hirata, "p44/42 MAP kinase and c-Jun N-terminal kinase contribute to the up-regulation of caspase-3 in manganese-induced apoptosis in PC12 cells," *Brain Research*, vol. 1099, no. 1, pp. 1–7, 2006.

[16] K. Prabhakaran, G. D. Chapman, and P. G. Gunasekar, "α-synuclein overexpression enhances manganese-induced neurotoxicity through the NF-κB-mediated pathway," *Toxicology Mechanisms and Methods*, vol. 21, no. 6, pp. 435–443, 2011.

[17] Z. Yin, J. L. Aschner, A. P. dos Santos, and M. Aschner, "Mitochondrial-dependent manganese neurotoxicity in rat primary astrocyte cultures," *Brain Research*, vol. 1203, pp. 1–11, 2008.

[18] E. K. Kim and E.-J. Choi, "Pathological roles of MAPK signaling pathways in human diseases," *Biochimica et Biophysica Acta*, vol. 1802, no. 4, pp. 396–405, 2010.

[19] G. M. Thomas and R. L. Huganir, "MAPK cascade signalling and synaptic plasticity," *Nature Reviews Neuroscience*, vol. 5, no. 3, pp. 173–183, 2004.

[20] T. R. Guilarte, N. C. Burton, J. L. McGlothan et al., "Impairment of nigrostriatal dopamine neurotransmission by manganese is mediated by pre-synaptic mechanism(s): implications to manganese-induced parkinsonism," *Journal of Neurochemistry*, vol. 107, no. 5, pp. 1236–1247, 2008.

[21] K. M. Erikson, K. Thompson, J. Aschner, and M. Aschner, "Manganese neurotoxicity: a focus on the neonate," *Pharmacology & Therapeutics*, vol. 113, no. 2, pp. 369–377, 2007.

[22] S. C. Sistrunk, M. K. Ross, and N. M. Filipov, "Direct effects of manganese compounds on dopamine and its metabolite Dopac: an *in vitro* study," *Environmental Toxicology and Pharmacology*, vol. 23, no. 3, pp. 286–296, 2007.

[23] T. Posser, J. L. Franco, L. Bobrovskaya, R. B. Leal, P. W. Dickson, and P. R. Dunkley, "Manganese induces sustained Ser40 phosphorylation and activation of tyrosine hydroxylase in PC12 cells," *Journal of Neurochemistry*, vol. 110, no. 3, pp. 848–856, 2009.

[24] P. Sengupta, "The laboratory rat: relating its age with human's," *International Journal of Preventive Medicine*, vol. 4, no. 6, pp. 624–630, 2013.

[25] F. M. Cordova, A. L. S. Rodrigues, M. B. O. Giacomelli et al., "Lead stimulates ERK1/2 and p38MAPK phosphorylation in the hippocampus of immature rats," *Brain Research*, vol. 998, no. 1, pp. 65–72, 2004.

[26] A. V. Jacques, D. K. Rieger, M. Maestri et al., "Lectin from *Canavalia brasiliensis* (ConBr) protects hippocampal slices against glutamate neurotoxicity in a manner dependent of PI3K/Akt pathway," *Neurochemistry International*, vol. 62, no. 6, pp. 836–842, 2013.

[27] S. Molz, H. Decker, T. Dal-Cim et al., "Glutamate-induced toxicity in hippocampal slices involves apoptotic features and p38MAPK signaling," *Neurochemical Research*, vol. 33, no. 1, pp. 27–36, 2008.

[28] Y. Suzuki, T. Mouri, and Y. Suzuki, "Study of subacute toxicity of manganese dioxide in monkeys," *Tokushima Journal of Experimental Medicine*, vol. 22, pp. 5–10, 1975.

[29] Y. Liu, D. A. Peterson, H. Kimura, and D. Schubert, "Mechanism of cellular 3-(4,5-dimethylthiazol-2-yl)-2,5- diphenyltetrazolium bromide (MTT) reduction," *Journal of Neurochemistry*, vol. 69, no. 2, pp. 581–593, 1997.

[30] A. P. Rigon, F. M. Cordova, C. S. Oliveira et al., "Neurotoxicity of cadmium on immature hippocampus and a neuroprotective role for p38MAPK," *NeuroToxicology*, vol. 29, no. 4, pp. 727–734, 2008.

[31] R. B. Leal, F. M. Cordova, L. Herd, L. Bobrovskaya, and P. R. Dunkley, "Lead-stimulated p38MAPK-dependent Hsp27 phosphorylation," *Toxicology and Applied Pharmacology*, vol. 178, no. 1, pp. 44–51, 2002.

[32] G. L. Peterson, "A simplification of the protein assay method of Lowry et al. Which is more generally applicable," *Analytical Biochemistry*, vol. 83, no. 2, pp. 346–356, 1977.

[33] P. R. Dunkley, L. Bobrovskaya, M. E. Graham, E. I. Von Nagy-Felsobuki, and P. W. Dickson, "Tyrosine hydroxylase phosphorylation: regulation and consequences," *Journal of Neurochemistry*, vol. 91, no. 5, pp. 1025–1043, 2004.

[34] S. C. Kumer and K. E. Vrana, "Intricate regulation of tyrosine hydroxylase activity and gene expression," *Journal of Neurochemistry*, vol. 67, no. 2, pp. 443–462, 1996.

[35] T. Cai, H. Che, T. Yao et al., "Manganese induces Tau hyperphosphorylation through the activation of ERK MAPK pathway in PC12 cells," *Toxicological Sciences*, vol. 119, no. 1, pp. 169–177, 2011.

[36] J.-H. Bae, B.-C. Jang, S.-I. Suh et al., "Manganese induces inducible nitric oxide synthase (iNOS) expression via activation of both MAP kinase and PI3K/Akt pathways in BV2 microglial cells," *Neuroscience Letters*, vol. 398, no. 1-2, pp. 151–154, 2006.

[37] P. L. Crittenden and N. M. Filipov, "Manganese modulation of MAPK pathways: effects on upstream mitogen activated protein kinase kinases and mitogen activated kinase phosphatase-1 in microglial cells," *Journal of Applied Toxicology*, vol. 31, no. 1, pp. 1–10, 2011.

[38] P. Grandjean and P. Landrigan, "Developmental neurotoxicity of industrial chemicals," *The Lancet*, vol. 368, no. 9553, pp. 2167–2178, 2006.

[39] D. Zhang, A. Kanthasamy, V. Anantharam, and A. Kanthasamy, "Effects of manganese on Tyrosine Hydroxylase (TH) activity and TH-phosphorylation in a dopaminergic neural cell line," *Toxicology and Applied Pharmacology*, vol. 254, no. 2, pp. 65–71, 2011.

[40] N. M. Filipov and C. A. Dodd, "Role of glial cells in manganese neurotoxicity," *Journal of Applied Toxicology*, vol. 32, no. 5, pp. 310–317, 2012.

[41] F. Zhao, T. Cai, M. Liu, G. Zheng, W. Luo, and J. Chen, "Manganese induces dopaminergic neurodegeneration via microglial activation in a rat model of manganism," *Toxicological Sciences*, vol. 107, no. 1, pp. 156–164, 2009.

[42] C.-X. Gong, T. Lidsky, J. Wegiel, I. Grundke-Iqbal, and K. Iqbal, "Metabolically active rat brain slices as a model to study the regulation of protein phosphorylation in mammalian brain," *Brain Research Protocols*, vol. 6, no. 3, pp. 134–140, 2001.

[43] Y. Hirata and T. Nagatsu, "Rotenone and CCCP inhibit tyrosine hydroxylation in rat striatal tissue slices," *Toxicology*, vol. 216, no. 1, pp. 9–14, 2005.

[44] R. Rodnight and R. Leal, "Regional variations in protein phosphorylating activity in rat brain studied in micro-slices labeled with [32P]phosphate," *Journal of Molecular Neuroscience*, vol. 2, no. 2, pp. 115–122, 1990.

[45] G. Díaz-Véliz, S. Mora, P. Gómez et al., "Behavioral effects of manganese injected in the rat substantia nigra are potentiated by dicumarol, a DT-diaphorase inhibitor," *Pharmacology Biochemistry and Behavior*, vol. 77, no. 2, pp. 245–251, 2004.

[46] E. J. Martinez-Finley, C. E. Gavin, M. Aschner, and T. E. Gunter, "Manganese neurotoxicity and the role of reactive oxygen species," *Free Radical Biology and Medicine*, vol. 62, pp. 65–75, 2013.

[47] K. Prabhakaran, D. Ghosh, G. D. Chapman, and P. G. Gunasekar, "Molecular mechanism of manganese exposure-induced dopaminergic toxicity," *Brain Research Bulletin*, vol. 76, no. 4, pp. 361–367, 2008.

[48] A. Benedetto, C. Au, D. S. Avila, D. Milatovic, and M. Aschner, "Extracellular dopamine potentiates Mn-induced oxidative stress, lifespan reduction, and dopaminergic neurodegeneration in a BLI-3-dependent manner in caenorhabditis elegans," *PLoS Genetics*, vol. 6, no. 8, Article ID e1001084, 2010.

[49] C. Au, A. Benedetto, and M. Aschner, "Manganese transport in eukaryotes: the role of DMT1," *NeuroToxicology*, vol. 29, no. 4, pp. 569–576, 2008.

[50] E. N. Martins, N. T. C. Pessano, L. Leal et al., "Protective effect of Melissa officinalis aqueous extract against Mn-induced oxidative stress in chronically exposed mice," *Brain Research Bulletin*, vol. 87, no. 1, pp. 74–79, 2012.